

Survey of Period Variations of Superhumps in SU UMa-Type Dwarf Novae. VII: The Seventh Year (2014–2015)

Taichi KATO,^{1*} Franz-Josef HAMBSCH,^{2,3,4} Pavol A. DUBOVSKY,⁵ Igor KUDZEJ,⁵ Berto MONARD,^{6,7} Ian MILLER,⁸
Hiroshi ITOH,⁹ Seiichiro KIYOTA,¹⁰ Kazunari MASUMOTO,¹¹ Daiki FUKUSHIMA,¹¹ Hiroki KINOSHITA,¹¹
Kazuki MAEDA,¹¹ Jyunya MIKAMI,¹¹ Risa MATSUDA,¹¹ Naoto KOJIGUCHI,¹¹ Miho KAWABATA,¹¹
Megumi TAKENAKA,¹¹ Katsura MATSUMOTO,¹¹ Enrique de MIGUEL,^{12,13} Yutaka MAEDA,¹⁴ Tomohito OHSHIMA,¹
Keisuke ISOGAI,¹ Roger D. PICKARD,^{15,16} Arne HENDEN,¹⁷ Stella KAFKA,¹⁷ Hidehiko AKAZAWA,¹⁸
Noritoshi OTANI,¹⁸ Sakiko ISHIBASHI,¹⁸ Minako OGI,¹⁸ Kenji TANABE,¹⁸ Kazuyoshi IMAMURA,¹⁸ William STEIN,¹⁹
Kiyoshi KASAI,²⁰ Tonny VANMUNSTER,²¹ Peter STARR,²² Arto OKSANEN,²³ Elena P. PAVLENKO,²⁴
Oksana I. ANTONYUK,²⁴ Kirill A. ANTONYUK,²⁴ Aleksei A. SOSNOVSKIY,²⁴ Nikolaj V. PIT,²⁴ Julia V. BABINA,²⁴
Aleksandr SKLYANOV,²⁶ Rudolf NOVÁK,²⁵ Shawn DVORAK,²⁷ Raúl MICHEL,²⁸ Gianluca MASI,²⁹
Colin LITTLEFIELD,³⁰ Joseph ULOWETZ,³¹ Sergey Yu. SHUGAROV,^{32,33} Polina Yu. GOLYSHEVA,³²
Drahomir CHOCHOL,³³ Viktoriia KRUSHEVSKA,³⁴ Javier RUIZ,^{35,36,37} Tamás TORDAI,³⁸ Etienne MORELLE,³⁹
Richard SABO,⁴⁰ Hiroyuki MAEHARA,⁴¹ Michael RICHMOND,⁴² Natalia KATYSHEVA,³² Kenji HIROSAWA,⁴³
William N. GOFF,⁴⁴ Franky DUBOIS,⁴⁵ Ludwig LOGIE,⁴⁶ Steve RAU,⁴⁷ Irina B. VOLOSHINA,³²
Maksim V. ANDREEV,^{48,49} Kazuhiko SHIOKAWA,⁵⁰ Vitaly V. NEUSTROEV,⁵¹ George SJOBERG,^{52,17}
Sergey ZHARIKOV,²⁸ Nick JAMES,⁵³ Greg BOLT,⁵⁴ Tim CRAWFORD,⁵⁵ Denis BUCZYNSKI,⁵⁶ Lewis M. COOK,⁵⁷
Christopher S. KOCHANKE,⁵⁸ Benjamin SHAPPEE,⁵⁸ Krzysztof Z. STANEK,⁵⁸ José L. PRIETO,^{59,60}
Denis DENISENKO,⁶¹ Hideo NISHIMURA,⁶² Masaru MUKAI,⁶³ Shizuo KANEKO,⁶⁴ Seiji UEDA,⁶⁵ Rod STUBBINGS,⁶⁶
Masayuki MORIYAMA,⁶⁷ Patrick SCHMEER,⁶⁸ Eddy MUYLLAERT,⁶⁹ Jeremy SHEARS,^{70,15} Robert J. MODIC,⁷¹
Kevin B. PAXSON,⁷²

¹ Department of Astronomy, Kyoto University, Kyoto 606-8502, Japan

*tkato@kusastro.kyoto-u.ac.jp

² Groupe Européen d'Observations Stellaires (GEOS), 23 Parc de Levesville, 28300 Bailleau l'Evêque, France

³ Bundesdeutsche Arbeitsgemeinschaft für Veränderliche Sterne (BAV), Munsterdamm 90, 12169 Berlin, Germany

⁴ Vereniging Voor Sterrenkunde (VVS), Oude Bleken 12, 2400 Mol, Belgium

⁵ Vihorlat Observatory, Mierova 4, Humenne, Slovakia

⁶ Bronberg Observatory, Center for Backyard Astrophysics Pretoria, PO Box 11426, Tiegerpoort 0056, South Africa

⁷ Kleinkaroo Observatory, Center for Backyard Astrophysics Kleinkaroo, Sint Helena 1B, PO Box 281, Calitzdorp 6660, South Africa

⁸ Furzehill House, Ilston, Swansea, SA2 7LE, UK

⁹ Variable Star Observers League in Japan (VSOLJ), 1001-105 Nishiterakata, Hachioji, Tokyo 192-0153, Japan

¹⁰ VSOLJ, 7-1 Kitahatsutomi, Kamagaya, Chiba 273-0126, Japan

¹¹ Osaka Kyoiku University, 4-698-1 Asahigaoka, Osaka 582-8582, Japan

¹² Departamento de Física Aplicada, Facultad de Ciencias Experimentales, Universidad de Huelva, 21071 Huelva, Spain

¹³ Center for Backyard Astrophysics, Observatorio del CIECEM, Parque Dunar, Matalascañas, 21760 Almonte, Huelva, Spain

¹⁴ Kaminishiyamamachi 12-14, Nagasaki, Nagasaki 850-0006, Japan

¹⁵ The British Astronomical Association, Variable Star Section (BAA VSS), Burlington House, Piccadilly, London, W1J 0DU, UK

¹⁶ 3 The Birches, Shobdon, Leominster, Herefordshire, HR6 9NG, UK

¹⁷ American Association of Variable Star Observers, 49 Bay State Rd., Cambridge, MA 02138, USA

¹⁸ Department of Biosphere-Geosphere System Science, Faculty of Informatics, Okayama University of Science, 1-1 Ridai-cho, Okayama, Okayama 700-0005, Japan

¹⁹ 6025 Calle Paraiso, Las Cruces, New Mexico 88012, USA

²⁰ Baselstrasse 133D, CH-4132 Muttenz, Switzerland

²¹ Center for Backyard Astrophysics Belgium, Walhostraat 1A, B-3401 Landen, Belgium

²² Warrumbungle Observatory, Tenby, 841 Timor Rd, Coonabarabran NSW 2357, Australia

²³ Hankasalmi observatory, Jyväskylä Sirius ry, Vertaalantie 419, FI-40270 Palokka, Finland

²⁴ Crimean Astrophysical Observatory, p/o Naychny, 298409, Republic of Crimea

²⁵ Research Centre for Toxic Compounds in the Environment, Faculty of Science, Masaryk University, Kamenice 3, 625 00 Brno, Czech Republic

²⁶ Kazan Federal University, Kremlevskaya str., 18, Kazan, 420008, Russia

²⁷ Rolling Hills Observatory, 1643 Nightfall Drive, Clermont, Florida 34711, USA

²⁸ Instituto de Astronomía UNAM, Apartado Postal 877, 22800 Ensenada B.C., México

²⁹ The Virtual Telescope Project, Via Madonna del Loco 47, 03023 Ceccano (FR), Italy

- ³⁰ *Department of Physics, University of Notre Dame, Notre Dame, Indiana 46556, USA*
- ³¹ *Center for Backyard Astrophysics Illinois, Northbrook Meadow Observatory, 855 Fair Ln, Northbrook, Illinois 60062, USA*
- ³² *Sternberg Astronomical Institute, Lomonosov Moscow State University, Universitetsky Ave., 13, Moscow 119992, Russia*
- ³³ *Astronomical Institute of the Slovak Academy of Sciences, 05960, Tatranska Lomnica, the Slovak Republic*
- ³⁴ *Main astronomical observatory of the National Academy of Sciences of Ukraine, 27 Akademika Zabolotnoho ave., 03680 Kyiv, Ukraine*
- ³⁵ *Observatorio de Cantabria, Ctra. de Rocamundo s/n, Valderredible, Cantabria, Spain*
- ³⁶ *Instituto de Física de Cantabria (CSIC-UC), Avenida Los Castros s/n, E-39005 Santander, Cantabria, Spain*
- ³⁷ *Agrupación Astronómica Cantabria, Apartado 573, 39080, Santander, Spain*
- ³⁸ *Polaris Observatory, Hungarian Astronomical Association, Laborc utca 2/c, 1037 Budapest, Hungary*
- ³⁹ *9 rue Vasco de GAMA, 59553 Lauwin Planque, France*
- ⁴⁰ *2336 Trailcrest Dr., Bozeman, Montana 59718, USA*
- ⁴¹ *Okayama Astrophysical Observatory, National Astronomical Observatory of Japan, Asakuchi, Okayama 719-0232, Japan*
- ⁴² *Physics Department, Rochester Institute of Technology, Rochester, New York 14623, USA*
- ⁴³ *216-4 Maeda, Inazawa-cho, Inazawa-shi, Aichi 492-8217, Japan*
- ⁴⁴ *13508 Monitor Ln., Sutter Creek, California 95685, USA*
- ⁴⁵ *Astrolab team, Poelkapellestraat 57 Langemark, Belgium*
- ⁴⁶ *Astrolab team, Gezellestraat 9, 8908 Vlamertinge, Belgium*
- ⁴⁷ *Astrolab team, Veldstraat 6, 8400 Oostende, Belgium*
- ⁴⁸ *Institute of Astronomy, Russian Academy of Sciences, 361605 Peak Terskol, Kabardino-Balkaria, Russia*
- ⁴⁹ *International Center for Astronomical, Medical and Ecological Research of NASU, Ukraine 27 Akademika Zabolotnoho Str. 03680 Kyiv, Ukraine*
- ⁵⁰ *Moriyama 810, Komoro, Nagano 384-0085, Japan*
- ⁵¹ *Astronomy and Space Physics, PO Box 3000, FIN-90014 University of Oulu, Finland*
- ⁵² *The George-Elma Observatory, 9 Contentment Crest, #182, Mayhill, New Mexico 88339, USA*
- ⁵³ *11 Tavistock Road, Chelmsford, Essex CM1 6JL, UK*
- ⁵⁴ *Camberwarra Drive, Craigie, Western Australia 6025, Australia*
- ⁵⁵ *Arch Cape Observatory, 79916 W. Beach Road, Arch Cape, Oregon 97102, USA*
- ⁵⁶ *Conder Brow Observatory, Fell Acre, Conder Brow, Little Fell Lane, Scotforth, Lancs LA2 0RQ, England*
- ⁵⁷ *Center for Backyard Astrophysics Concord, 1730 Helix Ct. Concord, California 94518, USA*
- ⁵⁸ *Department of Astronomy, the Ohio State University, Columbia, OH 43210, USA*
- ⁵⁹ *Núcleo de Astronomía de la Facultad de Ingeniería, Universidad Diego Portales, Av. Ejército 441, Santiago, Chile*
- ⁶⁰ *Department of Astrophysical Sciences, Princeton University, NJ 08544, USA*
- ⁶¹ *Space Research Institute (IKI), Russian Academy of Sciences, Moscow, Russia*
- ⁶² *Miyawaki 302-6, Kakegawa, Shizuoka 436-0086, Japan*
- ⁶³ *JCPM Kagoshima Station, Kagoshima City, Kagoshima 892-0871, Japan*
- ⁶⁴ *14-7 Kami-Yashiki, Kakegawa, Shizuoka 436-0049, Japan*
- ⁶⁵ *6-23-9 Syowa-Minami, Kushiro City, Hokkaido 084-0909, Japan*
- ⁶⁶ *Tetoora Observatory, Tetoora Road, Victoria, Australia*
- ⁶⁷ *290-383, Ogata-cho, Sasebo, Nagasaki 858-0926, Japan*
- ⁶⁸ *Bischmisheim, Am Probstbaum 10, 66132 Saarbrücken, Germany*
- ⁶⁹ *Vereniging Voor Sterrenkunde (VVS), Moffelstraat 13 3370 Boutersem, Belgium*
- ⁷⁰ *"Pemberton", School Lane, Bunbury, Tarporley, Cheshire, CW6 9NR, UK*
- ⁷¹ *351 Fairlawn Dr., Richmond Heights, Ohio 44143, USA*
- ⁷² *20219 Eden Pines, Spring, Texas 77379, USA*

(Received 201 0; accepted 201 0)

Abstract

Continuing the project described by Kato et al. (2009), we collected times of superhump maxima for 102 SU UMa-type dwarf novae observed mainly during the 2014–2015 season and characterized these objects. Our project has greatly improved the statistics of the distribution of orbital periods, which is a good approximation of the distribution of cataclysmic variables at the terminal evolutionary stage, and confirmed the presence of a period minimum at a period of 0.053 d and a period spike just above this period. The number density monotonically decreased toward the longer period and there was no strong indication of a period gap. We detected possible negative superhumps in Z Cha. It is possible that normal outbursts are also suppressed by the presence of a disk tilt in this system. There was no indication of enhanced orbital humps just preceding the superoutburst, and this result favors the thermal-tidal disk instability as the origin of superoutbursts. We detected superhumps in three AM CVn-type dwarf novae. Our observations and

recent other detections suggest that 8% of objects showing dwarf nova-type outbursts are AM CVn-type objects. AM CVn-type objects and EI Psc-type object may be more abundant than previously recognized. OT J213806, a WZ Sge-type object, exhibited a remarkably different feature between the 2010 and 2014 superoutbursts. Although the 2014 superoutburst was much fainter the plateau phase was shorter than the 2010 one, the course of the rebrightening phase was similar. This object indicates that the $O-C$ diagrams of superhumps can be indeed variable at least in WZ Sge-type objects. Four deeply eclipsing SU UMa-type dwarf novae (ASASSN-13cx, ASASSN-14ag, ASASSN-15bu, NSV 4618) were identified. We studied long-term trends in supercycles in MM Hya and CY UMa and found systematic variations of supercycles of $\sim 20\%$.

Key words: accretion, accretion disks — stars: novae, cataclysmic variables — stars: dwarf novae

1. Introduction

Cataclysmic variables (CVs) are close binary systems transferring matter from a low-mass dwarf secondary to a white dwarf. The transferred matter forms an accretion disk. Thermal instability of the disk caused by partial ionization of hydrogen results outbursts in dwarf novae (DNe), a subclass of CVs. Tidal instability of the disk caused by the 3:1 resonance with the orbiting secondary is considered to develop an eccentric (or flexing) disk in SU UMa-type dwarf novae, a subclass of DNe. This eccentric disk is responsible for superhumps, which have periods a few percent longer than the orbital period [see e.g. Whitehurst (1988); Hirose, Osaki (1990); Lubow (1991)]. The enhanced mass accretion by tidal instability causes long-lasting superoutbursts [thermal tidal instability (TTI) model: Osaki (1989); Osaki (1996)]. Although there had been intensive discussions whether superoutbursts are a result of tidal instability or an enhanced mass-transfer from the secondary [e.g. Smak (1991), Smak (2004), Smak (2008)], recent detailed analyses of high-precision Kepler observations have favored the TTI model as the only viable model for ordinary SU UMa-type dwarf novae (Osaki, Kato 2013a; Osaki, Kato 2013b; Osaki, Kato 2014). [For general information of CVs, DNe, SU UMa-type dwarf novae and superhumps, see e.g. Warner (1995)].

This paper is one of series of papers Kato et al. (2009), Kato et al. (2010), Kato et al. (2012a), Kato et al. (2013a), Kato et al. (2014b) and Kato et al. (2014a). These papers originally intended to clarify the period variations of superhumps in SU UMa-type dwarf novae and first succeeded in identifying superhump stages (stages A, B and C) in Kato et al. (2009). Among them, stage A superhumps have recently been identified to be reflect the precession of the eccentric disk at the radius of the 3:1 resonance, and have been one of the most promising tools in determining the mass-ratios in SU UMa-type dwarf novae and in following the terminal evolution of CVs (Kato, Osaki 2013b).

Continuing this project, we report observations of superhumps and associated phenomena in SU UMa-type dwarf novae whose superoutbursts were observed in 2014–2015. In this paper, we report basic observational materials and discussions in relation to individual objects. General discussion related to WZ Sge-type dwarf novae, which are a subclass of SU UMa-type dwarf novae with

infrequent, large amplitude superoutbursts, will be given as in a planned summary paper by Kato (2015).

Starting from Kato et al. (2014a), we have been intending these series of papers to be also a source of compiled information, including historical, of individual dwarf novae since there have been no compiled publication since Glasby (1970).

The material and methods of analysis are given in section 2, observations and analysis of individual objects are given in section 3, including some discussions particular to the objects, the general discussion is given in section 4 and the summary is given in section 5.

2. Observation and Analysis

2.1. General Procedure

The data were obtained under campaigns led by the VSNET Collaboration (Kato et al. 2004c). For some objects, we used the public data from the AAVSO International Database¹.

The majority of the data were acquired by time-resolved CCD photometry by using 30cm-class telescopes located world-wide, whose observational details will be presented in future papers dealing with analysis and discussion on individual objects of interest. The list of outbursts and observers is summarized in table 1. The data analysis was performed just in the same way described in Kato et al. (2009) and Kato et al. (2014a) and we mainly used R software² for data analysis. In de-trending the data, we used both lower (1–5th order) polynomial fitting and locally-weighted polynomial regression (LOWESS: Cleveland 1979). The times of superhumps maxima were determined by the template fitting method as described in Kato et al. (2009). The times of all observations are expressed in barycentric Julian Days (BJD).

The abbreviations used in this paper are the same as in Kato et al. (2014a): P_{orb} means the orbital period and $\varepsilon \equiv P_{\text{SH}}/P_{\text{orb}} - 1$ for the fractional superhump excess. Following Osaki, Kato (2013a), the alternative fractional superhump excess in the frequency unit $\varepsilon^* \equiv 1 - P_{\text{orb}}/P_{\text{SH}} - 1 = \varepsilon/(1 + \varepsilon)$ has been introduced because this fractional superhump excess can be directly compared to the precession rate. We therefore used ε^* in referring the precession rate.

¹ <<http://www.aavso.org/data-download>>.

² The R Foundation for Statistical Computing:
<<http://cran.r-project.org/>>.

We used phase dispersion minimization (PDM; Stellingwerf 1978) for period analysis and 1σ errors for the PDM analysis was estimated by the methods of Fernie (1989) and Kato et al. (2010). We present evidence for an SU UMa-type dwarf nova by presenting period analysis and averaged superhump profile if the paper provides the first solid presentation of individual objects as such.

The resultant P_{SH} , P_{dot} and other parameters are listed in table 2 in same format as in Kato et al. (2009). The definitions of parameters P_1, P_2, E_1, E_2 and P_{dot} are the same as in Kato et al. (2009).³ Comparisons of $O-C$ diagrams between different superoutbursts are also presented whenever available, since this comparison was one of the main motivations in of these series papers (cf. Uemura et al. 2005). Combined $O-C$ diagrams also help identifying superhump stages particularly when observations are insufficient. In drawing combined $O-C$ diagrams, we usually used $E=0$ for the start of the superoutburst, which usually refers to the first positive detection of the outburst. This epoch usually has an accuracy of ~ 1 d for well-observed objects, and if the outburst was not sufficiently observed, we mentioned in the figure caption how to estimate E in such an outburst. We also present $O-C$ diagrams and light curves especially for WZ Sge-type dwarf novae, which are not expected to undergo outbursts in the near future. In all figures, the binned magnitudes and $O-C$ values are accompanied by 1σ error bars, which are omitted when the error is smaller than the plot mark.

We used the same terminology of superhumps summarized in Kato et al. (2012a). We especially call attention to the term “late superhumps”. Although this term has been used to refer to various phenomena, we only used the concept of “traditional” late superhumps when an ~ 0.5 phase shift is detected [Vogt (1983); see also table 1 in Kato et al. (2012a) for various types of superhumps], since we suspect that many of the past claims of detections of “late superhumps” were likely stage C superhumps [cf. Kato et al. (2009); note that the Kepler observation of V585 Lyr also demonstrated this persistent stage C superhumps without a phase shift (Kato, Osaki 2013a), and most recently it is confirmed in another Kepler CV by Brown et al. (2015)].

Early superhumps are double-wave humps seen during the early stages of WZ Sge-type dwarf novae, and have period close to the orbital periods (Kato et al. 1996; Kato 2002; Osaki, Meyer 2002). We are going to discuss this phenomenon in the planned paper (Kato 2015). We used the period of early superhumps as approximate orbital period (Kato et al. 2014a).

As in Kato et al. (2009), we have used coordinate-based optical transient (OT) designations for some objects, such as apparent dwarf nova candidates reported in the Transient Objects Confirmation Page of the Central Bureau for Astronomical Telegrams⁴ and listed the original identifiers in table 1. For objects detected in the

Catalina Real-time Transient Survey (CRTS; Drake et al. 2009)⁵ transients, we preferably used the names provided in Drake et al. (2014). If these names are not yet available, we used the International Astronomical Union (IAU)-format names provided by the CRTS team in the public data release⁶

Since ASAS-SN detectors have relatively poor angular resolutions (7.5 arcsec/pixel), we provided coordinates from our own astrometry and astrometric catalogs for ASAS-SN CVs. We used SDSS, the Initial Gaia Source List (IGSL, Smart 2013) and Guide Star Catalog 2.3.2. The coordinates used in this paper are J2000.0.

2.2. Period Selection

Questions have been raised to our surveys how to select the periods among the aliases and what is the uncertainty. Such question are natural if one only sees PDM diagrams. We should note that PDM (and most of other period finding algorithms) assumes “uncorrelated” (in time) observations and defines the statistics. The actual data have more information, such as the superhump timing data. Even if the PDM result shows strong aliases, we can resolve the alias problem if we have sufficiently long continuous observations (continuous data produce no aliases). Our period selection is mostly based on this principle, when alias selection is inconclusive by the PDM analysis only. The second approach is to examine the trends of $O-C$ values against the trial periods. A period longer than the actual one produces systematically decreasing $O-C$ values within each night, and our measurements of the superhump maxima have typical errors of 0.001 d, which is usually sufficient to select one-day aliases when multiple superhumps were detected each night. If the case is not, we describe the uncertainty of the selection.

We show an example how our method works by using the data of FI Cet (subsection 3.6). A PDM analysis over a wider range of periods (figure 1) gives an impression that there are many period candidates and a period of 0.057 d and 0.060 d are equally acceptable. If we rely on statistics assuming temporarily “uncorrelated” observations, this would give equal significance to these periods. An example for FI Cet is shown in figure 2. Scatter in the $O-C$ values and systematic trends within each night are apparent for trial period 0.06033 d, which is rejected. Although we do not show similar figures for other objects due to the limitation of space, we made similar analysis for objects when ambiguities in period selection remained.

Readers may be interested in the result of least absolute shrinkage and selection operator (Lasso) (Tibshirani 1996; Kato, Uemura 2012) analysis, which has been proven to be very effective in detecting rapidly varying periods in unevenly sampled data (e.g. Kato, Maehara 2013; Osaki, Kato 2013b; Kato, Osaki 2013a; Ohshima et al. 2014). The result is shown in figure 3, and the impression is so different from the PDM result (figure 1). However, we

³ The intervals (E_1 and E_2) for the stages B and C given in the table sometimes overlap because of occasional observational ambiguity in determining the stages.

⁴ <<http://www.cbat.eps.harvard.edu/unconf/tocp.html>>.

⁵ <<http://nessi.cacr.caltech.edu/catalina/>>. For the information of the individual Catalina CVs, see <<http://nessi.cacr.caltech.edu/catalina/AllCV.html>>.

⁶ <<http://nessi.cacr.caltech.edu/DataRelease/>>.

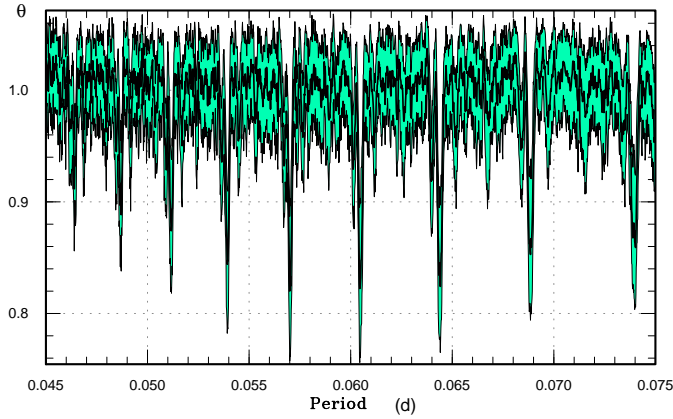


Fig. 1. PDM analysis of FI Cet (see subsection 3.6) in a wider period range.

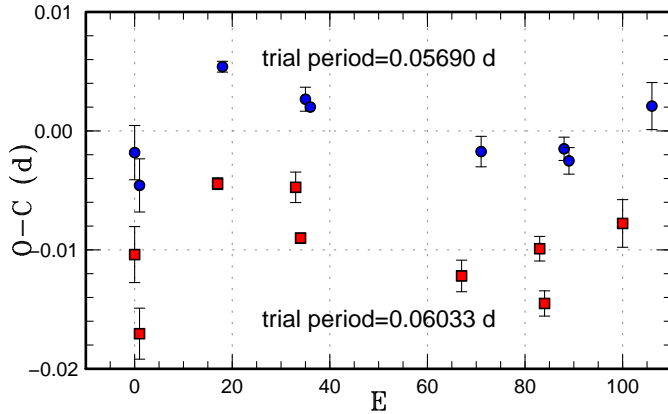


Fig. 2. $O - C$ diagrams assuming two trial periods (two aliases in figure 1). Scatter in the $O - C$ values and systematic trends within each night are apparent for trial period 0.06033 d, which is rejected.

didn't widely used this method in selecting the aliases since our model used in Lasso analysis also assumed temporarily uncorrelated observations, and the suppression of the aliases is simply a result of highly non-linear characteristics of compressed sensing. This figure (if compared to classical figures) would give misleading impression that there is no possibility for aliases and we have not used this type of figure in this paper.

3. Individual Objects

3.1. *KX Aquilae*

For the history of KX Aql, see Kato et al. (2010) and Kato et al. (2014b). The 2014 outburst was detected by C. Chiselbrook at a visual magnitude of 12.8 on December 15 (cf. BAAVSS alert 3897). The outburst was confirmed to be a superoutburst by the presence of a superhump and long outburst duration (vsnet-alert 18083,

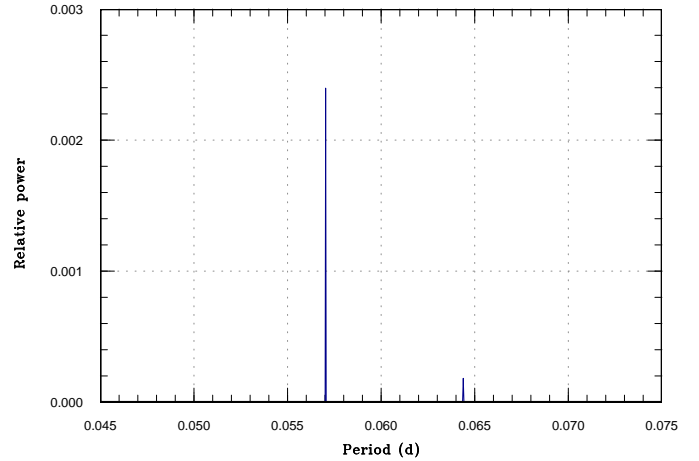


Fig. 3. Lasso period analysis of FI Cet. The period of 0.057 d is strongly selected.

18090).⁷ Only one superhump maximum was obtained: BJD 2457011.2633(15) ($N=38$).

3.2. *NN Camelopardalis*

NN Cam = NSV 1485 was recognized as a dwarf nova by Khruslov (2005). The object was given a GCVS designation in Kazarovets et al. (2008).⁸ The first superoutburst was detected in 2007 (Kato et al. 2009). The orbital period was reported to be 0.0717 d (vsnet-alert 9557).

The 2014 superoutburst was detected by M. Moriyama on February 19 (vsnet-alert 16934). The times of superhump maxima are listed in table 3. The observation covered the later stage of the superoutburst. A comparison of the $O - C$ diagrams (figure 4) suggests that we mainly observed stage C superhumps.

A list of recent outbursts is given in table 4. A linear regression to the epochs of superoutbursts yielded a mean supercycle of 386(6) d. The value of supercycle may be halved since this object is not well observed around solar conjunctions.

3.3. *V342 Camelopardalis*

For the history of this object (=1RXS J042332+745300 =HS 0417+7445), see Kato et al. (2014a). The 2014 superoutburst was detected on December 28 by E. Muylart (vsnet-alert 18128). Time-series observations started on 2015 January 3 and detected superhumps (vsnet-alert 18149, 18157, 18171). The times of superhump maxima are listed in table 5. Since the observation covered the final part of the superoutburst, we likely observed only stage C superhumps, which is also supported by a comparison of the $O - C$ diagrams (figure 5).

⁷ VSNET alert message can be accessed at <<http://ooruri.kusastro.kyoto-u.ac.jp/pipermail/vsnet-alert/>>.

⁸ The object is unofficially called "Samus's star", since the name can be read N. N. Samus, the editor in chief of the GCVS, in Russian spelling. <<http://www.kadar.ru/forum/index.php/topic,1040.15.html>>.

Table 1. List of Superoutbursts.

Subsection	Object	Year	Observers or references*	ID [†]
3.1	KX Aql	2014	RPc	
3.2	NN Cam	2014	DPV	
3.3	V342 Cam	2014	OKU, Kis, Ioh	
3.5	OY Car	2014	SPE	
		2015	SPE	
3.6	FI Cet	2014	HaC	
3.7	Z Cha	2014	HaC	
3.8	YZ Cnc	2014b	AAVSO	
3.9	V337 Cyg	2014	IMi	
3.10	V503 Cyg	2014	Kis, DPV	
		2014b	RPc	
3.11	BC Dor	2015	HaC, COO	
3.12	V660 Her	2014	Ioh	
3.13	CT Hya	2015	SPE, Kis	
3.14	LY Hya	2014	HaC	
3.15	MM Hya	2014	Mdy, Ioh	
3.16	RZ LMi	2014	Mic	
3.18	AY Lyr	2014	OUS, Aka	
3.19	V453 Nor	2014	HaC	
3.20	DT Oct	2014	HaC	
3.21	UV Per	2014	Ioh, DPV, IMi, Mdy, Kis, Nov, RPc	
3.22	HY Psc	2014	OKU, Ioh, IMi, Kis	

*Key to observers: Aka (H. Akazawa, OUS), Buc (D. Buczynski), COO (L. Cook), CRI (Crimean Astrophys. Obs.), CTX[†] (T. Crawford), deM (E. de Miguel), DKS[‡] (S. Dvorak), DPV (P. Dubovsky), Dub (F. Dubois team), GBo (G. Bolt), GFB[‡] (W. Goff), HaC (F.-J. Hambsch, remote obs. in Chile), Ham (F.-J. Hambsch), Han (Hankasalmi Obs., by A. Oksanen), Hsk (K. Hirose), IMi[‡] (I. Miller), Ioh (H. Itoh), Kai (K. Kasai), Kis (S. Kiyota), KU (Kyoto U., campus obs.), LCO (C. Littlefield), MEV[‡] (E. Morelle), MLF (B. Monard), Mas (G. Masi), Mdy (Y. Maeda), Mhh (H. Maehara), Mic (R. Michel-Murillo team), NDJ (N. James), Neu (V. Neustroev team), NKa (N. Katysheva and S. Shugarov), Nov (R. Novák), OKU (Osaya Kyoiku U.), OUS (Okayama U. of Science), OkC[‡] (A. Oksanen, remote obs. in Chile), RIT (M. Richmond), RPc[‡] (R. Pickard), Rui (J. Ruiz), SPE[‡] (P. Starr), SRI[‡] (R. Sabo), SWI[‡] (W. Stein), Shu (S. Shugarov team), Siz (K. Shiokawa), Ter (Terskol Obs.), Trt (T. Tordai), UJH[‡] (J. Ulowetz), Van (T. Vanmunster), Vol (I. Voloshina), AAVSO (AAVSO database)

[†]Original identifications, discoverers or data source.

[‡]Inclusive of observations from the AAVSO database.

Table 3. Superhump maxima of NN Cam (2014)

E	max*	error	$O - C^{\dagger}$	N^{\ddagger}
0	56713.2745	0.0005	-0.0017	76
1	56713.3519	0.0005	0.0018	75
2	56713.4233	0.0005	-0.0006	76
3	56713.4984	0.0034	0.0005	9
68	56718.3037	0.0005	0.0013	47
69	56718.3740	0.0004	-0.0023	72
70	56718.4512	0.0005	0.0010	58

*BJD-2400000.

[†]Against max = 2456713.2761 + 0.073916 E .

[‡]Number of points used to determine the maximum.

Table 5. Superhump maxima of V342 Cam (2014)

E	max*	error	$O - C^{\dagger}$	N^{\ddagger}
0	57026.0470	0.0003	0.0012	121
1	57026.1237	0.0003	-0.0001	168
14	57027.1454	0.0016	0.0067	85
15	57027.2134	0.0003	-0.0032	162
40	57029.1706	0.0029	0.0023	30
52	57030.0992	0.0033	-0.0058	162
53	57030.1831	0.0009	0.0000	162
54	57030.2536	0.0027	-0.0075	137
89	57032.9963	0.0183	0.0030	68
90	57033.0748	0.0021	0.0034	112

*BJD-2400000.

[†]Against max = 2457026.0457 + 0.078063 E .

[‡]Number of points used to determine the maximum.

Table 1. List of Superoutbursts (continued).

Subsection	Object	Year	Observers or references*	ID [†]
–	CC Scl	2014	Kato et al. (2015)	
3.23	QW Ser	2014	DPV	
3.24	V418 Ser	2014	CRI, AAVSO, LCO, SWI, KU, GFB, Mdy, deM, UJH, Ioh, SRI, DPV	
3.25	V701 Tau	2015	RPc, Kai, Trt	
3.26	SU UMa	2014	Kis, Nov, Dub, AAVSO	
3.27	CY UMa	2014	Nov, Aka, Kis, DPV, Mdy, Ham, Han	
3.29	NSV 1436	2014	IMi, DPV, Aka, NKa, KU, Hsk	
3.30	NSV 4618	2015	Ioh, HaC, SWI, Ter	
3.31	1RXS J185310	2014	IMi, LCO, Mdy, Ioh	1RXS J185310.0+594509
3.32	1RXS J231935	2014	Kai, OKU, CRI, Mdy, IMi, DPV	1RXS J231935.0+364705
3.33	2QZ J130441	2014	HaC, Mdy	2QZ J130441.7+010330
3.34	ASASSN-13cx	2014	deM, IMi, Han, OkC, Rui, RPc, SWI, Mdy, Ham	
3.35	ASASSN-14ag	2014	Mas, Kai, HaC, deM, Kis	
3.36	ASASSN-14aj	2014	HaC	
3.37	ASASSN-14au	2014	deM	
3.38	ASASSN-14aw	2014	deM	
3.39	ASASSN-14bh	2014	MLF	
3.40	ASASSN-14cl	2014	OkC, CRI, SWI, AAVSO, IMi, HaC, OKU, DPV, RIT, LCO, NDJ, Kai, DKS, SPE, CTX, UJH, deM	
3.41	ASASSN-14cq	2014	MLF, HaC	
—	ASASSN-14cv	2014	C. Nakata et al. in preparation	
3.42	ASASSN-14dm	2014	MLF	
3.43	ASASSN-14do	2014	MLF, HaC	
3.44	ASASSN-14dw	2014	HaC	
3.45	ASASSN-14eh	2014	HaC, Ioh	
3.46	ASASSN-14eq	2014	MLF	
3.47	ASASSN-14fr	2014	MLF	
3.48	ASASSN-14gd	2014	MLF	
3.49	ASASSN-14gq	2014	MLF	
3.50	ASASSN-14gx	2014	MLF, AAVSO, HaC, OKU	
3.51	ASASSN-14hk	2014	Ioh, OKU	
3.52	ASASSN-14hl	2014	MLF	
3.53	ASASSN-14hs	2014	MLF, HaC, Ioh	

3.4. *SY Capricorni*

SY Cap was originally discovered as a long-period variable star with a photographic range of 12.6 to fainter than 14.5 (=56.1927, Beljawsky 1927). The variable was independently discovered at a photographic magnitude of 11 on 1915 September 9 by Ross (1928) (Ross 328). Kholopov et al. (1985) listed this star as a possible Mira-type variable. Noting that there is no bright 2MASS counterpart, T. Kato identified this object as a dwarf nova (likely SU UMa-type one) using ASAS-3 (Pojmański 2002) observations (vsnet-alert 10025). D. Denisenko confirmed this identification (vsnet-alert 10027).

Soon after this re-classification, an outburst was detected by ASAS-3 on 2008 August 18 (vsnet-outburst 9336). The outburst turned out to be a superoutburst by the detection of superhumps (Kato et al. 2009). Thorstensen, Skinner (2012) made spectroscopic confir-

mation as a CV.⁹ Another superoutburst was observed in 2011 August–September (Kato et al. 2013a).

The 2014 superoutburst was detected by R. Stubbings at a visual magnitude of 12.8 on September 18 (vsnet-alert 17747). Subsequent observations detected superhumps (vsnet-alert 17750, 17764, 17769). The times of superhump maxima are listed in table 6. We most likely observed stage C superhump between $E=24$ and $E=89$ and the value in table 2 is based on this identification (figure 6). The maxima for $E \geq 119$ were post-superoutburst superhumps.

Recent outbursts of SY Cap are listed in table 7. The typical cycle length of normal outbursts is estimated to be ~ 30 d. The three shortest intervals between superoutbursts were 187, 220 and 235 d. The intervals between

⁹ Although the object is given CRTS designation in Thorstensen, Skinner (2012), we should note that the object was already recognized as a known dwarf nova at the time of CRTS detection.

Table 1. List of Superoutbursts (continued).

Subsection	Object	Year	Observers or references*	ID [†]
3.54	ASASSN-14ia	2014	OKU	
3.55	ASASSN-14id	2014	IMi, OKU, KU	
3.56	ASASSN-14it	2014	KU	
3.57	ASASSN-14iv	2014	Mdy, HaC	
3.58	ASASSN-14je	2014	MLF	
3.59	ASASSN-14jf	2014	HaC	
3.60	ASASSN-14jq	2014	LCO, DPV, KU, Kis, IMi, deM, Kai, Ioh	
3.61	ASASSN-14jv	2014	SWI, OUS, Van, DPV, AAVSO, CRI, OKU, Dub, Mdy, Buc, Aka, deM, Kis, DKS	
3.62	ASASSN-14kf	2014	MLF	
3.63	ASASSN-14kk	2014	MLF	
3.64	ASASSN-14ku	2014	MLF, HaC	
3.65	ASASSN-14lk	2014	MLF	
3.66	ASASSN-14mc	2014	MLF, HaC	
3.67	ASASSN-14md	2014	MLF, HaC	
3.68	ASASSN-14mh	2014	HaC, Ioh	
3.69	ASASSN-14mj	2014	Kis, Shu, Ioh, IMi, DPV	
3.70	ASASSN-15ah	2015	MLF, HaC, Ioh	
3.71	ASASSN-15ap	2015	MLF	
3.72	ASASSN-15aq	2015	MLF, HaC	
3.73	ASASSN-15aw	2015	Van	
3.74	ASASSN-15bg	2015	MLF, HaC	
3.75	ASASSN-15bp	2015	Kis, deM, SPE, DKS, Ioh, OKU, HaC, AAVSO, DPV, UJH, OUS, SWI, IMi, Van, Neu, Trt, CRI, Aka	
3.76	ASASSN-15bu	2015	deM, SWI, SRI, DPV, UJH	
3.77	ASASSN-15bv	2015	MLF	
3.78	ASASSN-15dq	2015	Van, HaC, Kai	
3.79	CRTS J081936	2013	Han	CRTS J081936.1+191540
3.80	CRTS J172038	2014	Mic	CRTS J172038.7+183802
3.82	CRTS J202731	2014	HaC, OKU	CRTS J202731.2–224002
3.83	CRTS J214738	2014	Kai, KU, Kis, DPV	CRTS J214738.4+244554
3.81	CSS J174033	2014	AAVSO, GFB, DPV, SRI, Mas, IMi, Nov, RPc, Ioh, RIT	CSS J174033.5+414756

superoutburst clustered around 317–353 d (six occasions). The cycle lengths of superoutbursts (supercycles) may be either bimodally distributed (187–235 d and 317–353 d) or the recorded longer supercycles represent two supercycles. If the latter is the case, the supercycle may be around 180 d.

3.5. *OY Carinae*

OY Car was discovered as a dwarf nova by Hoffmeister (1963). The object has been monitored by amateur astronomers (notably the Variable Star Section of the Royal Astronomical Society of New Zealand, VSS RASNZ) since 1963 and many outbursts were recorded. Warner (1976) listed the object as an SU UMa-type dwarf nova with a supercycle (called as super-period then) of ~ 300 d based on observations by the VSS RASNZ. The object received special attention after the discovery of the eclipsing na-

ture (Vogt 1979; Vogt et al. 1981). The object has been intensively studied since then (e.g. Ritter 1980; Bailey, Ward 1981; Sherrington et al. 1982; Schoembs, Hartmann 1983; Vogt 1983). Superhumps were first detected during the 1980 outburst (Krzeminski, Vogt 1985). Despite that the object is one of the best known SU UMa-type dwarf novae, no systematic study of superhumps has been reported. Since Kato et al. (2009), it has been established that objects with short superhumps periods almost always show positive P_{dot} . Although Kato et al. (2009) suggested a positive P_{dot} for the 1980 data by Krzeminski, Vogt (1985), a historical analysis by Patterson et al. (1993) suggested a negative P_{dot} . New observations of OY Car have therefore been desired.

A Markov-Chain Monte Carlo (MCMC) analysis (Kato et al. 2013a) of the eclipse observations of in the AAVSO database (2009–2015) yielded the following or-

Table 1. List of Superoutbursts (continued).

Subsection	Object	Year	Observers or references*	ID†
3.84	MASTER J031600	2014	Van	MASTER OT J031600.08+175824.4
3.85	MASTER J043915	2014	OKU	MASTER OT J043915.60+424232.3
3.86	MASTER J055845	2014	IMi	MASTER OT J055845.55+391533.4
3.87	MASTER J085854	2015	SPE, Kis, GBo, MLF	MASTER OT J085854.16−274030.7
3.88	MASTER J105545	2014	DPV, IMi	MASTER OT J105545.20+573109.7
3.89	OT J030929	2014	DPV, OKU, Mdy, deM, Kis, Ioh, Mas, Mic, Siz, Kai, MEV, Van, SPE	PNV J03093063+2638031
—	OT J060009	2014	C. Nakata et al. in preparation	PNV J06000985+1426152
3.90	OT J064833	2014	OKU, HaC, Mdy, DPV, IMi, Ioh, Van, Kis, Kai, Aka, NKa	PNV J06483343+0656236
3.91	OT J213806	2014	OKU, DPV, Trt, Aka, Vol, RPc, DKS, HaC, Kis, AAVSO, MEV, Han, Hsk	OT J213806.6+261957
3.92	OT J230523	2014	OKU, Kis, Mas	PNV J23052314−0225455
—	PNV J171442	2014	C. Nakata et al. in preparation	PNV J17144255−2943481
3.93	PNV J172929	2014	Kis, OKU, Mdy, HaC, Shu, Ioh, DPV, Mhh, deM, Aka, Rui	PNV J17292916+0054043
3.94	PTF1 J071912	2014	IMi, DPV	PTF1 J071912.13+485834.0
3.95	SDSS J033449	2014	Mdy	SDSS J033449.86−071047.8
3.96	SDSS J081408	2014	Mic, IMi, Rui, RPc	SDSS J081408.42+090759.1
3.97	SDSS J090221	2014	SWI, deM, DPV, AAVSO, IMi, KU, CRI, OKU, LCO, Han, Ioh, Mas, RPc, DKS, Kis, UJH, Mdy, Mic, Shu, Nov (Kato et al. 2014c)	SDSS J090221.35+381941.9
3.98	SDSS J120231	2014	MEV, deM, IMi	SDSS J120231.01+450349.1
3.99	SDSS J140037	2015	IMi, SWI, DPV, RPc	SDSS J140037.99+572341.3
3.100	SDSS J172325	2014	OKU, CRI, RPc, IMi, DPV	SDSS J172325.99+330414.1 =ASASSN-14gz
3.101	SDSS J173047	2014	deM, SWI, DKS, Nov, RPc, Mhh, DPV, Ham	SDSS J173047.59+554518.5
3.102	TCP J160548	2014	DPV, OKU, Van, AAVSO	TCP J16054809+2405338

bital ephemeris:

$$\text{Min(BJD)} = 2456502.09846(1) + 0.0631209050(6)E. (1)$$

The epoch of this ephemeris corresponds to the mean epoch of the observations. The decrease from the period in Greenhill et al. (2006) has been confirmed. The rate of secular decrease was about a half (-0.7×10^{-13}) of that reported in Greenhill et al. (2006). This value agrees with the one reported by Han et al. (2015) within a factor of two. The value corresponds to the time-scale of $P_{\text{orb}}/\dot{P}_{\text{orb}}$ of $\sim 2 \times 10^9$ yr. This timescale is similar to what is expected for angular momentum loss only by the gravitational wave radiation [1.1×10^9 yr, from equations 9.5b and 9.20 in Warner (1995) assuming conservative mass-transfer; the binary parameters are from RKcat 7.21 (Ritter, Kolb 2003)] One should be careful in interpreting secular period variations in CVs, however, since the same method is known to give much different timescales of variation, the well-known case being Z Cha (Cook, Warner 1981). We used this modern ephemeris in analyzing the data.

We observed two superoutbursts in 2014 and 2015. Although the initiation of the 2014 superoutburst was not recorded, the time-resolved observations started within two days of the start of the superoutburst. This superoutburst was followed by a post-superoutburst rebrightening. The 2015 superoutburst started with a precursor outburst (vsnet-alert 18313, 18325) and the early stage of the superoutburst was observed. This superoutburst was also followed by a post-superoutburst rebrightening (vsnet-alert 18408). The times of superhump maxima are listed in tables 8 and 9, respectively. Although the 2015 observations recorded stage A superhumps, the times of superhump maxima in this stage were not well determined because they happened to be close to eclipses. The cycle count between $E=18$ and $E=137$ for the 2015 data is uncertain. Note that the superhump period for the 2014 superoutburst listed in table 2 only refers to the initial part of stage B and it is expected to be significantly shorter than the mean period of stage B superhumps.

As shown in the comparison of $O-C$ diagrams (figure 7), the present observations were limited in coverage than

Table 2. Superhump Periods and Period Derivatives

Object	Year	P_1 (d)*	err	E_1^\dagger		P_{dot}^\ddagger	err ‡	P_2 (d)*	err	E_2^\dagger		P_{orb} (d) §	Q $^\parallel$
NN Cam	2014	—	—	—	—	—	—	0.073916	0.000019	0	70	0.0717	C
V342 Cam	2014	—	—	—	—	—	—	0.078063	0.000047	0	90	0.07531	C
SY Cap	2014	—	—	—	—	—	—	0.063414	0.000029	24	89	—	C
OY Car	2014	0.064595	0.000042	0	140	6.9	5.5	—	—	—	—	0.063121	CM
OY Car	2015	0.064464	0.000063	137	153	—	—	—	—	—	—	0.063121	C
FI Cet	2014	0.056911	0.000028	18	106	9.7	2.1	—	—	—	—	0.05594	BE
Z Cha	2014	0.077360	0.000082	25	65	—	—	0.076948	0.000023	64	143	0.074499	B
YZ Cnc	2014b	0.090707	0.000127	0	21	—	—	—	—	—	—	0.0868	C
V337 Cyg	2014	0.070190	0.000034	0	14	—	—	—	—	—	—	—	C
V503 Cyg	2014	0.081215	0.000209	0	17	—	—	—	—	—	—	0.077759	C
BC Dor	2003	0.068048	0.000036	44	145	—	—	—	—	—	—	—	C
BC Dor	2015	0.068026	0.000024	53	141	—	—	—	—	—	—	—	C
LY Hya	2014	—	—	—	—	—	—	0.076973	0.000025	—	—	0.0748	C
MM Hya	2014	0.058851	0.000030	0	119	−1.0	4.6	—	—	—	—	0.057590	CG
BR Lup	2014	0.082241	0.000037	23	97	1.1	4.5	0.081816	0.000090	96	145	0.07948	B
V453 Nor	2014	0.064977	0.000045	16	94	16.4	3.5	0.064590	0.000017	108	232	0.063381	B
DT Oct	2014b	0.074667	0.000043	0	67	−7.1	5.5	—	—	—	—	0.072707	CG
UV Per	2014	0.066750	0.000039	46	112	6.1	5.3	0.066124	0.000054	135	198	0.06489	C
HY Psc	2014	0.079942	0.000021	0	74	—	—	—	—	—	—	0.0767	C

* P_1 and P_2 are mean periods of stage B and C superhumps, respectively.

† Interval used for calculating the period (corresponding to E in the individual tables in section 3).

$^\ddagger P_{\dot{\text{dot}}} = \dot{P}/P$ for stage B superhumps, unit 10^{-5} .

§ References: NN Cam (Denisenko, D. 2007, vsnet-alert 9557), V342 Cam (Shears et al. 2011b), Z Cha (Dai et al. 2009), YZ Cnc (Shafter, Hessman 1988), V503 Cyg (Kato et al. 2014b), LY Hya (Still et al. 1994), MM Hya (Patterson et al. 2003), BR Lup (this work based in Mennickent, Sterken 1998, see text), V453 Nor (Imada, Monard 2006), DT Oct (Kato et al. 2014a), UV Per (Thorstensen, Taylor 1997), HY Psc Dillon et al. cited in Gänsicke et al. (2009), CC Scl (Kato et al. 2015), SU UMa (Thorstensen et al. 1986), CY UMa (Thorstensen et al. 1996), QZ Vir (Shafter, Szkody 1984), CRTS J214738 (Kato et al. 2013a), CSS J174033 (T. Ohshima et al. in preparation), OT J213806 (Kato et al. 2010), ASASSN-14cv, PNV J171442 (C. Nakata et al. in preparation), PTF1 J071912 (Levitan et al. 2011), SDSS J090221 (Rau et al. 2010), FI Cet, ASASSN-13cx, ASASSN-14ag, ASASSN-14cl, ASASSN-14cq, ASASSN-14gx, ASASSN-14id, ASASSN-14jf, ASASSN-14jv, ASASSN-15bp, OT J030929, OT J230523, PNV J172929 (this work)

$^\parallel$ Data quality and comments. A: excellent, B: partial coverage or slightly low quality, C: insufficient coverage or observations with large scatter, G: $P_{\dot{\text{dot}}}$ denotes global $P_{\dot{\text{dot}}}$, M: observational gap in middle stage, 2: late-stage coverage, the listed period may refer to P_2 , E: P_{orb} refers to the period of early superhumps, P: P_{orb} refers to a shorter stable periodicity recorded in outburst.

the 1980 one and the result was not conclusive. We hope we have a better luck next time to record the full evolution of superhumps.

3.6. FI Ceti

FI Cet was originally discovered as a transient ROTSE3 J015118.59–022300.1 on 2001 October 13 by ROTSE-IIIa telescope. The object was detected at 14.71 mag and faded by two magnitudes over 13 days. The object was originally suspected to be a nova based on the large amplitude, but it was also suspected to be either a recurrent nova or a WZ Sge-type dwarf nova (Smith et al. 2002). The object was named FI Cet in Kazarovets et al. (2006), which classified it as a possible dwarf nova.

Although amateur observers recognized that the object is most likely a larger-amplitude dwarf nova and started monitoring since 2002, no secure outburst had

been detected until the detection on 2014 June 27 by the ASAS-SN team (Davis et al. 2015) at $V=14.4$ (vsnet-alert 17423).

Subsequent observations initially did not detect superhumps (vsnet-alert 17428, 17436). The object started showing superhumps on July 2 and the amplitudes further grew over two days (vsnet-alert 17440, 17453; figure 8). The times of superhump maxima are listed in table 10. The period identification is based on the $O-C$ analysis on individual nights. The adopted period among the candidates only give acceptably small $O-C$ variations within the same nights. A stage A-B transition and stage B with a positive $P_{\dot{\text{dot}}}$ can be well recognized. Due to the faintness of the object, the times of superhump maxima could not be measured in the later part of the superoutburst. The light curve, however, showed a brightening trend around July 13. Since such a trend in the light curve

Table 2. Superhump Periods and Period Derivatives (continued)

Object	Year	P_1	err	E_1	P_{dot}	err	P_2	err	E_2	P_{orb}	Q		
CC Scl	2014	0.05998	0.00002	–	–	–	0.059523	0.000006	–	–	0.058567	C	
V418 Ser	2014	0.044669	0.000013	0	83	6.1	0.044408	0.000007	106	311	–	B	
V701 Tau	2015	0.068838	0.000141	13	72	–	–	–	–	–	–	C	
SU UMa	2014	0.079252	0.000037	0	25	–	–	–	–	–	0.07635	CG	
CY UMa	2014	0.072202	0.000018	5	35	−17.8	5.1	0.072017	0.000022	43	103	0.06957	B
QZ Vir	2014	0.060368	0.000015	20	126	8.9	1.1	0.059980	0.000086	125	170	0.05882	B
NSV 1436	2014	0.072843	0.000014	12	84	3.7	2.0	0.072403	0.000048	109	150	–	B
NSV 4618	2015	–	–	–	–	–	–	0.067506	0.000242	0	31	0.065769	C
1RXS J185310	2014	0.059521	0.000032	0	65	–	–	–	–	–	–	–	C
1RXS J231935	2014	0.066105	0.000059	0	51	–	–	0.065387	0.000059	81	140	–	C
2QZ J130441	2014	–	–	–	–	–	–	0.058069	0.000061	0	72	–	C
ASASSN-13cx	2014	0.083098	0.000042	7	52	–	–	0.082647	0.000035	48	133	0.079650	B
ASASSN-14ag	2014	0.062059	0.000055	0	38	–	–	–	–	–	–	0.060311	C
ASASSN-14aj	2014	0.082028	0.000041	0	90	−3.0	5.2	–	–	–	–	–	C2
ASASSN-14au	2014	0.082486	0.000084	0	37	–	–	–	–	–	–	–	C
ASASSN-14aw	2014	0.097586	0.000154	0	31	–	–	–	–	–	–	–	C
ASASSN-14bh	2014	–	–	–	–	–	–	0.061368	0.000065	0	35	–	C
ASASSN-14cl	2014	0.060008	0.000013	27	174	8.5	0.4	0.059738	0.000014	174	249	0.05838	AE
ASASSN-14cq	2014	0.057354	0.000011	34	194	4.6	0.4	–	–	–	–	0.05660	BE
ASASSN-14cv	2014	0.060413	0.000007	109	227	0.9	0.9	–	–	–	–	0.059917	AE
ASASSN-14dm	2014	0.068335	0.000042	0	76	–	–	0.068160	0.000130	73	104	–	C
ASASSN-14do	2014	0.056528	0.000032	14	105	4.6	3.2	–	–	–	–	–	C
ASASSN-14dw	2014	0.075630	0.000045	0	54	–	–	0.075195	0.000029	53	94	–	C
ASASSN-14eh	2014	0.062907	0.000027	0	96	6.0	3.0	–	–	–	–	–	C
ASASSN-14eq	2014	0.079467	0.000069	0	52	−40.2	10.0	–	–	–	–	–	CG
ASASSN-14gd	2014	0.078957	0.000054	0	14	–	–	–	–	–	–	–	C
ASASSN-14gx	2014	0.056088	0.000016	18	194	5.1	0.6	–	–	–	–	0.05488	BE
ASASSN-14hk	2014	0.060001	0.000019	0	135	2.8	2.1	–	–	–	–	–	CG
ASASSN-14hs	2014	0.093660	0.000059	10	102	−3.4	4.9	–	–	–	–	–	C2
ASASSN-14id	2014	0.079366	0.000028	0	137	−2.2	1.7	–	–	–	–	0.076857	CG
ASASSN-14iv	2014	0.069192	0.000051	0	22	–	–	–	–	–	–	–	C
ASASSN-14je	2014	–	–	–	–	–	–	0.069070	0.000054	0	74	–	C

is usually associated with development of stage C superhumps, superhumps after this epoch were likely stage C superhumps. Although we were not able to measure the period of stage A superhumps, an analysis of the first two nights yielded a period of 0.05594(3) d, which we tentatively identified to be the period of early superhumps (figure 9). Note that this identification of the period is not conclusive and awaits determination of the orbital period in quiescence. All the pieces of evidence support the WZ Sge-type classification as originally proposed. The large positive P_{dot} suggests that this object is not an extreme WZ Sge-type dwarf nova.

3.7. Z Chameleontis

3.7.1. Superhumps during the 2014 superoutburst

Z Cha is one of the best known SU UMa-type dwarf novae since the early history of research of SU UMa-type dwarf novae (e.g. Warner 1974; Bailey 1979; Vogt 1980). Its deep eclipses has provided us wealth of information about the structure of the accretion disk and its variation over the course of outburst and superoutburst (e.g. Vogt 1982; Horne 1984). Despite its importance, the object

was mostly observed in the era of photoelectric photometry and no publicly available data for superoutbursts are published. This has been an obstacle to compare the classical knowledge in SU UMa-type dwarf novae with the one with the modern CCD observations. In order to improve the situation, we undertook a campaign in 2013–2014 to cover a full supercycle. Since such a long-term campaign requires enormous effort, we did not attempt to record high time-resolution observations to resolve eclipses, instead we focused on longer-term (orbital modulations and superhumps) variations. The entire data are now publicly available in the AAVSO database.

As in the rest of this paper, we first deal with the superoutburst which occurred in 2014 April. The rise to the outburst was detected on April 15, and the object stayed the precursor part for three days, during which superhumps evolved (see bottom panel of figure 10). On April 20, fully grown superhumps were recorded associated with an increase of the brightness by ~ 0.2 mag. The object entered the post-superoutburst stage on April 30. The general behavior is in good agreement with the modern knowledge: a superoutburst is triggered by a normal

Table 2. Superhump Periods and Period Derivatives (continued)

Object	Year	P_1	err	E_1	P_{dot}	err	P_2	err	E_2	P_{orb}	Q
ASASSN-14jf	2014	0.055949	0.000005	54	341	1.1	0.2	—	—	0.05539	BE
ASASSN-14jq	2014	0.055178	0.000013	0	142	4.3	1.2	—	—	—	C
ASASSN-14jv	2014	0.055102	0.000013	59	210	4.9	0.7	—	—	0.05442	BE
ASASSN-14kf	2014	0.072095	0.000038	13	70	—	—	—	—	—	C
ASASSN-14kk	2014	0.056361	0.000060	0	89	—	—	—	—	—	C
ASASSN-14ku	2014	0.079066	0.000079	0	54	—	—	—	—	—	C2
ASASSN-14lk	2014	0.061432	0.000030	0	130	−2.7	3.5	—	—	—	CG
ASASSN-14mc	2014	0.055463	0.000017	18	127	1.7	2.1	—	—	—	C
ASASSN-14md	2014	0.066878	0.000074	28	74	—	—	—	—	—	C
ASASSN-14mh	2014	0.062754	0.000018	16	144	1.2	1.6	—	—	—	C
ASASSN-14mj	2014	0.060262	0.000032	18	63	—	—	—	—	—	C
ASASSN-15ah	2015	0.055469	0.000032	35	145	6.2	3.2	—	—	—	C
ASASSN-15ap	2015	0.091340	0.000042	0	67	−5.5	6.0	—	—	—	C
ASASSN-15aq	2015	0.072297	0.000064	0	80	6.6	7.3	0.071842	0.000035	80 139	C
ASASSN-15aw	2015	0.0615	0.0003	0	3	—	—	—	—	—	C
ASASSN-15bg	2015	0.065669	0.000071	0	32	—	—	—	—	—	C
ASASSN-15bp	2015	0.056702	0.000009	35	256	4.5	0.3	0.056656	0.000013	269 396	AE
ASASSN-15bu	2015	0.080049	0.000039	0	80	−8.3	4.8	—	—	0.076819	CG
ASASSN-15dq	2015	0.082062	0.000037	0	47	2.3	7.4	—	—	—	C
CRTS J214738	2014	0.096770	0.000137	41	80	—	—	—	—	0.09273	C
CRTS J202731	2014	0.071499	0.000064	0	78	—	—	0.071237	0.000050	78 164	C
CSS J174033	2014	0.045591	0.000003	0	166	2.0	0.3	0.045526	0.000008	59 332	A
MASTER J043915	2014	0.062452	0.000047	0	48	—	—	—	—	—	C
MASTER J055845	2014	—	—	—	—	—	—	0.056300	0.000400	0 3	C
MASTER J085854	2015	0.055560	0.000019	0	124	8.1	1.0	—	—	—	B
MASTER J105545	2014	0.066937	0.000052	0	46	−10.8	10.3	—	—	—	CG
OT J030929	2014	0.057437	0.000015	35	199	6.8	0.5	0.057076	0.000022	190 264	BE
OT J060009	2014	0.063311	0.000007	116	275	−1.2	0.6	—	—	—	A
OT J064833	2014	0.100326	0.000056	38	75	33.4	7.5	—	—	—	B
OT J213806	2014	0.055046	0.000011	16	174	6.5	0.5	0.054905	0.000040	190 228	AP
OT J230523	2014	0.055595	0.000023	34	125	8.2	1.3	—	—	0.05456	CE
PNV J171442	2014	0.060092	0.000009	67	188	4.4	0.7	—	—	0.059558	AE

Table 2. Superhump Periods and Period Derivatives (continued)

Object	Year	P_1	err	E_1	P_{dot}	err	P_2	err	E_2	P_{orb}	Q
PNV J172929	2014	0.060282	0.000015	32	173	2.6	1.2	—	—	0.05973	BE
PTF1 J071912	2014	0.018808	0.000011	0	159	—	—	—	—	0.01859	C
SDSS J081408	2014	0.100929	0.000112	0	27	−40.8	10.9	—	—	—	CG
SDSS J090221	2014	0.033714	0.000005	0	140	1.5	0.8	0.033593	0.000009	150 246	A
SDSS J120231	2014	0.059801	0.000042	0	134	9.0	1.3	0.059577	0.000024	134 202	B
SDSS J140037	2015	0.063954	0.000021	0	125	—	—	—	—	—	C
SDSS J172325	2014	0.059200	0.000021	6	110	5.3	2.6	—	—	—	C
SDSS J173047	2014	0.024609	0.000006	0	166	−0.7	0.9	—	—	—	BG
TCP J160548	2014	0.054989	0.000017	0	316	1.6	0.2	—	—	—	C

Table 4. List of recent outbursts of NN Cam.

Year	Month	max*	magnitude	type	source
2007	9	54354	12.6	precursor + super	vsnet-alert 9557; Kato et al. (2009); Shears et al. (2011a)
2008	3	54535	12.5	?	AAVSO
2008	10	54758	13.2	super	vsnet-alert 10588; Shears et al. (2011a)
2009	11	55137	13.0	super	BAAVSS alert 2130; Kato et al. (2010); Shears et al. (2011a)
2011	12	55905	12.4	super	vsnet-alert 13937; Kato et al. (2013a)
2012	11	56241	12.7	super	cvnet-outburst 5039; Kato et al. (2014b)
2013	9	56563	13.1	normal	AAVSO
2014	2	56708	12.8	super	this paper

*JD−2400000.

Table 7. List of recent outbursts of SY Cap.

Year	Month	max*	magnitude	type	source
2001	5	52040	13.2	super	ASAS-3
2002	4	52390	13.1	super	ASAS-3
2002	8	52502	13.7	normal? [†]	ASAS-3
2003	4	52741	13.5	normal? [†]	ASAS-3
2003	4	52756	14.3	normal? [†]	ASAS-3
2003	11	52945	13.6	super	ASAS-3
2004	6	53165	13.1	super	ASAS-3
2005	4	53467	13.0	super	ASAS-3
2005	7	53568	14.1	normal? [†]	ASAS-3
2005	9	53644	13.0	super	ASAS-3
2006	6	53914	14.7	normal?	ASAS-3
2007	4	54194	13.3	super? [†]	ASAS-3
2007	9	54344	13.2	super	ASAS-3
2008	4	54560	13.6	?	ASAS-3
2008	8	54697	13.1	super	ASAS-3, Kato et al. (2009)
2008	9	54725	13.9	normal [†]	ASAS-3
2008	10	54760	13.6	normal	ASAS-3, vsnet-outburst 9567
2009	4	54951	13.0	normal?	vsnet-outburst 10221, ASAS-3
2009	7	55014	12.9	super	ASAS-3
2009	7	55038	13.4	normal	vsnet-outburst 10408
2009	8	55060	14.1	normal	vsnet-outburst 10464
2009	10	56113	13.1	normal	vsnet-outburst 10611
2010	5	55340	14.1	normal	vsnet-outburst 11235
2010	7	55390	13.2	normal?	vsnet-outburst 11379
2010	10	55497	15.4	normal	vsnet-outburst 11720
2011	6	55742	13.1	normal	vsnet-outburst 12988
2011	8	55776	13.4	normal	cvnet-outburst 4252
2011	8	55799	13.0	super	Kato et al. (2013a)
2011	9	55827	14.1	normal	vsnet-outburst 13235
2011	10	55861	15.1	normal	vsnet-outburst 13363
2011	11	55890	15.0	normal	vsnet-outburst 13478
2012	7	56127	13.0	super	vsnet-outburst 14481
2013	5	56434	13.2	normal?	vsnet-outburst 15436

*JD−2400000.

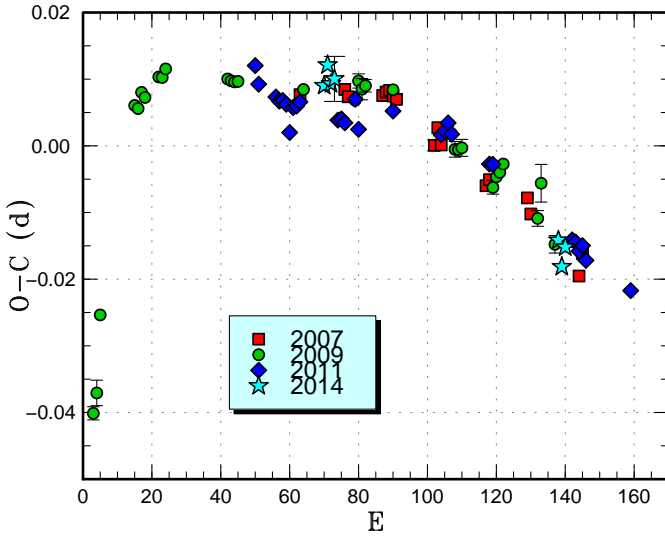
[†]Single detection.

Table 7. List of recent outbursts of SY Cap (continued).

Year	Month	max*	magnitude	type	source
2013	7	56500	13.2	normal?	vsnet-outburst 15721
2013	8	56532	13.6	normal	vsnet-alert 16296
2013	9	56560	13.0	normal	vsnet-outburst 16027
2013	10	56584	13.1	super	vsnet-alert 16550
2014	4	56753	13.0	normal?	vsnet-outburst 16749
2014	6	56817	13.4	normal?	vsnet-outburst 16970
2014	9	56819	12.8	super	this paper
2014	10	56847	13.2	normal	this paper
2014	11	56982	13.5	normal	this paper

*JD−2400000.

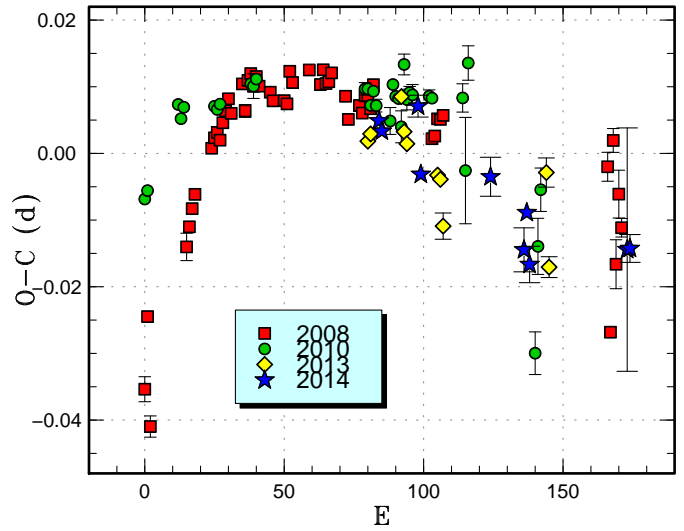
†Single detection.

**Fig. 4.** Comparison of $O - C$ diagrams of NN Cam between different superoutbursts. A period of 0.07430 d was used to draw this figure. Approximate cycle counts (E) after the start of the superoutburst were used.

outburst, which appears as a precursor, followed by development of superhumps (cf. Osaki, Kato 2013a).

The times of superhump maxima were determined during the superoutburst after subtracting the mean orbital variation (mostly eclipses) and template fitting as in other systems. This simple method assumes the constancy of the orbital light curve, which is obviously wrong because the orbital and superhump variations interact each other to produce a beat phenomenon. We used, however, this method since there is no other suitable method to determine times of superhumps. Readers should be careful in interpreting the resultant values (they should contain systematic errors due to this simple treatment other than the nominal errors given in the tables) in such a high-inclination system.

The result clearly indicates the presence of stage A ($E \leq 14$) and stage B to C transition around $E = 64$. The $O - C$ diagram for stage B superhumps is not as smooth as other non-eclipsing objects due to the strong beat phe-

**Fig. 5.** Comparison of $O - C$ diagrams of V342 Cam between different superoutbursts. A period of 0.07830 d was used to draw this figure. Approximate cycle counts (E) after the start of the superoutburst were used. Since the start of the 2013 superoutburst was not well constrained, we shifted the $O - C$ diagram to best fit the others.

nomenon. The measured periods of stage B and C superhumps are in good agreement with the previous values from re-identification of the published epochs in the literature (Kato et al. 2009) and analysis of recent limited data (Kato et al. 2010).

The three growing superhumps ($E \leq 14$) during the precursor phase (stage A superhumps) unfortunately happened around the phase of eclipses, and the times of maxima could not be determined around their peaks. The times of these superhump maxima should therefore contain considerable errors. Although the period of stage A superhumps can be measured as 0.08017(3) d, this value should be treated with caution. The fractional superhump excess corresponds to $q = 0.22(1)$. We hope observations in the future, when times of stage A superhumps do not overlap with eclipses, could provide a more reliable q value directly comparable to the one from eclipse observations.

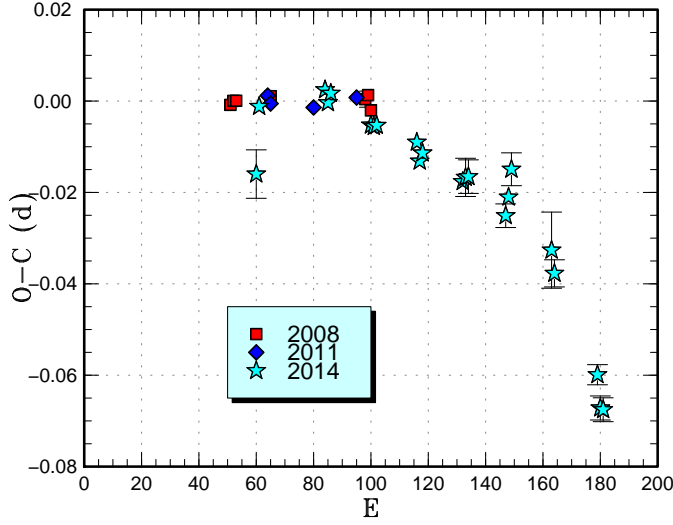


Fig. 6. Comparison of $O - C$ diagrams of SY Cap between different superoutbursts. A period of 0.06376 d was used to draw this figure. Approximate cycle counts (E) after the start of the superoutburst were used. The 2014 superoutburst was shifted by 60 cycles to best match the others.

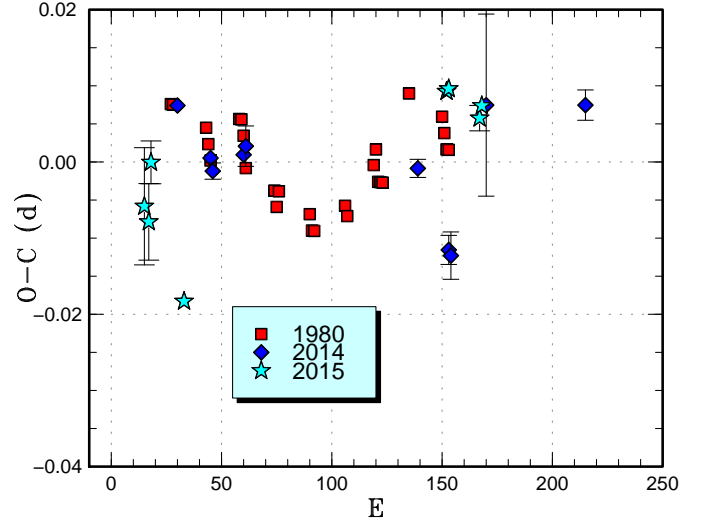


Fig. 7. Comparison of $O - C$ diagrams of OY Car between different superoutbursts. A period of 0.06465 d was used to draw this figure. Approximate cycle counts (E) after the starts of outbursts were used. The 2015 superoutburst with a separate precursor outburst was shifted by 15 cycles to best match the others.

Table 6. Superhump maxima of SY Cap (2014)

E	max*	error	$O - C^\dagger$	N^\ddagger
0	56920.9768	0.0053	-0.0268	27
1	56921.0554	0.0005	-0.0116	73
24	56922.5255	0.0007	0.0031	20
25	56922.5864	0.0008	0.0007	18
26	56922.6523	0.0015	0.0033	17
40	56923.5379	0.0012	0.0030	16
41	56923.6014	0.0008	0.0032	18
42	56923.6654	0.0007	0.0039	19
56	56924.5544	0.0009	0.0069	15
57	56924.6140	0.0007	0.0032	16
58	56924.6795	0.0010	0.0055	13
72	56925.5659	0.0021	0.0059	16
73	56925.6306	0.0042	0.0073	16
74	56925.6945	0.0037	0.0080	7
87	56926.5148	0.0026	0.0056	12
88	56926.5827	0.0019	0.0102	16
89	56926.6525	0.0036	0.0168	17
103	56927.5275	0.0083	0.0058	10
104	56927.5861	0.0030	0.0012	16
119	56928.5204	0.0022	-0.0138	14
120	56928.5768	0.0026	-0.0207	16
121	56928.6402	0.0026	-0.0206	16

*BJD-2400000.

† Against max = 2456921.0037 + 0.063282 E .

‡ Number of points used to determine the maximum.

Table 8. Superhump maxima of OY Car (2014)

E	max*	error	$O - C^\dagger$	phase ‡	N^\S
0	56818.0448	0.0009	0.0064	0.41	46
15	56819.0076	0.0008	-0.0003	0.67	37
16	56819.0706	0.0011	-0.0020	0.67	36
30	56819.9778	0.0010	0.0003	0.04	36
31	56820.0436	0.0027	0.0014	0.08	34
109	56825.0834	0.0012	-0.0004	0.92	34
123	56825.9778	0.0019	-0.0109	0.09	50
124	56826.0417	0.0031	-0.0117	0.11	54
140	56827.0958	0.0120	0.0083	0.81	28
185	56830.0051	0.0020	0.0089	0.90	28

*BJD-2400000.

† Against max = 2456818.0384 + 0.064636 E .

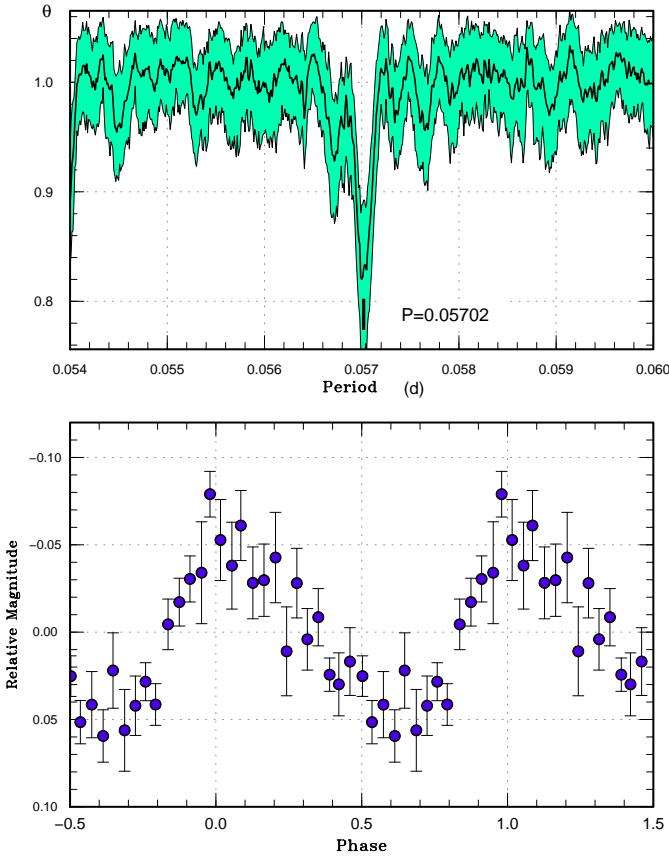
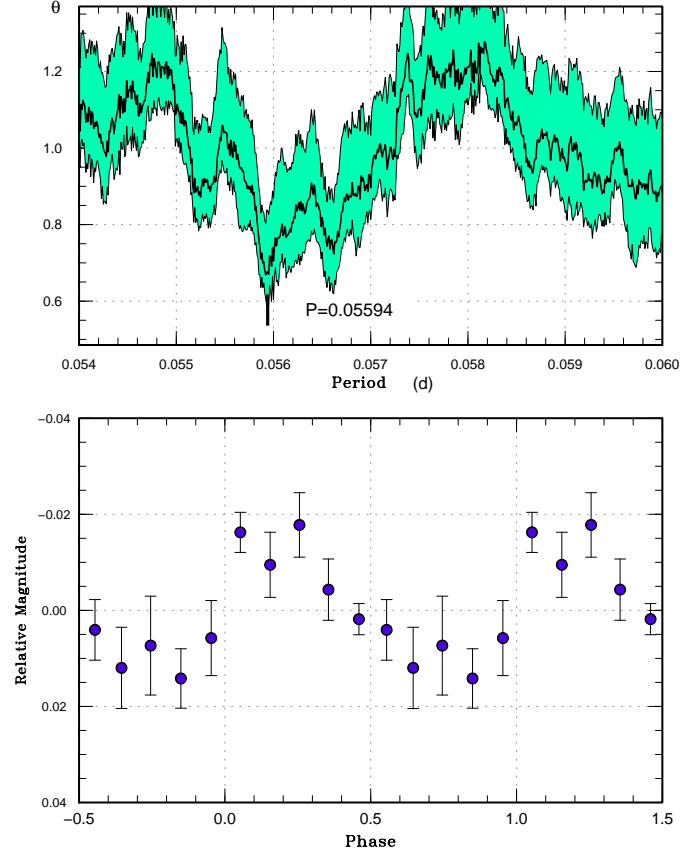
‡ Orbital phase.

§ Number of points used to determine the maximum.

Table 9. Superhump maxima of OY Car (2015)

E	max*	error	$O - C^\dagger$	phase ‡	N^\S
0	57067.0848	0.0077	0.0024	0.86	53
2	57067.2121	0.0050	0.0001	0.88	53
3	57067.2846	0.0028	0.0078	0.02	24
18	57068.2361	0.0009	-0.0121	0.10	43
137	57075.9570	0.0010	0.0026	0.42	51
138	57076.0220	0.0013	0.0028	0.45	63
152	57076.9232	0.0017	-0.0026	0.73	23
153	57076.9895	0.0006	-0.0010	0.78	45

*BJD-2400000.

 † Against max = 2457067.0825 + 0.064759 E . ‡ Orbital phase. § Number of points used to determine the maximum.**Fig. 8.** Superhumps in FI Cet (2014). (Upper): PDM analysis. (Lower): Phase-averaged profile.**Fig. 9.** Possible early superhumps in FI Cet (2014). (Upper): PDM analysis. (Lower): Phase-averaged profile.**Table 10.** Superhump maxima of FI Cet (2014)

E	max*	error	$O - C^\dagger$	N^\ddagger
0	56840.8397	0.0023	-0.0018	15
1	56840.8939	0.0022	-0.0046	19
18	56841.8724	0.0005	0.0054	19
35	56842.8382	0.0010	0.0027	16
36	56842.8945	0.0004	0.0020	19
71	56844.8847	0.0013	-0.0017	19
88	56845.8534	0.0010	-0.0015	17
89	56845.9094	0.0011	-0.0025	17
106	56846.8825	0.0020	0.0021	19

*BJD-2400000.

 † Against max = 2456840.8415 + 0.056971 E . ‡ Number of points used to determine the maximum.

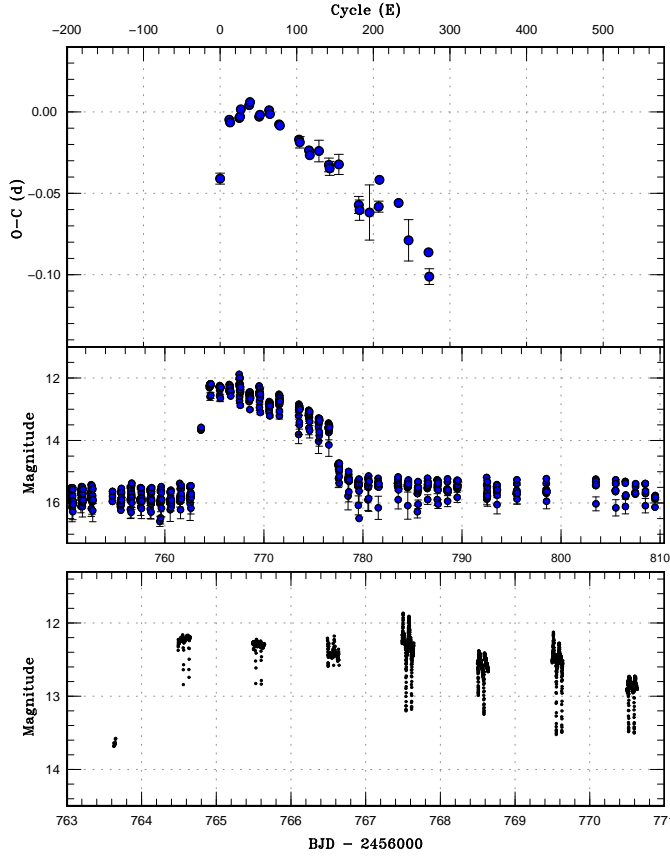


Fig. 10. $O - C$ diagram of superhumps in Z Cha (2014). (Upper): $O - C$. We used a period of 0.07736 d for calculating the $O - C$ residuals. (Middle): Light curve. The data were binned to 0.0077 d. (Lower): Enlarged light curve of showing the precursor and evolution of superhumps. After the full growth of superhumps, strong beat phenomena were present.

The superhumps persisted in the post-superoutburst phase (table 12), whose times were also determined after subtracting the mean orbital modulation. The period was similar to that of stage C superhumps. This superhump signal could be traced to BJD 2456790 with the PDM method, but became unclear after this.

A comparison of the $O - C$ diagrams between different superoutbursts is shown in figure 11. The 1982 superoutburst had a separate precursor outburst and we needed to shift 50 cycles for this superoutburst to make a match with the others. This indicates that superhumps started to grow 50 cycles (about 4 d) before the start of the main outburst. This value implies that superhumps started to develop 1 d after the precursor outburst, since it took five days before the main outburst occurs.

3.7.2. Search for negative superhumps

Our entire observation covered one complete supercycle consisting of the 2013 August superoutburst (BJD 2456524), three normal outbursts (BJD 2456572, 2456624, 2456676) and the 2014 April superoutburst (BJD 2456764).

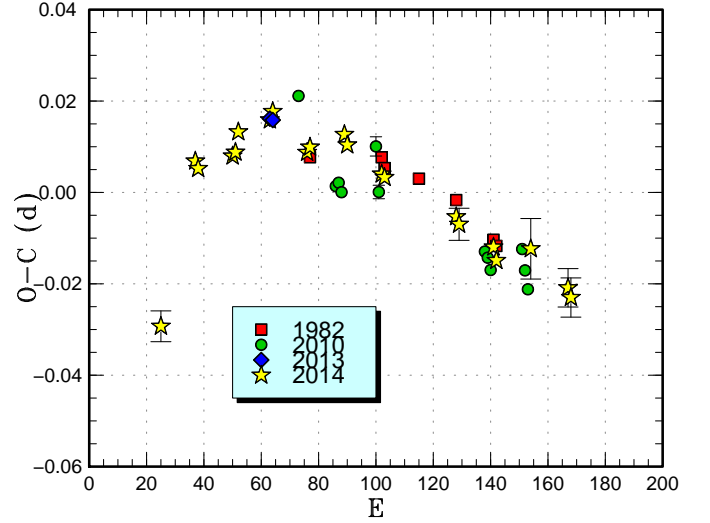


Fig. 11. Comparison of $O - C$ diagrams of Z Cha between different superoutbursts. A period of 0.07736 d was used to draw this figure. Approximate cycle counts (E) after the starts of outbursts were used. The 1982 superoutburst had a separate precursor outburst and the start of the outburst was defined as the start of the main outburst. The 1982 superoutburst was shifted by 50 cycles to best match the others.

Table 11. Superhump maxima of Z Cha (2014)

E	max*	error	$O - C^\dagger$	phase [‡]	N^\S
0	56765.5347	0.0034	-0.0410	0.10	26
12	56766.4992	0.0018	-0.0027	0.04	28
13	56766.5749	0.0016	-0.0042	0.06	33
25	56767.5060	0.0004	0.0006	0.56	91
26	56767.5842	0.0005	0.0016	0.61	147
27	56767.6660	0.0016	0.0062	0.71	38
38	56768.5195	0.0010	0.0107	0.16	133
39	56768.5987	0.0008	0.0128	0.23	147
51	56769.5181	0.0006	0.0059	0.57	122
52	56769.5966	0.0008	0.0072	0.62	147
64	56770.5277	0.0008	0.0121	0.12	148
65	56770.6028	0.0006	0.0099	0.13	140
77	56771.5247	0.0007	0.0056	0.50	142
78	56771.6014	0.0008	0.0050	0.53	148
103	56773.5268	0.0017	0.0008	0.38	41
104	56773.6025	0.0035	-0.0007	0.39	33
116	56774.5258	0.0013	-0.0036	0.79	40
117	56774.6002	0.0018	-0.0064	0.78	32
129	56775.5311	0.0066	-0.0018	0.28	34
142	56776.5283	0.0042	-0.0080	0.66	33
143	56776.6035	0.0043	-0.0100	0.67	21

*BJD-2400000.

[†]Against max = 2456765.5757 + 0.077187E.

[‡]Orbital phase.

[§]Number of points used to determine the maximum.

Table 12. Superhump maxima of Z Cha (2014) (post-super-outburst)

E	max*	error	$O - C^\dagger$	phase ‡	N^\S
0	56777.5343	0.0062	0.0047	0.17	32
26	56779.5207	0.0052	-0.0088	0.83	30
27	56779.5949	0.0062	-0.0115	0.83	24
40	56780.5991	0.0169	-0.0073	0.31	17
52	56781.5310	0.0034	0.0016	0.82	28
53	56781.6249	0.0011	0.0185	0.08	9
78	56783.5447	0.0025	0.0152	0.85	28
91	56784.5274	0.0127	-0.0020	0.04	28
117	56786.5314	0.0018	0.0020	0.94	80
118	56786.5938	0.0048	-0.0125	0.77	27

*BJD-2400000.

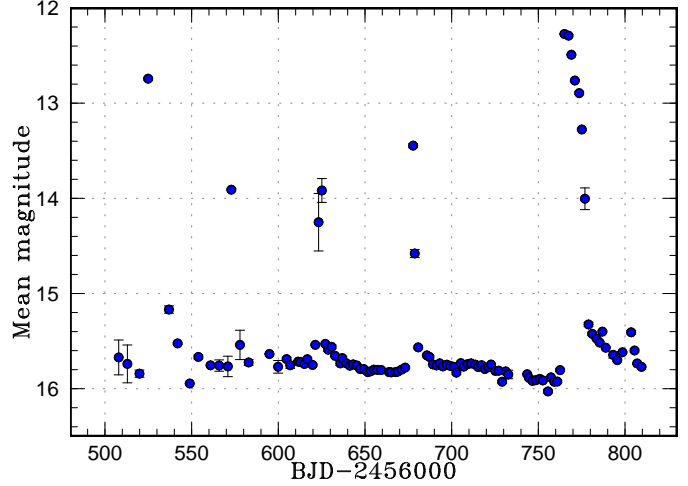
 † Against max = 2456777.5295 + 0.076922 E . ‡ Orbital phase. § Number of points used to determine the maximum.

We searched for possible negative superhumps. After dividing the quiescent data into 10–20 d bins (depending on the gaps in observations and the goodness of coverage), we subtracted the mean orbital variation and applied the PDM analysis. We detected possible signal of negative superhumps in the following three bins: BJD 2456610–2456623 (before the second normal outburst), period 0.07342(4) d and amplitude 0.05 mag; BJD 2456651–2456662 (before the third normal outburst), period of 0.07352(8) d and amplitude 0.05 mag; BJD 2456663–2456675 (after the third normal outburst), period of 0.07314(4) d and amplitude 0.04 mag. Although these possible detections were close to the detection limit and may have been affected by (probably variable) strong orbital modulations and uneven sampling of observations, these negative superhumps may have indeed transiently existed.

It may be noteworthy that the interval of the third normal outburst and the second superoutburst was relatively long (88 d). In VW Hyi, there exists “L” (long intervals of normal outbursts) and “S” (short intervals) type supercycles (Smak 1985), and it has been recently established by Kepler observations of that L-type and S-type supercycles are related to negative superhumps, which are considered to be a result of the tilted disk (Osaki, Kato 2013a). A similar suggestion was reported in VW Hyi (Kato et al. 2014a). The relatively long interval of outbursts after the third normal outburst in Z Cha might be also related to the existence of transient negative superhumps.

3.7.3. Secular brightness variation

van Amerongen et al. (1987) and van Amerongen et al. (1990) studied secular variation of the brightness of VW Hyi and Z Cha, respectively. Although van Amerongen et al. (1990) could not yield convincing results, our much improved and homogeneous data are expected to provide a better clue to understanding the quiescent disk. As in van Amerongen et al. (1987), we used phase 0.20 segment to represent the mean magnitude. Since Z Cha has an maximum of the quiescent orbital humps at around the

**Fig. 12.** Brightness variation of Z Cha outside orbital humps (orbital phase 0.26–0.46). Each dot represent 2-d average.

orbital phase 0.86, we used phase 0.36 ± 0.10 for this purpose.

The result clearly shows that the mean magnitude is variable in quiescence (figure 12). The mean magnitude in quiescence clearly monotonically faded between the third normal outburst and the second superoutburst. The situation is somewhat different in the quiescence between the second and third normal outburst, and there was a secular fading trend followed by a rising trend before the third normal outburst. It appears that the mean magnitude in quiescence shows a secular fading trend in a supercycle. The mean magnitude after the second superoutburst is much brighter than before the superoutburst, but this trend was not so evident in the first superoutburst. In any case, an explanation for such a trend is a future task for the disk instability model.

The variation of the orbital humps in quiescence was also examined (figure 13). The amplitude is defined here between magnitudes of orbital phase 0.76–0.96 and orbital phase 0.26–0.46. The amplitude of orbital humps increases during quiescence between normal outbursts. This most likely reflect the increased release of the gravitational potential energy as the disk shrinks in quiescence. There was no indication of enhanced orbital humps before any outburst, which severely constrain the mass-transfer instability model.

3.8. YZ Cancri

YZ Cnc is a well-known active SU UMa-type dwarf nova (e.g. Szkody, Mattei 1984). See Kato et al. (2014a) for more history. In 2014, another superoutburst in November–December was observed. The times of superhump maxima are listed in table 13. According to the AAVSO observations, there was an outburst (BJD 2456977.7, November 16) 5 d before the start of the superoutburst. Since the object did not reach the ordinary quiescent level after this outburst, it was likely that this outburst was a separate precursor outburst. Although the

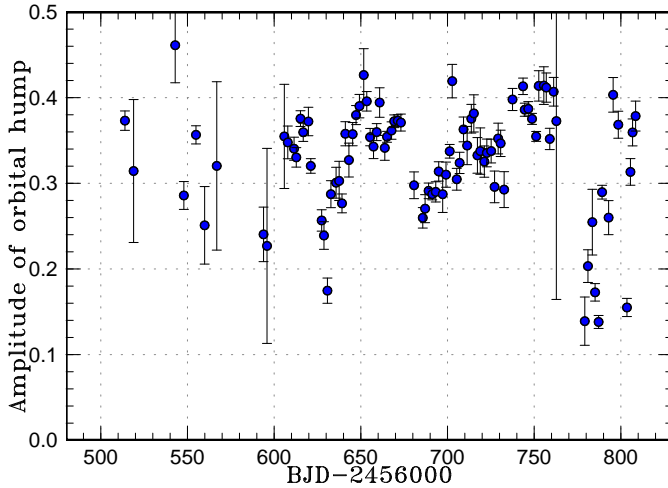


Fig. 13. Amplitude of orbital humps in Z Cha in quiescence (difference between orbital phase 0.76–0.96 and orbital phase 0.26–0.46). Each dot represent 2-d average.

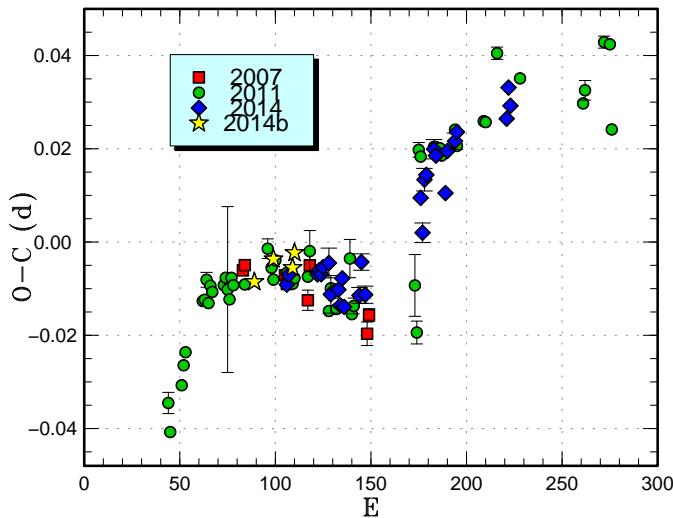


Fig. 14. Comparison of $O - C$ diagrams of YZ Cnc between different superoutbursts. A period of 0.09050 d was used to draw this figure. Approximate cycle counts (E) after the start of the superoutburst were used (in the case of YZ Cnc, this refers to the precursor outburst). Since the start of the 2014 superoutburst was not well constrained, we shifted the $O - C$ diagram to best fit the others. The figure was drawn based on an assumption that the preceding outburst before the 2014b superoutburst was a precursor outburst. The superhumps apparently appeared immediately following this precursor outburst.

superhump observations started only ~ 24 cycles after the final rise to the superoutburst, there was no hint of stage A superhumps. It was most likely that stage A superhumps appeared following the separate precursor outburst. This suggestion was supported by a comparison of $O - C$ diagrams (figure 14).

Table 13. Superhump maxima of YZ Cnc (2014b)

E	max*	error	$O - C^\dagger$	N^\ddagger
0	56985.9582	0.0002	-0.0009	72
10	56986.8680	0.0005	0.0019	169
20	56987.7712	0.0003	-0.0020	184
21	56987.8649	0.0004	0.0010	179

*BJD-2400000.

† Against max = 2456985.9591 + 0.090707 E .

‡ Number of points used to determine the maximum.

Table 14. Superhump maxima of V337 Cyg (2014)

E	max*	error	$O - C^\dagger$	N^\ddagger
0	56840.5108	0.0003	-0.0003	75
1	56840.5817	0.0006	0.0003	43
14	56841.4932	0.0005	-0.0000	67

*BJD-2400000.

† Against max = 2456840.5112 + 0.070150 E .

‡ Number of points used to determine the maximum.

3.9. V337 Cygni

V337 Cyg was discovered as a long-period variable (AN 101.1928) with a range of 14.2 to fainter than 16.4 (Baade 1928). Guthnick, Prager (1933) suggested that this object is likely a dwarf nova. The object had been long lost since then, and both Bruch et al. (1987) and Downes, Shara (1993) could not identify the object. In 1996, J. Manek identified three outbursts of this object in the Sonneberg archive (vsnet 775). J. Manek further supplied the dates of six outbursts (vsnet 782). In 2006 May, a new outburst was detected and subsequent observations confirmed the SU UMa-type nature of this object (Boyd et al. 2007; Kato et al. 2009). Kato et al. (2010) further studied the 2010 superoutburst.

The 2014 superoutburst was detected by J. Shears on June 29 (BAAVSS alert 3728; vsnet-alert 17427). Time-series observations were undertaken on two nights and the three times of superhump maxima were measured (table 14). A PDM analysis yielded a period of 0.07019(3) d. We probably observed stage B superhumps as judged from a comparison with the 2007 and 2010 data.

3.10. V503 Cygni

For this famous SU UMa-type dwarf nova, see Kato et al. (2014a) for a description. The 2014 July superoutburst was observed. On the initial two nights (BJD 2456864–2456865), typical superhumps were recorded. After BJD 2456867, the superhumps became double-humped. Since we could not distinguish which maxima correspond to the smooth continuation of the earlier superhump maxima, we listed both hump maxima in table 15. The value given in table 2 refers to the initial part only. Similar variation in the superhump profile can be found in Harvey et al. (1995).

Another superoutburst occurred in 2014 October

Table 15. Superhump maxima of V503 Cyg (2014)

E	max*	error	$O - C^\dagger$	N^\ddagger
0	56864.0992	0.0006	0.0031	133
1	56864.1776	0.0007	0.0000	142
12	56865.0712	0.0010	-0.0020	140
13	56865.1530	0.0008	-0.0017	142
14	56865.2391	0.0018	0.0030	45
16	56865.3917	0.0012	-0.0072	64
17	56865.4815	0.0007	0.0011	81
40	56867.3698	0.0017	0.0166	79
41	56867.4216	0.0009	-0.0129	74
65	56869.4034	0.0015	0.0146	74
66	56869.4532	0.0029	-0.0170	69
66	56869.4928	0.0018	0.0226	72
67	56869.5314	0.0036	-0.0202	65

*BJD-2400000.

 † Against max = 2456864.0961 + 0.081425 E . ‡ Number of points used to determine the maximum.

(vsnet-alert 17827; 2014b outburst in table 1). Time-series observations were obtained only on two nights and two superhumps maxima were obtained: BJD 2456942.4363(7) ($N=68$) and 2456952.4321(10) ($N=90$).

3.11. BC Doradus

This object was originally designated as CAL 86 in the direction of the Large Magellanic Cloud (LMC). This star was originally selected as an Einstein X-ray source. Cowley et al. (1984) provided an optical identification. Schmidtke et al. (2002) reported the detection of a short (0.066 d) orbital period and at least five outbursts in the MACHO observations. Some of these outbursts reached $V=14$. Kato et al. (2004a) confirmed the SU UMa-type nature by the detection of superhumps during the 2003 outburst.

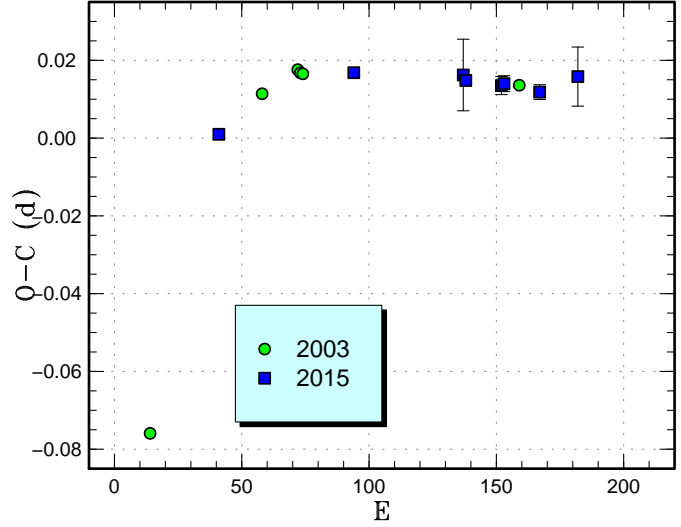
The 2015 superoutburst was visually detected by R. Stubbings on February 20 (vsnet-alert 18315). The outburst was also detected by ASAS-SN (vsnet-alert 18316). There was a gap in the observation in the early part of the superoutburst. The times of superhump maxima are listed in table 16. After a comparison with the 2003 result (figure 15), we noticed that the stage identifications for the 2003 superhumps were incorrect. We provide an updated result in table 2.

3.12. V660 Herculis

For the explanation of the history of this object, see Kato et al. (2014b). The 2014 superoutburst was detected by M. Moriyama at an unfiltered CCD magnitude of 14.4 on September 13 (vsnet-alert 17724). Only one superhump maximum was obtained: BJD 2456915.0538(8) ($N=97$).

3.13. CT Hydrae

For history of CT Hya, refer to Kato et al. (2014a). The 2015 superoutburst was visually detected by R. Stubbings (vsnet-alert 18285). The outburst was apparently de-

**Fig. 15.** Comparison of $O - C$ diagrams of BC Dor between different superoutbursts. A period of 0.06806 d was used to draw this figure. Approximate cycle counts (E) after the maximum of the superoutburst were used.**Table 16.** Superhump maxima of BC Dor (2015)

E	max*	error	$O - C^\dagger$	N^\ddagger
0	57076.9685	0.0014	-0.0049	24
53	57080.5915	0.0012	0.0068	16
96	57083.5175	0.0092	0.0029	10
97	57083.5841	0.0012	0.0014	17
111	57084.5356	0.0023	-0.0009	16
112	57084.6042	0.0020	-0.0006	12
126	57085.5549	0.0019	-0.0038	17
141	57086.5797	0.0076	-0.0010	17

*BJD-2400000.

 † Against max = 2457076.9734 + 0.068137 E . ‡ Number of points used to determine the maximum.

tected during the rising phase by P. Starr one night before Stubbings' detection. The times of superhump maxima are listed in table 17. A comparison of $O - C$ diagrams indicates that we observed stage B and C superhumps, although observations were not sufficient to determine individual periods.

3.14. LY Hydrae

LY Hya (=1329-294) was originally discovered as a CV selected for blue color (Echevarria et al. 1983). Double-peak emission lines suggested a high orbital inclination (Echevarria et al. 1983). Although Kubiak, Krzeminski (1989) reported a photometric period of 3.8 hr and Kubiak, Krzeminski (1992) reported photometric and spectroscopic observations indicating an orbital period of 0.13688 d, these observations were not confirmed. Still et al. (1994) obtained an orbital period of 0.0748(5) d and the Doppler tomogram suggested that the object likely

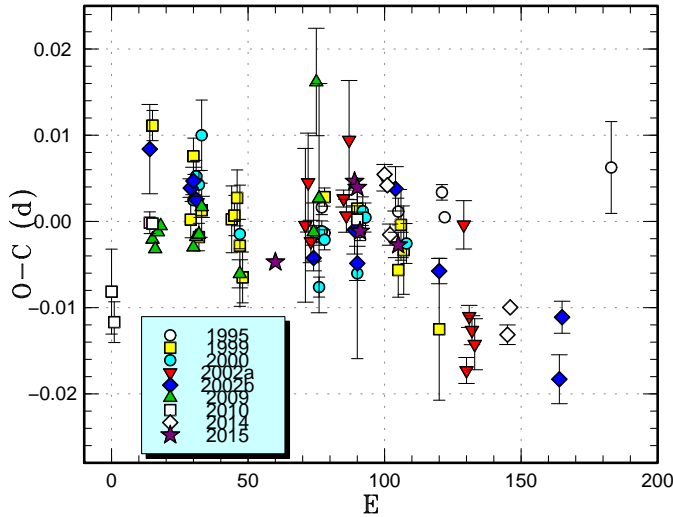


Fig. 16. Comparison of $O - C$ diagrams of CT Hya between different superoutbursts. A period of 0.06650 d was used to draw this figure. Approximate cycle counts (E) after the maximum of the superoutburst were used. Since the start of the 2014 superoutburst was not well constrained, we shifted the $O - C$ diagram to best fit the others.

Table 17. Superhump maxima of CT Hya (2015)

E	max*	error	$O - C^\dagger$	N^\ddagger
0	57067.0221	0.0010	-0.0024	51
29	57068.9599	0.0005	0.0045	65
30	57069.0257	0.0011	0.0037	208
31	57069.0872	0.0008	-0.0015	177
45	57070.0166	0.0015	-0.0043	50

*BJD-2400000.

† Against max = 2457067.0244 + 0.066587 E .

‡ Number of points used to determine the maximum.

belong SU UMa-type dwarf novae.

There was a report by T. Vanmunster that S. Howell observed an outburst in 1996 around $V=14.4$ (cf. vsnet-obs 2047). The details of this observation are not known. It was only in 1998 April when a fresh outburst was detected by R. Stubbings (vsnet-alert 1707). The object rapidly faded during this outburst (vsnet-alert 1713, 1714). In 2000 April, another brightening at 16.0 mag was reported by P. Schmeer (vsnet-alert 4559). This outburst also quickly faded (vsnet-alert 4563). Another outburst at 14.0 mag was reported visually by R. Stubbings in 2000 September (vsnet-outburst 462) but no further observation was available for this outburst. In 2009 May, R. Stubbings detected another outburst (vsnet-alert 11233) but it again faded rapidly (vsnet-alert 11236). After another faint outburst in 2011 February (vsnet-outburst 12296), there was a bright outburst reaching 13.1 mag in 2012 February (vsnet-alert 14206). No time-series observations were, however, obtained during this outburst.

The 2014 superoutburst was the first one during which

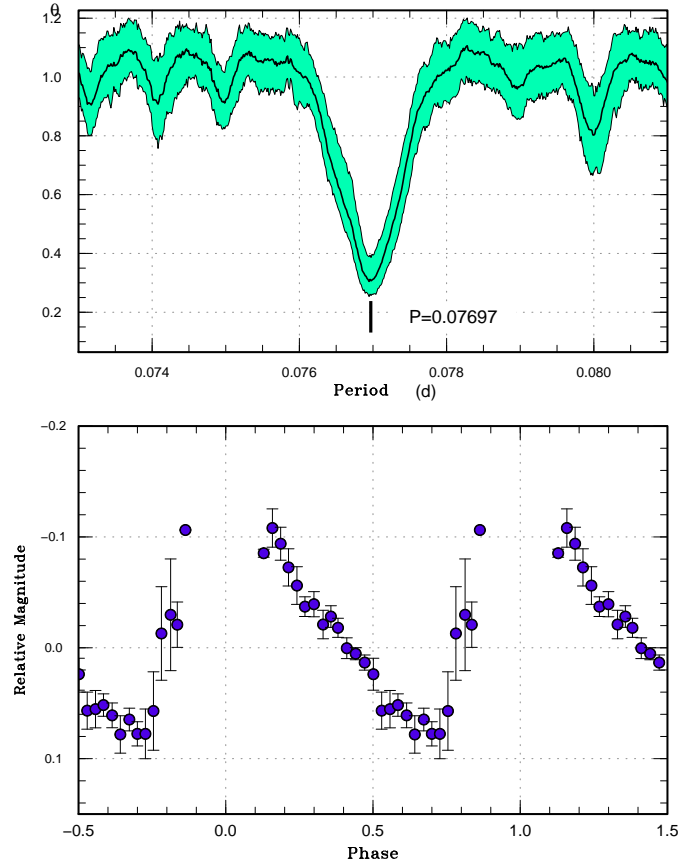


Fig. 17. Superhumps in LY Hya (2014). (Upper): PDM analysis. (Lower): Phase-averaged profile.

time-series observations were obtained. This outburst was detected at $V=13.25$ by the ASAS-SN team on August 9 (vsnet-alert 17632). Superhumps were finally detected (vsnet-alert 17640, 17644, 17653). Due to the unfavorable seasonal condition, observations were limited to short evening windows. Despite that individual superhump maxima were never recorded, a combined light curve yielded an unmistakable superhump signal (figure 17). Since we observed only the later part of the superoutburst until the rapid fading, we likely recorded stage C superhumps. In table 2, we list this identification.

3.15. *MM Hydrae*

MM Hya was originally selected as a CV by the Palomar-Green survey (Green et al. 1982). Although Misselt, Shafter (1995) suggested it to be a WZ Sge-type dwarf nova based on the very short orbital period, the object has been recognized as a rather ordinary SU UMa-type dwarf nova Patterson et al. (2003). Past superhump observations were given in Kato et al. (2009), Kato et al. (2012a), Kato et al. (2013a) and Kato et al. (2014b).

The 2014 superoutburst was detected by R. Stubbings on April 27 during its rising stage (vsnet-alert 17267). Six days later, time-resolved observations detected superhumps (vsnet-alert 17279). The times of superhump max-

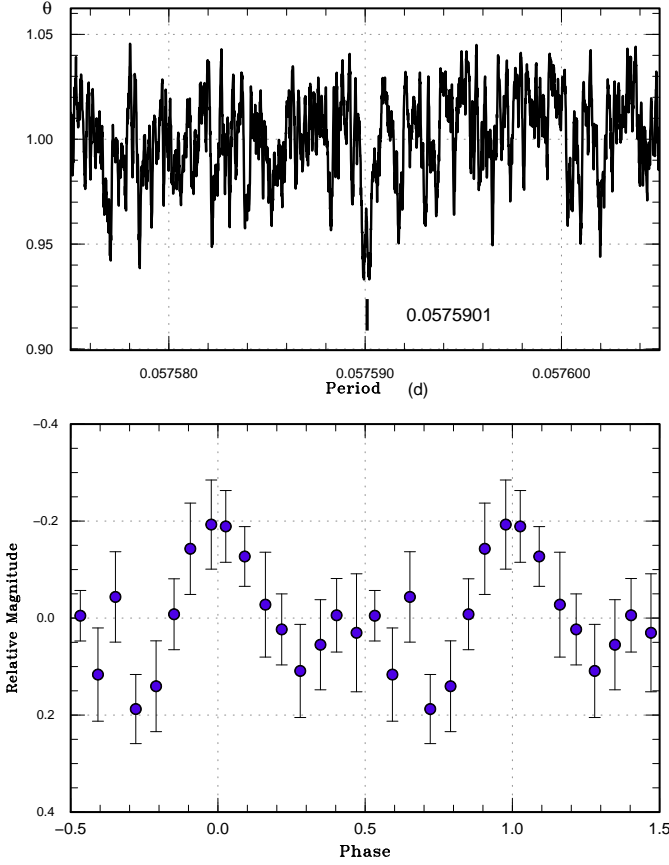


Fig. 18. Orbital variation of MM Hya in quiescence using the CRTS data. (Upper): PDM analysis. (Lower): Phase-averaged profile.

ima are listed in table 18. A comparison of the $O - C$ diagrams between different superoutbursts suggests that we observed stage B-C superhumps during the 2014 superoutburst (figure 19).

We have also refined the orbital period to be 0.0575901(1) using the quiescent CRTS data (figure 18; BJD 2453705–2456441).

We have also examined the recent outbursts of MM Hya (table 18). The $O - C$ diagram indicates that the supercycle was long [386(3) d] between 1998 and 2003, but it decreased to 330(2) d. Superoutbursts were not detected between 2007 and 2011 probably because superoutbursts occurred around solar conjunctions since the supercycle is close to one year. Although the shorter supercycle [347(8) d] was also recorded between 2011 and 2013, it again became longer in 2014. The number of normal outbursts has been rather small, although many of them may have escaped detection due to the faintness, particularly for visual observations.

3.16. RZ Leonis Minoris

This object is one of the ER UMA-type dwarf novae, and is renowned for its short supercycle length (19 d; cf. Robertson et al. 1995; Nogami et al. 1995). Two su-

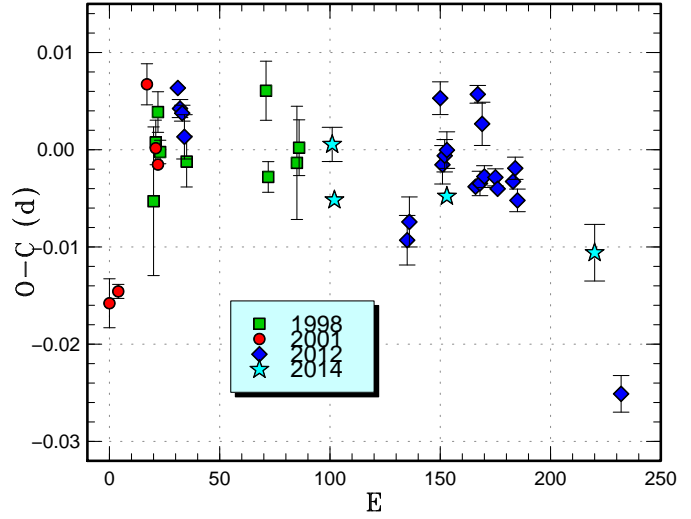


Fig. 19. Comparison of $O - C$ diagrams of MM Hya between different superoutbursts. A period of 0.05892 d was used to draw this figure. Approximate cycle counts (E) after the appearance of superhumps were used.

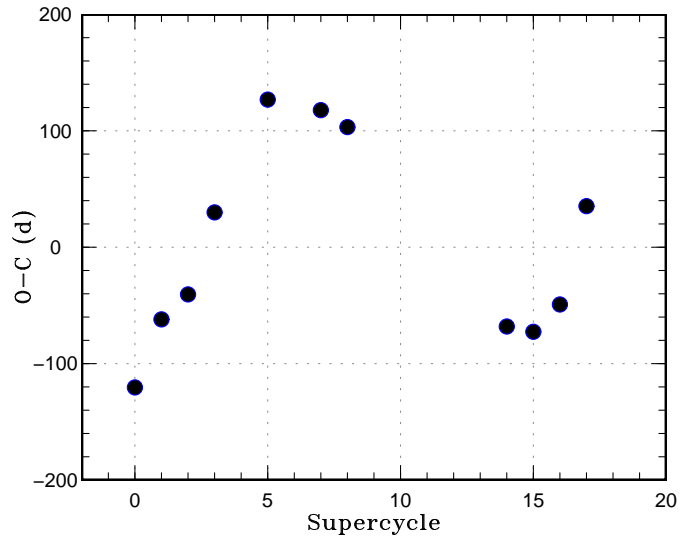


Fig. 20. $O - C$ diagram of superoutbursts in MM Hya. The ephemeris used was $\text{Max}(\text{JD}) = 2451001 + 337.5E$.

Table 18. Superhump maxima of MM Hya (2014)

E	max*	error	$O - C^\dagger$	N^\ddagger
0	56780.9808	0.0018	0.0026	122
1	56781.0340	0.0008	-0.0031	122
52	56784.0393	0.0006	0.0008	108
119	56787.9812	0.0029	-0.0003	58

*BJD-2400000.

† Against $\text{max} = 2456780.9782 + 0.058851E$.

‡ Number of points used to determine the maximum.

Table 19. List of recent outbursts of MM Hya.

Year	Month	max*	magnitude	type	source
1998	3	50881	13.7	super	J. Kemp, AAVSO; Patterson et al. (2003); Kato et al. (2009)
1999	4	51277	13.0	super	vsnet-alert 2842, AAVSO
2000	4	51636	13.0	super	vsnet-obs 27068, vsnet-alert 4565, AAVSO
2001	5	52044	13.0	super	AAVSO; Kato et al. (2009)
2002	11	52594	15.1 [†]	normal	AAVSO
2003	5	52816	13.2	super	AAVSO, ASAS-3
2004	1	53036	13.8	normal	AAVSO, ASAS-3
2004	7	53191	14.0 [‡]	?	vsnet-outburst 6354, AAVSO
2004	11	53320	14.1 [†]	normal	AAVSO
2005	5	53482	13.9	super	ASAS-3, VSOLJ, AAVSO
2006	3	53805	13.0	super	AAVSO
2006	10	54040	14.2	normal	AAVSO, VSOLJ
2011	4	55659	13.1	super	vsnet-alert 13113, AAVSO; Kato et al. (2012a)
2012	3	55992	13.4	super	AAVSO; Kato et al. (2013a)
2012	5	56055	15.1 [†]	normal	AAVSO
2013	3	56353	13.3	super	vsnet-alert 15487, AAVSO; Kato et al. (2014b)
2014	4	56775	13.1	super	vsnet-alert 17267; this paper

*JD−2400000.

[†]CCD single detection.[‡]Single visual detection and single positive detection by ASAS-3 5 d before.

perhump maxima were obtained: BJD 2456725.7181(2) ($N = 58$) and 2456725.7800(7) ($N = 31$).

3.17. *BR Lupi*

This object (=HV 4889) was discovered as a dwarf nova (although it was referred to as an SS Cyg-type, there was no distinction of subtypes at the time of this discovery) by Swope, Caldwell (1930) with a photographic range of 13.5 to fainter than 16.0 in the table. Swope, Caldwell (1930) reported ten outbursts and the photographic range was corrected to 13.1 to fainter than 16.4 in Prager, Shapley (1941). Walker, Olmsted (1958) provided a finding chart. Vogt, Bateson (1982) also provided a detailed finding chart.

O'Donoghue (1987) reported on the detection of superhumps during the 1986 outburst, establishing the SU UMa-type nature. Munari, Zwitter (1998) confirmed the CV nature by spectroscopy. Mennickent, Sterken (1998) reported a radial-velocity study and photometry in quiescence and during a superoutburst.

We conducted a time-series photometry in quiescence and superoutburst starting on 2014 July 31. The times of superhump maxima are listed in table 20. After BJD 2456878, the profile became double-humped. The two distinct hump maxima at $E = 194$ and $E = 218$ may be traditional late superhumps after an ~ 0.5 phase jump. The superhumps up to $E = 24$ correspond to stage A superhumps with growing amplitudes.

A comparison of $O - C$ diagrams between different superoutbursts is shown in figure 21. The trends were the same except the late part of the superoutburst, when superhump profiles became less regular or doubly humped. Since the mass-transfer rate is expected to be large to ac-

count for the short supercycle (140 d), the appearance of traditional late superhumps reflecting the bright hot spot is not a surprise.

The orbital period of this system has not been well-established. The period in the literature was 0.0795(5) d in Mennickent, Sterken (1998). We observed this object in quiescence to determine the orbital period (figure 22). The orbital signal was rather weak in contrast to the reported 0.4-mag variation in Mennickent, Sterken (1998). We adopted here a period of 0.07948(2) d because it is closer to the value by Mennickent, Sterken (1998) and the estimated orbital period (0.0795 d) based on the updated relation between the orbital and superhump periods (equation 6 in Kato et al. 2012a). There remains a possibility of 0.07904(2) d. The exact orbital period needs to be confirmed by further observations. This orbital period gives $\epsilon^* = 0.0488(12)$ for stage A superhumps and $q = 0.142(4)$. This value needs to be established by confirming the orbital period.

3.18. *AY Lyrae*

The 2014 October superoutburst of this well-known SU UMa-type dwarf nova was observed on two nights. Three superhump maxima were recorded: BJD 2456947.9590(7) ($N = 51$), 2456948.0347(7) ($N = 56$) and 2456954.9360(10) ($N = 96$).

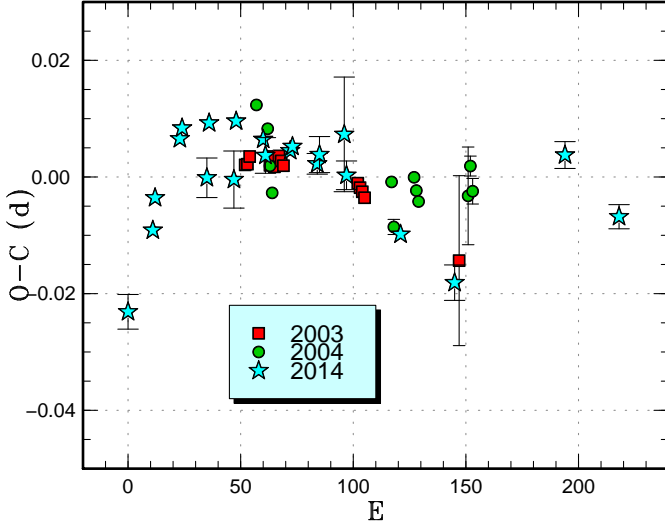
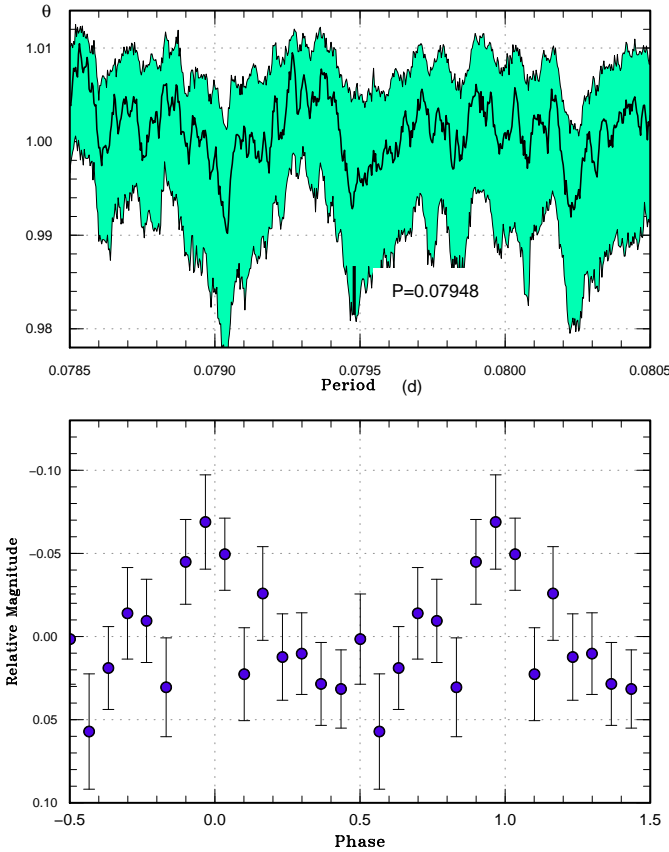
3.19. *V453 Normae*

This object (=ASAS J160048−4846.2) was discovered as a dwarf nova in 2005 June by Pojmanski (2005). Early observations of superhumps was reported by Monard, Africa (2005). Imada, Monard (2006) reported the possible detection of early superhumps and classified this ob-

Table 20. Superhump maxima of BR Lup (2014)

E	max*	error	$O - C^\dagger$	N^\ddagger
0	56869.5644	0.0030	-0.0242	15
11	56870.4835	0.0008	-0.0101	11
12	56870.5714	0.0006	-0.0045	14
23	56871.4865	0.0007	0.0058	15
24	56871.5707	0.0007	0.0076	16
35	56872.4672	0.0034	-0.0007	6
36	56872.5589	0.0007	0.0087	19
47	56873.4543	0.0049	-0.0008	6
48	56873.5466	0.0006	0.0092	19
60	56874.5308	0.0017	0.0062	15
61	56874.6103	0.0031	0.0035	6
72	56875.5162	0.0012	0.0045	14
73	56875.5992	0.0016	0.0052	8
84	56876.5013	0.0018	0.0024	14
85	56876.5852	0.0031	0.0040	11
96	56877.4937	0.0098	0.0077	11
97	56877.5690	0.0025	0.0007	10
121	56879.5336	0.0017	-0.0091	14
145	56881.5000	0.0030	-0.0170	15
194	56885.5536	0.0023	0.0056	20
218	56887.5178	0.0021	-0.0046	20

*BJD-2400000.

 † Against max = 2456869.5887 + 0.082265 E . ‡ Number of points used to determine the maximum.**Fig. 21.** Comparison of $O - C$ diagrams of BR Lup between different superoutbursts. A period of 0.08228 d was used to draw this figure. Approximate cycle counts (E) after the appearance of superhumps were used.**Fig. 22.** Period analysis of BR Lup in quiescence (BJD 2456835–2456864). (Upper): PDM analysis. (Lower): Phase-averaged profile.

ject as a WZ Sge-type dwarf nova. Soejima et al. (2009) provided the detailed analysis of the superhumps, and detected an increase in the superhump period which was later associated with the increase of the amplitude. Kato et al. (2009) made an extended analysis after combination with the AAVSO data, which generally confirmed the finding by Imada, Monard (2006).

After the 2005 superoutburst, there have been two detections of apparent normal outbursts: 2006 May 20 (14.2 mag) and 2009 January 5 (13.8), both detected by R. Stubbings.

The next superoutburst was detected on 2014 April 23 at 12.4 mag by R. Stubbings (vsnet-alert 17254). Growing superhumps were detected on April 25 and 26 (vsnet-alert 17262).

The times of superhump maxima are listed in table 21. This table includes superhumps observed after the rapid fading from the superoutburst. Although the end phase of stage A was probably observed on April 25 ($E = 1$ and $E = 2$), the period of stage A superhumps could not be determined. The P_{dot} of stage B superhumps was strikingly positive [$+16.4(3.5) \times 10^{-5}$], similar to the 2005 value [$+11.1(0.8) \times 10^{-5}$]. A very clear stage B-C transition was recorded (cf. figure 23). There was no phase jump during the rapid fading phase, and a single period (stage C superhumps) well explained the superhumps during the late course of the plateau phase and the post-superoutburst phase. An analysis of observations after the rebrightening (BJD 2456789.7–2456796) yielded weak modulations

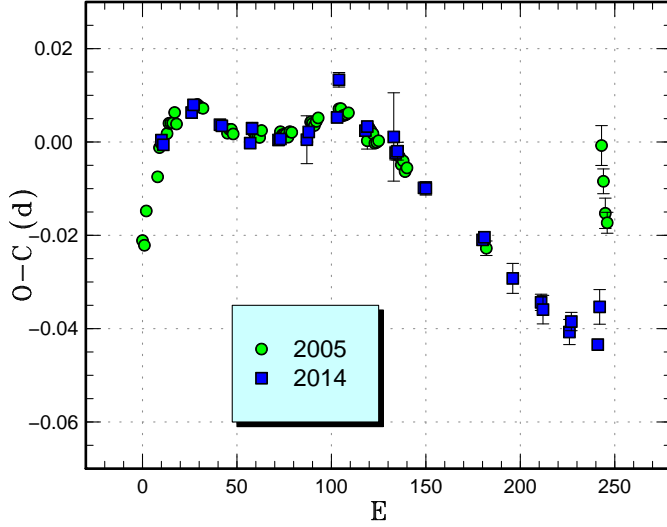


Fig. 23. Comparison of $O - C$ diagrams of V453 Nor between different superoutbursts. A period of 0.06497 d was used to draw this figure. Approximate cycle counts (E) after the appearance of superhumps were used. The 2014 superoutburst was shifted by 10 cycles to best match the 2005 one.

(0.05 mag) with period of 0.06416(13) d, which may be decaying superhumps.

The overall $O - C$ diagrams were very similar between 2005 and 2014 (figure 23) except the appearance of humps with different phases during the rebrightening in 2005 [see also discussion in Kato et al. 2009].

3.20. DT Octantis

For the history of this object, see Kato et al. (2014a). The 2014 December superoutburst was detected by R. Stubbings and the ASAS-SN team (vsnet-alert 18079). The times of superhump maxima are listed in table 22. The period listed in table 2 is probably a mixture of stage B and C superhumps (figure 24).

3.21. UV Persei

UV Per is a famous dwarf nova known more than for a century. The object was discovered as a nova or a new variable star (87.1911) in 1911 November by D'Esterre (1912). Since the object was initially suspected to be a nova, Wolf (1912) studied the counterpart and found that the object is a southern component of the close pair. This finding was confirmed by D'Esterre (1913). Nijland (1914) detected an outburst in 1914 June lasting 14 d and concluded that the object must be a U Gem-type variable. Hartwig (1915) recorded an outburst in 1915 September, which faded quickly. This outburst was also recorded by Nijland (1915), who confirmed the shortness of the outburst. Hartwig (1917) recorded a long outburst in 1916 December. Hartwig (1917) suggested that the intervals of three outbursts were 442 and 473 d. Nijland (1918) and Hartwig (1920) detected further outbursts in 1918 May and 1920 October, respectively. In the meantime, Harvard College Observatory reported the intervals of out-

Table 21. Superhump maxima of V453 Nor (2014)

E	max*	error	$O - C^\dagger$	N^\ddagger
0	56772.8084	0.0006	-0.0138	30
1	56772.8724	0.0005	-0.0146	37
16	56773.8538	0.0003	-0.0046	35
17	56773.9205	0.0010	-0.0027	15
31	56774.8258	0.0005	-0.0041	22
32	56774.8905	0.0004	-0.0041	35
47	56775.8614	0.0005	-0.0047	35
48	56775.9295	0.0013	-0.0013	10
62	56776.8366	0.0005	-0.0009	33
63	56776.9018	0.0005	-0.0005	29
77	56777.8112	0.0051	0.0023	10
78	56777.8778	0.0008	0.0041	35
93	56778.8555	0.0006	0.0104	35
94	56778.9285	0.0016	0.0186	12
108	56779.8272	0.0007	0.0106	33
109	56779.8931	0.0006	0.0117	35
123	56780.8004	0.0095	0.0124	16
124	56780.8619	0.0015	0.0092	35
125	56780.9273	0.0019	0.0098	15
139	56781.8290	0.0010	0.0048	35
140	56781.8939	0.0014	0.0049	35
170	56783.8319	0.0009	0.0001	31
171	56783.8975	0.0010	0.0009	29
186	56784.8632	0.0032	-0.0048	30
201	56785.8326	0.0017	-0.0068	27
202	56785.8960	0.0031	-0.0082	27
216	56786.8008	0.0027	-0.0101	27
217	56786.8680	0.0020	-0.0076	27
231	56787.7727	0.0009	-0.0097	16
232	56787.8457	0.0037	-0.0014	19

*BJD-2400000.

† Against max = 2456772.8222 + 0.064762 E .

‡ Number of points used to determine the maximum.

Table 22. Superhump maxima of DT Oct (2014b)

E	max*	error	$O - C^\dagger$	N^\ddagger
0	57012.5406	0.0010	-0.0031	24
14	57013.5926	0.0020	0.0035	11
27	57014.5603	0.0013	0.0005	26
40	57015.5309	0.0023	0.0005	18
54	57016.5750	0.0022	-0.0007	16
67	57017.5458	0.0035	-0.0007	25

*BJD-2400000.

† Against max = 2457012.5437 + 0.074667 E .

‡ Number of points used to determine the maximum.

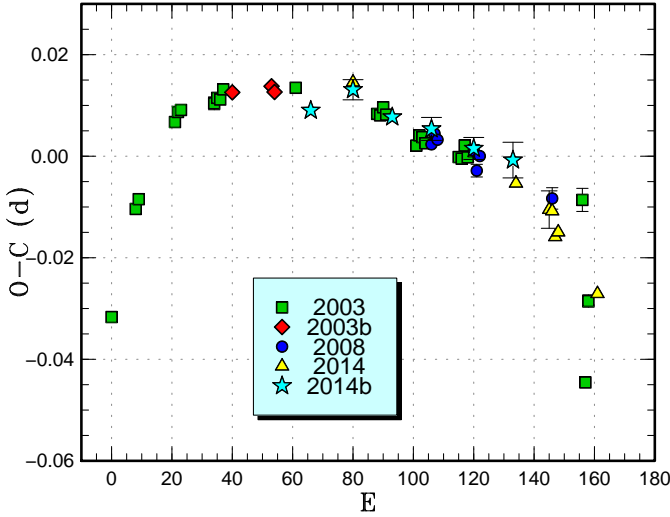


Fig. 24. Comparison of $O - C$ diagrams of DT Oct between different superoutbursts. A period of 0.07485 d was used to draw this figure. Approximate cycle counts (E) after the start of the superoutburst were used. Since the start of the 2014 and 2014b superoutbursts was not well constrained, we shifted the $O - C$ diagrams to best fit the others.

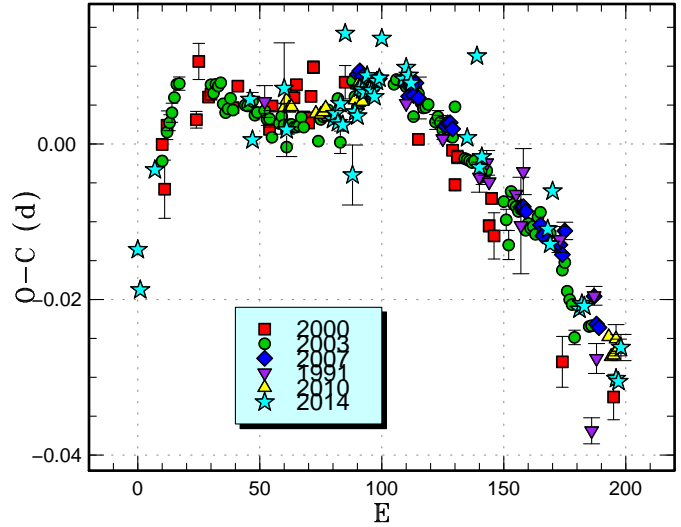


Fig. 25. Comparison of $O - C$ diagrams of UV Per between different superoutbursts. A period of 0.06665 d was used to draw this figure. Approximate cycle counts (E) after the appearance of superhumps were used. The superoutbursts before 2014 was shifted by 10 cycles against the figure in Kato et al. (2010) to best match the start of the 2014 one.

bursts to be 214 and 299 d, suggesting the irregularity. Nijland (1924) summarized nine known outbursts (five of them were long outbursts) and suggested that the intervals could be expressed by the basic period of 131.48 d.

Since then, the object has long been monitored by amateur observers (e.g. Petit, Brun 1956; Hornby 1975). Petit, Brun (1956) analyzed the outbursts in detail and obtained a mean interval of 359.8 d. Petit, Brun (1956) also classified outbursts into two types: type I lasting for 12 d and type II lasting for 4 d. Mayall (1966) was another summary article and reported a list of 32 outbursts between 1928 and 1966. The existence of long and short outbursts was clear from these data. Howarth (1978) also presented a list of 63 outbursts (dating back to Pickering's observation in 1896) and discussed outburst statistics. Howarth (1978) estimated the mean cycle length of 320 d.

The long cycle length of UV Per received attention, and the object was considered to be a good candidate for an SU UMa-type dwarf nova. It was only in 1989 when Udalski (1989) succeeded in detecting superhumps. Kato (1990) reported photometry in quiescence. Udalski, Pych (1992) reported both during the 1989 superoutburst and in quiescence. The orbital period was first reliably measured to be 0.06489(11) d by radial-velocity study by Thorstensen, Taylor (1997). The 1989 superoutburst was also notable that this was one of the first superoutbursts of SU UMa-type dwarf novae followed by a rebrightening.¹⁰ This rebrightening was best recorded by the VSOLJ members [although there were several detections in the present AAVSO data, they were not shown in Udalski,

Pych (1992)].

Although a number of superoutbursts were detected, there have not been many papers. Price et al. (2003) was the only publication before Kato et al. (2009) and dealt with the 2003 superoutburst. Kato et al. (2009) reported on the 2000, 2003 and 2007 superoutbursts and Kato et al. (2010) reported on the 2010 superoutburst. None of superoutbursts were better observed than the 2003 one.

The 2014 superoutburst was visually detected by C. Chiselbrook (cf. vsnet-alert 18000). Since the detection of the outburst was early enough to record the appearance of superhumps (vsnet-alert 18008, 18022). There was a single post-superoutburst rebrightening (vsnet-alert 18061).

The times of superhump maxima are listed in table 23. Stages B and C can be recognized. Although the maxima for $E \leq 7$ correspond to stage A superhumps, the period of stage A superhumps could not be determined. Since the early phase of stage B superhumps were not observed, the value of P_{dot} in table 2 is not as reliable as the 2003 one in Kato et al. (2009). A comparison of $O - C$ diagrams between different superoutbursts is given in figure 25.

3.22. *HY Piscium*

This object (=SDSSp J230351.64+010651.0) was originally selected as a CV by the SDSS (Szkody et al. 2002). Szkody et al. (2002) identified this object as a dwarf nova by obtaining spectra both in outburst and quiescence. A radial-velocity study by Szkody et al. (2002) yielded an orbital period of 100 ± 14 min. The first secure outburst since the discovery was detected on 2006 August 29 of 14.5 mag (magnitudes are unfiltered CCD ones for this object) by I. Miller (cvnet-outburst 1327). Although this outburst quickly faded, modulations with a period of 0.07 d were

¹⁰ The first documented record of a rebrightening was VY Aqr by R. McNaught (Perez, McNaught 1986) in 1986, which was later published (Patterson et al. 1993).

Table 23. Superhump maxima of UV Per (2014)

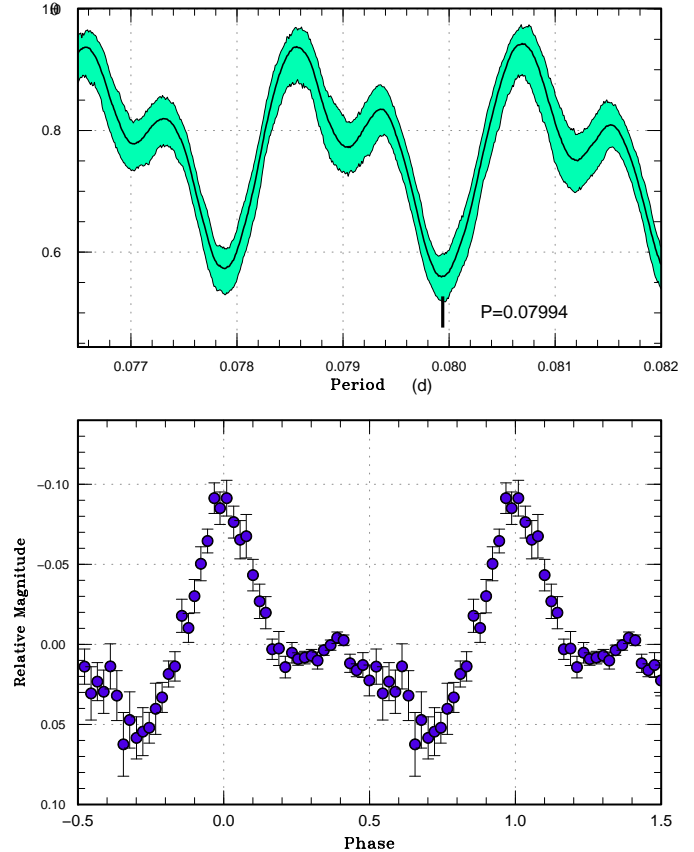
E	max*	error	$O - C^\dagger$	N^\ddagger
0	56984.9961	0.0008	-0.0253	79
1	56985.0576	0.0013	-0.0303	73
7	56985.4729	0.0012	-0.0142	229
46	56988.0813	0.0003	-0.0005	133
47	56988.1428	0.0004	-0.0056	134
60	56989.0158	0.0059	0.0026	21
61	56989.0772	0.0034	-0.0026	23
80	56990.3448	0.0004	0.0010	69
81	56990.4123	0.0003	0.0019	66
82	56990.4777	0.0004	0.0008	68
83	56990.5468	0.0005	0.0034	64
84	56990.6107	0.0005	0.0008	69
85	56990.6892	0.0007	0.0126	14
88	56990.8709	0.0039	-0.0052	25
89	56990.9457	0.0002	0.0030	248
90	56991.0118	0.0002	0.0026	248
91	56991.0820	0.0002	0.0063	249
92	56991.1485	0.0006	0.0062	55
93	56991.2148	0.0006	0.0060	68
94	56991.2836	0.0005	0.0083	69
95	56991.3484	0.0003	0.0066	191
96	56991.4150	0.0004	0.0066	69
97	56991.4808	0.0005	0.0059	66
98	56991.5494	0.0004	0.0080	67
99	56991.6165	0.0005	0.0086	69
100	56991.6883	0.0005	0.0138	24
109	56992.2829	0.0003	0.0096	107
110	56992.3510	0.0003	0.0112	200
111	56992.4167	0.0003	0.0104	154
112	56992.4823	0.0004	0.0095	66
135	56994.0082	0.0005	0.0052	84
139	56994.2853	0.0007	0.0162	86

*BJD-2400000.

 † Against max = 2456985.0214 + 0.066531 E . ‡ Number of points used to determine the maximum.**Table 23.** Superhump maxima of UV Per (2014) (continued)

E	max*	error	$O - C^\dagger$	N^\ddagger
140	56994.3377	0.0003	0.0020	132
141	56994.4057	0.0003	0.0034	111
168	56996.1959	0.0008	-0.0026	122
169	56996.2606	0.0008	-0.0045	144
170	56996.3341	0.0010	0.0025	137
181	56997.0521	0.0008	-0.0114	86
182	56997.1194	0.0005	-0.0106	215
183	56997.1858	0.0007	-0.0108	202
196	56998.0429	0.0010	-0.0185	65
197	56998.1092	0.0008	-0.0188	62
198	56998.1802	0.0017	-0.0143	49

*BJD-2400000.

 † Against max = 2456985.0214 + 0.066531 E . ‡ Number of points used to determine the maximum.**Fig. 26.** Superhumps in HY Psc (2014) before BJD 2456873. (Upper): PDM analysis. (Lower): Phase-averaged profile.

reported during the declining branch (vsnet-alert 9004). In Gänsicke et al. (2009), there was an orbital period of 110.51(24) min [0.07674(17) d] by Dillon et al., but this observation has not yet been published. On 2010 January 3, J. Shears detected a bright outburst at 13.6 mag (cvnet-outburst 3532). Although this outburst was a long one, superhumps were not confidently detected.

The 2014 outburst was detected by the ASAS-SN team (vsnet-alert 17560) at $V=13.27$ on July 28. Although superhumps were securely detected, the limited observation time in the morning sky did not enable an unique selection of the superhump period (vsnet-alert 17577, 17602). Based on the best observed part of the data (BJD before 2456873), two periods of 0.07994(2) d and 0.07788(2) d remained viable. Since the period 0.080 d better expressed nightly observations, we list the times of maxima based on this selection of the period (table 24). Both periods, however, give anomalous ϵ if assume an orbital period of 0.07674(17) d. Both the orbital and superhump periods need to be confirmed by further observations. The later part of the data (BJD after 2456873) gave a period of 0.07981(2) d with a more irregular profile. We are not confident whether this period corresponds to stage C superhump due to the lack of observations.

Table 24. Superhump maxima of HY Psc (2014)

E	max*	error	$O - C^\dagger$	N^\ddagger
0	56869.1790	0.0003	-0.0022	109
1	56869.2615	0.0002	0.0004	171
38	56872.2221	0.0004	0.0036	145
74	56875.0941	0.0011	-0.0019	40

*BJD-2400000.

 † Against max = 2456869.1811 + 0.079930 E . ‡ Number of points used to determine the maximum.

3.23. *QW Serpentis*

This object was identified as an SU UMa-type dwarf nova in 2003 (Patterson et al. 2003; Olech et al. 2003; Nogami et al. 2004). See Kato et al. (2014b) for more history.

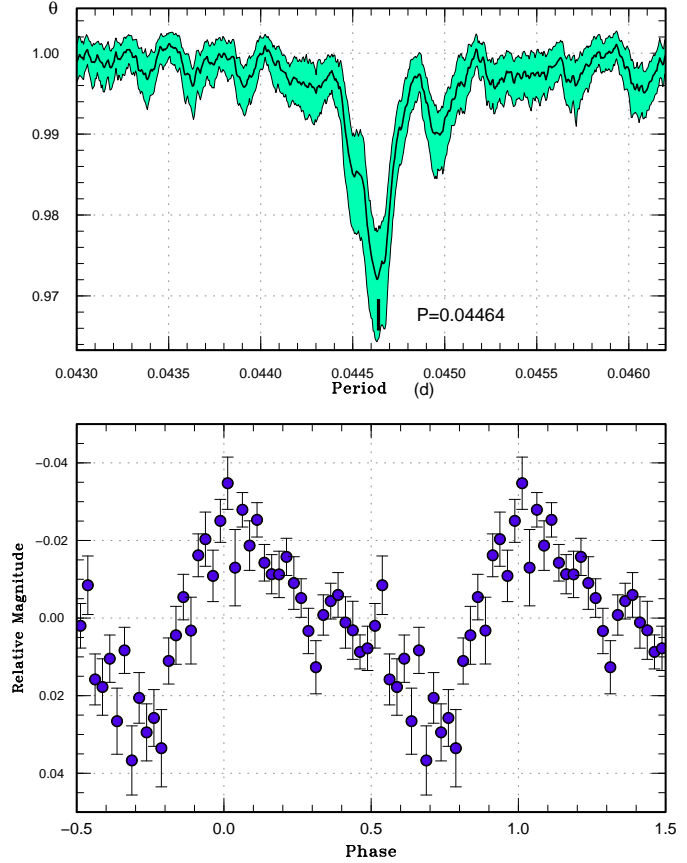
The 2014 superoutburst was detected by MASTER-Tunka on February 25 (vsnet-alert 16951). The observations on March 2 detected superhumps. Only two times of superhumps were obtained: BJD 2456718.5235(9) ($N = 79$), 2456718.5991(15) ($N = 77$).

3.24. *V418 Serpentis*

This object (=ROTSE3 J151453.6+020934.2) was discovered as a dwarf nova (Rykoff et al. 2004). Although the variable star designation was given in Kazarovets et al. (2011), only little had been known until the outburst detection by CRTS on 2014 May 21 (cf. vsnet-alert 17320). Subsequent time-resolved photometry indicated that this object is an SU UMa-type dwarf nova below the period minimum by the detection of superhumps (vsnet-alert 17321, 17322; figure 27). The times of superhump maxima are listed in table 25. A very clear stage B-C transition was recorded (vsnet-alert 17349, 17358). Spectroscopic observation clarified that this object contains hydrogen, ruling out the possibility of an AM CVn-type object (Garnavich et al. 2014). The spectroscopic appearance was very similar to SBS 1108+574 (Littlefield et al. 2013; Carter et al. 2013b) making this object a new member of EI Psc-type objects.

Among EI Psc-type objects, SBS 1108+574 was the first in which distinct stages B and C were recorded (Kato et al. 2013a). Another well-established object is CSS J174033.5+414756 (T. Ohshima et al. in preparation; subsection 3.81). V418 Ser is the third object in this class of objects in which distinct stages B and C are recorded (figure 28). It was likely the early phase of stage B was not observed. There was an apparent increase in the superhump period after the stage B-C transition, a phenomenon similar to what is observed in hydrogen-rich CVs (Kato et al. 2009) and in SBS 1108+574 (Kato et al. 2013a). The fractional decrease of the superhump period ($\sim 0.5\%$) between stage B and C was also similar to those in hydrogen-rich CVs (Kato et al. 2009). A comparison of these three objects has shown that the stage transition in EI Psc-type objects are similar to ordinary hydrogen-rich CVs.

In the AAVSO database, one observer detected a rise to

**Fig. 27.** Superhumps in V418 Ser (2014). (Upper): PDM analysis. (Lower): Phase-averaged profile.

$V=16.02$ on May 16. The entire duration of the superoutburst was 20–21 d, somewhat shorter than the one in SBS 1108+574 (Kato et al. 2013a) and CSS J174033.5+414756 (T. Ohshima et al. in preparation).

3.25. *V701 Tauri*

V701 Tau was discovered by Erastova (1973) as an eruptive object. Since this “eruption” lasted more than ten days, the object was considered to be a dwarf nova and has been monitored by amateur observers. The initial superoutburst was recorded in 1995 December (vsnet-alert 303). Shears, Boyd (2007) further reported the 2005 superoutburst and obtained a superhump period of 0.0690(2) d. The 1995 superoutburst was analyzed in (Kato et al. 2009) as well as the 2005 superoutburst. Although there was also a well-recorded superoutburst in 2007 March (e.g. vsnet-outburst 7535), superhumps were not sufficiently observed.

The 2015 superoutburst was detected by K. Paxson on February 16 (vsnet-alert 18301). This is the first secure superoutburst since 2007. Subsequent observations detected superhumps (vsnet-alert 18308, 18312). The times of superhump maxima are listed in table 26. Although $E = 0$ appears to be a stage A superhump (figure 29), the period of stage A superhumps could not be determined.

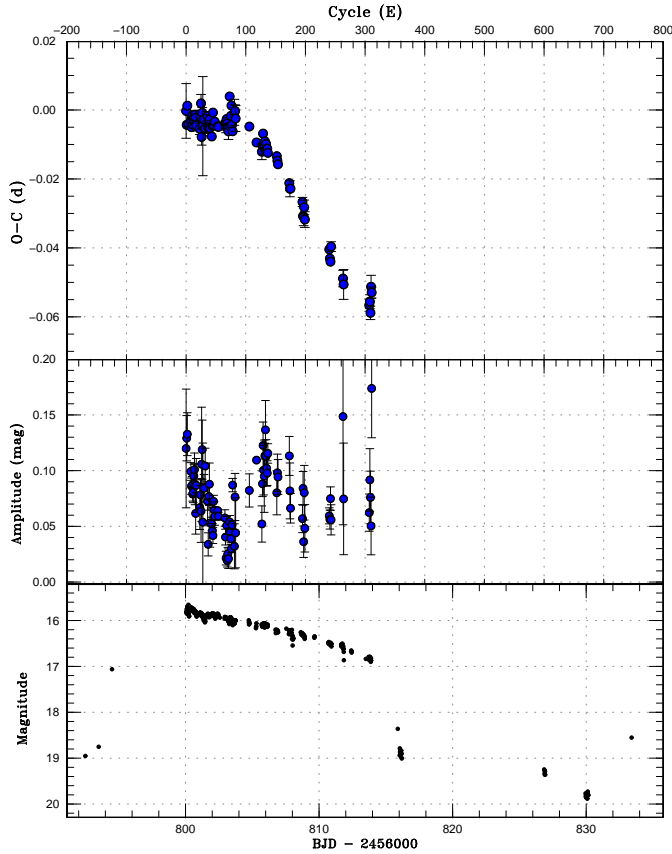


Fig. 28. $O - C$ diagram of superhumps in V418 Ser (2014). (Upper:) $O - C$ diagram. We used a period of 0.04467 d for calculating the $O - C$ residuals. (Middle:) Amplitudes of superhumps. There was a slight tendency of regrowth of superhumps after the stage B–C transition. (Lower:) Light curve. The data were binned to 0.015 d. The detection of an outburst on BJD 2456794 appears to be secure. The seemingly rebrightening on BJD 2456833 may not be real since this magnitude was similar to the pre-outburst observations of the same observer.

3.26. *SU Ursae Majoris*

This famous dwarf nova (=5.1908) was discovered by Ceraski (1908). Hoffmeister identified this object to be a U Gem-type object with cycle lengths of 10–20 d. Elvey, Babcock (1943) observed the object in outburst and obtained a spectrum B5 with $H\alpha$ emission. Petit (1960) reported a summary of outbursts and identified long and short outbursts. According to this literature, Brun and Petit considered a class of SU UMa-type variables and introduced a concept of supermaxima in 1952. Isles (1974) also reported historical variations in 1926–1954 and proposed a mean cycle length between long outbursts to be 170 d. Thorstensen et al. (1986) determined the orbital period by a radial-velocity study. Although the object had long been proposed to be the prototype of SU UMa-type dwarf novae, it was only in 1989 when superhumps were detected during a superoutburst Udalski (1990), after unsuccessful reports before a superoutburst (Barwig, Schoembs 1981) and during a normal outburst (Udalski

Table 25. Superhump maxima of V418 Ser (2014)

E	max*	error	$O - C^\dagger$	N^\ddagger
0	56800.0447	0.0079	−0.0051	41
1	56800.0854	0.0009	−0.0089	75
2	56800.1356	0.0008	−0.0032	78
4	56800.2196	0.0006	−0.0082	56
8	56800.3992	0.0004	−0.0065	52
9	56800.4420	0.0005	−0.0082	55
10	56800.4900	0.0005	−0.0048	51
11	56800.5322	0.0005	−0.0071	48
12	56800.5784	0.0006	−0.0053	48
13	56800.6223	0.0006	−0.0059	100
14	56800.6673	0.0008	−0.0054	78
15	56800.7137	0.0012	−0.0036	78
16	56800.7575	0.0021	−0.0043	64
17	56800.7999	0.0016	−0.0064	74
23	56801.0669	0.0016	−0.0063	48
24	56801.1151	0.0011	−0.0027	90
25	56801.1637	0.0026	0.0014	52
26	56801.1986	0.0024	−0.0081	57
27	56801.2503	0.0015	−0.0009	91
28	56801.2911	0.0144	−0.0047	39
30	56801.3824	0.0008	−0.0023	35
32	56801.4692	0.0008	−0.0046	35
36	56801.6513	0.0014	−0.0004	78
37	56801.6927	0.0017	−0.0035	120
38	56801.7381	0.0009	−0.0026	120
39	56801.7844	0.0014	−0.0009	83
40	56801.8266	0.0022	−0.0032	37
43	56801.9581	0.0007	−0.0051	44
44	56802.0059	0.0009	−0.0018	37
45	56802.0544	0.0010	0.0022	44
46	56802.0955	0.0004	−0.0012	42
47	56802.1400	0.0006	−0.0012	44
48	56802.1858	0.0007	0.0001	43

*BJD−2400000.

† Against max = 2456800.0498 + 0.044498 E .

‡ Number of points used to determine the maximum.

1988). This delay of detection of superhumps was partly caused by the decrease of frequency of superoutbursts between 1980 and 1989, which prevented scheduled observational campaigns (cf. Udalski 1990).

We reported observations of the 1999, 2010 and 2013 superoutbursts in Kato et al. (2009), Kato et al. (2010) and Kato et al. (2014a), respectively.

The rise to the 2014–2015 superoutburst took place on 2014 December 27 according to the AAVSO data. The outburst was a precursor outburst and the final rise to the superoutburst was on 2015 January 1–2 (vsnet-alert 18142; figure 30). There was a post-superoutburst rebrightening on January 18–19 (figure 30). Time-resolved photometry was obtained rather fragmentarily. Although there were also observations in the late stage of the plateau phase, superhumps became unclear. Only the times of superhump maxima in the earlier stage of the superoutburst

Table 25. Superhump maxima of V418 Ser (2014) (continued)

E	max*	error	$O - C^\dagger$	N^\ddagger
53	56802.4078	0.0003	-0.0004	131
54	56802.4523	0.0003	-0.0004	102
65	56802.9447	0.0007	0.0025	40
66	56802.9894	0.0010	0.0027	43
67	56803.0329	0.0016	0.0017	43
68	56803.0799	0.0009	0.0043	42
69	56803.1233	0.0017	0.0032	41
70	56803.1669	0.0013	0.0022	41
71	56803.2104	0.0023	0.0012	39
73	56803.3098	0.0007	0.0117	129
74	56803.3458	0.0005	0.0032	132
75	56803.3935	0.0005	0.0064	132
76	56803.4412	0.0007	0.0095	133
77	56803.4803	0.0004	0.0042	130
78	56803.5231	0.0004	0.0024	132
81	56803.6626	0.0038	0.0085	76
82	56803.7077	0.0018	0.0090	77
83	56803.7501	0.0038	0.0070	64
106	56804.7752	0.0010	0.0086	41
118	56805.3066	0.0002	0.0061	91
127	56805.7060	0.0023	0.0049	30
128	56805.7524	0.0007	0.0068	47
129	56805.8006	0.0006	0.0105	29
130	56805.8421	0.0012	0.0076	43
131	56805.8860	0.0020	0.0070	35
132	56805.9324	0.0006	0.0088	56
133	56805.9744	0.0012	0.0064	91
134	56806.0209	0.0007	0.0084	137
135	56806.0642	0.0010	0.0072	93
136	56806.1089	0.0006	0.0074	42
137	56806.1524	0.0004	0.0063	34
152	56806.8214	0.0011	0.0079	35

*BJD-2400000.

 † Against max = 2456800.0498 + 0.044498 E . ‡ Number of points used to determine the maximum.

are listed in table 27. A comparison of $O - C$ diagrams suggests that the superhumps started to grow around the maximum of the precursor outburst in the 2014 superoutburst (figure 31).

3.27. CY Ursae Majoris

This object was identified as an SU UMa-type dwarf nova in 1988 (Kato et al. 1988; Kato 1997b). The correct superhump period was established by Harvey, Patterson (1995). See Kato et al. (2014b) for more history.

The 2014 superoutburst was detected by H. Maehara (vsnet-alert 16967), which started as a separate precursor outburst on March 3. The object once faded, but was detected in outburst again after six days (vsnet-alert 16998). This outburst turned out to be a genuine superoutburst. Such a separate precursor was first observed in CY UMa.

The times of superhump maxima are listed in table 28. Although $E = 0$ corresponded to the growing stage of su-

Table 25. Superhump maxima of V418 Ser (2014) (continued)

E	max*	error	$O - C^\dagger$	N^\ddagger
153	56806.8648	0.0009	0.0068	40
154	56806.9084	0.0009	0.0059	41
173	56807.7517	0.0009	0.0037	35
174	56807.7947	0.0023	0.0023	32
175	56807.8394	0.0013	0.0025	41
195	56808.7290	0.0013	0.0021	66
196	56808.7696	0.0011	-0.0019	83
197	56808.8140	0.0026	-0.0019	68
198	56808.8614	0.0021	0.0010	55
199	56808.9026	0.0023	-0.0024	32
240	56810.7254	0.0008	-0.0040	74
241	56810.7674	0.0010	-0.0065	107
242	56810.8111	0.0008	-0.0072	88
243	56810.8602	0.0014	-0.0027	79
263	56811.7443	0.0024	-0.0085	16
264	56811.7873	0.0043	-0.0100	28
307	56813.7021	0.0018	-0.0086	31
308	56813.7478	0.0020	-0.0075	32
309	56813.7892	0.0019	-0.0105	32
310	56813.8414	0.0033	-0.0028	32
311	56813.8844	0.0016	-0.0043	32

*BJD-2400000.

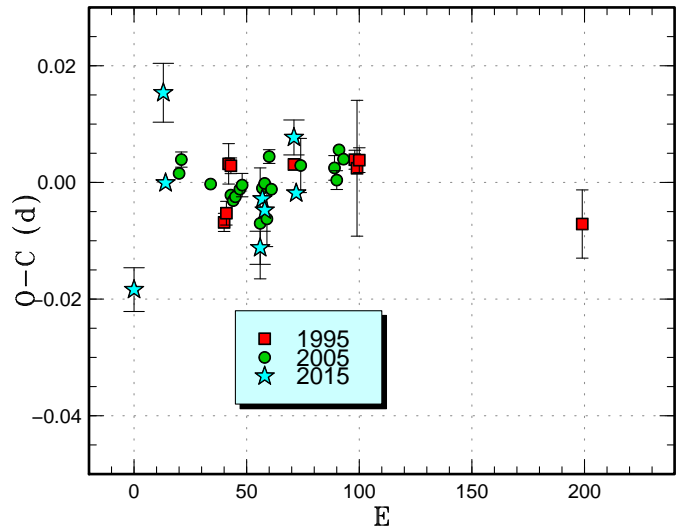
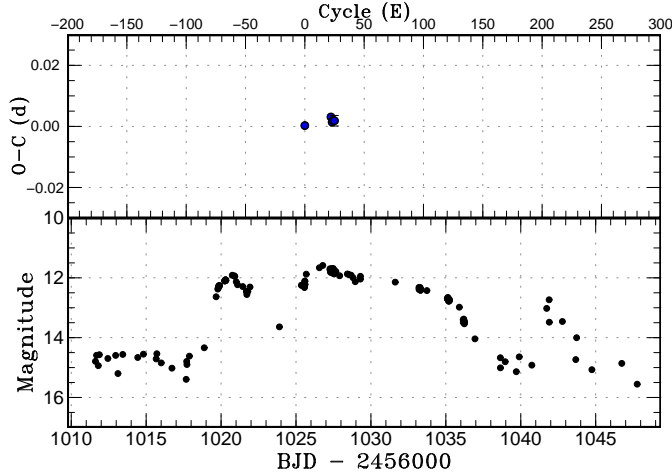
 † Against max = 2456800.0498 + 0.044498 E . ‡ Number of points used to determine the maximum.

Fig. 29. Comparison of $O - C$ diagrams of V701 Tau between different superoutbursts. A period of 0.06899 d was used to draw this figure. Approximate cycle counts (E) after the start of the superoutburst were used. We assumed that the 2015 superoutburst was detected soon after the maximum and shifted other superoutbursts to get the best fit.

Table 26. Superhump maxima of V701 Tau (2015)

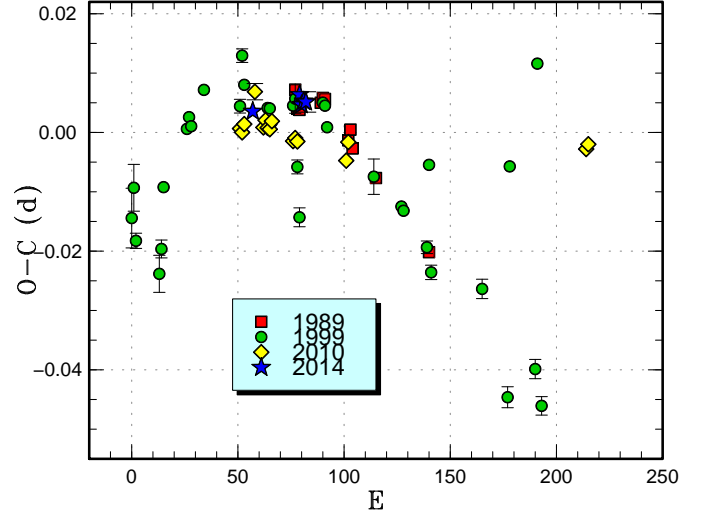
E	max*	error	$O - C^\dagger$	N^\ddagger
0	57070.3621	0.0038	-0.0147	68
13	57071.2927	0.0050	0.0186	41
14	57071.3462	0.0008	0.0031	75
56	57074.2327	0.0028	-0.0097	27
57	57074.3101	0.0005	-0.0014	77
58	57074.3771	0.0010	-0.0034	77
71	57075.2865	0.0030	0.0086	37
72	57075.3459	0.0006	-0.0010	67

*BJD-2400000.

 † Against max = 2457070.3768 + 0.069030 E . ‡ Number of points used to determine the maximum.**Fig. 30.** $O - C$ diagram of superhumps in SU UMa (2014). (Upper): $O - C$ diagram. A period of 0.07918 d was used to draw this figure. (Lower): Light curve. The observations were binned to 0.01 d. A precursor outburst and a post-superoutburst rebrightening were clearly recorded.**Table 27.** Superhump maxima of SU UMa (2014)

E	max*	error	$O - C^\dagger$	N^\ddagger
0	57025.5893	0.0006	-0.0001	36
22	57027.3341	0.0010	0.0011	166
23	57027.4115	0.0005	-0.0006	146
24	57027.4913	0.0006	-0.0001	160
25	57027.5704	0.0017	-0.0003	49

*BJD-2400000.

 † Against max = 2457025.5894 + 0.079252 E . ‡ Number of points used to determine the maximum.**Fig. 31.** Comparison of $O - C$ diagrams of SU UMa between different superoutbursts. A period of 0.07918 d was used to draw this figure. Approximate cycle counts (E) after the start of the superoutburst were used. For the 2014 superoutburst, the cycle count from the maximum of the precursor outburst was used. The two epochs in the 2010 data may be traditional late superhumps.

perhumps (during the final rise to the superoutburst), the period of stage A superhumps was not meaningfully determined. The transition from stage B to C was rather smooth in this object and the distinction between these stages is rather ambiguous. The epochs for $E \geq 125$ correspond to the rapid fading phase and post-superoutburst phase. Since the observations were rather fragmentary in these phases, we did not attempt to determine the period after the superoutburst.

A comparison of the $O - C$ diagrams (figure 32) indicates that the $O - C$ diagram of the 2014 superoutburst well matched the others if we assume that superhumps started to grow 22 cycles before $E = 0$. It implies that the duration of stage A was 2.0 d (up to $E = 5$), and it is evident that superhumps started to grow after the precursor outburst.

Since there is no published statistics of outbursts of CY UMa, we summarized the list of outbursts from the readily available data (table 29). It has become evident that normal outbursts were more frequently recorded in the late 1980s to early 1990s. Most of superoutbursts were detected except two between 1989 and 1991, one between 2006 and 2008 and likely three between 2010 and 2013. These outburst detections heavily relied on a few expert observers, and the variation of the activity of these observers strongly affected the detections. The lack of superoutburst between 2010 and 2013 was probably a result of the decrease of visual observers regularly watching this object. This decrease has been partly compensated by CCD monitoring, but it is not still sufficient particularly around solar conjunctions. It has also become evident that supercycle length has experienced a dramatic change

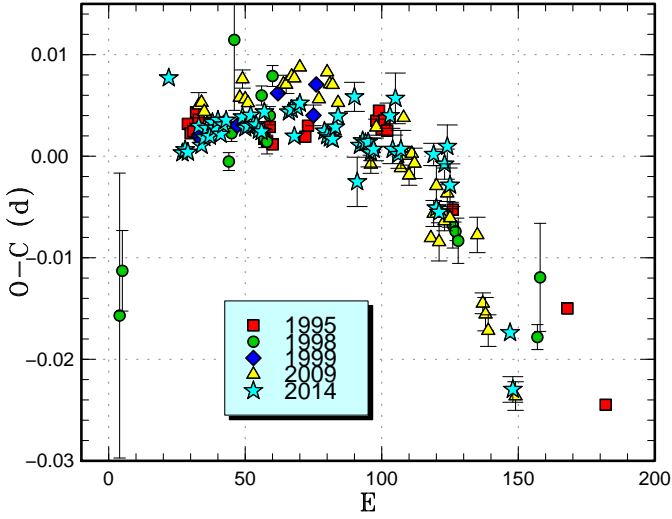


Fig. 32. Comparison of $O - C$ diagrams of CY UMa between different superoutbursts. A period of 0.07212 d was used to draw this figure. Approximate cycle counts (E) after the start of the superoutburst were used. The 2014 superoutburst was shifted by 22 cycles to best match the others.

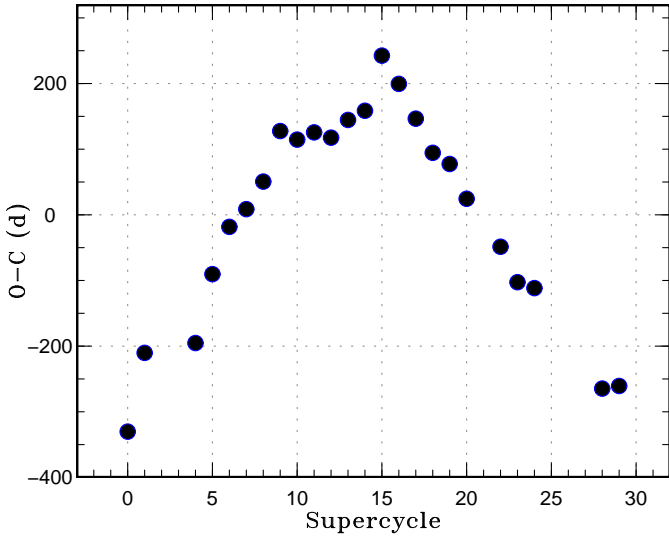


Fig. 33. $O - C$ diagram of superoutbursts in CY UMa. The ephemeris used was $\text{Max}(\text{JD}) = 2447824 + 327.0E$. In 2003, the supercycle suddenly decreased from 362 d to 290 d.

around 2003 (figure 33). Before 2003 (JD 2452545), the mean supercycle was 362(3) d. After this, the value decreased to 290(1) d. Since this change was not apparently associated with the increase of normal outbursts, it is less likely to be a result of an increased mass-transfer rate. It would be interesting to see the evolution of the supercycle length in future.

Table 28. Superhump maxima of CY UMa (2014)

E	max*	error	$O - C^\dagger$	N^\ddagger
0	56726.1519	0.0006	0.0080	131
5	56726.5052	0.0002	0.0003	101
6	56726.5776	0.0002	0.0006	158
7	56726.6495	0.0002	0.0003	137
11	56726.9405	0.0005	0.0026	71
12	56727.0107	0.0005	0.0007	79
13	56727.0836	0.0003	0.0014	155
14	56727.1567	0.0002	0.0022	177
15	56727.2280	0.0002	0.0014	220
16	56727.3015	0.0002	0.0027	238
17	56727.3730	0.0002	0.0021	155
18	56727.4459	0.0002	0.0028	149
19	56727.5167	0.0002	0.0014	153
20	56727.5897	0.0003	0.0022	154
21	56727.6623	0.0005	0.0026	67
27	56728.0953	0.0004	0.0026	127
28	56728.1664	0.0005	0.0015	233
29	56728.2387	0.0006	0.0016	205
30	56728.3119	0.0004	0.0026	231
31	56728.3830	0.0003	0.0017	127
32	56728.4552	0.0002	0.0016	189
33	56728.5268	0.0003	0.0010	199
34	56728.5987	0.0004	0.0008	155
35	56728.6728	0.0006	0.0027	46
44	56729.3219	0.0007	0.0022	99
45	56729.3942	0.0004	0.0024	116
46	56729.4637	0.0003	-0.0003	174
47	56729.5387	0.0003	0.0025	161
48	56729.6112	0.0003	0.0029	144
57	56730.2575	0.0007	-0.0004	137
58	56730.3292	0.0005	-0.0009	148
59	56730.4011	0.0003	-0.0012	120

*BJD-2400000.

† Against max = $2456726.1440 + 0.072174E$.

‡ Number of points used to determine the maximum.

3.28. QZ Virginis

QZ Vir (former T Leo) is the second dwarf nova discovered in the history. See Kato (1997a) for a summary of the history. In recent years, this object has shown superoutbursts approximately once a year.

The 2014 superoutburst was detected by R. Modic in relatively early phase (vsnet-alert 17291). After further brightening (vsnet-alert 17296), evolving superhumps were observed (vsnet-alert 17301). This part was later found to be a precursor part of a superoutburst and fully developed superhumps were recorded near the peak brightness. The times of superhump maxima during the superoutburst plateau are listed in table 30. All stages A–C were recorded (see also figure 34). After the plateau phase, superhumps were also continuously observed (table 31). The superhumps in the post-superoutburst phase were on a smooth continuation of stage C superhumps, and there was no phase ~ 0.5 jump as expected for “tradi-

Table 29. List of recent outbursts of CY UMa.

Year	Month	max*	magnitude	type	source
1988	1	47167	12.3	super	VSOLJ; Kato et al. (1988); Kato (1997b)
1988	5	47299	12.5	normal	VSOLJ; Watanabe et al. (1989)
1988	10	47464	12.2	normal	VSOLJ; Watanabe et al. (1989)
1989	1	47528	12.9	normal	VSOLJ; Watanabe et al. (1989)
1989	3	47614	12.3	super	P. Schmeer; Watanabe et al. (1989)
1989	6	47679	12.8	normal	VSOLJ
1990	1	47915	12.5	normal	VSOLJ
1990	4	47986	12.9	normal	VSOLJ, AAVSO
1990	9	48156	12.3	normal	VSOLJ, AAVSO
1990	12	48252	13.3	normal	Schmeer
1991	3	48335	13.3	normal	VSOLJ, AAVSO
1991	12	48610	12.8	super	VSOLJ, AAVSO; Kato (1995)
1993	2	49042	12.2	super	VSOLJ, AAVSO
1993	6	49155	12.9	normal	AAVSO
1994	3	49441	11.7	super	VSOLJ, AAVSO
1995	3	49795	12.1	super	VSOLJ, AAVSO; Harvey, Patterson (1995); Kato et al. (2009)
1995	5	49859	13.0	normal	AAVSO
1995	7	49915	13.3	normal	AAVSO
1996	3	50164	12.2	super	AAVSO, VSOLJ
1996	6	50245	13.4	normal	AAVSO
1996	12	50442	12.9	normal	AAVSO
1997	3	50516	14.1	? [†]	AAVSO
1997	3	50520	13.7	? [‡]	AAVSO
1997	4	50559	12.6	precursor? [†]	AAVSO
1997	4	50568	12.3	super	AAVSO, VSOLJ
1997	10	50726	12.6	normal	AAVSO
1998	3	50882	12.4	super	AAVSO, VSOLJ; Kato et al. (2009)
1998	5	50948	13.8	normal	AAVSO
1998	12	51167	13.2	normal [§]	VSOLJ
1999	2	51220	12.5	super	AAVSO, VSOLJ; Kato, Matsumoto (1999); Kato et al. (2009)
1999	6	51335	12.8	normal	AAVSO
1999	12	51539	12.5	super	AAVSO, VSOLJ
2000	2	51600	13.0	normal	AAVSO
2000	4	51654	13.2	normal	AAVSO

*JD−2400000.

[†]CCD single detection.[‡]Detection by two visual observers, but contradict a CCD observation two hours later.[§]Single visual detection.

Table 29. List of recent outbursts of CY UMa (continued).

Year	Month	max*	magnitude	type	source
2000	6	51716	13.1	normal	AAVSO
2000	12	51893	12.5	super	AAVSO, VSOLJ
2001	6	52064	13.1	normal	AAVSO
2001	11	52234	12.3	super	AAVSO
2002	1	52300	13.9	normal	AAVSO
2002	5	52422	12.9	normal	AAVSO
2002	11	52601	12.9	normal [†]	AAVSO
2003	1	52645	12.4	super	AAVSO, VSOLJ
2003	3	52717	12.7	normal	AAVSO
2003	6	52818	12.9	normal [†]	AAVSO
2003	10	52929	12.3	super	AAVSO
2003	12	52998	14.4 [§]	normal	AAVSO
2004	2	53055	13.0	normal	AAVSO, VSOLJ
2004	4	53122	12.9	normal	AAVSO
2004	7	53203	12.3	super	AAVSO
2004	11	53315	12.3	normal	AAVSO
2005	1	53398	12.9	normal	AAVSO
2005	4	53478	12.5	super	AAVSO, VSOLJ
2005	11	53676	12.5	normal	AAVSO
2006	2	53788	12.8	super	AAVSO
2006	6	53802	13.8	normal	AAVSO
2006	11	54062	12.4	super	vsnet-alert 9148; AAVSO
2007	4	54195	13.0	normal	AAVSO
2008	6	54643	12.5	super	AAVSO
2009	3	54916	12.6	super	vsnet-alert 11127; AAVSO; Kato et al. (2009)
2009	5	54972	12.6	normal	AAVSO
2010	2	55234	12.3	super	vsnet-alert 11811; AAVSO
2010	4	55302	13.2	normal [†]	AAVSO
2010	5	55330	15.1	normal [†]	AAVSO
2010	12	55558	13.5	normal	AAVSO
2011	2	55615	13.3	normal	AAVSO
2012	1	55944	14.6	normal [†]	AAVSO
2012	2	55986	13.1	normal [†]	AAVSO
2012	5	56078	13.7	normal [§]	AAVSO
2013	4	56389	12.5	super	vsnet-alert 15596; AAVSO
2014	3	56720	12.6	precursor + super	vsnet-alert 16967; this paper

*JD−2400000.

[†]CCD single detection.[‡]Detection by two visual observers, but contradict a CCD observation two hours later.[§]Single visual detection.

Table 28. Superhump maxima of CY UMa (2014) (continued)

E	max*	error	$O - C^\dagger$	N^\ddagger
60	56730.4731	0.0004	-0.0014	151
61	56730.5464	0.0003	-0.0002	155
62	56730.6196	0.0004	0.0008	104
68	56731.0542	0.0014	0.0024	41
69	56731.1180	0.0024	-0.0060	27
70	56731.1937	0.0004	-0.0025	235
71	56731.2663	0.0004	-0.0021	244
72	56731.3382	0.0003	-0.0023	230
73	56731.4104	0.0007	-0.0023	79
74	56731.4815	0.0014	-0.0034	57
75	56731.5539	0.0011	-0.0032	68
81	56731.9899	0.0012	-0.0002	54
82	56732.0587	0.0014	-0.0035	54
83	56732.1359	0.0025	0.0014	127
84	56732.2025	0.0009	-0.0042	215
85	56732.2751	0.0019	-0.0037	71
97	56733.1400	0.0011	-0.0048	138
98	56733.2069	0.0009	-0.0102	167
99	56733.2786	0.0004	-0.0107	133
101	56733.4276	0.0015	-0.0060	18
102	56733.5014	0.0021	-0.0043	34
103	56733.5697	0.0021	-0.0082	35
125	56735.1419	0.0007	-0.0239	68
126	56735.2084	0.0013	-0.0296	110
156	56737.4295	0.0014	0.0263	36
170	56738.4478	0.0008	0.0342	38
181	56739.2186	0.0006	0.0111	73
182	56739.2815	0.0011	0.0018	76

*BJD-2400000.

 † Against max = 2456726.1440 + 0.072174 E . ‡ Number of points used to determine the maximum.

tional" late superhumps. This finding confirmed the earlier finding (Kato et al. 2009).

Although stage A superhumps were detected, the coverage of the 2014 observation was not good enough to determine the period sufficiently. An analysis of the $O - C$ data suggested a period of 0.0625(3) d, which corresponds to $q=0.18(2)$. However, since the baseline is only 1 d and the coverage was not so good, we should not heavily rely on this value. The absence of stage A superhumps during the 1993 superoutburst still remains a mystery (Kato 1997a; Kato et al. 2009). If we can shift the $O - C$ diagram of the 1993 superoutburst by 50 cycles, the resultant $O - C$ diagram appears to fit the others (figure 34; this figure used the data in Ohshima et al. 2011). This implies that superhumps started to grow 3 d earlier than the precursor outburst. If superhumps had already grown at the time of the precursor outburst, the lack of stage A superhumps may be reconciled, although such early development of superhumps may be a challenge to the standard thermal-tidal disk instability model.

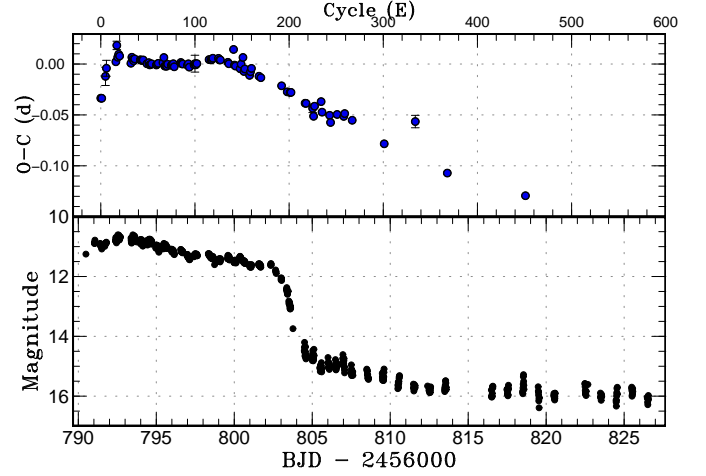
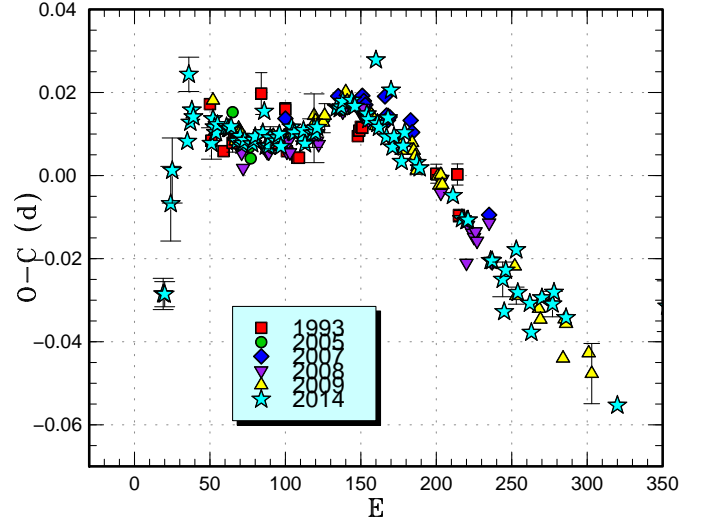
**Fig. 34.** $O - C$ diagram of superhumps in QZ Vir (2014). (Upper): $O - C$ diagram. A period of 0.06038 d was used to draw this figure. (Lower): Light curve. The observations were binned to 0.01 d.**Fig. 35.** Comparison of $O - C$ diagrams of QZ Vir between different superoutbursts. A period of 0.06032 d was used to draw this figure. Approximate cycle counts (E) after the starts of outbursts were used. Since the starts of the 2005, 2007 and 2008 superoutbursts were not well constrained, we shifted the $O - C$ diagrams to best fit the others. The 1993 superoutburst was shifted by 50 cycles, which implies that superhumps started to grow 3 d before the precursor.

Table 30. Superhump maxima of QZ Vir (2014)

E	max*	error	$O - C^\dagger$	N^\ddagger
0	56791.4075	0.0038	-0.0334	27
1	56791.4677	0.0030	-0.0335	23
5	56791.7308	0.0090	-0.0120	83
6	56791.7991	0.0078	-0.0041	78
16	56792.4093	0.0017	0.0024	56
17	56792.4858	0.0041	0.0185	26
18	56792.5345	0.0005	0.0069	32
19	56792.5978	0.0005	0.0097	19
20	56792.6565	0.0018	0.0080	6
32	56793.3739	0.0038	0.0010	22
33	56793.4402	0.0008	0.0068	28
34	56793.4985	0.0004	0.0048	22
35	56793.5575	0.0006	0.0034	31
36	56793.6197	0.0006	0.0052	25
42	56793.9811	0.0005	0.0044	437
43	56794.0410	0.0001	0.0039	1235
44	56794.1013	0.0002	0.0038	1248
45	56794.1621	0.0008	0.0043	137
49	56794.3999	0.0011	0.0005	29
51	56794.5217	0.0007	0.0016	32
52	56794.5799	0.0003	-0.0006	82
53	56794.6406	0.0004	-0.0003	100
54	56794.7017	0.0002	0.0005	159
59	56795.0025	0.0003	-0.0007	339
60	56795.0637	0.0002	0.0002	326
61	56795.1248	0.0003	0.0009	474
66	56795.4274	0.0003	0.0016	242
67	56795.4929	0.0009	0.0067	25
68	56795.5448	0.0009	-0.0018	49
69	56795.6053	0.0004	-0.0016	110
70	56795.6654	0.0005	-0.0019	86
71	56795.7278	0.0027	0.0001	26
75	56795.9682	0.0018	-0.0009	101
76	56796.0294	0.0002	-0.0002	450

*BJD-2400000.

 † Against max = 2456791.4409 + 0.060377*E*. ‡ Number of points used to determine the maximum.**Table 30.** Superhump maxima of QZ Vir (2014) (continued)

E	max*	error	$O - C^\dagger$	N^\ddagger
77	56796.0906	0.0002	0.0006	513
78	56796.1479	0.0009	-0.0024	259
85	56796.5748	0.0017	0.0019	26
86	56796.6339	0.0006	0.0006	83
87	56796.6941	0.0011	0.0004	81
92	56796.9947	0.0009	-0.0009	142
93	56797.0566	0.0003	0.0006	485
94	56797.1136	0.0007	-0.0027	394
99	56797.4179	0.0034	-0.0004	18
100	56797.4793	0.0083	0.0007	10
101	56797.5386	0.0016	-0.0004	41
102	56797.6002	0.0006	0.0008	100
115	56798.3891	0.0006	0.0048	132
117	56798.5095	0.0016	0.0044	29
118	56798.5702	0.0008	0.0048	84
119	56798.6319	0.0005	0.0061	93
125	56798.9941	0.0007	0.0060	65
126	56799.0529	0.0006	0.0044	64
127	56799.1133	0.0009	0.0045	39
135	56799.5940	0.0003	0.0022	85
136	56799.6529	0.0005	0.0007	88
141	56799.9689	0.0016	0.0148	48
142	56800.0139	0.0006	-0.0005	76
143	56800.0733	0.0006	-0.0015	79
148	56800.3726	0.0006	-0.0041	114
149	56800.4375	0.0012	0.0004	63
151	56800.5648	0.0014	0.0070	55
152	56800.6114	0.0007	-0.0068	82
153	56800.6743	0.0007	-0.0043	82
158	56800.9699	0.0012	-0.0106	64
159	56801.0339	0.0010	-0.0069	104
160	56801.0975	0.0012	-0.0038	26
168	56801.5729	0.0008	-0.0114	67
170	56801.6922	0.0010	-0.0128	54

*BJD-2400000.

 † Against max = 2456791.4409 + 0.060377*E*. ‡ Number of points used to determine the maximum.

3.29. NSV 1436

NSV 1436 was one of variable stars (Ross 4) reported in Ross (1925). Although Ross (1925) gave a photographic range of 12–16 mag, the variability type was not known. T. Kato pointed out in 2000 that the object can be identified with an ROSAT X-ray source (vsnet-chat 3326).¹¹ Starting from 2000, a search for outburst started mostly by visual observers. This attempt had been unsuccessful up to 2010. In Brown et al. (2010), studied the historical photographic material and characterized two outbursts in 1904 and 1948. The object was mostly in faint state fainter than 15.8 mag and occasionally observed in outburst. Brown et al. (2010) suggested that the object might be a recurrent nova.

¹¹ Brown et al. (2010) incorrectly gave the first reference of the ROSAT identification of this object.

In 2011, a fresh outburst was reported by E. Muyliaert at an unfiltered CCD magnitude of 13.49 on March 28, and the outburst was confirmed by M. Linnolt a visual magnitude of 12.8. There was a suspected fainter outburst on March 9 (Templeton 2011). Despite an intensive observing campaign, the object rapidly faded. Osborne et al. (2011) observed this outburst with Swift satellite and found that the X-ray properties were not those of a recurrent nova. The optical light variation suggested the dwarf nova classification (Osborne et al. 2011).

A total of 14 outbursts were recorded between 2011 and 2014 March, and the object was found to undergo outbursts more frequently than supposed. Pagnotta, Schaefer (2014) also listed this object as an ordinary dwarf nova.

In 2014 September, a bright outburst of this object was visually detected by P. Schmeer (11.8 mag on September 15, vsnet-alert 17729). Subsequent observations finally

Table 31. Superhump maxima of QZ Vir (2014) (post-superoutburst)

E	max*	error	$O - C^\dagger$	N^\ddagger
0	56803.0126	0.0002	0.0059	240
6	56803.3689	0.0005	0.0022	131
9	56803.5494	0.0007	0.0028	28
10	56803.6099	0.0007	0.0033	19
25	56804.5049	0.0010	-0.0015	27
26	56804.5652	0.0011	-0.0013	27
33	56804.9830	0.0042	-0.0034	22
34	56805.0355	0.0004	-0.0109	331
35	56805.1058	0.0005	-0.0006	266
42	56805.5330	0.0019	0.0067	28
43	56805.5830	0.0015	-0.0033	26
51	56806.0630	0.0012	-0.0033	60
52	56806.1163	0.0021	-0.0099	35
59	56806.5468	0.0015	0.0007	27
66	56806.9676	0.0031	0.0015	44
67	56807.0307	0.0011	0.0047	64
75	56807.5072	0.0015	0.0012	29
109	56809.5370	0.0014	-0.0086	27
142	56811.5514	0.0061	0.0261	24
176	56813.5537	0.0017	-0.0112	19
259	56818.5430	0.0012	-0.0011	23

*BJD-2400000.

 † Against max = 2456803.0067 + 0.059990 E . ‡ Number of points used to determine the maximum.

revealed the emergence of superhumps after a rise from a precursor outburst (figure 36; vsnet-alert 17736). Further observations confirmed superhump (vsnet-alert 17754, 17770; figure 37).

The times of superhump maxima are listed in table 32. The maxima for $E \leq 2$ were likely the final part of stage A. Although there were observations on the preceding night, the amplitudes were too small to determine the period of stage A superhumps. As is usual for an object with this moderate superhump period, the transition between stages was not very sharp. We could, however, identify stages B and C. The resultant behavior was typical for an SU UMa-type dwarf nova.

3.30. NSV 4618

NSV 4618 was discovered by Luyten (1938) as a variable object. A photographic range of 14.0 to fainter than 16 was reported. Although the identity of the object had long been unknown, CRTS Siding Spring Survey (SSS) detected an outburst on 2013 April 13 (cf. vsnet-alert 15611). The object was recorded in outburst several times in ASAS-3 data. The brightest outburst reached $V=13.3$. The eclipsing nature of this object was inferred (vsnet-alert 15612, 15613, 15614). Using the CRTS data, an orbital period was determined (vsnet-alert 15615) and the object was recognized as a candidate eclipsing SU UMa-type dwarf nova. The 2015 outburst was detected on February 14 by the ASAS-SN team (vsnet-alert 18297). Subsequent observations detected deep eclipses and super-

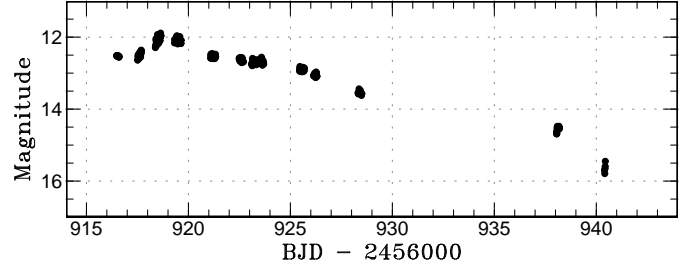
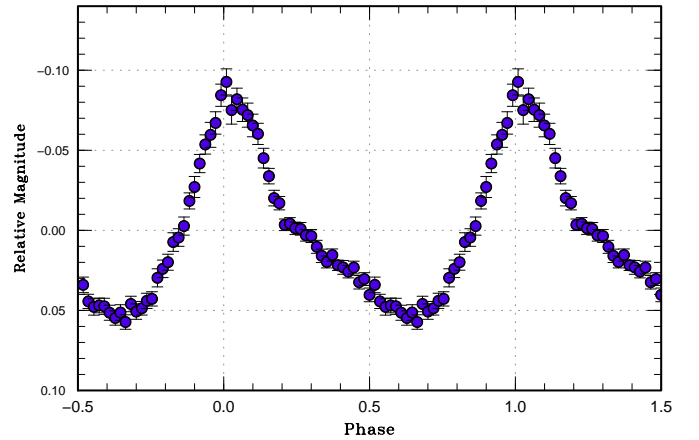
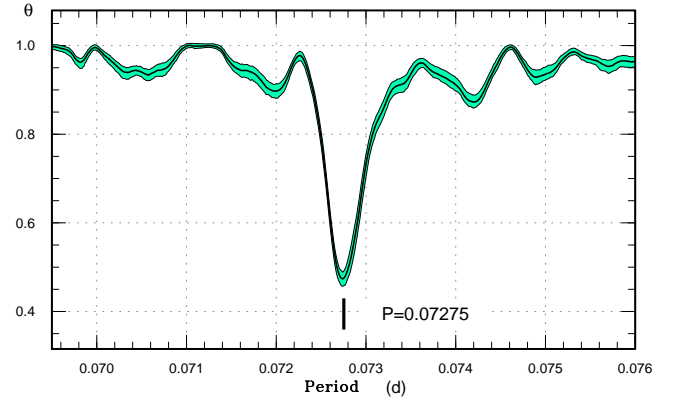
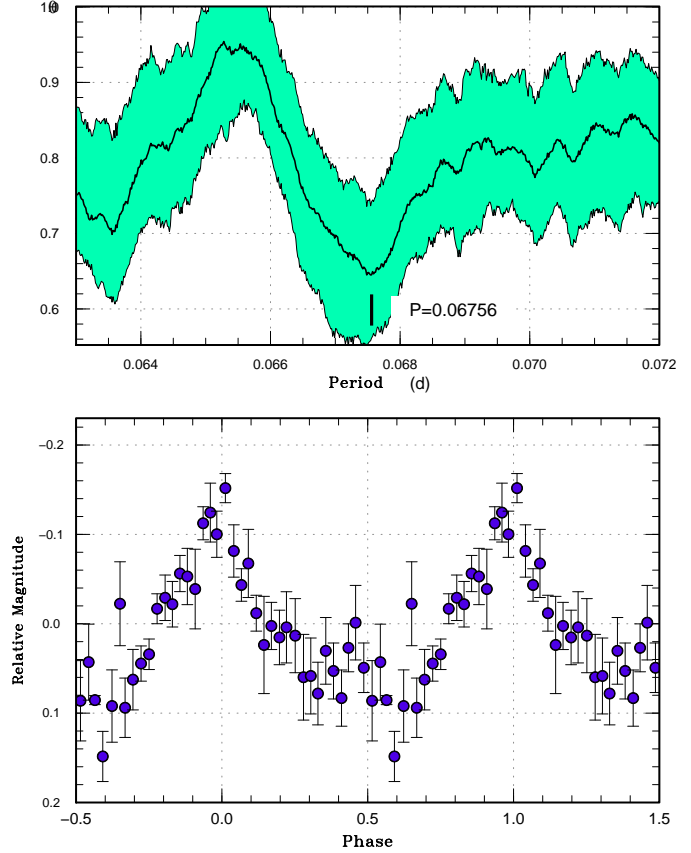
**Fig. 36.** Light curve of the superoutburst of NSV 1436 (2014). The data were binned to 0.01 d. The initial precursor part of the outburst and subsequent rise to the superoutburst maximum are clearly depicted. The widths of the light curve mainly reflect the amplitudes of superhumps.**Fig. 37.** Superhumps in NSV 1436 during the superoutburst plateau (2014). (Upper): PDM analysis. (Lower): Phase-averaged profile.

Table 32. Superhump maxima of NSV 1436 (2014)

E	max*	error	$O - C^\dagger$	N^\ddagger
0	56917.5356	0.0004	-0.0071	71
1	56917.6102	0.0003	-0.0053	77
2	56917.6816	0.0004	-0.0065	63
12	56918.4124	0.0003	-0.0030	80
13	56918.4862	0.0003	-0.0019	109
14	56918.5589	0.0003	-0.0019	109
15	56918.6323	0.0003	-0.0013	154
26	56919.4332	0.0004	-0.0002	113
27	56919.5075	0.0003	0.0014	106
28	56919.5782	0.0003	-0.0007	95
29	56919.6517	0.0057	0.0001	29
49	56921.1041	0.0005	-0.0019	127
50	56921.1796	0.0005	0.0010	142
51	56921.2519	0.0017	0.0005	50
52	56921.3246	0.0009	0.0005	56
68	56922.4948	0.0015	0.0071	53
69	56922.5628	0.0007	0.0025	76
70	56922.6393	0.0007	0.0062	76
77	56923.1497	0.0007	0.0076	53
78	56923.2208	0.0007	0.0060	55
79	56923.2940	0.0005	0.0065	54
82	56923.5114	0.0005	0.0058	77
83	56923.5856	0.0003	0.0072	78
84	56923.6569	0.0008	0.0058	77
109	56925.4690	0.0005	-0.0001	66
110	56925.5404	0.0006	-0.0014	78
111	56925.6123	0.0004	-0.0022	75
112	56925.6895	0.0016	0.0023	36
119	56926.1949	0.0008	-0.0014	53
120	56926.2684	0.0007	-0.0005	53
149	56928.3673	0.0008	-0.0105	80
150	56928.4361	0.0009	-0.0144	76

*BJD-2400000.

 † Against max = 2456917.5428 + 0.072719*E*. ‡ Number of points used to determine the maximum.**Fig. 38.** Superhumps in NSV 4618 outside the eclipses (2015). Due to the limited data segment, the error is relatively large. Post-superoutburst observations were not included in the analysis. (Upper): PDM analysis. (Lower): Phase-averaged profile.

humps (vsnet-alert 18305, 18306; figures 39, figure 38).

An MCMC analysis of both the CRTS data and the present data in outburst yielded the following orbital ephemeris:

$$\text{Min(BJD)} = 2454884.13441(2) + 0.0657692860(6)E. (2)$$

The times of superhump maxima outside the eclipses are listed in table 33. Since the object faded three days after the initial observation, it was likely we only observed the terminal stage of the superoutburst.

3.31. 1RXS J185310.0+594509

This object (hereafter 1RXS J185310) was originally selected as a variable optical counterpart of an ROSAT X-ray source (Denisenko, Sokolovsky 2011). The designation DDE 14 was also given (Denisenko 2011).¹² The

Table 33. Superhump maxima of NSV 4618 (2015)

E	max*	error	$O - C^\dagger$	phase ‡	N^\S
0	57070.5565	0.0014	-0.0080	0.82	17
1	57070.6404	0.0020	0.0084	0.09	24
15	57071.5842	0.0128	0.0071	0.44	17
18	57071.7727	0.0005	-0.0069	0.31	56
19	57071.8445	0.0006	-0.0027	0.40	49
30	57072.5944	0.0212	0.0047	0.80	19
31	57072.6545	0.0036	-0.0027	0.72	18

*BJD-2400000.

 † Against max = 2457070.5645 + 0.067506*E*. ‡ Orbital phase. § Number of points used to determine the maximum.

¹² For a list of DDE variables, see <http://hea.iki.rssi.ru/~denis/VarDDE.html>.

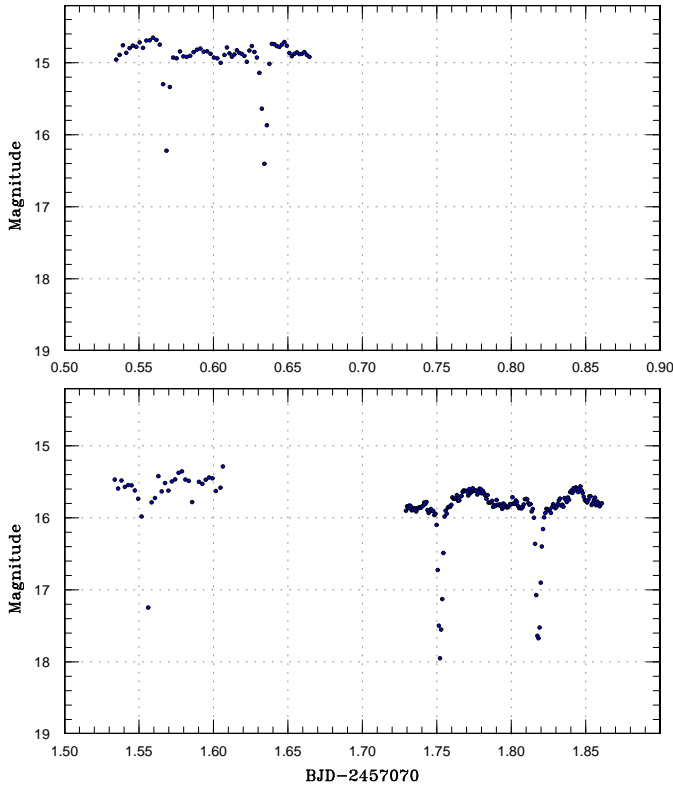


Fig. 39. Sample light curve of NSV 4618 in superoutburst. Superposition of superhumps and eclipse are well visible.

object was found in outburst on Palomar Observatory Sky Survey II infrared plate on 1992 June 28. On 2011 May 8, J. Shears detected an outburst at an unfiltered CCD magnitude of 15.9 (all magnitudes are unfiltered for this object unless otherwise noted; cvnet-outburst 4145). On 2011 November 22, J. Shears also detected an outburst at a magnitude of 15.1 (cvnet-outburst 4405). During this outburst, J. Shears detected superhump-like modulations, but it was not confirmed because the observations were obtained only for a night. Two further outbursts were recorded on 2012 December 5–11 (peak brightness at 15.16 on December 9) and 2013 August 16 (16.6 mag) by J. Shears. The 2013 August outburst was recorded by the ASAS-SN team at $V=15.18$ on August 15 (vsnet-alert 16247). Two faint outbursts in 2014 were detected by MASTER network (vsnet-alert 17500).

The 2014 July outburst was detected by J. Shears at a magnitude of 14.8 on July 16 (vsnet-outburst 17115). Subsequent observations detected superhumps (vsnet-alert 17514, 17532; figure 40).

The times of superhump maxima are listed in table 34. Although the superhump stage was not identified, these superhumps were likely stage B superhumps as judged from the large amplitudes.

The two long outbursts in 2011 November and 2012 December must have been superoutbursts. The interval between these two superoutburst was 379 d. The interval between the 2012 and current superoutbursts was 590 d.

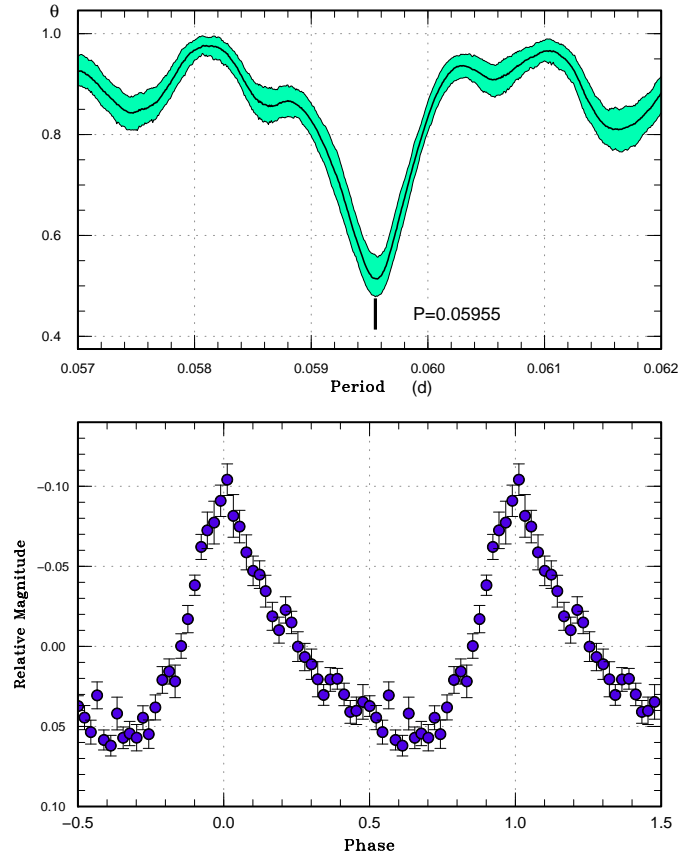


Fig. 40. Superhumps in 1RXS J185310 (2014). (Upper): PDM analysis. (Lower): Phase-averaged profile.

The supercycle may be around 190 d, which needs to be confirmed by further observations.

3.32. 1RXS J231935.0+364705

This object (=DDE 8, hereafter 1RXS J231935) was selected as a likely dwarf nova during the course of identification of the ROSAT sources (Denisenko, Sokolovsky 2011). The 2011 outburst was a superoutburst during which superhumps were detected (Kato et al. 2013a). The 2013 outburst also a superoutburst (Kato et al. 2014a). The 2005 outburst was also most likely a superoutburst which was recorded by CRTS. The 2010 May outburst was also bright (CRTS data) but only single night observation was available.

The 2014 outburst was detected by D. Denisenko at an unfiltered CCD magnitude of 13.9 (vsnet-alert 17701). Subsequent observations detected superhumps (vsnet-alert 17703, 17717, 17739). The times of superhump maxima are listed in table 35. Although observations were not dense enough in the middle part of the outburst, stages B and C were recorded. The $O-C$ diagrams were very similar between the 2011 and 2014 superoutbursts (figure 41).

The known outburst of this object is listed in table 36. The shortest interval between outbursts was 74 d.

Table 34. Superhump maxima of 1RXS J185310 (2014)

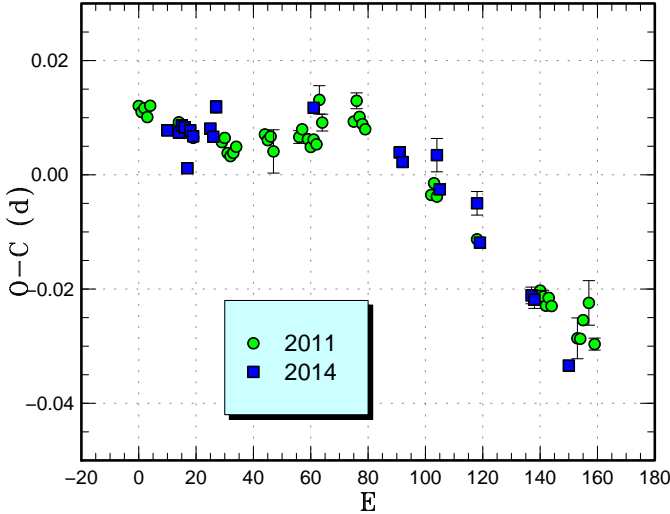
E	max*	error	$O - C^\dagger$	N^\ddagger
0	56857.6878	0.0020	0.0016	54
1	56857.7458	0.0003	0.0001	104
2	56857.8060	0.0004	0.0008	104
3	56857.8639	0.0005	-0.0009	104
14	56858.5174	0.0004	-0.0021	64
15	56858.5863	0.0009	0.0073	20
23	56859.0538	0.0008	-0.0014	22
24	56859.1098	0.0033	-0.0050	49
25	56859.1747	0.0012	0.0005	95
30	56859.4746	0.0028	0.0027	29
31	56859.5276	0.0004	-0.0037	64
32	56859.5879	0.0006	-0.0029	62
57	56861.0800	0.0009	0.0011	57
58	56861.1392	0.0012	0.0008	58
59	56861.1978	0.0011	-0.0001	19
64	56861.4936	0.0024	-0.0019	44
65	56861.5583	0.0010	0.0033	63

*BJD-2400000.

 † Against max = 2456857.6862 + 0.059521 E . ‡ Number of points used to determine the maximum.**Table 35.** Superhump maxima of 1RXS J231935 (2014)

E	max*	error	$O - C^\dagger$	N^\ddagger
0	56908.0625	0.0002	-0.0035	73
4	56908.3262	0.0003	-0.0030	100
5	56908.3934	0.0003	-0.0015	133
6	56908.4591	0.0003	-0.0017	131
7	56908.5179	0.0008	-0.0086	111
8	56908.5905	0.0003	-0.0018	207
9	56908.6555	0.0004	-0.0026	192
15	56909.0529	0.0005	-0.0001	130
16	56909.1174	0.0004	-0.0013	171
17	56909.1886	0.0011	0.0041	52
51	56911.4325	0.0009	0.0109	46
81	56913.4047	0.0004	0.0092	71
82	56913.4690	0.0008	0.0077	50
94	56914.2622	0.0029	0.0114	36
95	56914.3222	0.0004	0.0056	99
108	56915.1778	0.0021	0.0058	39
109	56915.2369	0.0007	-0.0009	48
127	56916.4156	0.0015	-0.0065	24
128	56916.4809	0.0016	-0.0070	25
140	56917.2614	0.0010	-0.0161	49

*BJD-2400000.

 † Against max = 2456908.0660 + 0.065796 E . ‡ Number of points used to determine the maximum.**Fig. 41.** Comparison of $O - C$ diagrams of 1RXS J231935 between different superoutbursts. A period of 0.06600 d was used to draw this figure. Approximate cycle counts (E) after the start of observations were used. The 2014 superoutburst was shifted by 10 cycles to best match the 2011 one.

Although supercycle was not well determined, the shortest known interval between superoutbursts was ~ 420 d.

3.33. 2QZ J130441.7+010330

This object (hereafter 2QZ J130441) was identified as a CV during the course of the 2dF QSO Redshift Survey (Croom et al. 2004). Although little had been known about this object, Kato et al. (2012b) estimated the orbital period to be 0.064–0.069 d from the SDSS colors,

suggesting an SU UMa-type dwarf nova. ASAS-SN team detected this object in outburst on 2014 March 20 at 15.65 mag.

Subsequent observation detected superhumps (vsnet-alert 17079, 17087; figure 42). The times of superhump maxima are listed in table 37. Since the object started fading rapidly on the fifth night of the observation, we probably observed only stage C superhumps.

3.34. ASASSN-13cx

This object was detected as a transient at $V=15.47$ on 2013 September 14 by ASAS-SN team. The coordinates are $00^{\text{h}}02^{\text{m}}22^{\text{s}}34$, $+42^{\circ}42'13''4$ (the Initial Gaia Source List). CRTS data detected six past outbursts. This object was detected in outburst again by E. Muylaert on 2014 August 31 (cvnet-outburst 6073). Noting that there were two faint measurements in the CRTS data, an observational campaign started to verify possible eclipses (vsnet-alert 17682). The object immediately turned out to be an SU UMa-type dwarf nova with deep eclipses (vsnet-alert 17684; figure 44).

An MCMC analysis of both the CRTS data and the present data in outburst yielded the following orbital ephemeris (vsnet-alert 17691):

$$\text{Min(BJD)} = 2456901.69823(5) + 0.079650075(5)E. \quad (3)$$

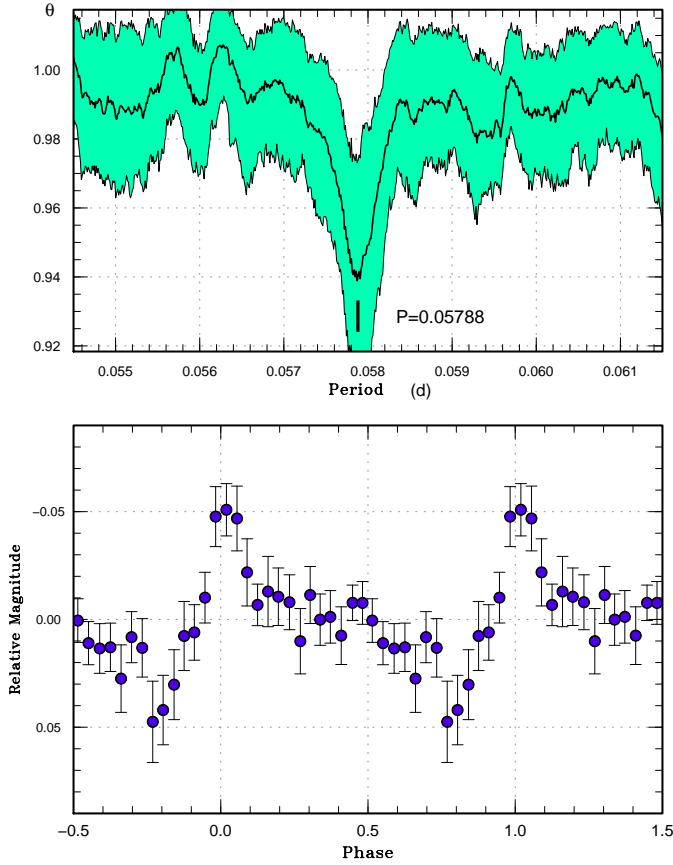
The orbital light curve in quiescence based on this ephemeris is in figure 43. Orbital humps before eclipses were present.

The times of superhump maxima are listed in table 38. Stages B and C can be identified. Although $E \leq 2$ ap-

Table 36. List of outbursts of 1RXS J231935

Year	Month	max*	magnitude	type	source
1999	11	51496	13.7	super	NSVS [†]
2005	10	53675	13.9	super	CRTS
2009	11	55140	14.5	normal	Denisenko (2009)
2010	5	55347	13.9	super?	CRTS
2010	12	55557	14.2	normal	vsnet-alert 12532
2011	9	55834	13.7	super	Kato et al. (2013a)
2012	10	56230	14.4	normal	vsnet-alert 15072
2013	7	56489	14.4	super?	vsnet-alert 15998
2013	9	56563	15.2	normal	vsnet-alert 16460
2014	9	56908	14.0	super	this paper

*JD–2400000.

[†]NSVS 9022680, see Denisenko (2009).**Fig. 42.** Superhumps in 2QZ J130441 (2014). (Upper): PDM analysis. (Lower): Phase-averaged profile.**Table 37.** Superhump maxima of 2QZ J130441 (2014)

E	max*	error	$O - C^{\dagger}$	N^{\ddagger}
0	56740.6716	0.0019	0.0061	20
1	56740.7227	0.0058	−0.0009	20
2	56740.7843	0.0016	0.0027	21
3	56740.8399	0.0040	0.0002	25
17	56741.6542	0.0020	0.0016	21
18	56741.7064	0.0017	−0.0043	20
19	56741.7653	0.0011	−0.0035	20
20	56741.8290	0.0015	0.0022	22
34	56742.6373	0.0064	−0.0025	22
35	56742.6940	0.0029	−0.0039	19
36	56742.7534	0.0023	−0.0025	21
37	56742.8175	0.0017	0.0035	21
38	56742.8690	0.0028	−0.0031	21
51	56743.6258	0.0021	−0.0012	24
52	56743.6816	0.0035	−0.0034	21
53	56743.7330	0.0031	−0.0101	20
54	56743.7959	0.0023	−0.0053	19
59	56744.0991	0.0018	0.0076	45
60	56744.1743	0.0020	0.0247	63
63	56744.3159	0.0014	−0.0079	43
69	56744.6750	0.0117	0.0028	22
70	56744.7259	0.0047	−0.0044	21
71	56744.7946	0.0265	0.0062	19
72	56744.8419	0.0030	−0.0046	18

*BJD–2400000.

[†]Against max = 2456740.6655 + 0.058069 E .[‡]Number of points used to determine the maximum.

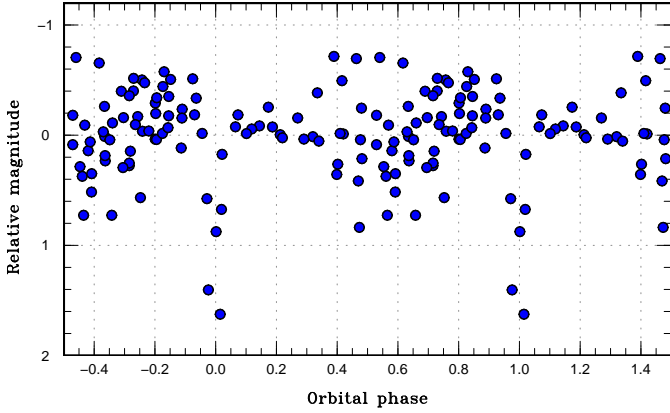


Fig. 43. Orbital light curve of ASASSN-13cx in the CRTS data.

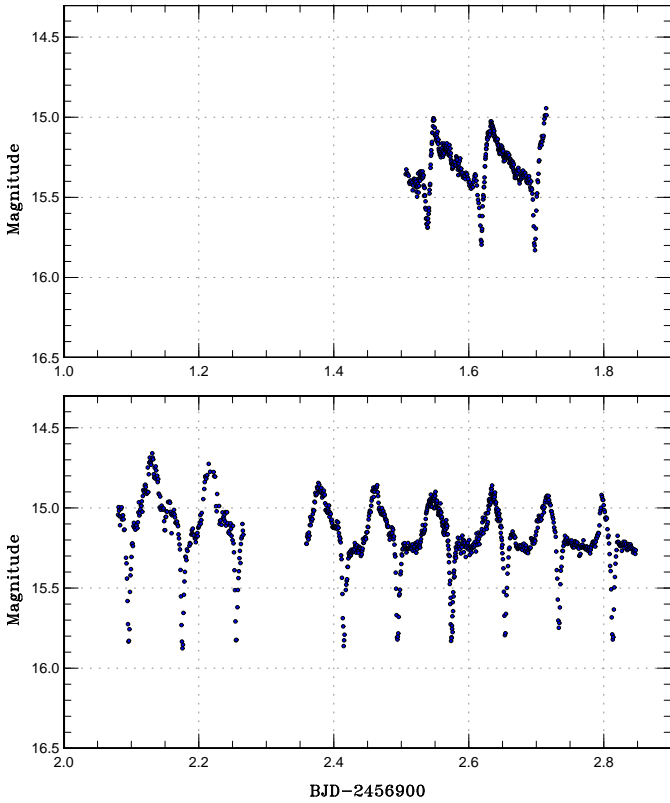


Fig. 44. Sample light curve of ASASSN-13cx in superoutburst. Superposition of superhumps and eclipse are well visible.

pears to corresponds to stage A superhumps, the period of stage A superhumps could not be determined. The mean superhump profile outside the eclipses is shown in figure 45.

Since the 2013 outburst was likely a superoutburst as judged from the magnitude, the supercycle can be estimated to be ~ 350 d or possibly its half.

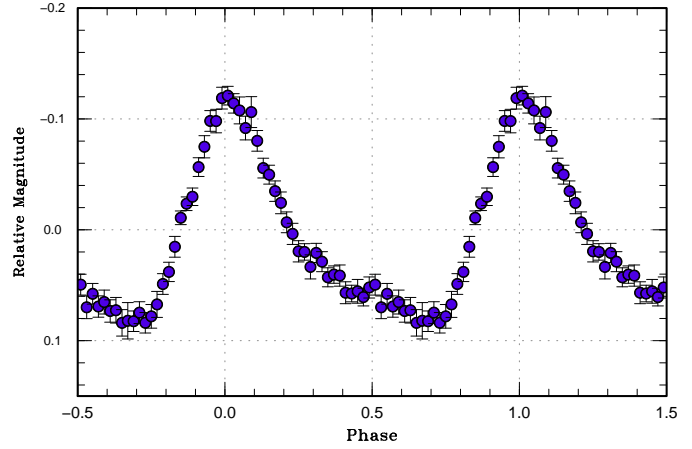
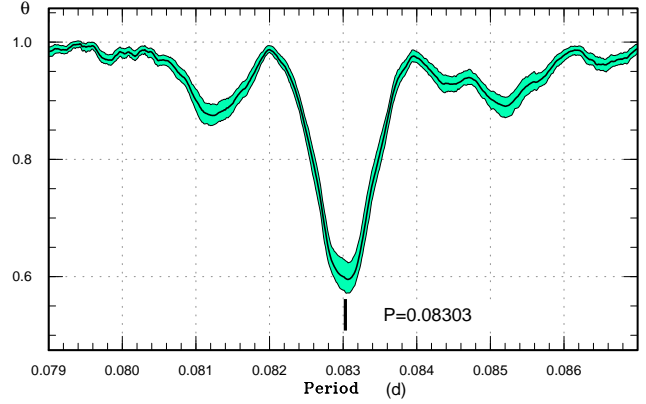


Fig. 45. Superhumps in ASASSN-13cx outside the eclipses (2014). (Upper): PDM analysis. (Lower): Phase-averaged profile.

3.35. ASASSN-14ag

This object was detected as a transient at $V=13.5$ on 2014 March 14 by ASAS-SN team. The coordinates are $08^h13^m18^s.51$, $-01^\circ03'28''.5$ (2MASS position). CRTS recorded five more outbursts in the past data. One of the authors (TK) noticed that the CRTS light curve showed evidence of eclipses, and obtained a period below the period gap (vsnet-alert 17036; figure 46). This suggestion was confirmed by photometry in outburst (vsnet-alert 17041, 17042; figure 47). An MCMC analysis of both the CRTS data and the present data in outburst yielded the following orbital ephemeris:

$$\text{Min(BJD)} = 2454413.99168(7) + 0.060310651(2)E. \quad (4)$$

There was a strong beat phenomenon between the superhump period and the orbital period (figure 47). The mean profile of superhumps outside the eclipses is shown in figure 48. The times of superhump maxima determined outside the eclipses are listed in table 39.

The relatively low outburst amplitude (2–3 mag in the CRTS data; the outburst data in ASAS-SN data appear to be brighter than the real magnitude by ~ 1 mag) is probably due to the high orbital inclination. Since such a bright, deeply eclipsing SU UMa-type dwarf nova with

Table 38. Superhump maxima of ASASSN-13cx (2014)

E	max*	error	$O - C^\dagger$	phase ‡	N^\S
0	56901.5524	0.0006	-0.0069	0.17	133
1	56901.6357	0.0004	-0.0064	0.22	136
2	56901.7257	0.0012	0.0007	0.35	19
7	56902.1313	0.0005	-0.0079	0.44	80
8	56902.2185	0.0005	-0.0035	0.53	64
10	56902.3819	0.0003	-0.0059	0.58	80
11	56902.4646	0.0004	-0.0060	0.62	91
12	56902.5500	0.0005	-0.0034	0.69	123
13	56902.6340	0.0008	-0.0023	0.75	102
14	56902.7172	0.0004	-0.0019	0.79	73
15	56902.8031	0.0009	0.0012	0.87	71
34	56904.3712	0.0041	-0.0047	0.56	26
35	56904.4609	0.0004	0.0021	0.68	85
36	56904.5450	0.0005	0.0034	0.74	87
38	56904.7142	0.0075	0.0069	0.87	18
47	56905.4597	0.0009	0.0068	0.23	215
48	56905.5433	0.0008	0.0076	0.27	211
49	56905.6253	0.0004	0.0068	0.30	86
50	56905.7075	0.0006	0.0061	0.34	57
52	56905.8692	0.0007	0.0021	0.37	71
58	56906.3684	0.0012	0.0043	0.63	43
59	56906.4487	0.0008	0.0018	0.64	54
60	56906.5305	0.0013	0.0007	0.67	64
61	56906.6176	0.0013	0.0049	0.76	54
63	56906.7817	0.0006	0.0034	0.82	93
64	56906.8728	0.0015	0.0116	0.97	80
72	56907.5217	0.0018	-0.0022	0.11	130
73	56907.6051	0.0014	-0.0016	0.16	116
83	56908.4406	0.0024	0.0054	0.65	63
84	56908.5243	0.0024	0.0062	0.70	53
118	56911.3291	0.0027	-0.0055	0.92	46
130	56912.3164	0.0042	-0.0124	0.31	39
133	56912.5658	0.0077	-0.0115	0.44	33

*BJD-2400000.

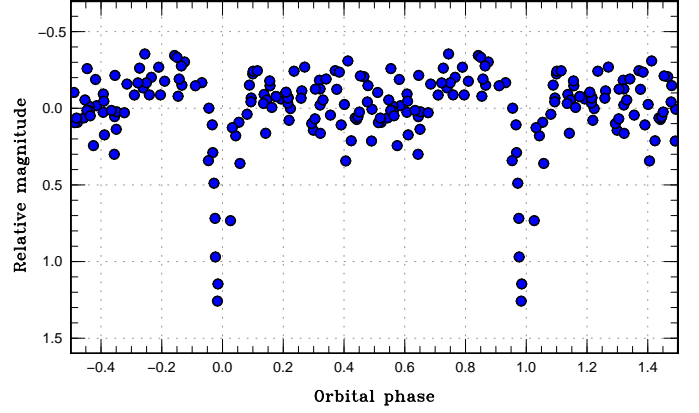
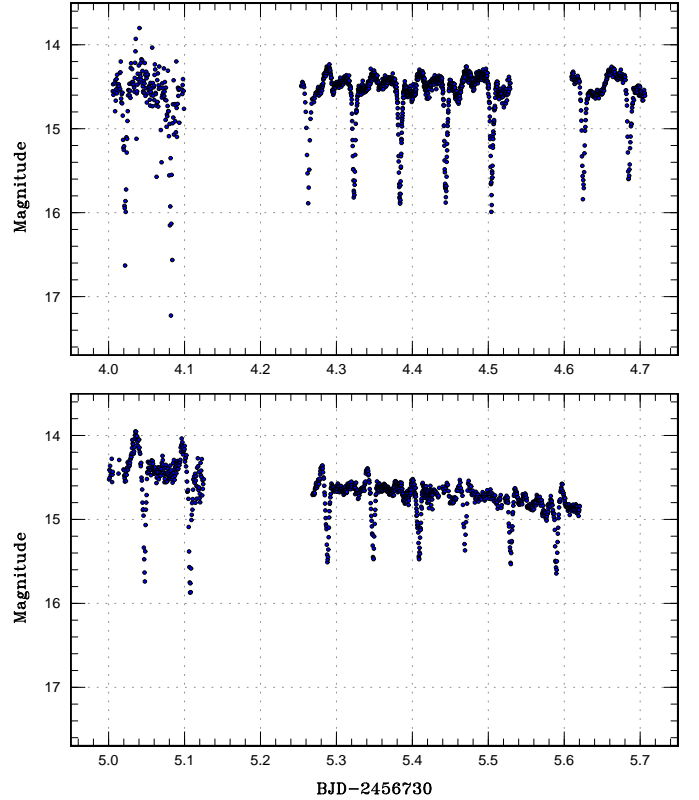
 † Against max = 2456901.5593 + 0.082842*E*. ‡ Orbital phase. § Number of points used to determine the maximum.

a short orbital period is rare, further detailed study will be promising in resolving the superhump light source in different stages.

3.36. ASASSN-14aj

This object was detected as a transient at $V=15.1$ on 2014 March 27 by ASAS-SN team (vsnet-alert 17101). The coordinates are $17^{\text{h}}36^{\text{m}}15^{\text{s}}09$, $+07^{\circ}16'56''0$ (SDSS $g = 21.7$ counterpart). This object was also independently discovered on the same day as TCP J17361506+0716560.¹³ There were also two past outbursts (vsnet-alert 17130).

Subsequent observation detected superhumps (vsnet-alert 17119, 17128, 17131). The times of superhump max-

**Fig. 46.** Orbital light curve of ASASSN-14ag in the CRTS data.**Fig. 47.** Sample light curve of ASASSN-14ag in superoutburst. Superposition of superhumps and eclipse are well visible.

¹³ <<http://www.cbat.eps.harvard.edu/unconf/followups/J17361506+0716560.html>>.

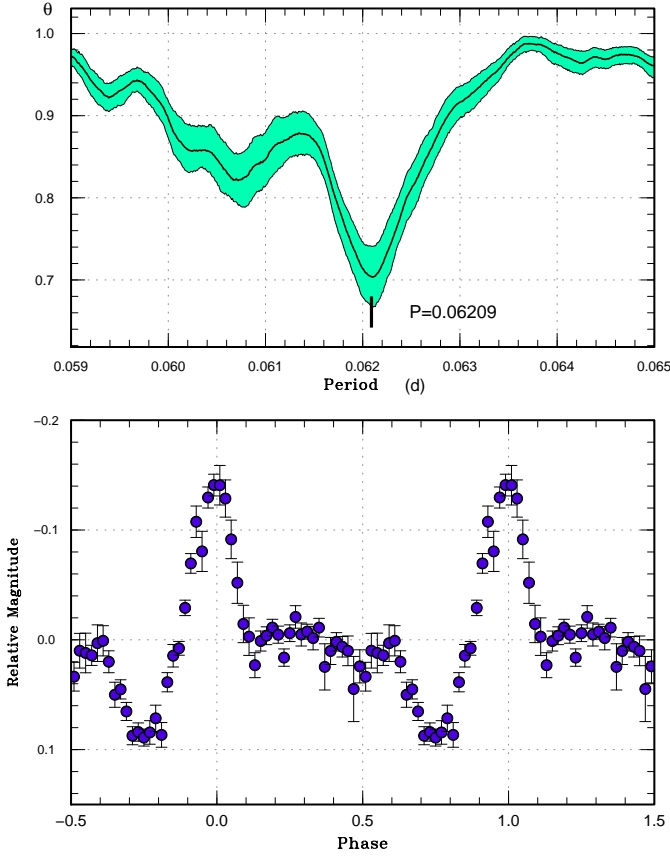


Fig. 48. Superhumps in ASASSN-14ag outside the eclipses (2014). (Upper): PDM analysis. (Lower): Phase-averaged profile.

Table 39. Superhump maxima of ASASSN-14ag (2014)

E	max*	error	$O - C^\dagger$	phase [‡]	N^\S
0	56734.0403	0.0025	-0.0027	0.31	85
1	56734.0969	0.0025	-0.0081	0.25	19
4	56734.2909	0.0008	-0.0003	0.46	166
5	56734.3530	0.0011	-0.0003	0.49	201
6	56734.4172	0.0012	0.0018	0.56	222
7	56734.4788	0.0011	0.0014	0.58	207
8	56734.5431	0.0042	0.0036	0.64	30
10	56734.6670	0.0004	0.0034	0.70	96
16	56735.0392	0.0004	0.0033	0.87	77
17	56735.0983	0.0011	0.0003	0.85	88
20	56735.2854	0.0004	0.0012	0.95	79
21	56735.3453	0.0007	-0.0009	0.95	117
22	56735.4083	0.0014	-0.0000	0.99	132
23	56735.4706	0.0009	0.0003	0.02	56
24	56735.5349	0.0014	0.0025	0.09	80
25	56735.5946	0.0006	0.0001	0.08	96
36	56736.2739	0.0012	-0.0032	0.34	100
37	56736.3379	0.0008	-0.0013	0.40	100
38	56736.4001	0.0054	-0.0011	0.43	111

*BJD-2400000.

[†]Against max = 2456734.0430 + 0.062059 E .

[‡]Orbital phase.

[§]Number of points used to determine the maximum.

Table 40. Superhump maxima of ASASSN-14aj (2014)

E	max*	error	$O - C^\dagger$	N^\ddagger
0	56746.7697	0.0017	-0.0057	15
1	56746.8528	0.0009	-0.0046	21
12	56747.7625	0.0023	0.0036	16
13	56747.8434	0.0011	0.0025	27
25	56748.8266	0.0012	0.0022	27
37	56749.8076	0.0010	-0.0003	26
38	56749.8930	0.0022	0.0031	11
49	56750.7932	0.0016	0.0018	25
50	56750.8692	0.0020	-0.0042	19
61	56751.7750	0.0013	0.0000	25
62	56751.8612	0.0013	0.0043	24
73	56752.7631	0.0040	0.0047	22
98	56754.8000	0.0058	-0.0074	26

*BJD-2400000.

[†]Against max = 2456746.7754 + 0.081959 E .

[‡]Number of points used to determine the maximum.

ima are listed in table 40. Although we only observed the late phase of the superoutburst, we left the stage classification as an open question since the stages tend to become unclear for long- P_{orb} systems. If there were distinct stage transitions in this system, we may have only observed stage C superhumps.

3.37. ASASSN-14au

This object was detected as a transient at $V=16.4$. on 2014 May 8 by ASAS-SN team (vsnet-alert 17290). The coordinates are $18^{\text{h}}17^{\text{m}}52^{\text{s}}54$, $+67^{\circ}08'08''.0$. There is a GALEX counterpart with an NUV magnitude of 21.6. Subsequent observations detected superhumps (vsnet-alert 17295; figure 50). The times of superhump maxima are listed in table 41.

3.38. ASASSN-14aw

This object was detected as a transient at $V=15.8$. on 2014 May 10 by ASAS-SN team (vsnet-alert 17290). The coordinates are $18^{\text{h}}47^{\text{m}}02^{\text{s}}57$, $+53^{\circ}00'30''.6$. Subsequent observations detected superhumps (vsnet-alert 17295; figure 51). The times of superhump maxima are listed in table 42. The superhump period indicates that this object is located in the period gap.

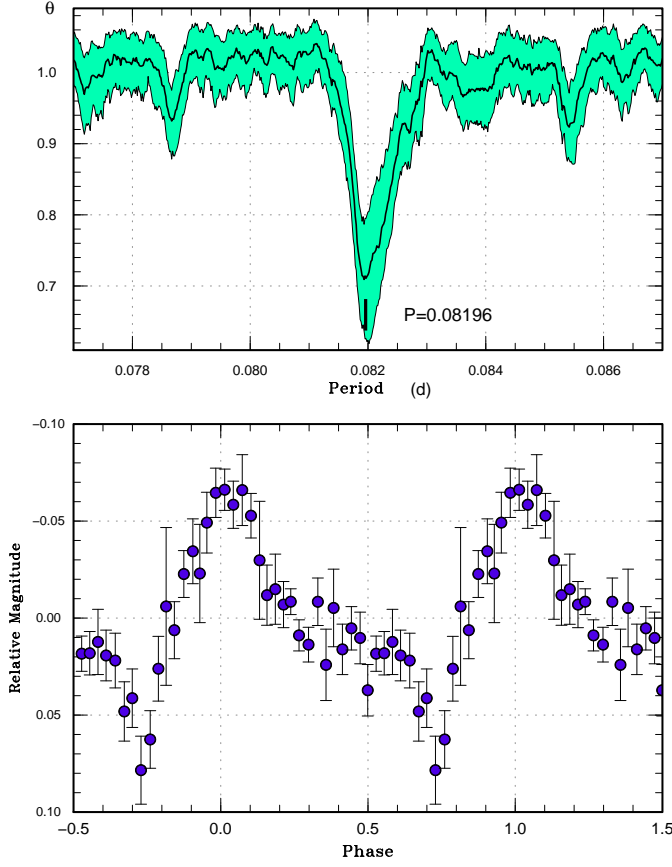


Fig. 49. Superhumps in ASASSN-14aj (2014). (Upper): PDM analysis. (Lower): Phase-averaged profile.

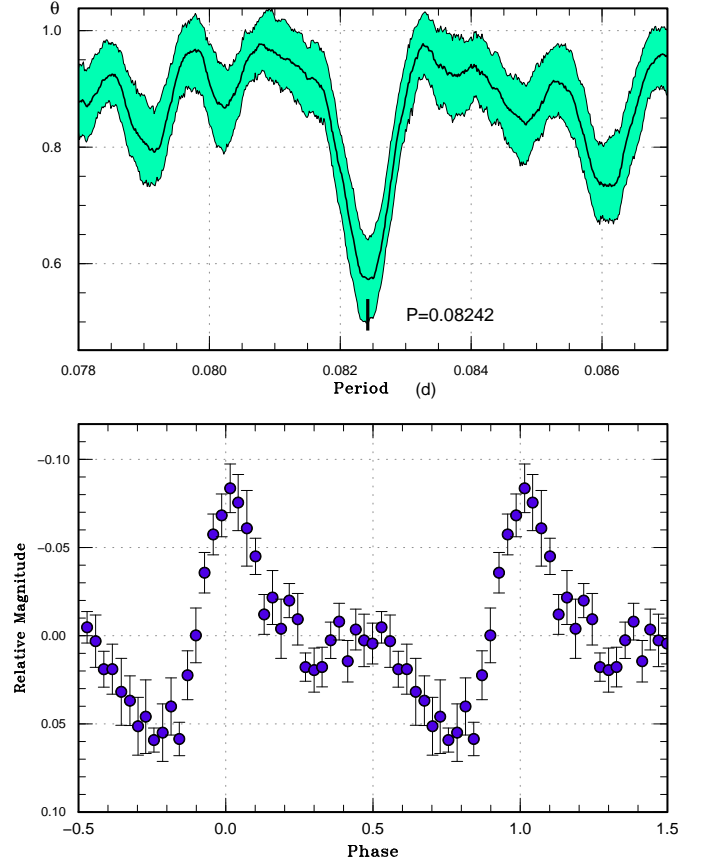


Fig. 50. Superhumps in ASASSN-14au (2014). (Upper): PDM analysis. (Lower): Phase-averaged profile.

Table 41. Superhump maxima of ASASSN-14au (2014)

E	max*	error	$O - C^\dagger$	N^\ddagger
0	56790.6007	0.0020	-0.0013	58
1	56790.6816	0.0050	-0.0029	30
12	56791.5916	0.0012	-0.0002	43
13	56791.6810	0.0038	0.0067	23
35	56793.4876	0.0016	-0.0014	37
36	56793.5703	0.0012	-0.0012	43
37	56793.6542	0.0025	0.0003	40

*BJD-2400000.

† Against max = 2456790.6020 + 0.082486 E .

‡ Number of points used to determine the maximum.

Table 42. Superhump maxima of ASASSN-14aw (2014)

E	max*	error	$O - C^\dagger$	N^\ddagger
0	56790.6159	0.0007	-0.0013	105
10	56791.5945	0.0011	0.0014	89
29	56793.4530	0.0042	0.0057	58
30	56793.5430	0.0010	-0.0018	77
31	56793.6383	0.0014	-0.0041	63

*BJD-2400000.

† Against max = 2456790.6172 + 0.097586 E .

‡ Number of points used to determine the maximum.

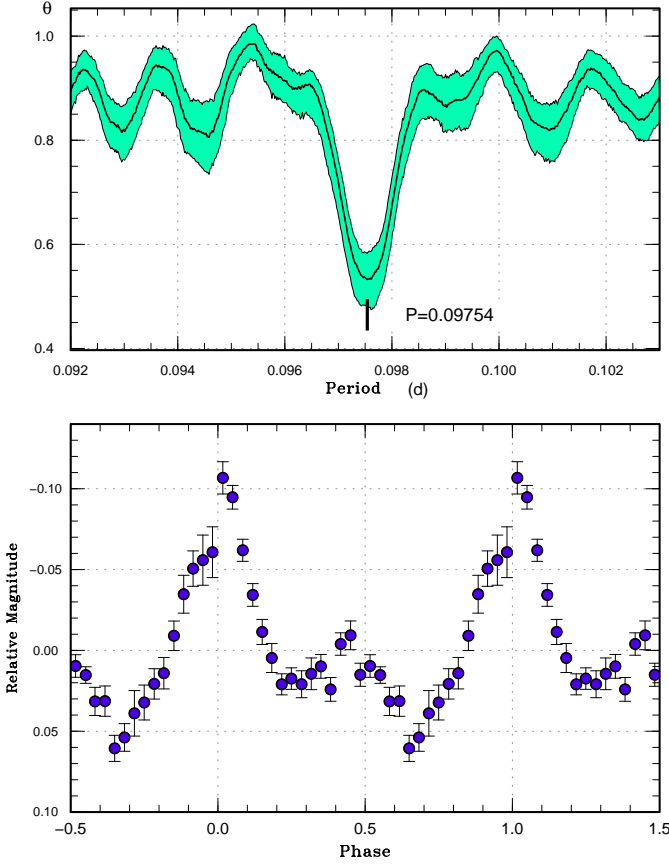


Fig. 51. Superhumps in ASASSN-14aw (2014). (Upper): PDM analysis. (Lower): Phase-averaged profile.

3.39. ASASSN-14bh

This object was detected as a transient at $V=14.66$, on 2014 May 21 by ASAS-SN team (vsnet-alert 17334). The coordinates given by the ASAS-SN team are $13^{\text{h}}24^{\text{m}}40^{\text{s}}0$, $-19^{\circ}51'31''.4$, which is $3''$ distant from a 20.4 mag (blue plate) USNO B1.0 object. Subsequent observations detected superhumps (vsnet-alert 17359; figure 52). The times of superhump maxima are listed in table 43. The object started fading rapidly five nights after the start of this observation. We only observed the final part of the superoutburst, and we most likely observed stage C superhumps.

3.40. ASASSN-14cl

This object was detected as a bright transient at $V=10.66$, on 2014 June 14 by ASAS-SN team (Stanek et al. 2014a; vsnet-alert 17376). The coordinates are $21^{\text{h}}54^{\text{m}}57^{\text{s}}70$, $+26^{\circ}41'12''.9$ (vsnet-alert 17429). The quiescent counterpart in SDSS was a $g = 18.8$ star. No previous outbursts are known. The SDSS colors expected a short orbital period of 0.066 d by using the neural network analysis (Kato et al. 2012b). The large outburst amplitude suggested a WZ Sge-type dwarf nova caught in the early stage (vsnet-alert 17377). Teyssier (2014) spectroscopically confirmed that this object is an outbursting

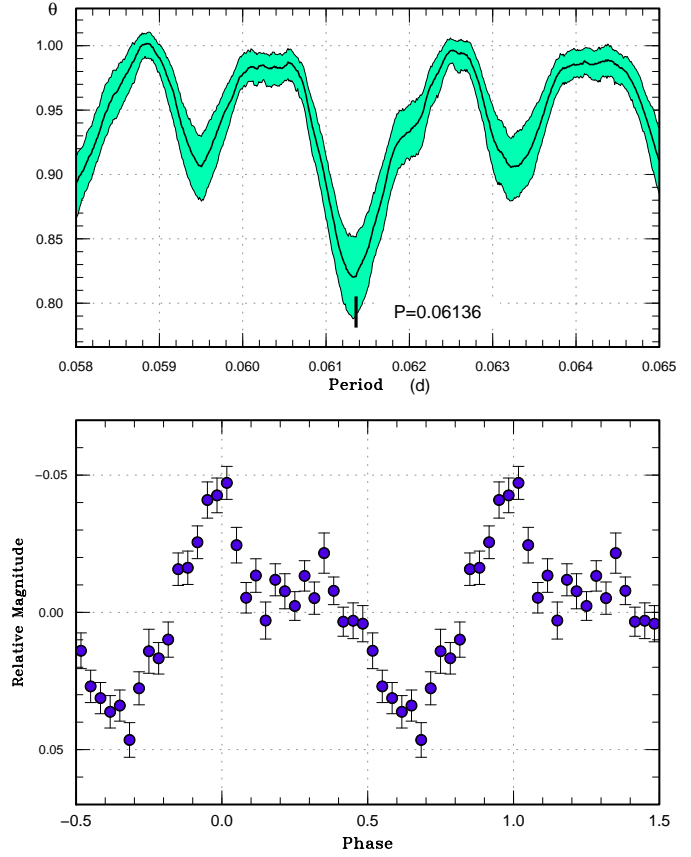


Fig. 52. Superhumps in ASASSN-14bh (2014). (Upper): PDM analysis. (Lower): Phase-averaged profile.

Table 43. Superhump maxima of ASASSN-14bh (2014)

E	max*	error	$O - C^\dagger$	N^\ddagger
0	56808.2910	0.0007	-0.0035	139
1	56808.3567	0.0009	0.0009	141
2	56808.4156	0.0011	-0.0016	135
16	56809.2791	0.0014	0.0027	136
17	56809.3420	0.0015	0.0043	46
18	56809.4007	0.0014	0.0016	128
32	56810.2569	0.0018	-0.0013	140
33	56810.3189	0.0031	-0.0008	136
34	56810.3773	0.0020	-0.0037	140
35	56810.4438	0.0023	0.0015	140

*BJD-2400000.

† Against max = 2456808.2945 + 0.061368 E .

‡ Number of points used to determine the maximum.

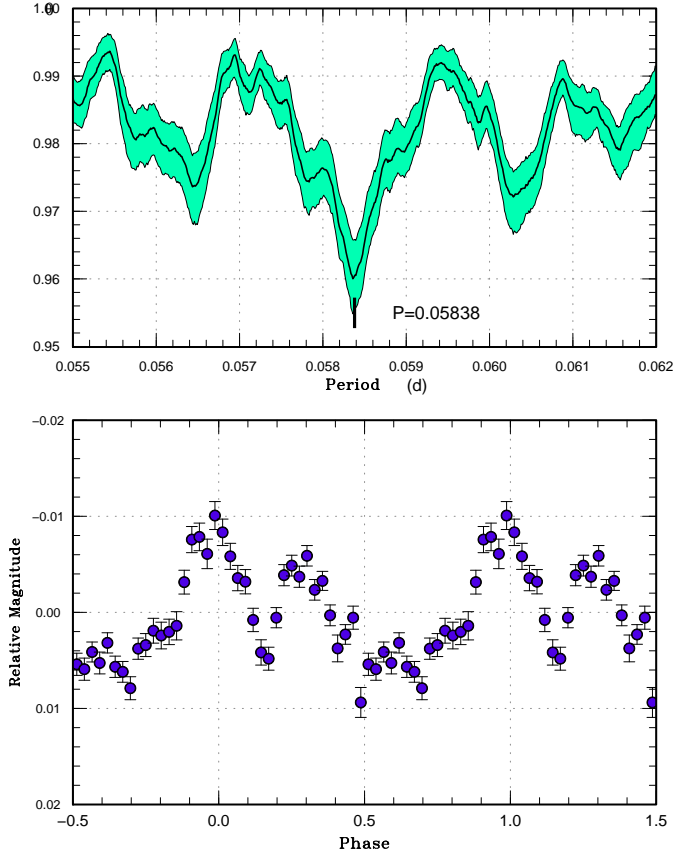


Fig. 53. Early superhumps in ASASSN-14cl (2014). (Upper): PDM analysis. (Lower): Phase-averaged profile

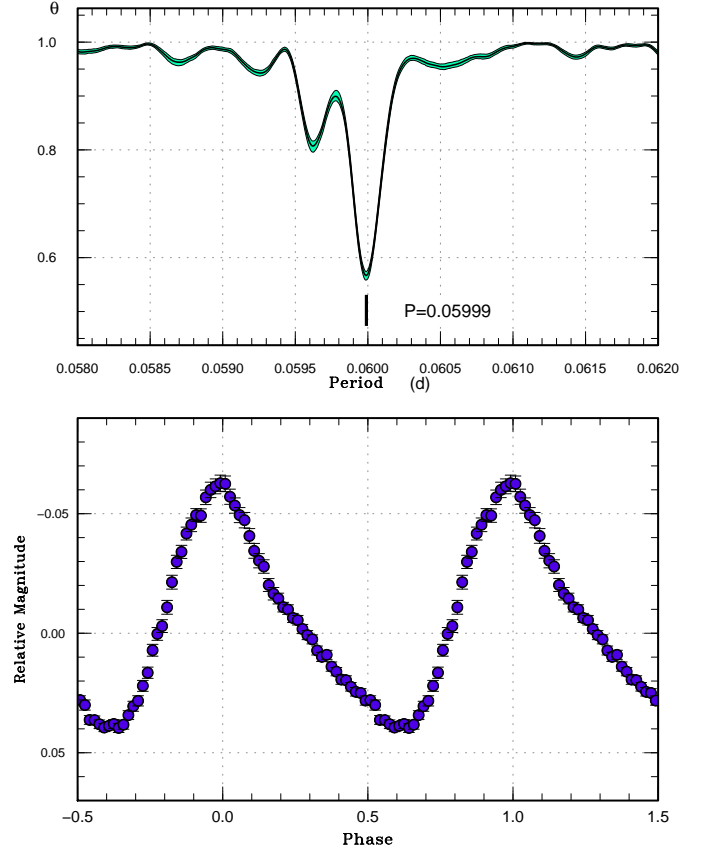


Fig. 54. Ordinary superhumps in ASASSN-14cl (2014) during the plateau phase (BJD 2456829–2456843). (Upper): PDM analysis. (Lower): Phase-averaged profile

dwarf nova. The spectrum was characterized by broad Balmer absorption lines with an emission core in $H\alpha$. The $HeII$ line was recorded in emission, which is known to be a frequent signature of a WZ Sge-type dwarf nova (cf. Baba et al. 2002).

Soon after the discovery, possible early superhumps were detected (vsnet-alert 17383, 17384, 17387; figure 53). The object then started to show ordinary superhumps (vsnet-alert 17392, 17398, 17413; figure 54).

The times of superhump maxima during the superoutburst plateau are listed in table 44. The $O - C$ values showed very prominent stages A–C with a definitely positive P_{dot} for stage B. The times of superhumps in the post-superoutburst stage are listed in table 45. The post-superoutburst superhumps were on very good extension of stage C superhumps (figure 55).

The presence of distinct stage B with a definitely positive P_{dot} , the presence of stage C and the persistence of stage C superhumps after the rapid fading from the plateau phase indicate that ASASSN-14cl resembles a rather ordinary large-amplitude SU UMa-type dwarf nova rather than an extreme WZ Sge-type object.

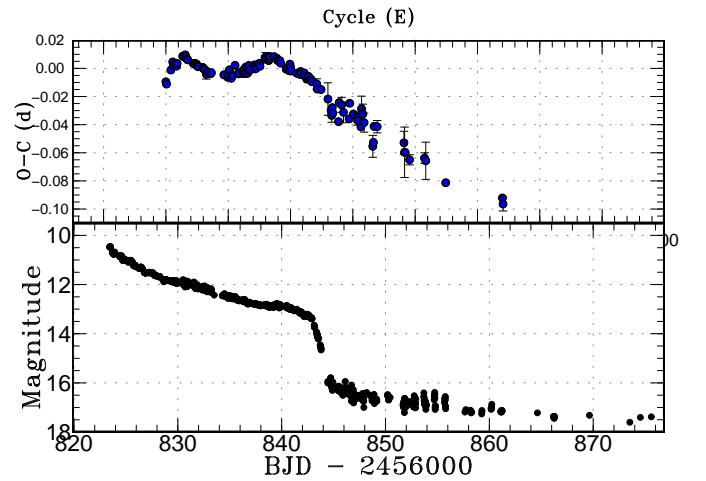


Fig. 55. $O - C$ diagram of superhumps in ASASSN-14cl (2014). (Upper): $O - C$ diagram. A period of 0.06001 d was used to draw this figure. (Lower): Light curve. The observations were binned to 0.012 d.

Table 44. Superhump maxima of ASASSN-14cl (2014)

E	max*	error	$O - C^\dagger$	N^\ddagger
0	56828.8437	0.0013	-0.0122	207
1	56828.9019	0.0006	-0.0139	187
8	56829.3319	0.0007	-0.0039	99
11	56829.5177	0.0007	0.0020	68
12	56829.5750	0.0004	-0.0007	63
15	56829.7567	0.0017	0.0010	32
16	56829.8167	0.0001	0.0011	358
17	56829.8748	0.0001	-0.0009	448
18	56829.9367	0.0001	0.0010	250
27	56830.4819	0.0004	0.0064	37
28	56830.5417	0.0002	0.0062	52
31	56830.7230	0.0002	0.0075	142
32	56830.7815	0.0001	0.0061	277
33	56830.8402	0.0001	0.0048	224
34	56830.9001	0.0001	0.0047	214
35	56830.9594	0.0002	0.0040	46
44	56831.4970	0.0002	0.0017	110
45	56831.5571	0.0003	0.0018	89
46	56831.6170	0.0003	0.0018	85
47	56831.6766	0.0012	0.0014	19
48	56831.7368	0.0002	0.0016	92
49	56831.7966	0.0001	0.0014	284
50	56831.8553	0.0001	0.0002	291
51	56831.9150	0.0001	-0.0002	244
52	56831.9747	0.0006	-0.0005	49
59	56832.3944	0.0002	-0.0007	58
60	56832.4537	0.0002	-0.0014	84
61	56832.5134	0.0002	-0.0017	153
62	56832.5728	0.0002	-0.0022	111
65	56832.7494	0.0034	-0.0055	11
66	56832.8112	0.0006	-0.0037	18
67	56832.8713	0.0006	-0.0036	26
72	56833.1700	0.0003	-0.0049	125

*BJD-2400000.

 † Against max = 2456828.8559 + 0.059986*E*. ‡ Number of points used to determine the maximum.**Table 44.** Superhump maxima of ASASSN-14cl (2014) (continued)

E	max*	error	$O - C^\dagger$	N^\ddagger
73	56833.2306	0.0002	-0.0042	125
93	56834.4293	0.0024	-0.0053	69
94	56834.4895	0.0002	-0.0051	229
99	56834.7877	0.0006	-0.0068	224
100	56834.8494	0.0003	-0.0051	245
101	56834.9094	0.0002	-0.0050	228
102	56834.9730	0.0005	-0.0014	51
105	56835.1470	0.0007	-0.0074	88
106	56835.2094	0.0002	-0.0049	147
107	56835.2689	0.0002	-0.0054	138
111	56835.5163	0.0004	0.0020	116
116	56835.8102	0.0004	-0.0040	193
117	56835.8710	0.0005	-0.0032	137
123	56836.2322	0.0004	-0.0019	121
124	56836.2929	0.0006	-0.0012	115
125	56836.3510	0.0032	-0.0031	53
126	56836.4134	0.0005	-0.0007	62
127	56836.4709	0.0005	-0.0032	60
128	56836.5351	0.0019	0.0011	19
131	56836.7108	0.0006	-0.0032	55
132	56836.7737	0.0004	-0.0003	258
133	56836.8364	0.0004	0.0025	216
134	56836.8928	0.0003	-0.0012	263
135	56836.9534	0.0003	-0.0006	94
142	56837.3770	0.0010	0.0031	97
143	56837.4341	0.0005	0.0002	119
144	56837.4965	0.0006	0.0027	107
145	56837.5545	0.0010	0.0006	32
149	56837.7976	0.0007	0.0039	137
150	56837.8581	0.0006	0.0043	129
151	56837.9160	0.0006	0.0023	132
159	56838.4023	0.0008	0.0087	91
160	56838.4626	0.0032	0.0090	82

*BJD-2400000.

 † Against max = 2456828.8559 + 0.059986*E*. ‡ Number of points used to determine the maximum.

3.41. ASASSN-14cq

This object was detected as a transient at $V=13.72$ on 2014 June 18 by ASAS-SN team (vsnet-alert 17386). The coordinates are 15^h32^m00^s.29, -28°33'57".2 (vsnet-alert 17429).

Subsequent observations recorded prominent early superhumps (vsnet-alert 17403, 17405; figure 56). Although ordinary superhumps (figure 57) started to be observed on June 26 (vsnet-alert 17426), the early phase of the development of superhumps fell in the 1.8-d gap in the observation. The times of superhump maxima are listed in table 46. Although there were short gaps in the observation in the late stage of the superoutburst, the times of maxima for $34 \leq E \leq 194$ appear to be expressed by a single, positive P_{dot} . We identified this part as stage B. There was some hint of stage C superhump after $E=194$, but the stage was not well observed because the object

became too faint. Although $E=0$ corresponds to one of stage A superhumps, the period of stage A superhumps (and q) could not be estimated.

3.42. ASASSN-14dm

This object was detected as a transient at $V=15.02$ on 2014 July 1 by ASAS-SN team (vsnet-alert 17434). The coordinates are 14^h09^m32^s.07, -29°17'04".5. (GSC 2.3.2 position). The object has a GALEX UV counterpart with an NUV magnitude of 20.6. Subsequent observations detected superhumps (vsnet-alert 17452; figure 58). The times of superhump maxima are listed in table 47. The $O - C$ values suggest that we recorded stage B-C transition around $E=75$.

Table 44. Superhump maxima of ASASSN-14cl (2014) (continued)

E	max*	error	$O - C^\dagger$	N^\ddagger
161	56838.5214	0.0007	0.0078	160
162	56838.5808	0.0014	0.0072	44
165	56838.7602	0.0011	0.0067	23
166	56838.8212	0.0013	0.0077	19
167	56838.8831	0.0016	0.0096	16
173	56839.2429	0.0004	0.0095	129
174	56839.3030	0.0006	0.0096	35
178	56839.5420	0.0004	0.0086	120
179	56839.6004	0.0003	0.0071	86
182	56839.7801	0.0003	0.0069	119
183	56839.8402	0.0003	0.0070	117
184	56839.8985	0.0003	0.0053	116
193	56840.4343	0.0006	0.0012	123
194	56840.4954	0.0003	0.0023	252
195	56840.5544	0.0003	0.0014	228
198	56840.7333	0.0012	0.0002	28
199	56840.7980	0.0007	0.0050	62
200	56840.8559	0.0007	0.0029	102
201	56840.9131	0.0005	0.0001	85
210	56841.4517	0.0017	-0.0012	26
215	56841.7509	0.0013	-0.0019	34
216	56841.8130	0.0020	0.0002	29
217	56841.8722	0.0023	-0.0006	20
222	56842.1720	0.0017	-0.0007	45
223	56842.2298	0.0015	-0.0029	27
226	56842.4076	0.0008	-0.0051	99
227	56842.4685	0.0005	-0.0041	153
228	56842.5281	0.0008	-0.0045	128
229	56842.5895	0.0007	-0.0031	48
232	56842.7678	0.0012	-0.0047	75
233	56842.8276	0.0006	-0.0049	128
234	56842.8859	0.0008	-0.0066	131
242	56843.3644	0.0036	-0.0080	45
243	56843.4207	0.0012	-0.0117	61
249	56843.7805	0.0021	-0.0119	86

*BJD-2400000.

 † Against max = 2456828.8559 + 0.059986 E . ‡ Number of points used to determine the maximum.**Table 45.** Superhump maxima of ASASSN-14cl (2014) (post-superoutburst)

E	max*	error	$O - C^\dagger$	N^\ddagger
0	56844.4338	0.0116	0.0034	14
5	56844.7257	0.0021	-0.0034	81
6	56844.7822	0.0048	-0.0067	108
7	56844.8478	0.0018	-0.0009	76
8	56844.9039	0.0026	-0.0045	64
17	56845.4379	0.0015	-0.0082	42
18	56845.5115	0.0007	0.0056	44
22	56845.7499	0.0053	0.0050	14
25	56845.9245	0.0073	0.0003	33
34	56846.4600	0.0019	-0.0020	27
35	56846.5312	0.0010	0.0094	27
41	56846.8836	0.0023	0.0034	45
47	56847.2415	0.0035	0.0027	58
48	56847.2989	0.0032	0.0004	56
53	56847.5945	0.0012	-0.0027	39
54	56847.6675	0.0089	0.0104	9
56	56847.7838	0.0070	0.0072	42
58	56847.8976	0.0067	0.0016	51
72	56848.7209	0.0078	-0.0117	18
73	56848.7837	0.0018	-0.0086	49
74	56848.8551	0.0027	0.0030	71
79	56849.1549	0.0044	0.0041	16
122	56851.7239	0.0082	0.0037	17
123	56851.7772	0.0179	-0.0028	15
124	56851.8371	0.0026	-0.0027	14
131	56852.2519	0.0036	-0.0061	55
155	56853.6934	0.0037	0.0013	14
157	56853.8115	0.0132	-0.0001	15
189	56855.7162	0.0024	-0.0075	19
280	56861.1663	0.0018	0.0051	58
281	56861.2220	0.0049	0.0010	40

*BJD-2400000.

 † Against max = 2456844.4304 + 0.059753 E . ‡ Number of points used to determine the maximum.

3.43. ASASSN-14do

This object was detected as a transient at $V=15.08$ on 2014 July 1 by ASAS-SN team (vsnet-alert 17447). The coordinates are $20^{\text{h}}37^{\text{m}}06^{\text{s}}.79$, $-30^{\circ}12'21''.7$. The object has been spectroscopically confirmed to be a CV (Prieto et al. 2014b).

Although initial observations did not show strong superhumps (vsnet-alert 17464), the object soon developed superhumps (vsnet-alert 17467, 17476, 17506; figure 59). The times of superhump maxima are listed in table 48. Although $E = 0$ corresponds to stage A superhumps, the period of stage A superhumps could not have been determined.

3.44. ASASSN-14dw

This object was detected as a transient at $V=14.23$ on 2014 July 10 by ASAS-SN team (vsnet-alert 17487). The coordinates are $13^{\text{h}}43^{\text{m}}37^{\text{s}}.18$, $-44^{\circ}26'42''.0$ (2MASS po-

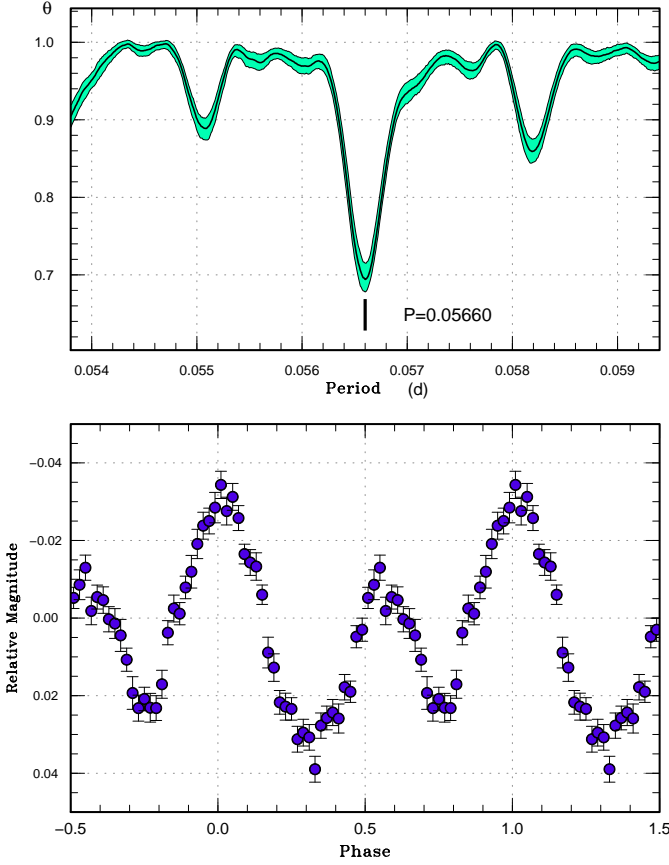


Fig. 56. Early superhumps in ASASSN-14cq (2014). (Upper): PDM analysis. (Lower): Phase-averaged profile

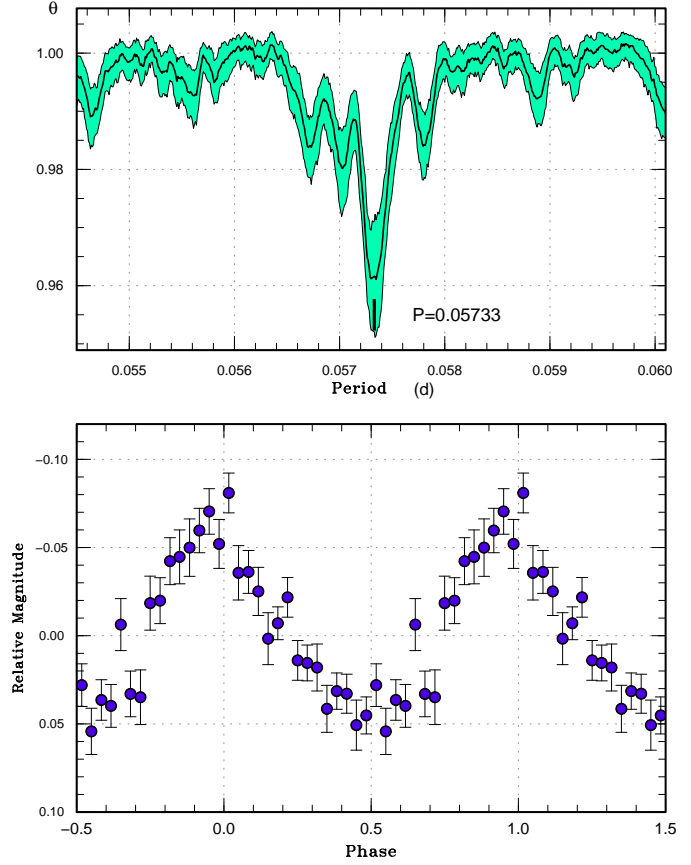


Fig. 57. Ordinary superhumps in ASASSN-14cq (2014). (Upper): PDM analysis. (Lower): Phase-averaged profile

sition). The object further brightened to $V=13.4$ on July 12 in the ASAS-SN data. Time-resolved photometry detected superhumps (vsnet-alert 17495, 17498; figure 60). The times of superhump maxima are listed in table 49. Both stages B and C can be identified. The object started fading rapidly on July 22. The duration of the superoutburst was ~ 12 d, which was not particularly long as in objects with similar P_{SH} , such as TT Boo (Olech et al. 2004). During the post-superoutburst period, the object stayed around 17 mag for at least eight days. Although individual superhump maxima were not measured, an analysis of the entire post-superoutburst data yielded a strong period of 0.07498(6) d. A PDM analysis of the combined data of stage C during the superoutburst plateau and post-superoutburst yielded a period of 0.07491(3) d. This period can express well both observations of stage C during the superoutburst plateau and post-superoutburst without a phase shift. It is most likely that there was no phase jump around the termination of the superoutburst.

3.45. ASASSN-14eh

This object was detected as a transient at $V=16.7$ on 2014 July 21 by ASAS-SN team (vsnet-alert 17533). The coordinates are $20^{\text{h}}32^{\text{m}}37^{\text{s}}.49$, $+03^{\circ}05'25''.3$ (GSC 2.3.2

position). The object has a GALEX UV counterpart with an NUV magnitude of 22.4. The object further brightened to $V=14.94$ on July 23. On July 28, the object started to show prominent superhumps (vsnet-alert 17568; figure 61) accompanied by a slight rise of the brightness. The times of superhump maxima are listed in table 50. Although there was possibility of early superhumps or stage A superhumps before July 28, we could not detect variations securely due to the limited observational coverage. The superoutburst lasted at least 13 d.

3.46. ASASSN-14eq

This object was detected as a transient at $V=13.53$ on 2014 July 28 by ASAS-SN team (vsnet-alert 17561). The coordinates are $00^{\text{h}}21^{\text{m}}30^{\text{s}}.92$, $-57^{\circ}19'22''.0$ (2MASS position). The object has a GALEX UV counterpart with an NUV magnitude of 18.1. ASAS-3 data indicated at least five past outbursts and at least one of them (2005 November-December one) looked like a superoutburst. Subsequent observations detected superhumps (vsnet-alert 17576; figure 62). The times of superhump maxima are listed in table 51. The large negative P_{dot} for the entire observation appears to be a result of a stage transition. We could not distinguish whether it was stage

Table 46. Superhump maxima of ASASSN-14cq (2014)

E	max*	error	$O - C^\dagger$	N^\ddagger
0	56833.3147	0.0040	-0.0019	59
34	56835.2705	0.0003	0.0035	132
35	56835.3281	0.0004	0.0037	111
36	56835.3838	0.0002	0.0021	130
37	56835.4422	0.0003	0.0030	132
38	56835.4988	0.0008	0.0023	19
39	56835.5558	0.0005	0.0020	15
40	56835.6149	0.0011	0.0037	11
41	56835.6724	0.0005	0.0039	19
42	56835.7277	0.0007	0.0017	11
52	56836.3009	0.0004	0.0013	132
53	56836.3598	0.0004	0.0028	132
54	56836.4162	0.0004	0.0019	131
55	56836.4730	0.0004	0.0013	140
56	56836.5306	0.0013	0.0016	37
57	56836.5876	0.0007	0.0011	15
68	56837.2147	0.0010	-0.0027	77
69	56837.2747	0.0004	-0.0001	132
70	56837.3316	0.0004	-0.0006	132
71	56837.3873	0.0005	-0.0022	129
72	56837.4473	0.0008	0.0004	128
73	56837.5025	0.0007	-0.0018	84
74	56837.5610	0.0007	-0.0006	15
75	56837.6181	0.0005	-0.0009	11
76	56837.6739	0.0007	-0.0024	17
90	56838.4779	0.0014	-0.0015	12
91	56838.5345	0.0010	-0.0024	15
92	56838.5923	0.0008	-0.0019	13
93	56838.6487	0.0009	-0.0029	16
94	56838.7067	0.0007	-0.0023	15
108	56839.5077	0.0014	-0.0043	17
109	56839.5671	0.0011	-0.0023	15

*BJD-2400000.

 † Against max = 2456833.3166 + 0.057365 E . ‡ Number of points used to determine the maximum.

A-B or stage B-C transition due to the lack of observations before the ASAS-SN detection.

A list of known outbursts is given in table 52. It looks likely only superoutbursts were recorded by ASAS-3. The shortest interval between the outbursts was ~ 410 d, which may be the supercycle. Since the object is relatively bright, the object would also be a good target for visual monitoring.

3.47. ASASSN-14fr

This object was detected as a transient at $V=15.9$ on 2014 August 16 by ASAS-SN team (vsnet-alert 17628). The coordinates are $21^{\text{h}}59^{\text{m}}06^{\text{s}}90$, $-35^{\circ}29'56''8$ (The Initial Gaia Source List). The object was spectroscopically confirmed as a CV in outburst (Hodgkin et al. 2014). Based on a single-night observation, a period of 0.073 d was reported (vsnet-alert 17631; figure 63). The times of superhump maxima from these data are

Table 46. Superhump maxima of ASASSN-14cq (2014) (continued)

E	max*	error	$O - C^\dagger$	N^\ddagger
111	56839.6814	0.0009	-0.0027	16
125	56840.4861	0.0006	-0.0011	14
126	56840.5423	0.0008	-0.0022	14
127	56840.6021	0.0007	0.0001	10
128	56840.6572	0.0009	-0.0021	15
139	56841.2865	0.0010	-0.0038	92
141	56841.4044	0.0010	-0.0007	101
142	56841.4585	0.0009	-0.0039	124
143	56841.5176	0.0009	-0.0022	15
144	56841.5717	0.0016	-0.0054	14
145	56841.6307	0.0008	-0.0039	12
146	56841.6865	0.0015	-0.0054	15
192	56844.3392	0.0016	0.0085	119
193	56844.3934	0.0010	0.0053	132
194	56844.4534	0.0020	0.0080	96
225	56846.2213	0.0030	-0.0025	132
226	56846.2855	0.0019	0.0044	131
227	56846.3427	0.0018	0.0043	132

*BJD-2400000.

 † Against max = 2456833.3166 + 0.057365 E . ‡ Number of points used to determine the maximum.**Table 47.** Superhump maxima of ASASSN-14dm (2014)

E	max*	error	$O - C^\dagger$	N^\ddagger
0	56842.2076	0.0003	0.0003	116
1	56842.2752	0.0002	-0.0003	157
2	56842.3417	0.0003	-0.0022	153
31	56844.3220	0.0005	-0.0026	154
32	56844.3910	0.0005	-0.0019	157
33	56844.4662	0.0018	0.0050	43
73	56847.1864	0.0043	-0.0068	50
74	56847.2667	0.0007	0.0051	157
75	56847.3351	0.0010	0.0053	157
76	56847.4008	0.0010	0.0026	134
90	56848.3549	0.0007	0.0005	151
91	56848.4250	0.0047	0.0023	54
103	56849.2399	0.0008	-0.0024	157
104	56849.3058	0.0010	-0.0048	146

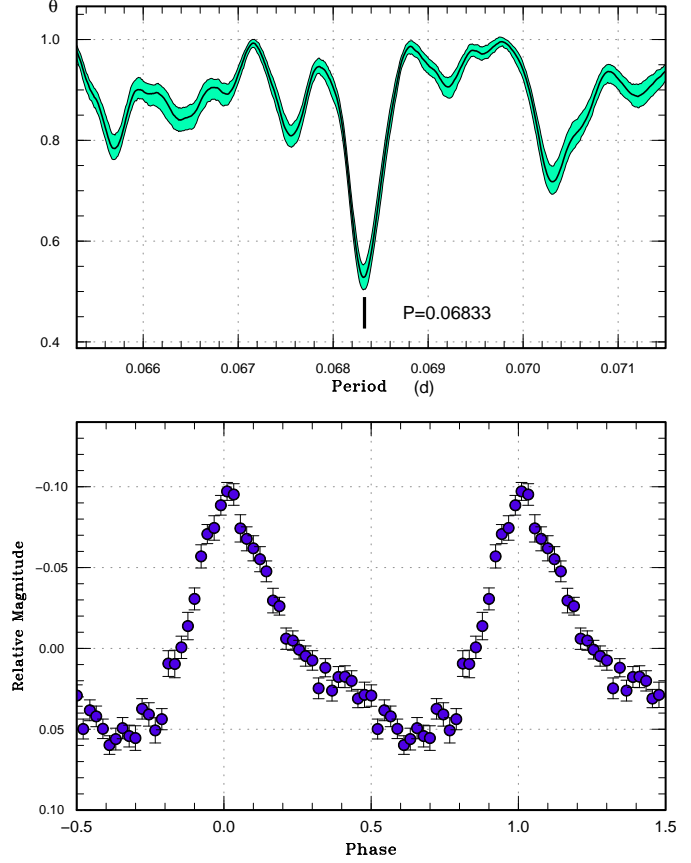
*BJD-2400000.

 † Against max = 2456842.2073 + 0.068301 E . ‡ Number of points used to determine the maximum.

Table 48. Superhump maxima of ASASSN-14do (2014)

E	max*	error	$O - C^\dagger$	N^\ddagger
0	56845.7565	0.0029	-0.0083	19
14	56846.5539	0.0005	-0.0028	130
15	56846.6156	0.0005	0.0023	130
17	56846.7277	0.0016	0.0013	19
18	56846.7866	0.0016	0.0036	17
19	56846.8439	0.0013	0.0043	8
30	56847.4636	0.0005	0.0018	131
31	56847.5202	0.0005	0.0019	131
32	56847.5770	0.0005	0.0021	130
33	56847.6333	0.0005	0.0018	130
34	56847.6920	0.0008	0.0039	90
47	56848.4187	0.0058	-0.0047	60
48	56848.4764	0.0010	-0.0036	130
49	56848.5365	0.0006	-0.0001	130
50	56848.5938	0.0006	0.0007	131
51	56848.6498	0.0062	0.0001	45
52	56848.7094	0.0010	0.0032	12
53	56848.7601	0.0017	-0.0028	16
54	56848.8136	0.0027	-0.0058	15
105	56851.7056	0.0029	0.0012	14

*BJD-2400000.

 † Against max = 2456845.7648 + 0.056568 E . ‡ Number of points used to determine the maximum.**Fig. 58.** Superhumps in ASASSN-14dm (2014). (Upper): PDM analysis. (Lower): Phase-averaged profile**Table 49.** Superhump maxima of ASASSN-14dw (2014)

E	max*	error	$O - C^\dagger$	N^\ddagger
0	56852.4711	0.0011	-0.0080	10
1	56852.5542	0.0022	-0.0003	14
14	56853.5352	0.0013	-0.0003	17
15	56853.6093	0.0011	-0.0016	17
27	56854.5197	0.0013	0.0034	16
28	56854.5943	0.0006	0.0025	16
53	56856.4832	0.0009	0.0051	14
54	56856.5588	0.0012	0.0053	16
67	56857.5379	0.0010	0.0035	16
68	56857.6115	0.0012	0.0017	14
80	56858.5150	0.0019	-0.0002	17
81	56858.5899	0.0021	-0.0008	17
93	56859.4895	0.0025	-0.0066	15
94	56859.5679	0.0053	-0.0036	17

*BJD-2400000.

 † Against max = 2456852.4791 + 0.075451 E . ‡ Number of points used to determine the maximum.**Table 50.** Superhump maxima of ASASSN-14eh (2014)

E	max*	error	$O - C^\dagger$	N^\ddagger
0	56866.6506	0.0011	0.0001	7
1	56866.7139	0.0007	0.0005	12
16	56867.6592	0.0005	0.0022	10
17	56867.7214	0.0013	0.0015	10
33	56868.7278	0.0017	0.0014	7
48	56869.6684	0.0012	-0.0016	12
49	56869.7314	0.0034	-0.0015	9
64	56870.6711	0.0022	-0.0055	13
65	56870.7339	0.0017	-0.0056	7
80	56871.6850	0.0024	0.0019	14
86	56872.0644	0.0020	0.0039	71
87	56872.1225	0.0030	-0.0009	66
96	56872.6933	0.0026	0.0037	12

*BJD-2400000.

 † Against max = 2456866.6505 + 0.062907 E . ‡ Number of points used to determine the maximum.

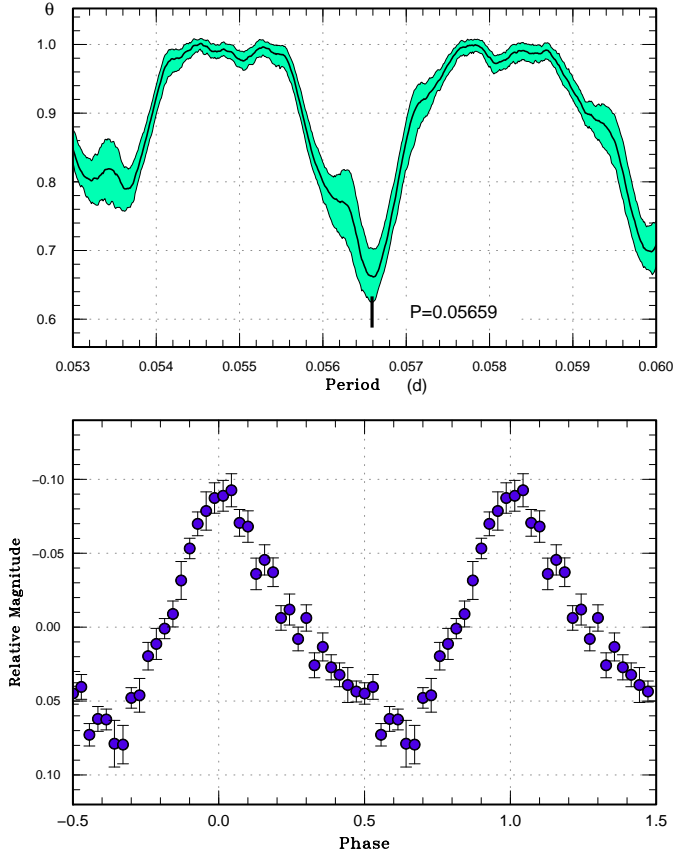


Fig. 59. Superhumps in ASASSN-14do (2014). (Upper): PDM analysis. (Lower): Phase-averaged profile

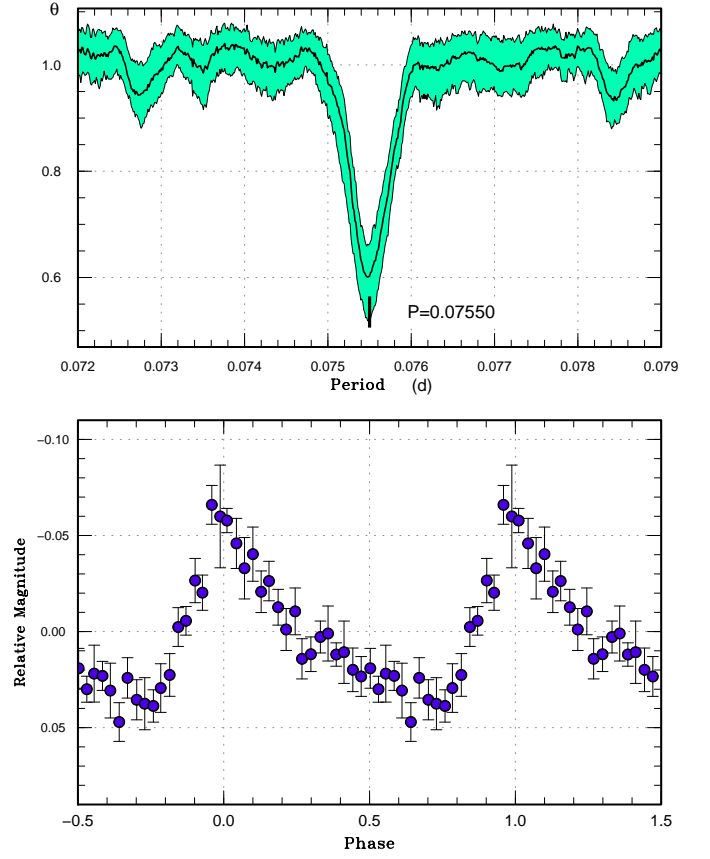


Fig. 60. Superhumps in ASASSN-14dw during the super-outburst plateau (2014). (Upper): PDM analysis. (Lower): Phase-averaged profile

Table 51. Superhump maxima of ASASSN-14eq (2014)

E	max*	error	$O - C^\dagger$	N^\ddagger
0	56868.5150	0.0040	-0.0050	64
1	56868.5970	0.0005	-0.0025	185
2	56868.6762	0.0005	-0.0027	148
12	56869.4779	0.0003	0.0043	183
13	56869.5612	0.0004	0.0082	184
14	56869.6333	0.0004	0.0008	184
50	56872.4948	0.0007	0.0015	183
51	56872.5706	0.0007	-0.0022	184
52	56872.6499	0.0008	-0.0024	164

*BJD-2400000.

† Against max = 2456868.5200 + 0.079467 E .

‡ Number of points used to determine the maximum.

Table 52. List of known outbursts of ASASSN-14eq.

Year	Month	max*	magnitude	type	source
2001	9	52168	14.0	?	ASAS-3
2002	10	52578	13.3	?	ASAS-3
2004	1	53005	13.6	?	ASAS-3
2005	11	53702	13.5	super	ASAS-3
2007	5	54231	13.5:	super?	ASAS-3
2014	7	56867	13.5	super	ASAS-SN

*JD-2400000.

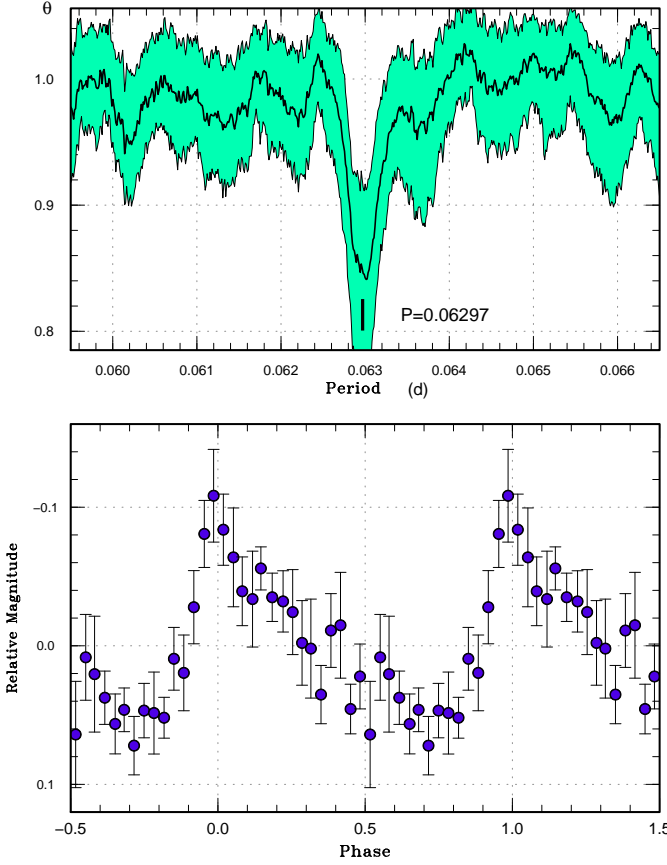


Fig. 61. Superhumps in ASASSN-14eh (2014). (Upper): PDM analysis. (Lower): Phase-averaged profile

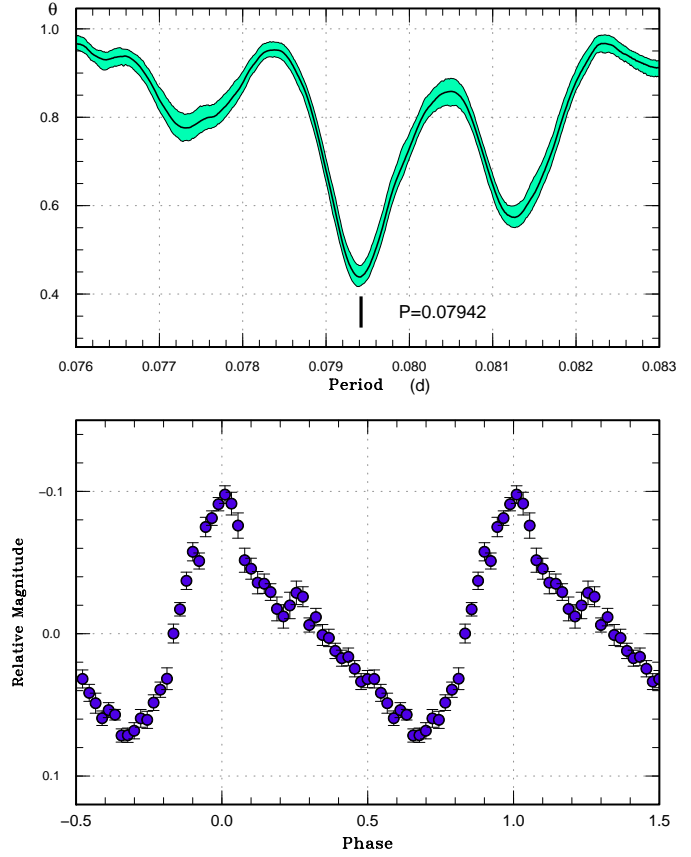


Fig. 62. Superhumps in ASASSN-14eq (2014). (Upper): PDM analysis. (Lower): Phase-averaged profile

BJD 2456886.5052(18) ($N=169$) and 2456886.6289(26) ($N=169$). The observation was not long enough to constrain the period better than the initial report.

3.48. ASASSN-14qd

This object was detected as a transient at $V=16.23$ on 2014 August 23 by ASAS-SN team (vsnet-alert 17670). The coordinates are $19^{\text{h}}26^{\text{m}}08^{\text{s}}.92$, $-65^{\circ}26'21''.0$ (GSC 2.3.2 position). There is a GALEX counterpart with an NUV magnitude of 21.9. Superhumps were detected in observations on two nights (vsnet-alert 17669; figure 64). The times of superhump maxima are listed in table 53. The superhump period in table 2 was obtained by the PDM method.

3.49. ASASSN-14qq

This object was detected as a transient at $V=13.92$ on 2014 September 4 by ASAS-SN team (vsnet-alert 17695). The coordinates are $19^{\text{h}}27^{\text{m}}10^{\text{s}}.15$, $-48^{\circ}47'52''.3$ (2MASS position). At least six past outbursts were recorded by CRTS. Superhumps with a period of ~ 0.072 d were recorded (vsnet-alert 17731; figure 65x). Two superhump maxima were recorded: BJD 2456908.2970(7) ($N=164$) and 2456908.3687(8) ($N=166$). Although there were ob-

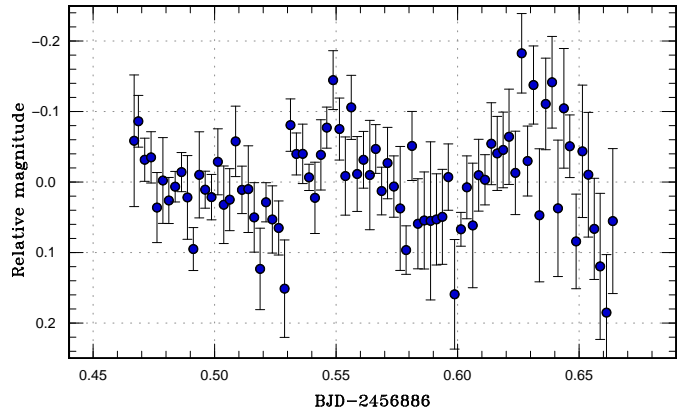


Fig. 63. Superhumps in ASASSN-14fr (2014). The data were binned to 0.0025 d.

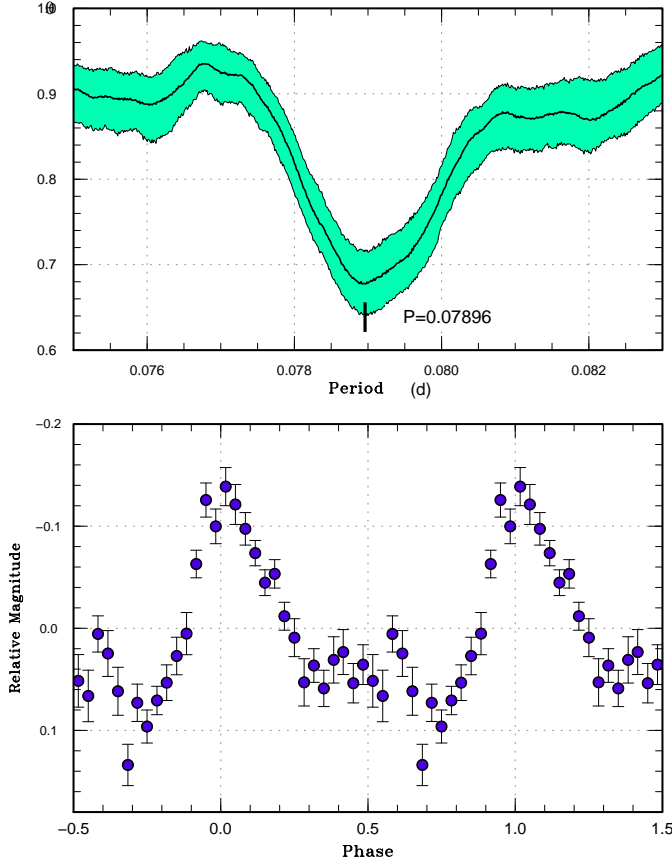


Fig. 64. Superhumps in ASASSN-14gd (2014). (Upper): PDM analysis. (Lower): Phase-averaged profile

Table 53. Superhump maxima of ASASSN-14gd (2014)

E	max*	error	$O - C^\dagger$	N^\ddagger
0	56895.3042	0.0011	0.0010	182
1	56895.3813	0.0013	-0.0010	179
12	56896.2528	0.0008	0.0003	177
13	56896.3298	0.0009	-0.0018	180
14	56896.4121	0.0010	0.0014	148

*BJD-2400000.

† Against max = 2456895.3032 + 0.079109 E .

‡ Number of points used to determine the maximum.

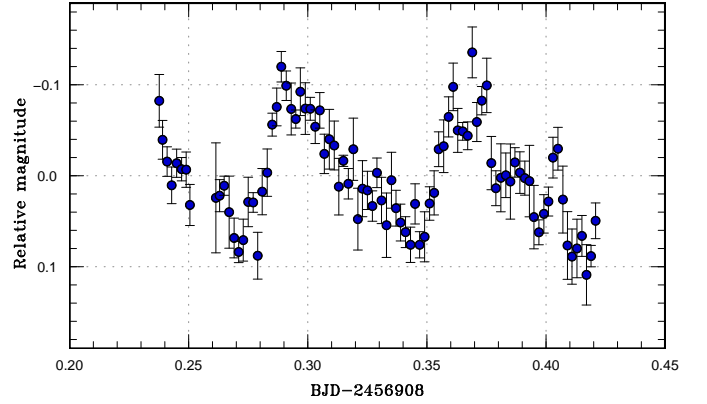


Fig. 65. Superhumps in ASASSN-14gq (2014). The data were binned to 0.002 d.

servation on BJD 2456916, the amplitudes of superhumps were too small to determine the times of maxima.

3.50. ASASSN-14gx

This object was detected as a transient at $V=14.9$ on 2014 September 6 by ASAS-SN team (vsnet-alert 17702). The object further brightened to $V=13.8$ on September 8. The coordinates are $23^{\text{h}}51^{\text{m}}23^{\text{s}}.92$, $-30^{\circ}27'25''.1$ (GSC 2.3.2 position). A signature of early superhumps was immediately reported (vsnet-alert 17715). The period of early superhumps was updated to 0.05488(3) d (figure 66). On September 15, the object showed ordinary superhumps (vsnet-alert 17738, 17748; figure 67). During the terminal stage of the plateau phase, the object slightly brightened (vsnet-alert 17768; figure 68). The times of superhumps maxima are listed in table 54. The maxima $E \leq 1$ correspond to stage A superhumps. Although stage A superhumps were recorded, we could not determine the period due to the shortness of the observation. Despite the brightening in the later part, there was no apparent indication of stage B-C transition and maxima up to $E=194$ were well expressed by an ephemeris up to $E=124$. We cannot, however, exclude a discontinuous period change due to the gap of 70 cycles. A PDM analysis after the brightening (BJD 2456924-2456928) yielded a possible period of 0.05592(9) d. Although this period may be that of stage C superhumps, observations were not sufficient to confirm this identification. Despite the large outburst amplitude, the behavior of this object did not look like that of an extreme WZ Sge-type dwarf nova.

3.51. ASASSN-14hk

This object was detected as a transient at $V=14.61$ on 2014 September 16 by ASAS-SN team (Stanek et al. 2014b). The coordinates are $01^{\text{h}}39^{\text{m}}35^{\text{s}}.62$, $+35^{\circ}38'40''.8$ (GSC 2.3.2 position). There is a GALEX counterpart with an NUV magnitude of 21.9. The large outburst amplitude (~ 6 mag) made the object a good candidate for an SU UMa-type dwarf nova. Subsequent observations initially detect no apparent modulations on September 20.

Table 54. Superhump maxima of ASASSN-14gx (2014)

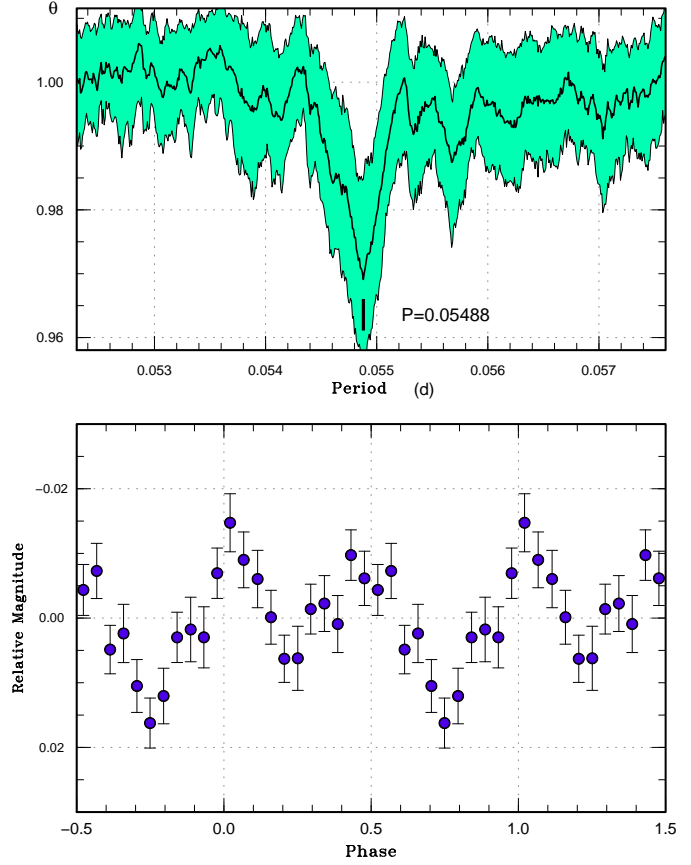
E	max*	error	$O - C^\dagger$	N^\ddagger
0	56914.6027	0.0050	-0.0065	144
1	56914.6627	0.0008	-0.0026	14
18	56915.6259	0.0011	0.0070	14
19	56915.6821	0.0005	0.0070	15
31	56916.3527	0.0006	0.0044	101
32	56916.4078	0.0006	0.0035	90
33	56916.4642	0.0008	0.0038	90
34	56916.5184	0.0007	0.0019	91
35	56916.5763	0.0007	0.0037	131
36	56916.6319	0.0018	0.0032	64
37	56916.6878	0.0010	0.0030	15
41	56916.9112	0.0002	0.0021	47
42	56916.9670	0.0003	0.0017	55
43	56917.0286	0.0010	0.0072	21
45	56917.1327	0.0009	-0.0009	42
46	56917.1875	0.0009	-0.0022	41
53	56917.5819	0.0012	-0.0004	15
54	56917.6370	0.0013	-0.0014	14
55	56917.6919	0.0014	-0.0026	15
59	56917.9178	0.0005	-0.0011	55
60	56917.9717	0.0004	-0.0034	56
61	56918.0324	0.0023	0.0013	13
77	56918.9229	0.0005	-0.0058	56
78	56918.9798	0.0005	-0.0050	56
89	56919.6021	0.0025	0.0003	15
90	56919.6493	0.0017	-0.0086	14
95	56919.9324	0.0007	-0.0060	56
96	56919.9901	0.0006	-0.0044	56
107	56920.6047	0.0022	-0.0068	14
113	56920.9405	0.0012	-0.0076	51
114	56921.0000	0.0006	-0.0041	46

*BJD-2400000.

 † Against max = 2456914.6092 + 0.056096 E . ‡ Number of points used to determine the maximum.**Table 54.** Superhump maxima of ASASSN-14gx (2014)
(continued)

E	max*	error	$O - C^\dagger$	N^\ddagger
120	56921.3467	0.0055	0.0059	76
121	56921.3951	0.0013	-0.0018	127
123	56921.5067	0.0019	-0.0023	129
124	56921.5638	0.0030	-0.0013	141
192	56925.3855	0.0013	0.0058	129
193	56925.4436	0.0017	0.0078	129
194	56925.4971	0.0021	0.0052	136

*BJD-2400000.

 † Against max = 2456914.6092 + 0.056096 E . ‡ Number of points used to determine the maximum.**Fig. 66.** Early superhumps in ASASSN-14gx (2014).
(Upper): PDM analysis. (Lower): Phase-averaged profile**Table 55.** Superhump maxima of ASASSN-14hk (2014)

E	max*	error	$O - C^\dagger$	N^\ddagger
0	56921.0890	0.0035	0.0026	51
1	56921.1463	0.0026	-0.0002	71
2	56921.2101	0.0026	0.0037	120
3	56921.2638	0.0016	-0.0026	128
36	56923.2428	0.0010	-0.0036	45
37	56923.3049	0.0008	-0.0016	45
118	56928.1686	0.0050	0.0021	61
135	56929.1861	0.0018	-0.0005	27

*BJD-2400000.

 † Against max = 2456921.0864 + 0.060001 E . ‡ Number of points used to determine the maximum.

Superhumps were present on September 22 (BJD 2456921, vsnet-alert 17773). The superhumps took 4–6 d to develop. Although there remained some ambiguity in period selection, we selected the superhump period to best match the result from the long single-night observation on BJD 2456921 (figure 69). The times of superhump maxima are listed in table 55. The epochs for $E \leq 118$ were not very certain due to the low signal-to-noise ratio.

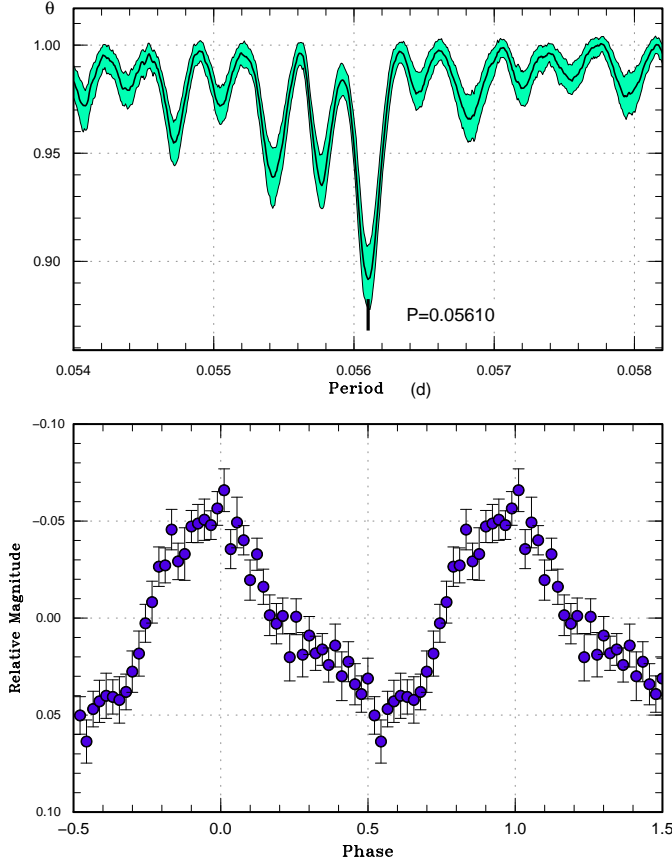


Fig. 67. Ordinary superhumps in ASASSN-14gx during the plateau phase (2014). (Upper): PDM analysis. (Lower): Phase-averaged profile

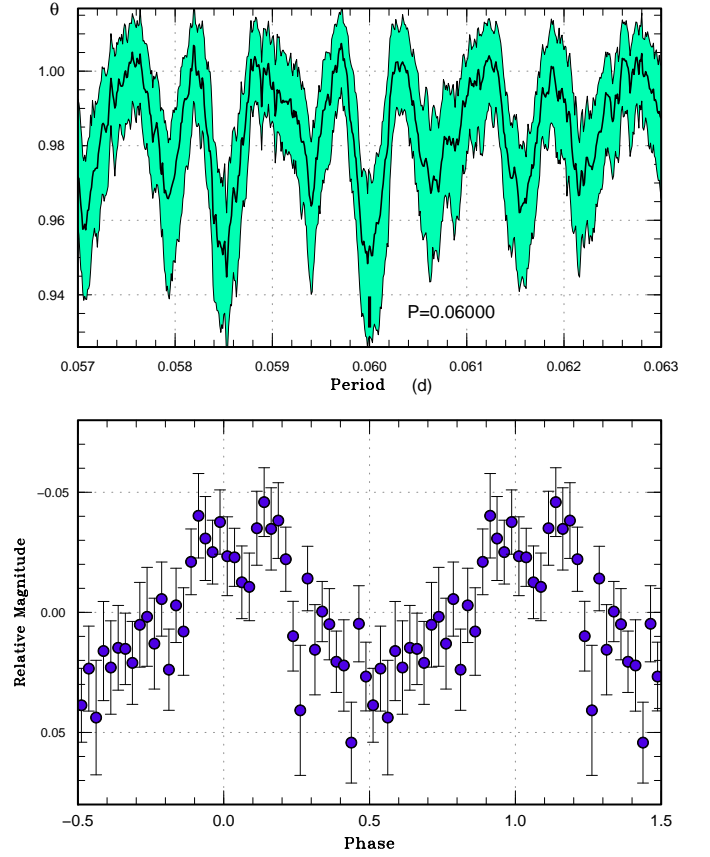


Fig. 69. Superhumps in ASASSN-14hk after BJD 2456923 (2014). (Upper): PDM analysis. (Lower): Phase-averaged profile

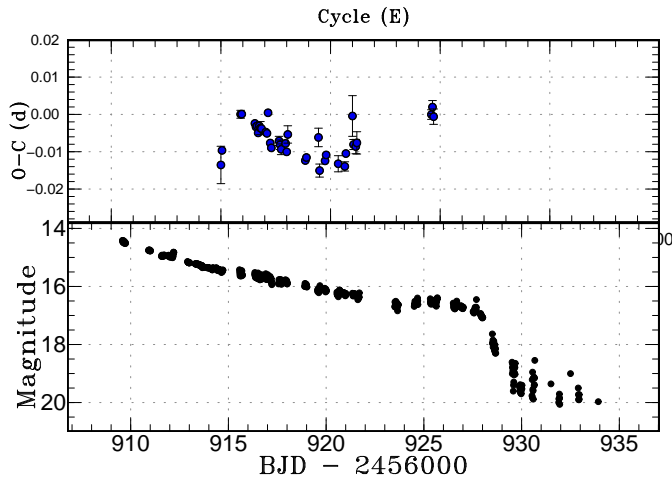


Fig. 68. $O - C$ diagram of superhumps in ASASSN-14gx (2014). (Upper): $O - C$ diagram. A period of 0.05609 d was used to draw this figure. (Lower): Light curve. The observations were binned to 0.011 d.

3.52. ASASSN-14hl

This object was detected as a transient at $V=15.42$ on 2014 September 18 by ASAS-SN team (vsnet-alert 17746). The coordinates are $23^{\text{h}}49^{\text{m}}55^{\text{s}}.12$, $-60^{\circ}54'17''.1$ (the Initial Gaia Source List). Two superhumps were detected from a single-night observation (vsnet-alert 17772, figure 70): BJD 2456925.3196(6) ($N=157$) and 2456925.3885(7) ($N=158$). The superhump period is 0.0685(5) d.

3.53. ASASSN-14hs

This object was detected as a transient at $V=13.99$ on 2014 September 26 by ASAS-SN team (vsnet-alert 17777). The coordinates are $22^{\text{h}}42^{\text{m}}58^{\text{s}}.04$, $-19^{\circ}45'51''.5$ (the Initial Gaia Source List). There is a GALEX counterpart with an NUV magnitude of 20.0. Subsequent observations detected superhumps (vsnet-alert 17785, 17802, 17809; figure 71). The period suggests that the object is located in the lower edge of the period gap. The times of superhumps maxima are listed in table 56. Except $E \leq 1$, the maxima could be expressed by a relatively constant period. The last two epochs correspond to the rapidly fading part. Since $O - C$ variations in long- P_{orb} systems strongly depends on object, we could not identify the su-

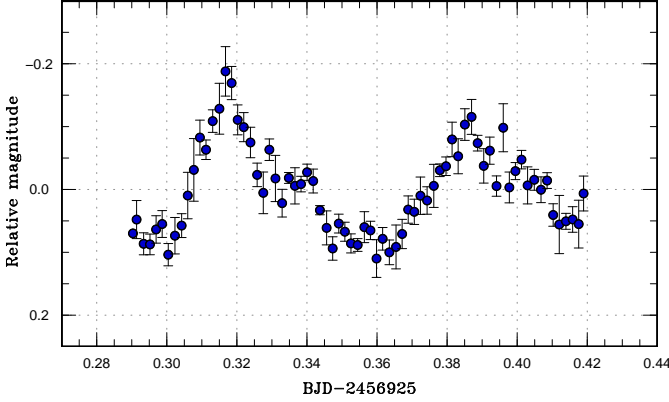


Fig. 70. Superhumps in ASASSN-14hl (2014). The data were binned to 0.0018 d.

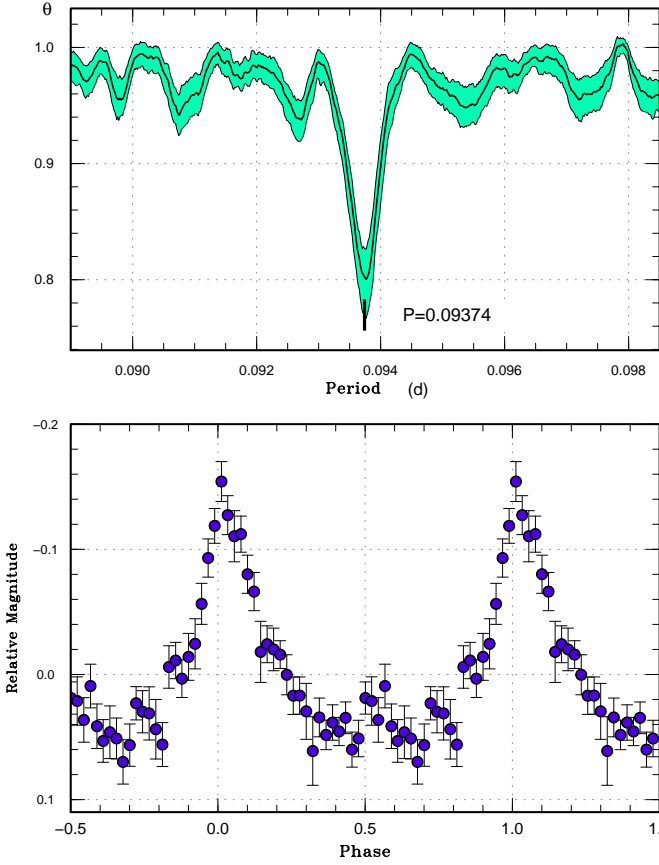


Fig. 71. Superhumps in ASASSN-14hs (2014). (Upper): PDM analysis. (Lower): Phase-averaged profile

Table 56. Superhump maxima of ASASSN-14hs (2014)

E	max*	error	$O - C^\dagger$	N^\ddagger
0	56929.0606	0.0005	-0.0092	97
1	56929.1540	0.0005	-0.0096	118
10	56930.0118	0.0020	0.0047	51
11	56930.1008	0.0069	-0.0001	9
26	56931.5084	0.0118	0.0016	8
27	56931.6067	0.0009	0.0062	18
27	56931.6071	0.0010	0.0065	18
37	56932.5417	0.0006	0.0039	22
38	56932.6277	0.0065	-0.0038	10
55	56934.2313	0.0069	0.0064	97
56	56934.3167	0.0005	-0.0020	193
57	56934.4112	0.0021	-0.0012	65
66	56935.2541	0.0008	-0.0019	162
67	56935.3500	0.0011	0.0003	195
69	56935.5386	0.0014	0.0014	39
70	56935.6408	0.0018	0.0099	41
80	56936.5526	0.0027	-0.0156	47
81	56936.6670	0.0070	0.0050	22
88	56937.3185	0.0025	0.0005	216
90	56937.5213	0.0080	0.0158	30
101	56938.5340	0.0027	-0.0026	29
102	56938.6143	0.0032	-0.0160	50

*BJD-2400000.

† Against max = 2456929.0698 + 0.093730 E .

‡ Number of points used to determine the maximum.

The coordinates are $06^{\text{h}}40^{\text{m}}20^{\text{s}}.89$, $+44^{\circ}21'26''.4$ (the Initial Gaia Source List). Only rather fragmentary observations on two nights were obtained. The resultant superhump maxima were BJD 2456930.2213(29) ($N=15$), 2456930.2910(6) ($N=24$) and 2456932.2452(9) ($N=19$). The superhump period was not very well constrained. In figure 72, we selected one of the possible aliases.

3.55. ASASSN-14id

This object was detected as a transient at $V=14.3$ on 2014 September 29 by ASAS-SN team (vsnet-alert 17791). The coordinates are $07^{\text{h}}26^{\text{m}}37^{\text{s}}.23$, $+83^{\circ}32'18''.6$ (SDSS $g=20.8$ counterpart). Subsequent observations detected large-amplitude superhumps (vsnet-alert 17814, 17826; figures 73, 74). The times superhumps maxima are listed in table 57. Although the PDM figure is not so clear, it is probably a result of beat modulation because this object is eclipsing (as shown later). The period selection is secure from the $O - C$ analysis of the best observed segment of $E \leq 24$. The superhump stage was not clear from these observations.

On BJD 2456942 and 2456952, shallow eclipses (~ 0.3 mag) were observed. Since superhumps were strongly seen on BJD 2456942, we subtracted the superhump signal. After combining with the data on BJD 2456952, we applied an MCMC analysis (cf. Kato et al. 2013a) to determine the eclipse ephemeris. The result was

$$\text{Min(BJD)} = 2456942.3720(5) + 0.076857(4)E. \quad (5)$$

perhump stage confidently in this system.

3.54. ASASSN-14ia

This object was first detected as a transient at $V=14.3$ on 2014 September 19 by ASAS-SN team but was recognized at $V=15.6$ on September 24 (vsnet-alert 17786).

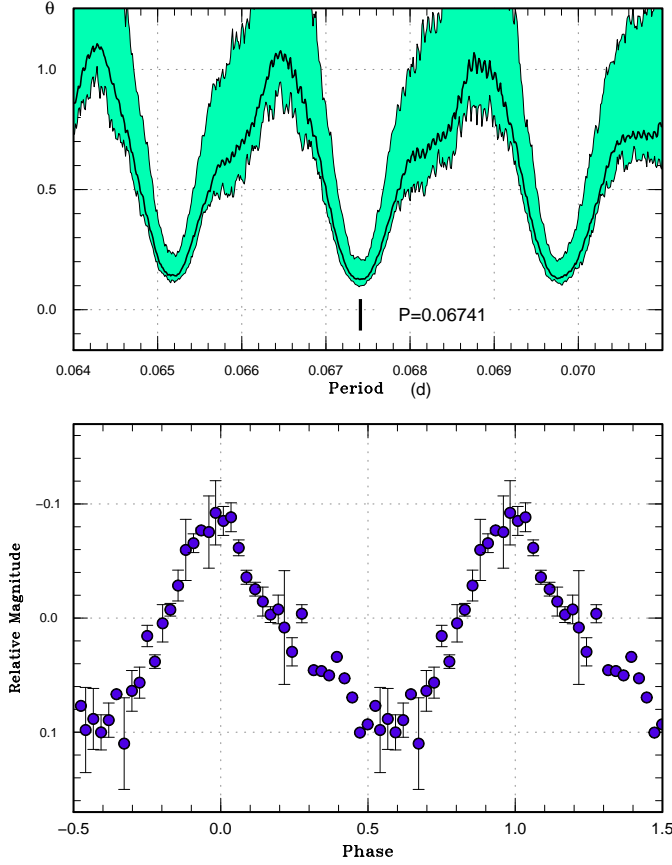


Fig. 72. Superhumps in ASASSN-14ia (2014). (Upper): PDM analysis. (Lower): Phase-averaged profile

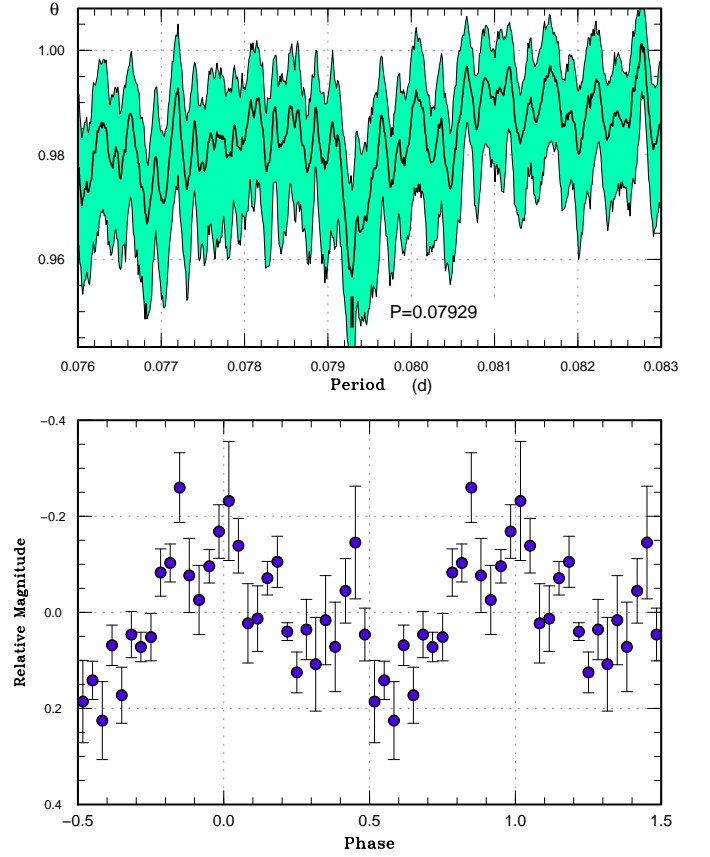


Fig. 73. Superhumps in ASASSN-14id (2014). (Upper): PDM analysis. A weak signal near 0.0769 d is likely the orbital one. (Lower): Phase-averaged profile

Although there were several possibilities of the orbital period due to the long gap between two nights, this period was selected because it gives a reasonably acceptable ϵ of 0.033. This period selection is confirmed by the detection of shallow eclipse-like features at zero orbital phase on earlier nights (figure 74). Since the eclipse profile was likely affected by superhumps, this ephemeris is not intended for long-term prediction of eclipse times. The observed large superhump amplitudes on the initial two nights were most likely a result of a high orbital inclination.

3.56. ASASSN-14it

This object was detected as a transient at $V=15.6$ on 2014 October 10 by ASAS-SN team. The coordinates are $20^{\text{h}}11^{\text{m}}09^{\text{s}}.13$, $+53^{\circ}39'01''.7$ (R. Nesci, vsnet-alert 17840). The absence of a quiescent counterpart in past catalogs suggested a large (≥ 6 mag) outburst amplitude. Only a short run on a single night was obtained. Although possible superhumps were detected (figure 75), the period was difficult to estimate due to the shortness of the observation.

Table 57. Superhump maxima of ASASSN-14id (2014)

E	max*	error	$O - C^{\dagger}$	phase ‡	N^{\S}
0	56935.3475	0.0003	-0.0012	0.60	75
1	56935.4267	0.0002	-0.0014	0.63	103
2	56935.5066	0.0002	-0.0009	0.67	77
24	56937.2530	0.0003	-0.0006	0.40	52
25	56937.3256	0.0008	-0.0074	0.34	36
36	56938.2071	0.0016	0.0012	0.81	46
37	56938.2945	0.0005	0.0092	0.95	46
48	56939.1624	0.0038	0.0041	0.24	31
88	56942.3328	0.0007	-0.0002	0.49	40
89	56942.4127	0.0005	0.0004	0.53	54
90	56942.4908	0.0006	-0.0009	0.55	40
137	56946.2196	0.0024	-0.0023	0.06	26

*BJD-2400000.

† Against max = $2456935.3488 + 0.079366E$.

‡ Orbital phase.

§ Number of points used to determine the maximum.

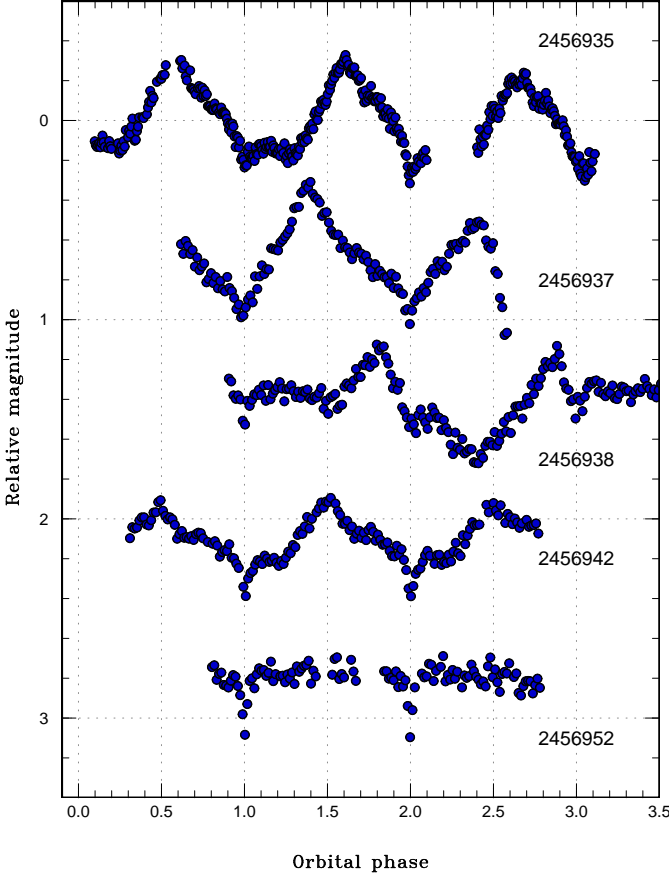


Fig. 74. Superhumps and eclipses in ASASSN-14id (2014). The orbital phase refers to equation (5). Shallow signatures of eclipses were also detected in all observations. The data were binned to 0.0025 d.

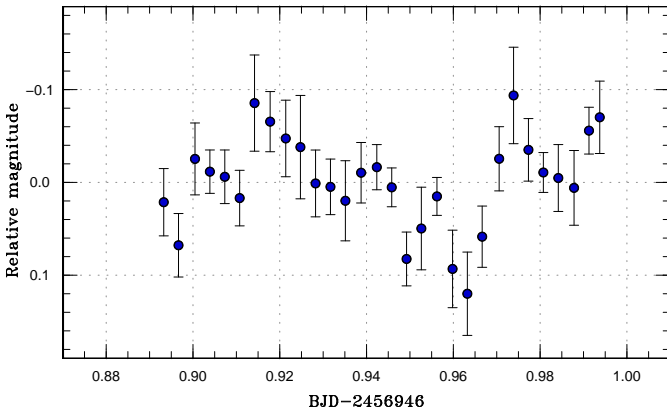


Fig. 75. Possible superhumps in ASASSN-14it (2014). The data were binned to 0.0035 d.

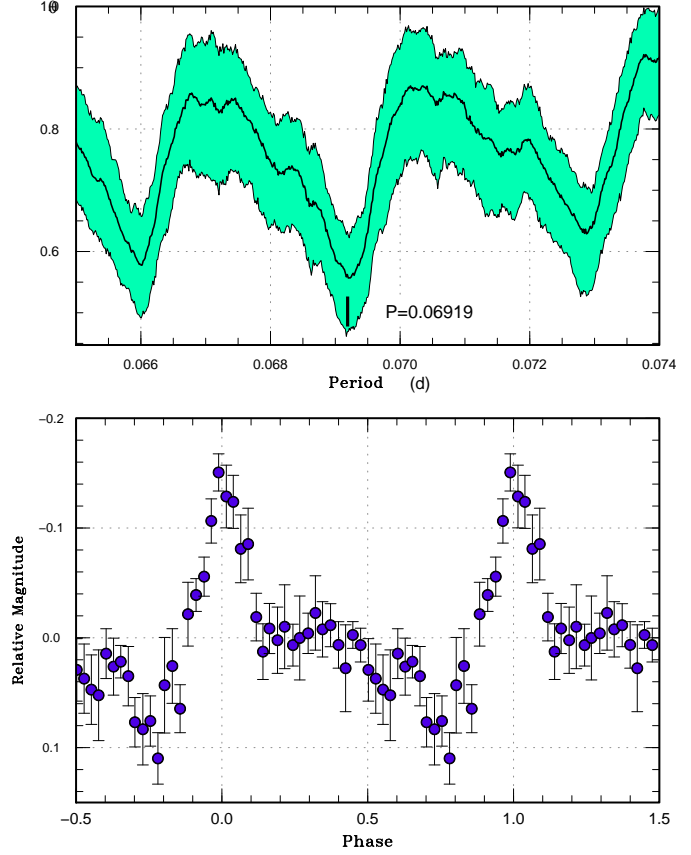


Fig. 76. Superhumps in ASASSN-14iv (2014). (Upper): PDM analysis. The selection of the alias was based on $O - C$ analysis. (Lower): Phase-averaged profile

Table 58. Superhump maxima of ASASSN-14iv (2014)

E	max*	error	$O - C^\dagger$	N^\ddagger
0	56944.5019	0.0255	-0.0073	9
1	56944.5829	0.0019	0.0042	33
2	56944.6516	0.0030	0.0035	15
21	56945.9698	0.0010	0.0028	72
22	56946.0333	0.0018	-0.0031	71

*BJD-2400000.

† Against max = 2456944.5092 + 0.069418 E .

‡ Number of points used to determine the maximum.

3.57. ASASSN-14iv

This object was detected as a transient at $V=15.6$ on 2014 October 10 by ASAS-SN team. The coordinates are $20^{\text{h}}35^{\text{m}}09^{\text{s}}.75$, $+09^{\circ}20'46''.4$ (SDSS $g=20.7$ counterpart). Subsequent observations detected superhumps (vsnet-alert 17844, 17850; figure 76). The times of superhump maxima are listed in table 58.

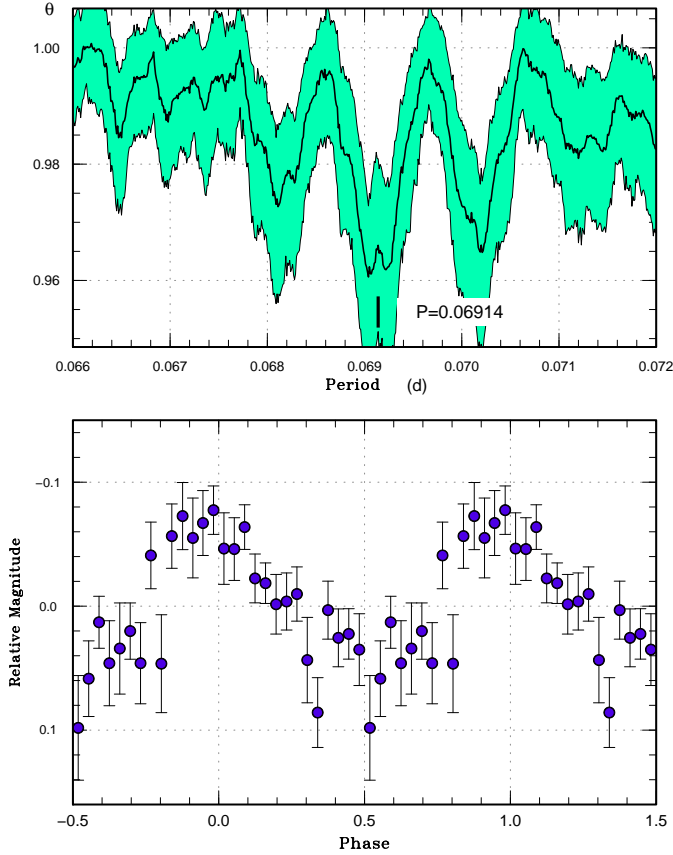


Fig. 77. Superhumps in ASASSN-14je (2014). (Upper): PDM analysis. (Lower): Phase-averaged profile

3.58. ASASSN-14je

This object was detected as a transient at $V=14.26$ on 2014 October 20 by ASAS-SN team (vsnet-alert 17880). The coordinates are $06^{\text{h}}32^{\text{m}}27^{\text{s}}.68$, $-56^{\circ}38'52''.6$ (the Initial Gaia Source List). Subsequent observations detected superhumps (vsnet-alert 17883, 17889; figure 77). The times of superhumps maxima are listed in table 59. The maxima for $E \geq 73$ correspond to the rapid fading phase. Since the object started fading rapidly within five days of the start of our outburst, the superhumps we observed were most likely stage C superhumps.

3.59. ASASSN-14jf

This object was detected as a transient at $V=13.3$ on 2014 October 22 by ASAS-SN team Simonian et al. (2014). The coordinates are $06^{\text{h}}06^{\text{m}}02^{\text{s}}.61$, $-60^{\circ}39'41''.5$ (the Initial Gaia Source List). There is a GALEX counterpart with an NUV magnitude of 20.9. The large outburst amplitude (~ 7.9 mag) suggested a WZ Sge-type dwarf nova. Subsequent observations indeed detected early superhumps (vsnet-alert 17897, 17898, 17901, 17923; figure 78). Nine days after the outburst detection, this object started to show ordinary superhumps (vsnet-alert 17928, 17930, 17938, 17960; figure 79). The times of superhump

Table 59. Superhump maxima of ASASSN-14je (2014)

E	max*	error	$O - C^{\dagger}$	N^{\ddagger}
0	56952.4237	0.0037	-0.0029	85
1	56952.4958	0.0003	0.0002	159
2	56952.5637	0.0004	-0.0010	160
3	56952.6372	0.0013	0.0035	33
14	56953.3908	0.0037	-0.0027	84
15	56953.4654	0.0004	0.0028	160
16	56953.5328	0.0005	0.0011	160
17	56953.6002	0.0012	-0.0005	76
73	56957.4603	0.0025	-0.0083	159
74	56957.5456	0.0057	0.0079	160

*BJD-2400000.

† Against max = $2456952.4266 + 0.069070E$.

‡ Number of points used to determine the maximum.

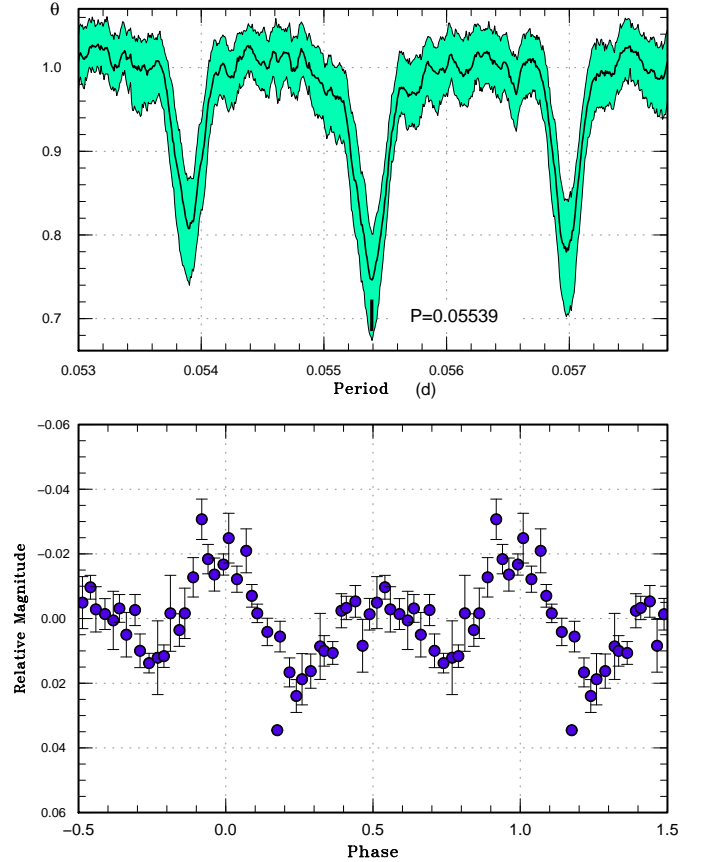


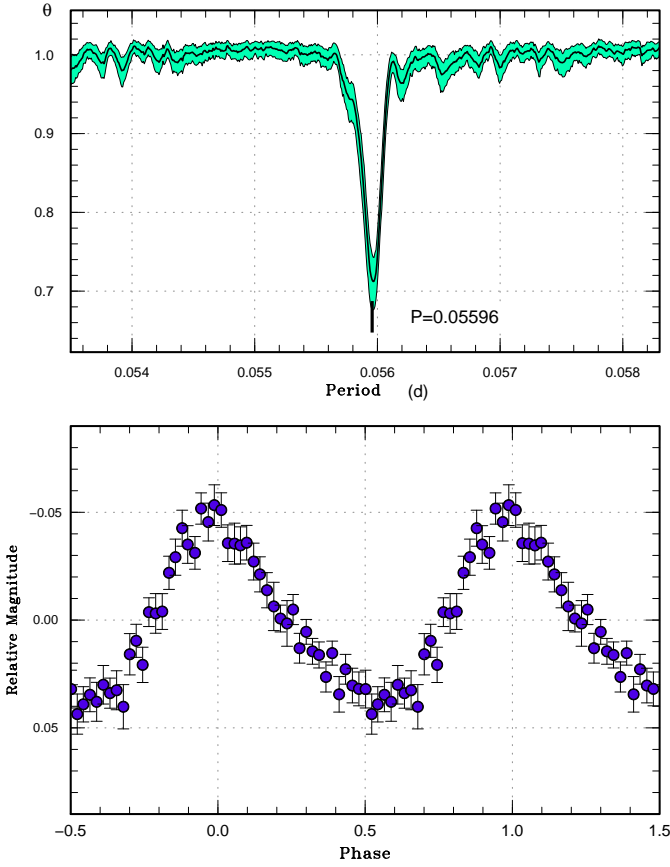
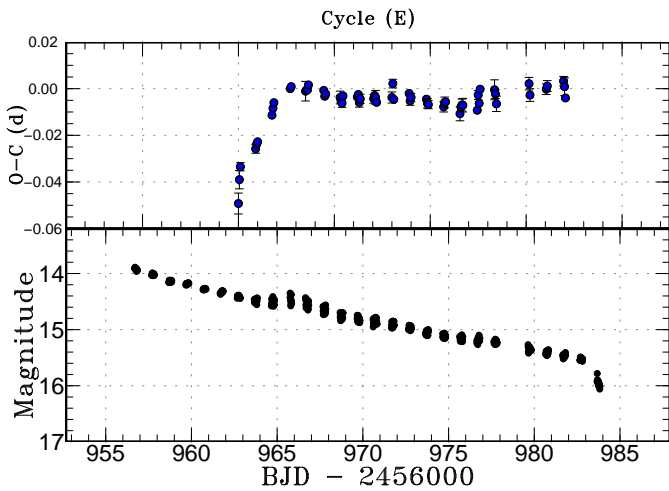
Fig. 78. Early superhumps in ASASSN-14jf (2014). (Upper): PDM analysis. (Lower): Phase-averaged profile

maxima are listed in table 60. Stages A and B can be clearly identified (figure 80). There was no evidence of transition to stage C superhumps during the superoutburst plateau, as is usual the case in WZ Sge-type dwarf novae. The period of stage A superhumps corresponds to $\epsilon^*=0.026(2)$ and $q=0.070(5)$.

Table 60. Superhump maxima of ASASSN-14jf (2014)

E	max*	error	$O - C^\dagger$	N^\ddagger
0	56962.6916	0.0045	-0.0347	16
1	56962.7577	0.0039	-0.0245	16
2	56962.8192	0.0018	-0.0190	20
18	56963.7221	0.0019	-0.0121	16
19	56963.7800	0.0011	-0.0102	17
20	56963.8370	0.0015	-0.0093	14
35	56964.6877	0.0010	0.0014	17
36	56964.7466	0.0010	0.0043	16
37	56964.8049	0.0007	0.0067	19
54	56965.7621	0.0008	0.0118	16
55	56965.8189	0.0005	0.0126	21
70	56966.6562	0.0042	0.0100	10
71	56966.7127	0.0009	0.0105	17
72	56966.7687	0.0010	0.0104	16
73	56966.8267	0.0005	0.0125	19
89	56967.7196	0.0014	0.0093	19
90	56967.7731	0.0009	0.0068	19
91	56967.8299	0.0010	0.0077	17
106	56968.6677	0.0027	0.0055	11
107	56968.7221	0.0010	0.0039	19
108	56968.7772	0.0018	0.0030	19
109	56968.8362	0.0016	0.0060	14
124	56969.6750	0.0011	0.0047	17
125	56969.7321	0.0012	0.0058	20
126	56969.7846	0.0020	0.0023	20
127	56969.8421	0.0020	0.0038	6
141	56970.6254	0.0019	0.0032	18
142	56970.6828	0.0015	0.0045	16
143	56970.7379	0.0030	0.0037	17
144	56970.7917	0.0009	0.0015	20
160	56971.6890	0.0024	0.0027	17
161	56971.7509	0.0018	0.0087	17
162	56971.8001	0.0017	0.0018	17

*BJD-2400000.

 † Against max = 2456962.7263 + 0.056000 E . ‡ Number of points used to determine the maximum.**Fig. 79.** Ordinary superhumps in ASASSN-14jf (2014). (Upper): PDM analysis. (Lower): Phase-averaged profile**Fig. 80.** $O - C$ diagram of superhumps in ASASSN-14jf (2014). (Upper): $O - C$ diagram. A period of 0.05595 d was used to draw this figure. (Lower): Light curve. The observations were binned to 0.011 d.

3.60. ASASSN-14jq

This object was detected as a transient at $V=13.74$ on 2014 November 6 by ASAS-SN team (vsnet-alert 17943). The coordinates are $02^{\text{h}}21^{\text{m}}02^{\text{s}}.78$, $+73^{\circ}22'45''.2$ (SDSS $g=20.5$ counterpart). Subsequent observations detected superhumps (vsnet-alert 17957, 17974; figure 81). The object then faded after the plateau phase (a dip around BJD 2456979, vsnet-alert 17978). The object faded again (BJD 2456982) and a long rebrightening followed, which lasted more than 5 d (vsnet-alert 17997, 18010; figure 82). During this rebrightening, the superhumps grew again (figure 83).

The times of superhump maxima during the superoutburst plateau are listed in table 62. During the dip, the superhump signal became very weak (See the middle panel of figure 82. The amplitudes are shown in magnitudes and the pulsed flux during the dip remarkably decreased). The

Table 61. Superhump maxima of ASASSN-14jf (2014) (continued)

E	max*	error	$O - C^\dagger$	N^\ddagger
178	56972.6979	0.0016	0.0036	16
179	56972.7506	0.0019	0.0003	16
180	56972.8081	0.0017	0.0018	17
196	56973.7025	0.0011	0.0002	17
197	56973.7567	0.0021	-0.0016	16
198	56973.8121	0.0018	-0.0022	14
214	56974.7063	0.0022	-0.0040	16
215	56974.7641	0.0023	-0.0021	15
216	56974.8203	0.0014	-0.0019	10
231	56975.6545	0.0030	-0.0078	11
232	56975.7133	0.0015	-0.0050	17
233	56975.7701	0.0025	-0.0041	15
234	56975.8260	0.0029	-0.0043	9
249	56976.6631	0.0015	-0.0072	15
250	56976.7256	0.0019	-0.0007	17
251	56976.7780	0.0014	-0.0043	16
252	56976.8400	0.0016	0.0017	5
267	56977.6790	0.0043	0.0007	16
268	56977.7331	0.0019	-0.0012	17
269	56977.7848	0.0033	-0.0054	16
303	56979.6958	0.0027	0.0015	16
304	56979.7469	0.0027	-0.0034	15
321	56980.7005	0.0023	-0.0018	17
322	56980.7578	0.0023	-0.0005	16
339	56981.7111	0.0020	0.0008	16
340	56981.7646	0.0038	-0.0016	16
341	56981.8158	0.0014	-0.0065	10

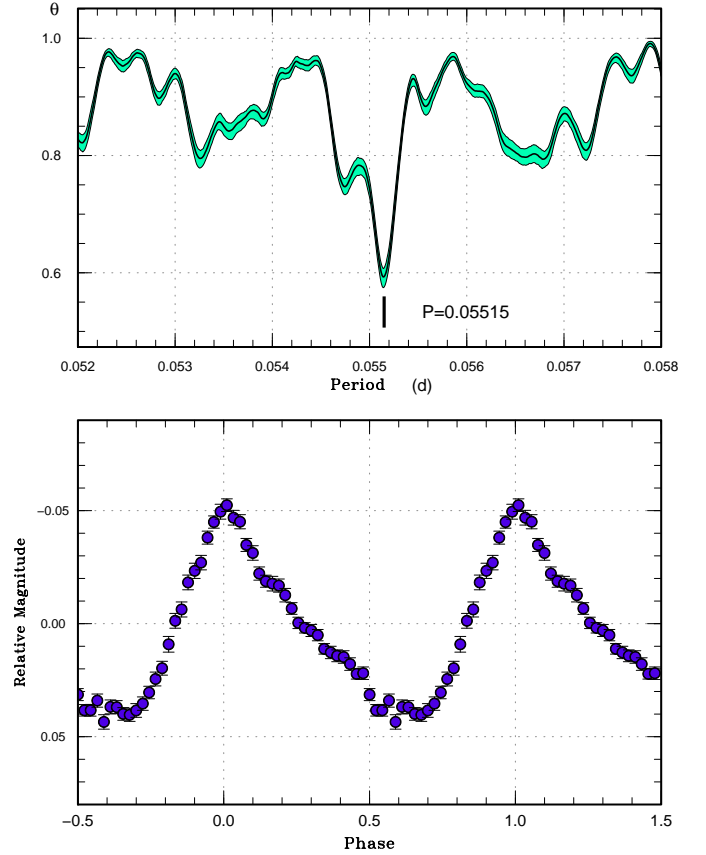
*BJD-2400000.

 † Against max = 2456962.7263 + 0.056000 E . ‡ Number of points used to determine the maximum.

times of superhump maxima during the dip and the rebrightening are listed in table 63. The maxima for $E \leq 4$ correspond to maxima observed during the dip and the rising phase from the dip. There was no marked period variation compared to the superhumps observed during the superoutburst plateau (figure 83). The $O - C$ values between the plateau and the rebrightening showed a jump by a phase ~ 0.3 (figure 82). Since the periods were almost the same between the plateau and the rebrightening, it was unlikely a continuous period change gave rise to this shift. Since the amplitudes of superhumps grew again during the rebrightening, it is most likely these superhumps were newly excited during the rebrightening.

The last ASAS-SN observation was 25 d before the outburst detection, and it was very likely the true maximum was missed. Although early superhump were not recorded, we consider that the object is likely a WZ Sge-type dwarf nova because it showed a dip and a long rebrightening, characteristic to WZ Sge-type dwarf novae (type-A rebrightening, cf. Imada et al. 2006; Kato et al. 2009).

There has been an attempt to explain WZ Sge-type rebrightenings by an enhanced mass-transfer (originally proposed by Patterson et al. 2002 and modeled by Buat-

**Fig. 81.** Ordinary superhumps in ASASSN-14jq during the superoutburst plateau (2014). (Upper): PDM analysis. (Lower): Phase-averaged profile

Ménard, Hameury 2002). This model predicts the shrinkage of the disk radius (see figure 5 in Buat-Ménard, Hameury 2002) by an addition of matter with low-angular momentum. The present observation did not detect noticeable period variation, indicating that the disk radius was almost constant (we consider that we can reasonably neglect the pressure effect since the amplitudes of superhumps were very small around the dip and during the rebrightening). This observation does not favor the enhanced mass-transfer model.

3.61. ASASSN-14jv

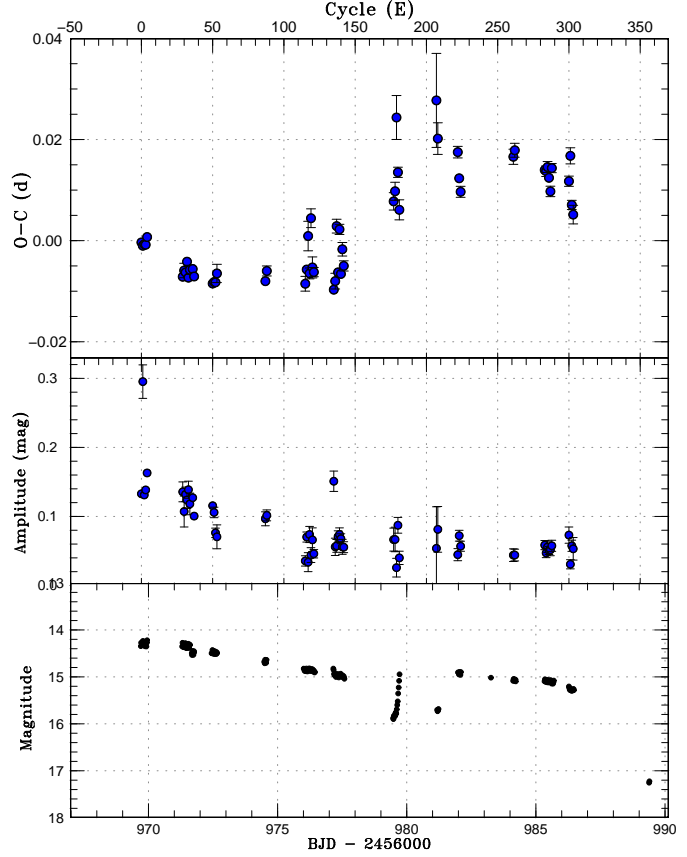
This object was detected as a transient at $V=11.3$ on 2014 November 9 by ASAS-SN team Shappee et al. (2014b). The coordinates are $18^{\text{h}}53^{\text{m}}28^{\text{s}}.81$, $+42^{\circ}03'43''.3$ (the Initial Gaia Source List). Berardi (2014) spectroscopically confirmed the object to be an outbursting dwarf nova. Early superhumps were immediately reported (vsnet-alert 17950, 17953, 17956, 17966; figure 84). Following this phase, ordinary superhumps appeared (vsnet-alert 17973, 17985, 18015; figure 85).

The times of superhump maxima are listed in table 64. Both stages A and B were clearly recorded. Instead of stage C superhumps, either a phase shift or a large de-

Table 62. Superhump maxima of ASASSN-14jq during the plateau phase (2014)

E	max*	error	$O - C^\dagger$	N^\ddagger
0	56969.7257	0.0001	0.0041	569
1	56969.7802	0.0002	0.0034	165
2	56969.8356	0.0002	0.0037	400
3	56969.8907	0.0001	0.0036	569
4	56969.9474	0.0003	0.0051	320
29	56971.3191	0.0007	-0.0027	50
30	56971.3755	0.0014	-0.0014	61
31	56971.4303	0.0006	-0.0018	65
32	56971.4876	0.0007	0.0003	63
33	56971.5396	0.0006	-0.0028	64
34	56971.5964	0.0009	-0.0013	50
36	56971.7069	0.0001	-0.0011	568
37	56971.7606	0.0002	-0.0026	430
50	56972.4765	0.0003	-0.0040	150
51	56972.5320	0.0005	-0.0037	121
52	56972.5871	0.0007	-0.0037	123
53	56972.6441	0.0018	-0.0019	51
87	56974.5186	0.0007	-0.0034	60
88	56974.5758	0.0010	-0.0014	31
115	56976.0632	0.0015	-0.0039	115
116	56976.1212	0.0007	-0.0010	116
117	56976.1830	0.0029	0.0056	137
118	56976.2308	0.0011	-0.0018	145
119	56976.2969	0.0019	0.0091	87
120	56976.3423	0.0021	-0.0006	65
121	56976.3966	0.0009	-0.0015	57
135	56977.1656	0.0007	-0.0050	40
136	56977.2225	0.0016	-0.0033	148
137	56977.2885	0.0014	0.0076	106
138	56977.3346	0.0008	-0.0016	109
139	56977.3982	0.0010	0.0069	53
140	56977.4446	0.0007	-0.0019	57
141	56977.5047	0.0013	0.0030	57
142	56977.5566	0.0010	-0.0003	54

*BJD-2400000.

 † Against max = 2456969.7216 + 0.055178*E*. ‡ Number of points used to determine the maximum.**Fig. 82.** $O - C$ diagram of superhumps in ASASSN-14jq (2014). (Upper:) $O - C$ diagram. We used a period of 0.05518 d for calculating the $O - C$ residuals. (Middle:) Amplitudes of superhumps. (Lower:) Light curve. The data were binned to 0.011 d.

crease in the period was recorded during the rapid fading phase (figure 86). This phenomenon appears similar to what was observed in FL Psc and GW Lib (Kato et al. 2009).

The period of early superhumps was determined to be 0.054417(15) d. The period of stage A superhumps corresponds to $\epsilon^* = 0.0278(9)$ and $q = 0.074(3)$.

3.62. ASASSN-14kf

This object was detected as a transient at $V=15.36$ on 2014 November 11 by ASAS-SN team (vsnet-alert 17880). The coordinates are $05^{\text{h}}13^{\text{m}}06^{\text{s}}59$, $-26^{\circ}19'52''0$ (the Initial Gaia Source List). Superhumps were immediately detected (vsnet-alert 17992; figure 87). The times of superhump maxima are listed in table 65. Although $E=0$ corresponds to stage A superhump, the period of stage A superhumps could not be determined.

3.63. ASASSN-14kk

This object was detected as a transient at $V=16.17$ on 2014 November 12 by ASAS-SN team (vsnet-alert 17988). The coordinates are $01^{\text{h}}32^{\text{m}}02^{\text{s}}77$, $-10^{\circ}43'57''8$ (SDSS $g=20.8$ counterpart). The object brightened to $V=15.87$

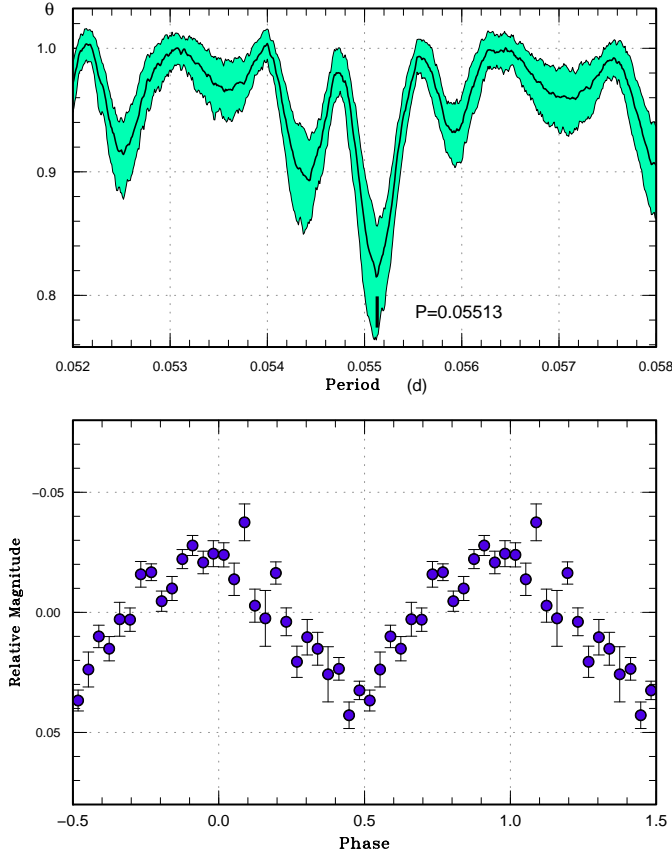


Fig. 83. Ordinary superhumps in ASASSN-14jq during the rebrightening (2014). (Upper): PDM analysis. (Lower): Phase-averaged profile

on November 17 (vsnet-alert 17989). Observations starting on November 16 detected superhumps (vsnet-alert 18011; figure 88). The times of superhump maxima are listed in table 66.

3.64. ASASSN-14ku

This object was detected as a transient at $V=15.45$ on 2014 November 23 by ASAS-SN team. The coordinates are $23^{\text{h}}43^{\text{m}}38^{\text{s}}.18$, $-58^{\circ}52'47''.3$ (the Initial Gaia Source List). Subsequent observations detected superhumps (vsnet-alert 18019, 18023, 18028; figure 89). The times of superhump maxima are listed in table 67. The superhump stage is unknown.

3.65. ASASSN-14lk

This object was detected as a transient at $V=13.48$ on 2014 December 1 by ASAS-SN team (vsnet-alert 18032). The coordinates are $20^{\text{h}}09^{\text{m}}24^{\text{s}}.09$, $-63^{\circ}26'22''.8$ (the Initial Gaia Source List). No previous outbursts were recorded in ASAS-3 data. Although the object may be identical with NSV 12802 (=HV 9672) and NLTT 161-48 (vsnet-alert 18032), the identification requires further investigation because no finding chart is available for these objects.

Table 63. Superhump maxima of ASASSN-14jq during the dip and rebrightening (2014)

E	max*	error	$O - C^{\dagger}$	N^{\ddagger}
0	56979.5006	0.0017	-0.0076	60
1	56979.5578	0.0018	-0.0056	58
2	56979.6276	0.0043	0.0091	59
3	56979.6719	0.0010	-0.0018	59
4	56979.7197	0.0020	-0.0092	36
30	56981.1760	0.0093	0.0131	61
31	56981.2236	0.0031	0.0055	75
45	56981.9935	0.0011	0.0032	106
46	56982.0435	0.0008	-0.0020	115
47	56982.0960	0.0011	-0.0046	88
84	56984.1446	0.0015	0.0032	54
85	56984.2010	0.0014	0.0045	52
106	56985.3559	0.0008	0.0010	57
107	56985.4109	0.0010	0.0008	54
108	56985.4669	0.0011	0.0017	57
109	56985.5199	0.0008	-0.0004	55
110	56985.5724	0.0010	-0.0031	53
111	56985.6322	0.0009	0.0015	57
123	56986.2918	0.0010	-0.0008	49
124	56986.3520	0.0016	0.0043	54
125	56986.3974	0.0009	-0.0054	57
126	56986.4507	0.0018	-0.0073	46

*BJD-2400000.

\dagger Against max = $2456979.5082 + 0.055157E$.

\ddagger Number of points used to determine the maximum.

Superhumps were immediately recorded (vsnet-alert 18038; figure 90). The times of superhump maxima are listed in table 68. Although the superhump stage is not very clear, the large superhump amplitudes suggest that at least early observations recorded stage B superhumps. The resultant $O - C$ values and mean period are likely a mixture of stage B and C superhumps. The selection of the period is based on the initial two nights. If the object showed anomalous period variation, the cycle counts of the later part may contain errors due to the observational gap.

3.66. ASASSN-14mc

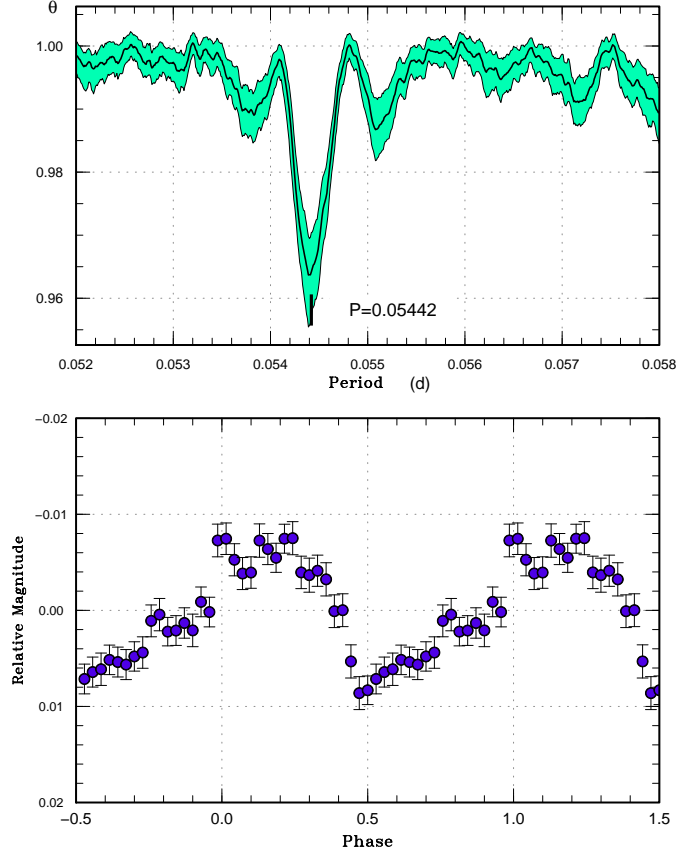
This object was detected as a transient at $V=16.5$ on 2014 December 14 by ASAS-SN team. The object further brightened to $V=14.3$ on December 15 (vsnet-alert 18063). The coordinates are $04^{\text{h}}47^{\text{m}}23^{\text{s}}.27$, $-36^{\circ}56'01''.8$ (ASAS-SN position). Superhumps were detected 10 d after the outburst detection (vsnet-alert 18104, 18129; figure 91).

The times of superhump maxima are listed in table 69. The maxima for $E \leq 1$ correspond to stage A superhumps. Although stage A superhumps were detected, neither $O - C$ analysis nor PDM method could not yield a reliable period of stage A superhumps. Although this object is likely a WZ Sge-type dwarf nova, no significant signal of early superhumps was detected in the earlier part of the observation. This was probably due to a low orbital

Table 64. Superhump maxima of ASASSN-14jv (2014)

E	max*	error	$O - C^\dagger$	N^\ddagger
0	56978.5970	0.0017	-0.0281	182
1	56978.6539	0.0015	-0.0263	185
18	56979.6121	0.0005	-0.0052	103
18	56979.6124	0.0005	-0.0048	103
23	56979.8903	0.0004	-0.0026	80
24	56979.9435	0.0004	-0.0044	103
25	56979.9957	0.0004	-0.0074	96
35	56980.5600	0.0003	0.0058	96
36	56980.6147	0.0001	0.0053	108
37	56980.6722	0.0004	0.0076	52
42	56980.9484	0.0002	0.0083	116
43	56981.0050	0.0003	0.0097	69
59	56981.8863	0.0003	0.0091	138
60	56981.9404	0.0003	0.0081	165
61	56981.9948	0.0003	0.0074	155
67	56982.3249	0.0002	0.0068	78
68	56982.3767	0.0003	0.0035	68
69	56982.4327	0.0004	0.0044	87
71	56982.5427	0.0005	0.0042	60
72	56982.5997	0.0002	0.0060	107
73	56982.6535	0.0003	0.0047	90
84	56983.2515	0.0001	-0.0036	83
85	56983.3131	0.0005	0.0029	32
108	56984.5794	0.0003	0.0014	103
109	56984.6345	0.0003	0.0014	108
114	56984.9090	0.0013	0.0003	92
137	56986.1774	0.0003	0.0009	75
138	56986.2312	0.0003	-0.0004	181
139	56986.2871	0.0008	0.0004	140
140	56986.3414	0.0003	-0.0004	90
141	56986.3965	0.0005	-0.0005	57

*BJD-2400000.

 † Against max = 2456978.6251 + 0.055119 E . ‡ Number of points used to determine the maximum.**Fig. 84.** Early superhumps in ASASSN-14jv (2014). (Upper): PDM analysis. (Lower): Phase-averaged profile**Table 64.** Superhump maxima of ASASSN-14jv (2014) (continued)

E	max*	error	$O - C^\dagger$	N^\ddagger
162	56987.5553	0.0004	0.0008	97
163	56987.6108	0.0004	0.0012	107
164	56987.6667	0.0014	0.0020	45
175	56988.2757	0.0004	0.0047	25
180	56988.5527	0.0008	0.0061	60
181	56988.6063	0.0006	0.0046	68
182	56988.6595	0.0012	0.0027	37
210	56990.2070	0.0009	0.0069	35
229	56991.2396	0.0016	-0.0078	103
230	56991.2874	0.0013	-0.0151	124
231	56991.3369	0.0025	-0.0207	49

*BJD-2400000.

 † Against max = 2456978.6251 + 0.055119 E . ‡ Number of points used to determine the maximum.**Table 65.** Superhump maxima of ASASSN-14kf (2014)

E	max*	error	$O - C^\dagger$	N^\ddagger
0	56978.5438	0.0009	-0.0030	158
13	56979.4857	0.0009	0.0013	167
14	56979.5566	0.0008	0.0000	167
27	56980.4963	0.0010	0.0021	166
28	56980.5662	0.0011	-0.0001	166
54	56982.4440	0.0039	0.0024	145
55	56982.5161	0.0017	0.0024	165
56	56982.5836	0.0018	-0.0022	139
69	56983.5252	0.0025	0.0017	166
70	56983.5910	0.0042	-0.0046	126

*BJD-2400000.

 † Against max = 2456978.5468 + 0.072127 E . ‡ Number of points used to determine the maximum.

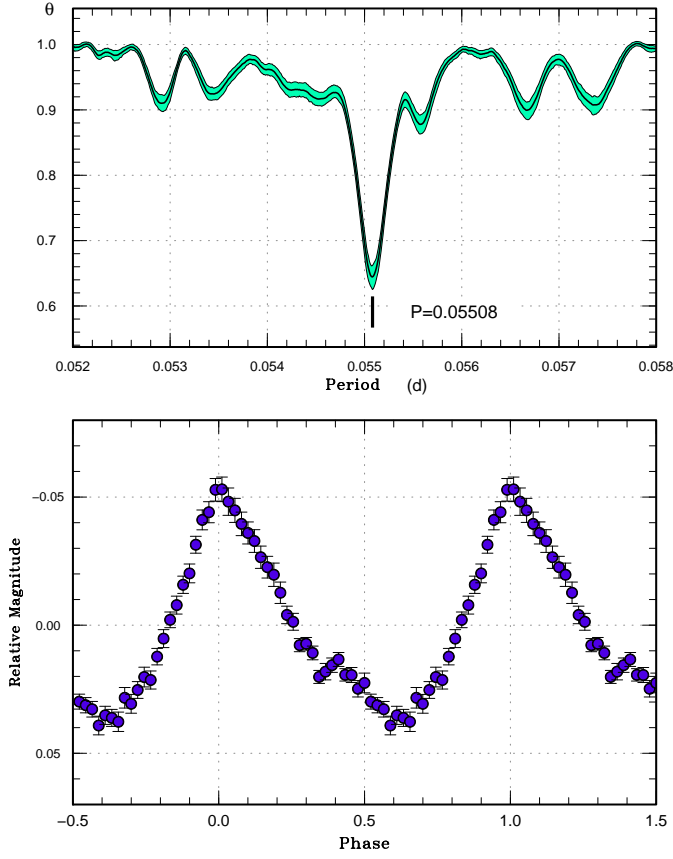


Fig. 85. Ordinary superhumps in ASASSN-14jv during the superoutburst plateau (2014). (Upper): PDM analysis. (Lower): Phase-averaged profile

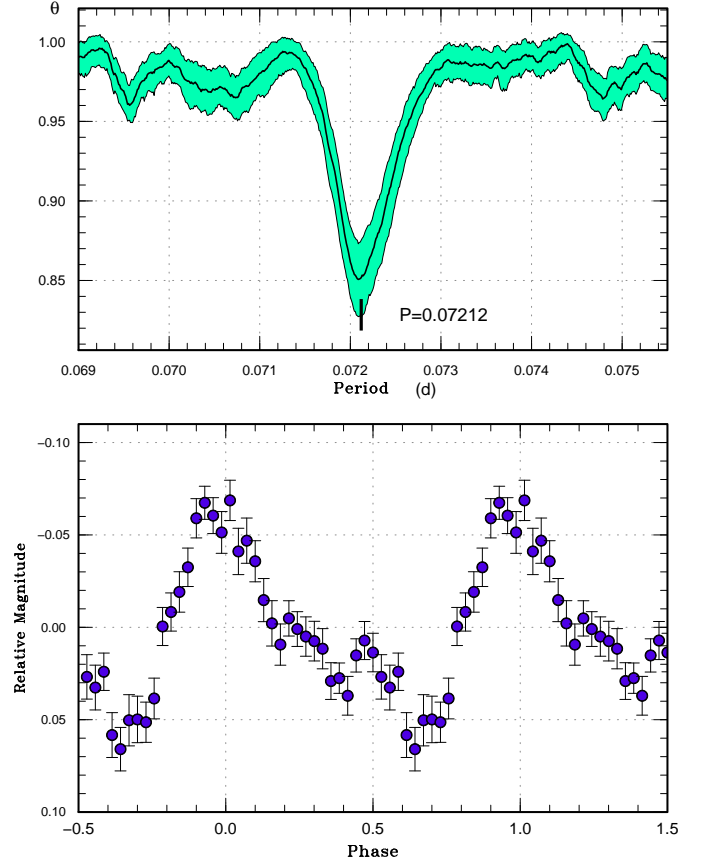


Fig. 87. Superhumps in ASASSN-14kf (2014). (Upper): PDM analysis. (Lower): Phase-averaged profile

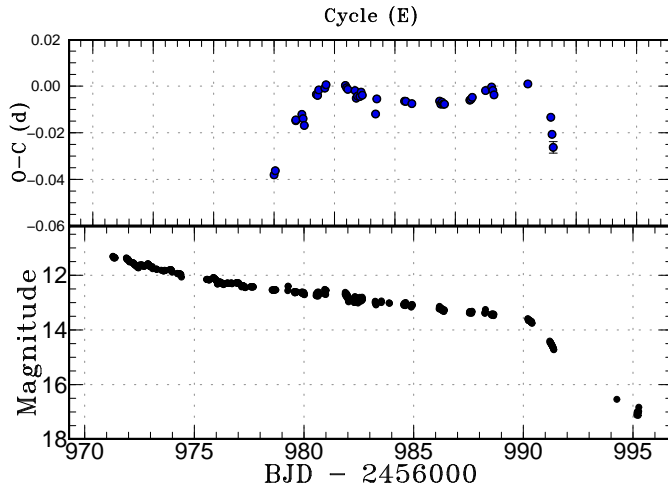


Fig. 86. $O - C$ diagram of superhumps in ASASSN-14jv (2014). (Upper): $O - C$ diagram. A period of 0.05510 d was used to draw this figure. (Lower): Light curve. The observations were binned to 0.011 d.

Table 66. Superhump maxima of ASASSN-14kk (2014)

E	max*	error	$O - C^\dagger$	N^\ddagger
0	56978.4042	0.0009	-0.0071	80
1	56978.4650	0.0006	-0.0026	129
16	56979.3286	0.0041	0.0156	130
17	56979.3704	0.0030	0.0010	129
18	56979.4197	0.0021	-0.0060	77
69	56982.3067	0.0014	0.0065	84
70	56982.3501	0.0009	-0.0065	128
71	56982.4164	0.0032	0.0035	74
87	56983.3139	0.0063	-0.0007	47
88	56983.3692	0.0012	-0.0019	129
89	56983.4254	0.0015	-0.0020	124

*BJD-2400000.

† Against max = 2456978.4112 + 0.056361E.

‡ Number of points used to determine the maximum.

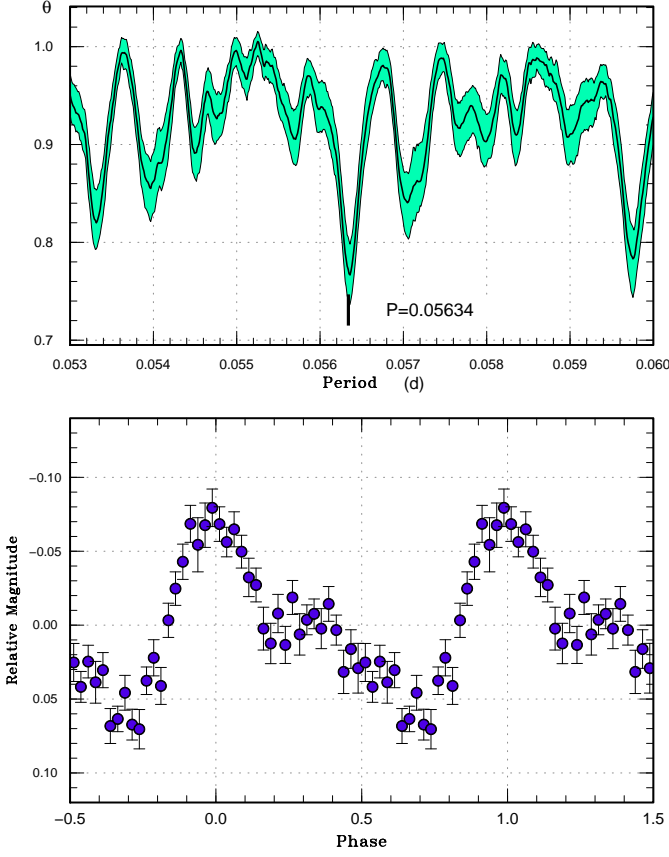


Fig. 88. Superhumps in ASASSN-14kk (2014). (Upper): PDM analysis. (Lower): Phase-averaged profile

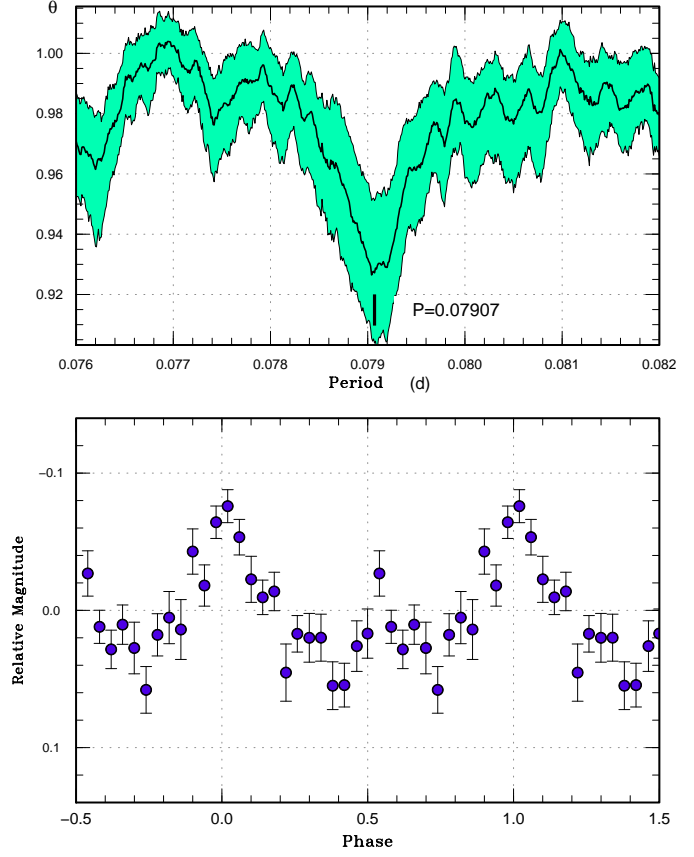


Fig. 89. Superhumps in ASASSN-14ku (2014). (Upper): PDM analysis. (Lower): Phase-averaged profile

Table 67. Superhump maxima of ASASSN-14ku (2014)

E	max*	error	$O - C^\dagger$	N^\ddagger
0	56988.3239	0.0022	0.0021	133
1	56988.3986	0.0017	-0.0022	183
3	56988.5632	0.0024	0.0042	29
13	56989.3492	0.0016	-0.0005	182
14	56989.4234	0.0021	-0.0053	140
16	56989.5877	0.0038	0.0009	28
25	56990.3036	0.0073	0.0052	82
26	56990.3772	0.0040	-0.0003	135
28	56990.5300	0.0145	-0.0056	15
29	56990.6175	0.0048	0.0028	22
38	56991.3279	0.0083	0.0017	142
41	56991.5551	0.0059	-0.0083	27
54	56992.5967	0.0059	0.0053	29

*BJD-2400000.

† Against max = 2456988.3218 + 0.079066 E .

‡ Number of points used to determine the maximum.

Table 68. Superhump maxima of ASASSN-14lk (2014)

E	max*	error	$O - C^\dagger$	N^\ddagger
0	56997.3080	0.0003	0.0018	137
16	56998.2864	0.0004	-0.0027	122
17	56998.3494	0.0005	-0.0012	134
81	57002.2863	0.0013	0.0041	58
130	57005.2903	0.0026	-0.0021	94

*BJD-2400000.

† Against max = 2456997.3062 + 0.061432 E .

‡ Number of points used to determine the maximum.

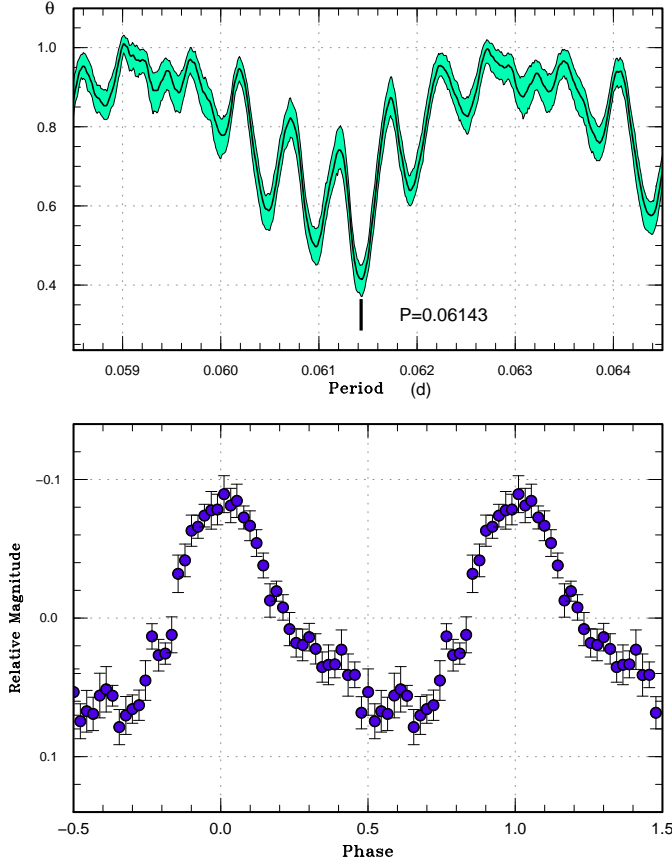


Fig. 90. Superhumps in ASASSN-14lk (2014). (Upper): PDM analysis. (Lower): Phase-averaged profile

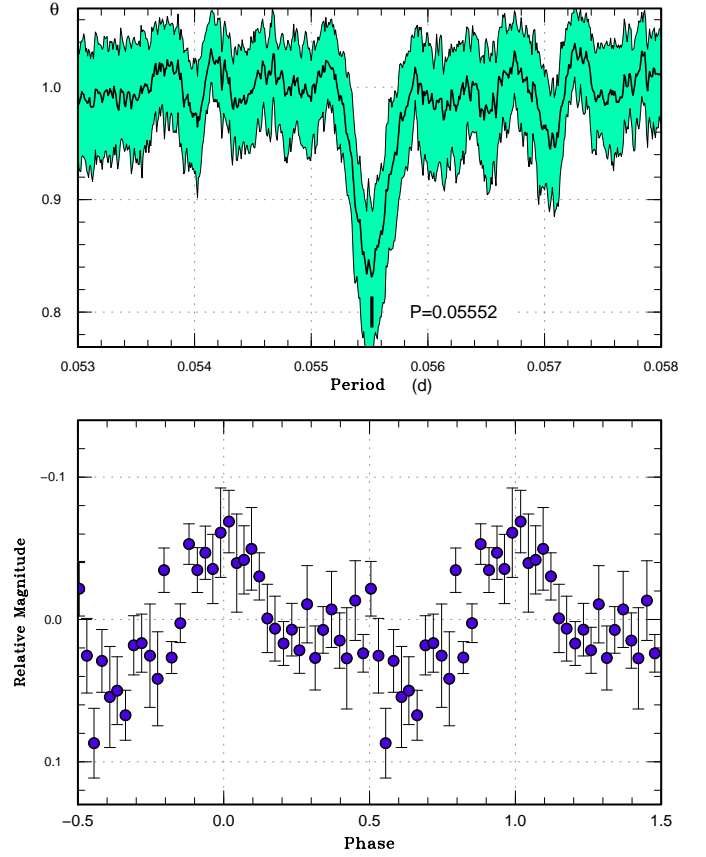


Fig. 91. Superhumps in ASASSN-14mc (2014). (Upper): PDM analysis. (Lower): Phase-averaged profile

inclination.

3.67. ASASSN-14md

This object was detected as a transient at $V=15.7$ on 2014 December 15 by ASAS-SN team (vsnet-alert 18074). The coordinates are $04^{\text{h}}43^{\text{m}}45^{\text{s}}.41$, $-21^{\circ}08'34''.1$ (refined astrometry, vsnet-alert 18078). Superhumps appeared accompanied by brightening of the brightness of the object (vsnet-alert 18095, 18099, 18105, 18130; figure 92). The times of superhump maxima are listed in table 70. Stages A and B can be clearly recognized. Since the object is very faint ($V \sim 17$), no secure superhumps were detected in the later part of the superoutburst. The alias selection was made to express the $O - C$ values for the best observed data on BJD 2457014 and 2457015.

3.68. ASASSN-14mh

This object was detected as a transient at $V=15.1$ on 2014 December 20 by ASAS-SN team (vsnet-alert 18074). The coordinates are $11^{\text{h}}27^{\text{m}}25^{\text{s}}.99$, $-28^{\circ}22'11''.8$ (the Initial Gaia Source List). The object initially showed rapid fading and subsequent brightening (vsnet-alert 18094), which turned out to be a precursor outburst and rise to a superoutburst accompanied by superhumps

Table 69. Superhump maxima of ASASSN-14mc (2014)

E	max*	error	$O - C^{\dagger}$	N^{\ddagger}
0	57015.6156	0.0035	-0.0074	28
1	57015.6675	0.0035	-0.0110	30
18	57016.6291	0.0009	0.0062	30
19	57016.6841	0.0009	0.0057	26
36	57017.6277	0.0018	0.0049	30
37	57017.6828	0.0021	0.0044	25
55	57018.6826	0.0012	0.0042	21
73	57019.6801	0.0027	0.0017	21
91	57020.6747	0.0014	-0.0036	22
109	57021.6741	0.0022	-0.0042	19
127	57022.6774	0.0035	-0.0009	25

*BJD-2400000.

† Against max = 2457015.6229 + 0.055554 E .

‡ Number of points used to determine the maximum.

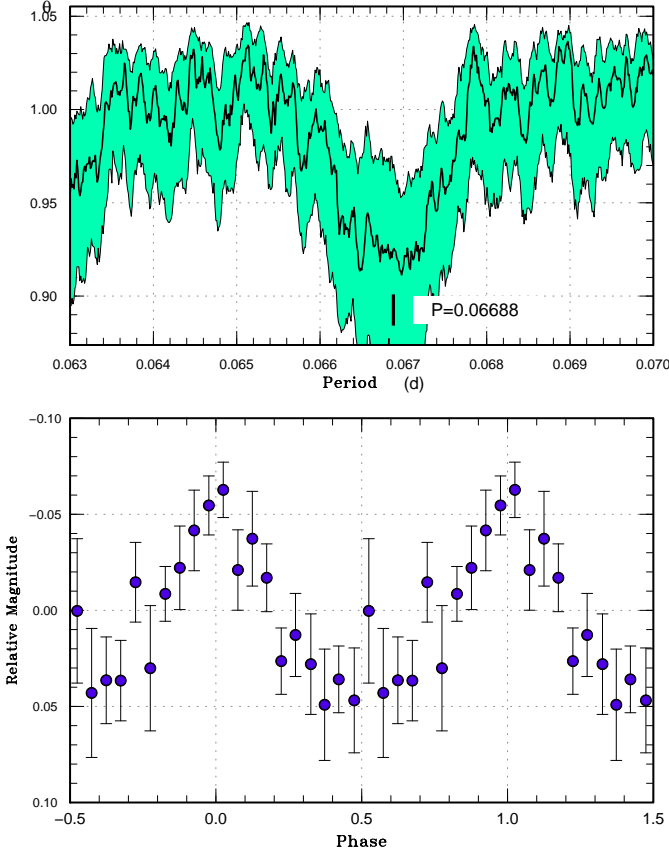


Fig. 92. Superhumps in ASASSN-14md (2014). The data after BJD 2457014 were used. (Upper): PDM analysis. (Lower): Phase-averaged profile

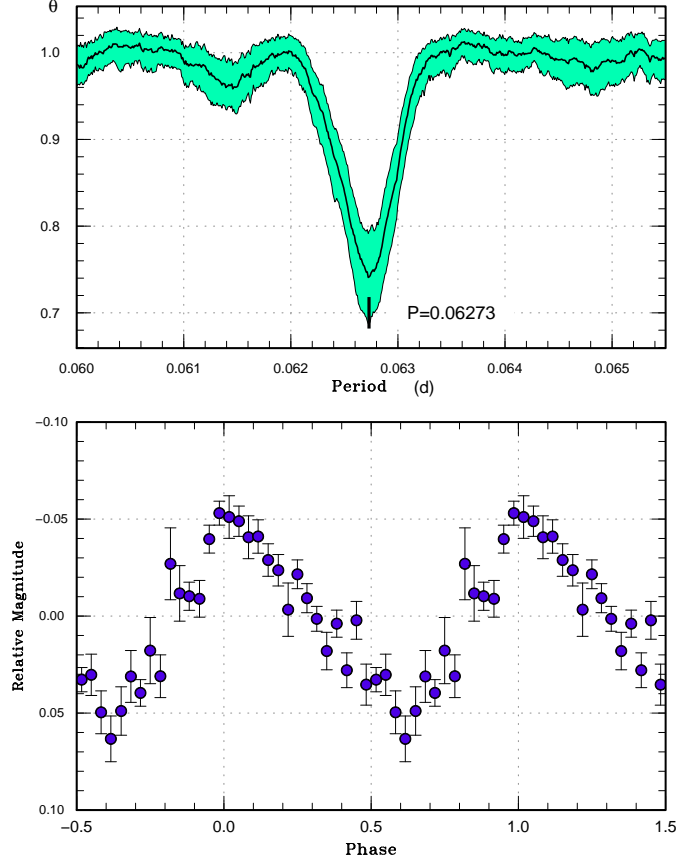


Fig. 93. Superhumps in ASASSN-14mh (2014). The data between BJD 2457015 and 2457024 were used. (Upper): PDM analysis. (Lower): Phase-averaged profile

Table 70. Superhump maxima of ASASSN-14md (2014)

E	max*	error	$O - C^\dagger$	N^\ddagger
0	57012.6905	0.0045	-0.0119	23
1	57012.7571	0.0024	-0.0128	21
2	57012.8216	0.0033	-0.0159	17
14	57013.6598	0.0029	0.0111	32
28	57014.6129	0.0023	0.0178	16
29	57014.6787	0.0027	0.0160	34
43	57015.6226	0.0012	0.0136	31
44	57015.6875	0.0015	0.0109	29
58	57016.6258	0.0015	0.0028	35
59	57016.6891	0.0018	-0.0014	26
73	57017.6235	0.0021	-0.0134	35
74	57017.6878	0.0075	-0.0167	25

*BJD-2400000.

† Against max = 2457012.7023 + 0.067597 E .

‡ Number of points used to determine the maximum.

(vsnet-alert 18098; figure 93). The times of superhump maxima are listed in table 71. The maxima for $E \leq 1$ correspond to stage A superhumps.

3.69. ASASSN-14mj

This object was detected as a transient at $V=13.7$ on 2014 December 21 by ASAS-SN team (vsnet-alert 18092). The coordinates are $06^{\text{h}}43^{\text{m}}35^{\text{s}}.15$, $+74^{\circ}10'15''.5$ (GSC 2.3.2 position). Although the object was originally suspected to be a WZ Sge-type dwarf nova based on the apparent large outburst amplitude, it showed development of superhumps as in ordinary SU UMa-type dwarf novae (vsnet-alert 18103, 18114, 18118, 18125; figure 94). The object significantly brightened as superhumps grew. The times of superhump maxima are listed in table 72. Although the epochs for $E \leq 5$ correspond to stage A superhumps, we could not determine the period of stage A superhumps.

3.70. ASASSN-15ah

This object was detected as a transient at $V=13.69$ on 2015 January 7 by ASAS-SN team (vsnet-alert 18153). The coordinates are $06^{\text{h}}00^{\text{m}}30^{\text{s}}.00$, $-32^{\circ}07'35''.6$ (GSC 2.3.2 position). Although the outburst amplitude sug-

Table 71. Superhump maxima of ASASSN-14mh (2014)

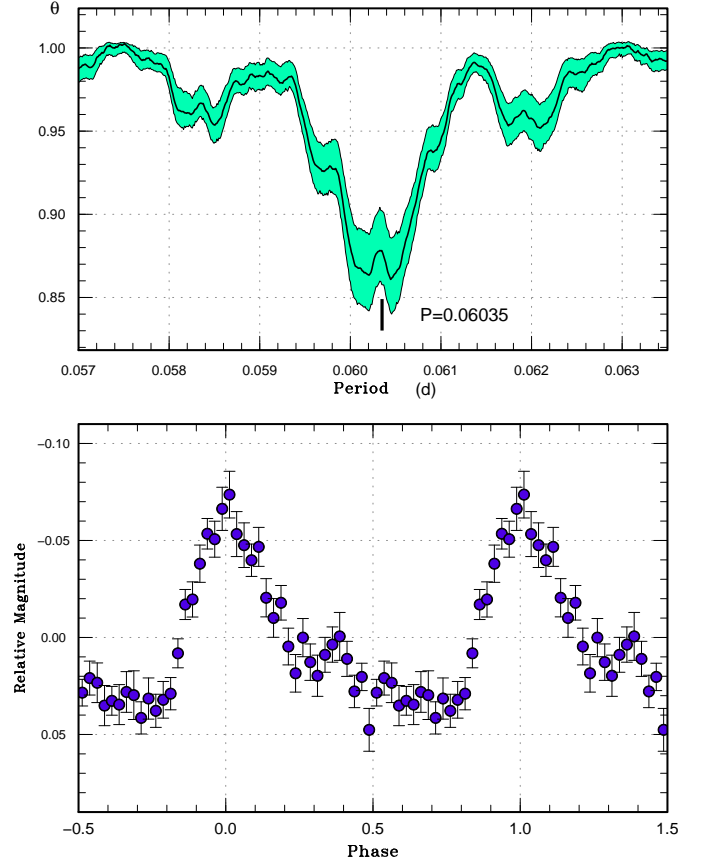
E	max*	error	$O - C^\dagger$	N^\ddagger
0	57014.7329	0.0020	-0.0029	28
1	57014.7916	0.0017	-0.0070	28
16	57015.7409	0.0005	0.0007	28
17	57015.8051	0.0006	0.0021	27
32	57016.7468	0.0008	0.0020	28
33	57016.8087	0.0006	0.0012	28
47	57017.6909	0.0051	0.0045	11
48	57017.7507	0.0008	0.0015	28
49	57017.8125	0.0008	0.0006	28
56	57018.2584	0.0068	0.0070	43
57	57018.3187	0.0018	0.0045	64
65	57018.8100	0.0021	-0.0064	23
73	57019.3181	0.0021	-0.0005	54
79	57019.6931	0.0054	-0.0022	16
80	57019.7568	0.0018	-0.0013	28
96	57020.7613	0.0013	-0.0013	27
111	57021.7051	0.0017	0.0009	25
112	57021.7623	0.0010	-0.0047	27
128	57022.7724	0.0023	0.0009	15
143	57023.7155	0.0076	0.0023	15
144	57023.7741	0.0050	-0.0019	13

*BJD-2400000.

 † Against max = 2457014.7358 + 0.062779 E . ‡ Number of points used to determine the maximum.**Table 72.** Superhump maxima of ASASSN-14mj (2014)

E	max*	error	$O - C^\dagger$	N^\ddagger
0	57019.1881	0.0029	-0.0094	199
4	57019.4351	0.0013	-0.0041	56
5	57019.4915	0.0010	-0.0082	61
18	57020.2919	0.0003	0.0063	54
19	57020.3512	0.0002	0.0053	63
20	57020.4123	0.0002	0.0059	65
21	57020.4718	0.0003	0.0050	64
22	57020.5326	0.0003	0.0053	45
33	57021.1948	0.0006	0.0026	59
34	57021.2538	0.0005	0.0011	59
35	57021.3153	0.0006	0.0022	58
45	57021.9209	0.0012	0.0034	122
51	57022.2796	0.0005	-0.0006	102
52	57022.3397	0.0006	-0.0009	117
53	57022.3997	0.0003	-0.0014	61
54	57022.4588	0.0004	-0.0027	59
55	57022.5208	0.0003	-0.0012	62
56	57022.5808	0.0002	-0.0016	61
57	57022.6404	0.0003	-0.0025	62
58	57022.6994	0.0024	-0.0039	22
62	57022.9399	0.0040	-0.0052	47
63	57023.0103	0.0018	0.0047	44

*BJD-2400000.

 † Against max = 2457019.1975 + 0.060445 E . ‡ Number of points used to determine the maximum.**Fig. 94.** Superhumps in ASASSN-14mj (2014). The data after BJD 2457019 were used. (Upper): PDM analysis. (Lower): Phase-averaged profile

gested a WZ Sge-type dwarf nova, no evident early superhumps were detected. Eight days after the detection, this object started to show ordinary superhumps (vsnet-alert 18189, 18200; figure 95). The times of superhump maxima are listed in table 73. The epochs for $E \leq 2$ correspond to stage A superhumps. Despite the large outburst amplitude, the shortness of the segment before the appearance of ordinary superhumps suggests that ASASSN-15ah is not an extreme WZ Sge-type dwarf nova.

3.71. ASASSN-15ap

This object was detected as a transient at $V=17.0$ on 2015 January 8 by ASAS-SN team. The brightened to $V=15.55$ on January 11. The coordinates are $06^{\text{h}}37^{\text{m}}47^{\text{s}}.51$, $-25^{\circ}41'20''.1$ (the Initial Gaia Source List). Superhumps were observed since our initial observation on January 17 (vsnet-alert 18198, 18222; figure 96). The times of superhump maxima are listed in table 74. The superhump stage is not known. The superhump period was relatively constant for this long- P_{SH} system.

3.72. ASASSN-15aq

This object was detected as a transient at $V=14.2$ on 2015 January 13 by ASAS-SN team (vsnet-alert 18175).

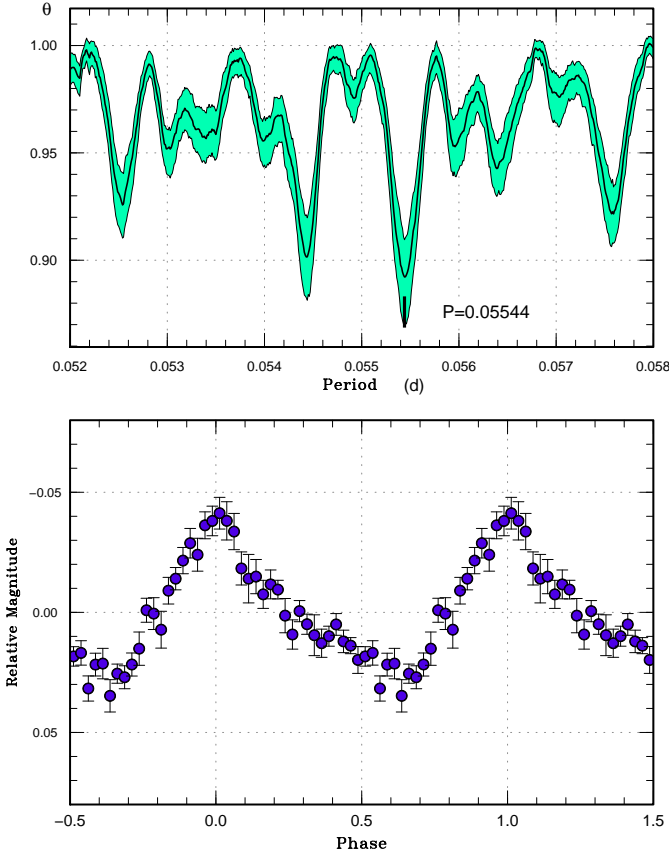


Fig. 95. Superhumps in ASASSN-15ah (2015). The data after BJD 2457038 were used. (Upper): PDM analysis. (Lower): Phase-averaged profile

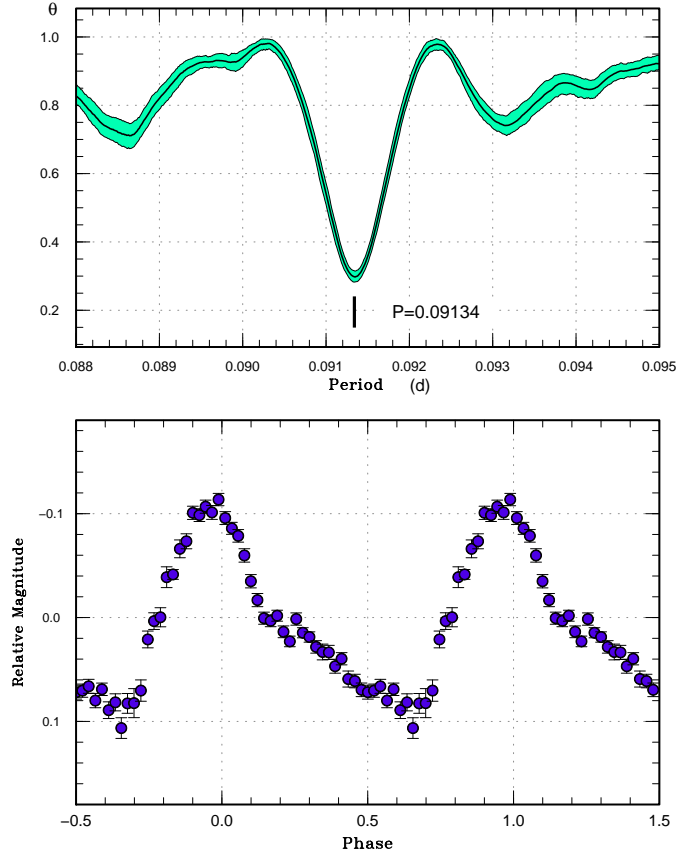


Fig. 96. Superhumps in ASASSN-15ap (2015). (Upper): PDM analysis. (Lower): Phase-averaged profile

Table 73. Superhump maxima of ASASSN-15ah (2015)

E	max*	error	$O - C^\dagger$	N^\ddagger
0	57038.3679	0.0006	-0.0028	128
1	57038.4223	0.0006	-0.0040	128
2	57038.4741	0.0033	-0.0077	33
35	57040.3212	0.0003	0.0069	127
36	57040.3760	0.0002	0.0061	127
37	57040.4306	0.0003	0.0052	127
38	57040.4873	0.0003	0.0064	128
85	57043.0859	0.0035	-0.0049	70
89	57043.3102	0.0004	-0.0027	127
90	57043.3662	0.0003	-0.0023	127
107	57044.3073	0.0007	-0.0052	95
108	57044.3739	0.0021	0.0059	78
109	57044.4210	0.0013	-0.0026	56
139	57046.0969	0.0033	0.0075	54
144	57046.3651	0.0008	-0.0020	128
145	57046.4185	0.0007	-0.0041	127

*BJD-2400000.

† Against max = 2457038.3708 + 0.055530 E .

‡ Number of points used to determine the maximum.

Table 74. Superhump maxima of ASASSN-15ap (2015)

E	max*	error	$O - C^\dagger$	N^\ddagger
0	57038.4067	0.0010	-0.0058	122
1	57038.5068	0.0042	0.0031	28
22	57040.4233	0.0008	0.0014	124
23	57040.5166	0.0004	0.0034	211
55	57043.4353	0.0004	-0.0009	166
56	57043.5259	0.0005	-0.0016	211
66	57044.4410	0.0006	0.0001	166
67	57044.5326	0.0006	0.0004	210

*BJD-2400000.

† Against max = 2457038.4125 + 0.091340 E .

‡ Number of points used to determine the maximum.

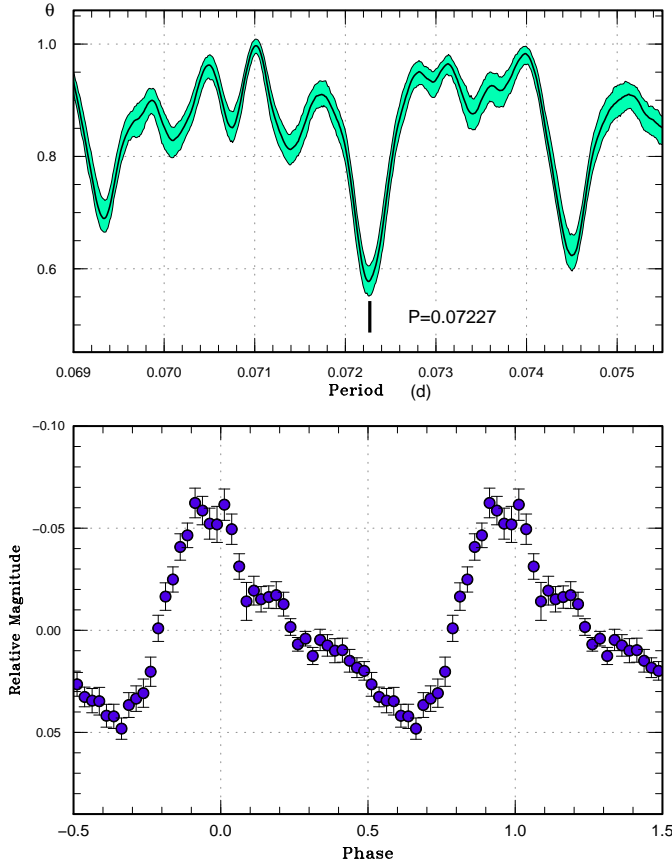


Fig. 97. Superhumps in ASASSN-15aq during the plateau phase (2015). (Upper): PDM analysis. (Lower): Phase-averaged profile

The coordinates are $00^{\text{h}}42^{\text{m}}14^{\text{s}}24$, $-56^{\circ}09'19''.9$ (2MASS position). There were several outbursts in the ASAS-3. The 2007 outburst looked like superoutbursts (vsnet-alert 18175). Superhumps were immediately detected (vsnet-alert 18186, 18199; figure 97). The times of superhump maxima are listed in table 75. Both stages B and C can be recognized. It was likely that the outburst detection was not early enough to detect stage A superhumps.

3.73. ASASSN-15aw

This object was detected as a transient at $V=15.8$ on 2015 January 15 by ASAS-SN team. The coordinates are $01^{\text{h}}57^{\text{m}}46^{\text{s}}13$, $+51^{\circ}10'24''.1$ (The Initial Gaia Source List). There is a GALEX counterpart with an NUV magnitude of 21.1. MASTER team also detected this object (MASTER OT J015746.16+511023.2) three days later (Balanutsa et al. 2015b). Superhumps were recorded in single-night observations (vsnet-alert 18203; figure 98). Three superhump maxima were recorded: BJD 2457044.3558(18) ($N=39$), 2457044.4104(9) ($N=42$) and 2457044.4720(10) ($N=43$). The superhump period determined by the PDM method is listed in table 2.

Table 75. Superhump maxima of ASASSN-15aq (2015)

E	max*	error	$O - C^{\dagger}$	N^{\ddagger}
0	57037.5159	0.0076	-0.0110	9
1	57037.6044	0.0028	0.0054	9
11	57038.3208	0.0003	0.0001	167
12	57038.3946	0.0005	0.0017	80
14	57038.5341	0.0015	-0.0032	15
39	57040.3398	0.0004	-0.0016	166
40	57040.4175	0.0010	0.0039	59
42	57040.5562	0.0007	-0.0017	37
56	57041.5701	0.0021	0.0018	26
80	57043.3113	0.0005	0.0110	167
108	57045.3254	0.0004	0.0044	167
125	57046.5455	0.0016	-0.0024	23
139	57047.5499	0.0030	-0.0084	24

*BJD-2400000.

† Against max = 2457037.5269 + 0.072168 E .

‡ Number of points used to determine the maximum.

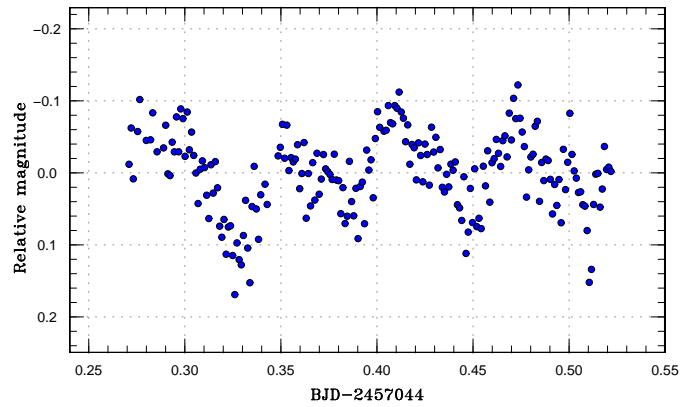


Fig. 98. Superhumps in ASASSN-15aw (2015).

3.74. ASASSN-15bg

This object was detected as a transient at $V=15.6$ on 2015 January 20 by ASAS-SN team. The coordinates are $01^{\text{h}}27^{\text{m}}54^{\text{s}}61$, $-58^{\circ}17'16''.8$ (the Initial Gaia Source List). Subsequent observations detected superhumps (vsnet-alert 18223; figure 99). The times of superhump maxima are listed in table 76.

3.75. ASASSN-15bp

This object was detected as a transient at $V=11.9$ on 2015 January 23 by ASAS-SN team (Simonian et al. 2015). The coordinates are $12^{\text{h}}12^{\text{m}}40^{\text{s}}43$, $+04^{\circ}16'55''.8$ (SDSS $g=20.5$ counterpart). There is a GALEX counterpart with a NUV magnitude of 20.9. The object was spectroscopically confirmed as an outbursting CV (Williams et al. 2015). The object was immediately identified as a WZ Sge-type dwarf nova by the detection of early superhumps (vsnet-alert 18219, 18325, 18241; figure 100). The object then started to show ordinary superhumps (vsnet-alert

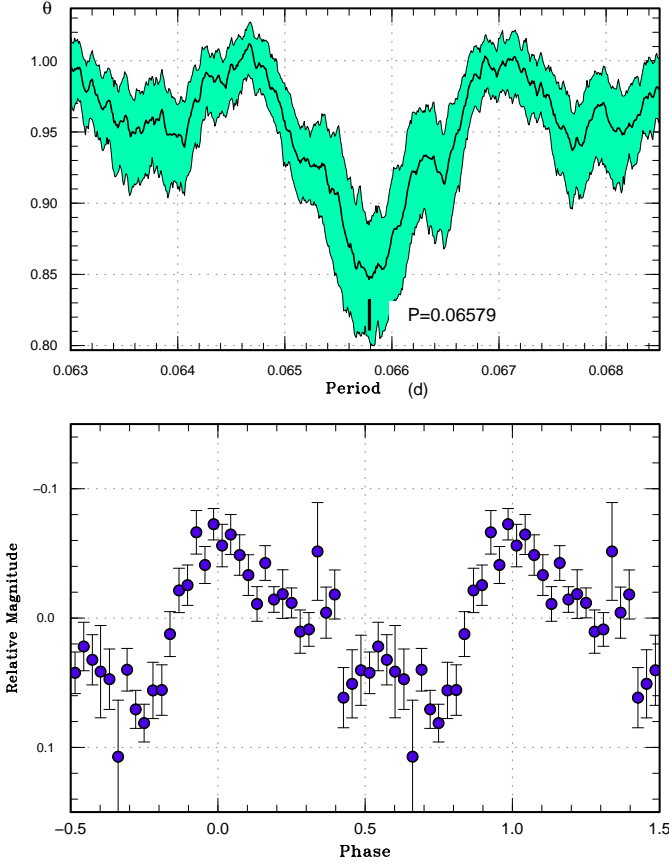


Fig. 99. Superhumps in ASASSN-15bg (2015). (Upper): PDM analysis. (Lower): Phase-averaged profile

Table 76. Superhump maxima of ASASSN-15bg (2015)

E	max [*]	error	$O - C^{\dagger}$	N^{\ddagger}
0	57044.3073	0.0022	-0.0019	73
1	57044.3782	0.0013	0.0034	104
15	57045.2932	0.0041	-0.0011	108
16	57045.3583	0.0014	-0.0016	148
31	57046.3456	0.0010	0.0006	151
32	57046.4112	0.0019	0.0006	103

^{*}BJD-2400000.

[†]Against max = 2457044.3092 + 0.065669 E .

[‡]Number of points used to determine the maximum.

18250, 18255, 18262, 18269, 18277, 18300, 18311; figure 101). The object then started fading rapidly on February 23 (31 d after the outburst detection, vsnet-alert 18331). Although there was some hint of post-superoutburst rebrightenings (figure 102), they were not confirmed by independent observers.

The times of superhump maxima during the plateau phase are listed in table 77. The times $E \leq 35$ are clearly growing superhumps (cf. figure 102). Using the data for $E \leq 33$ (BJD 2457054–2457056), we could determine the period of stage A superhumps as 0.05731(3) d with the PDM method. The maxima for $35 \leq E \leq 256$ represent characteristic stage B superhumps with a small positive P_{dot} . As is usual for a WZ Sge-type dwarf nova, this object did not show a smooth transition to stage C superhumps. There was an apparent phase jump after $E=256$. This jump corresponds to the later part of the plateau phase, and it looks like the superhumps observed after this phase jump appear to be on a smooth extension of early stage B superhumps (figure 102), just as seen in GW Lib during the 2007 superoutburst (figure 33 in Kato et al. 2009). There is difference, however, in that this jump occurred during the rapid fading in GW Lib while it occurred during the plateau phase in ASASSN-15bp. The superhump period after $E = 256$ (BJD 2457069–2457076.8) was determined to be 0.05666(1) d by the PDM method. We listed this period as stage C superhumps in table 2. The times of superhump maxima in the post-superoutburst stage are listed in table 78. The period was determined as 0.05651(2) d with the PDM method.

The variation of the superhump period is also well visualized in two-dimensional period analysis (figure 103) using Lasso.

The period of stage A superhumps corresponds to $\epsilon^* = 0.0293(6)$ and $q = 0.079(2)$. Following the formulation in Kato, Osaki (2013b), the period of superhump in the post-superoutburst phase is found to correspond to a disk radius of 0.355(5) A , where A is the binary separation. This value is close to those recorded in WZ Sge-type dwarf novae without multiple rebrightenings (Kato, Osaki 2013b).

3.76. ASASSN-15bu

This object was detected as a transient at $V=15.8$ on 2015 January 22 by ASAS-SN team. The coordinates are 02^h54^m43^s.77, +22°44′01″.9 (2MASS position). There is a GALEX counterpart with a NUV magnitude of 19.7. The object was suspected to be an eclipsing SU UMa-type dwarf nova based on apparent eclipses in the CRTS data (vsnet-alert 18228). Although the outburst amplitude was small, the outburst turned out to be a superoutburst with superhumps (vsnet-alert 18234, 18242; figure 104).

An MCMC analysis of both the CRTS data and the present data in outburst yielded the following orbital ephemeris:

$$\text{Min(BJD)} = 2455129.74232(3) + 0.076819040(1)E. \quad (6)$$

Like ASASSN-14ag, the object showed a strong beat phenomenon between the superhump period and the or-

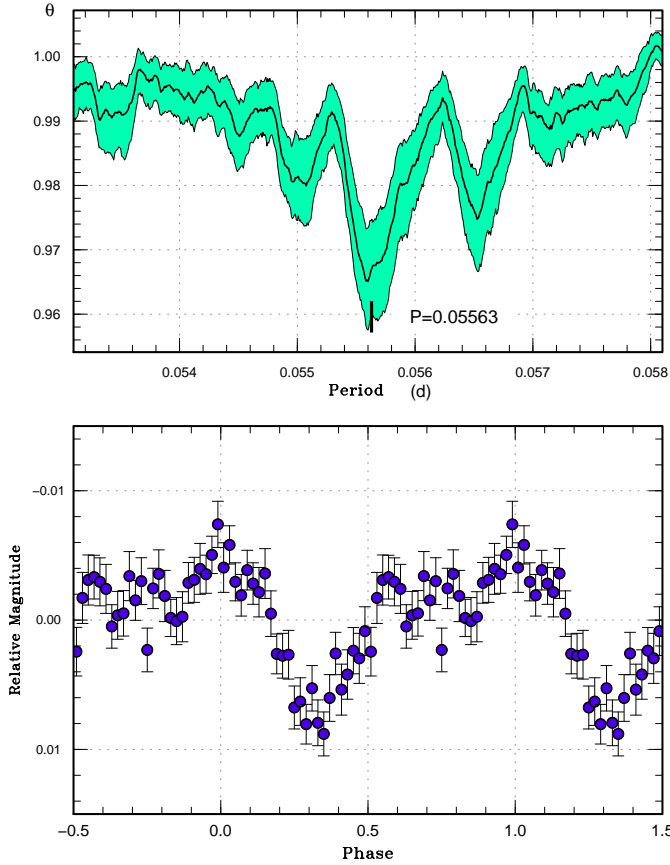


Fig. 100. Early superhumps in ASASSN-15bp (2015). (Upper): PDM analysis. (Lower): Phase-averaged profile

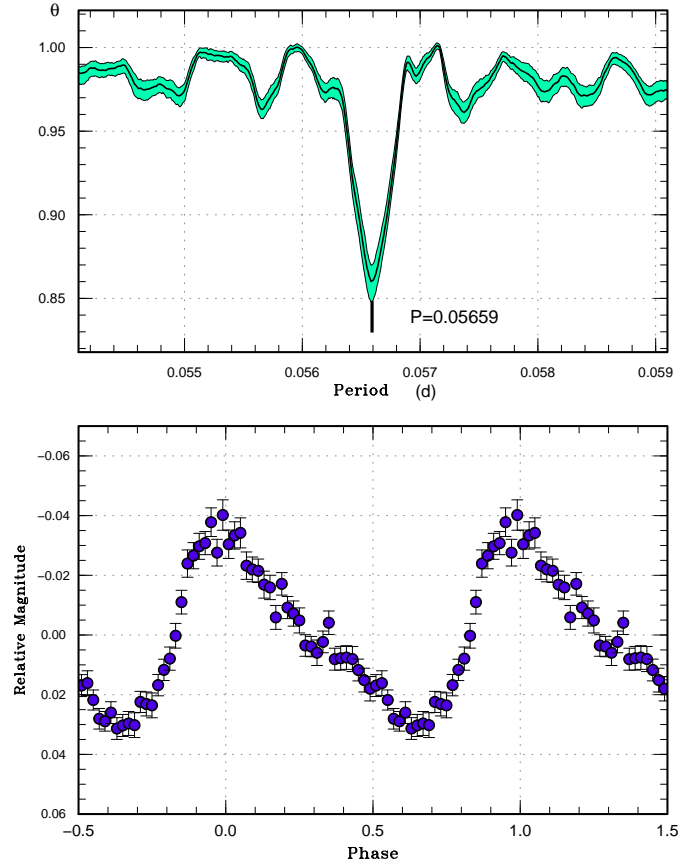


Fig. 101. Ordinary superhumps in ASASSN-15bp (2015). The data for BJD 2457056–2457069 were used. (Upper): PDM analysis. (Lower): Phase-averaged profile

bital period (figure 105).

The times of superhump maxima outside the eclipses are listed in table 79. Since the object started fading rapidly ~ 9 d after the ASAS-SN detection, it was likely that we observed the only the later part of the super-outburst. The superhumps were possibly mostly stage C superhumps although the superhump amplitudes (sometimes reaching 0.6 mag) were much larger than those of typical stage C superhumps in non-eclipsing systems.

3.77. ASASSN-15bv

This object was detected as a transient at $V=15.5$ on 2015 January 22 by ASAS-SN team. The coordinates are $06^{\text{h}}25^{\text{m}}01^{\text{s}}.75$, $-02^{\circ}47'58''.6$ (the Initial Gaia Source List). A single-night observations detected likely superhumps (vsnet-alert 18244, figure 106). Although a period of 0.101(1) d can be determined, the reality of superhumps needs to be confirmed by future observations.

3.78. ASASSN-15dq

This object was detected as a transient at $V=14.5$ on 2015 February 22 by ASAS-SN team. The coordinates are $09^{\text{h}}46^{\text{m}}06^{\text{s}}.91$, $-00^{\circ}56'01''.6$ (SDSS $g=20.4$ counterpart). CRTS also detected the object four days later (cf. vsnet-

alert 18348). The SDSS colors suggested an SU UMa-type dwarf nova (vsnet-alert 18329). Superhumps were immediately detected (vsnet-alert 18333, 18352, 18362; figure 107). The times of superhump maxima are listed in table 80. Although superhump stage is now known, no strong period variation was detected except $E \geq 61$. The object rapidly faded on March 7, 13 d after the outburst detection.

3.79. CRTS J081936.1+191540

This object (hereafter CRTS J081936) was originally detected as a CV by CRTS on 2010 February 2 (=CSS100202:081936+191540). Although it was a faint (17.35 mag), there was another brighter outburst (16.33 mag) on 2011 February 4. The object was given a CRTS designation in Drake et al. (2014). The 2013 bright (15.02 mag) outburst was by MASTER network (vsnet-alert 15562). Subsequent observations detected superhumps (vsnet-alert 15565, 15574; figure 108). The times of superhump maxima are listed in table 81. The superhump stage is unknown.

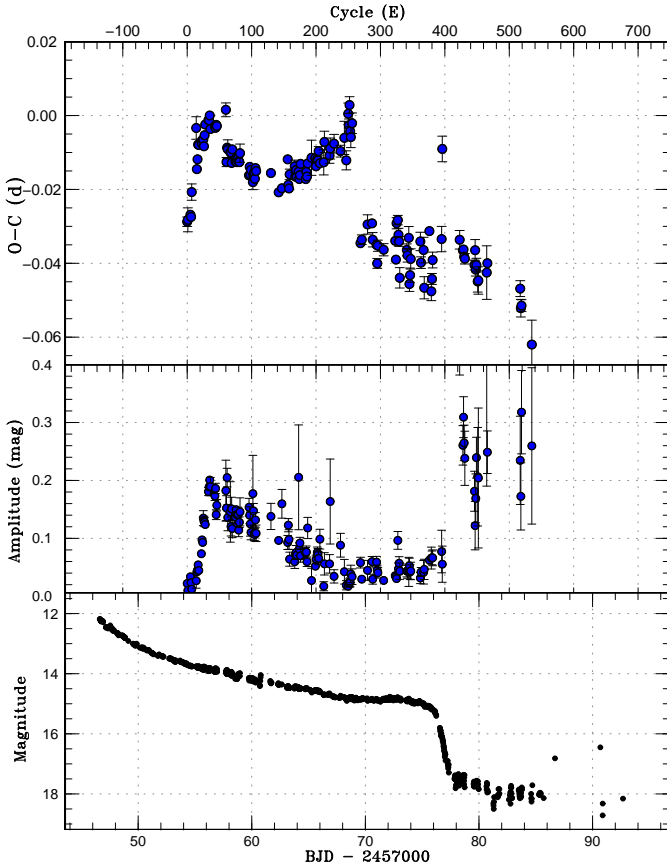


Fig. 102. $O - C$ diagram of superhumps in ASASSN-15bp (2015). (Upper:) $O - C$ diagram. We used a period of 0.05670 d for calculating the $O - C$ residuals. (Middle:) Amplitudes of superhumps. (Lower:) Light curve. The data were binned to 0.018 d.

3.80. CRTS J172038.7+183802

This object (hereafter CRTS J172038) was originally detected as a CV by CRTS on 2009 September 29 (=CSS090929:172039+183802). The object was given a CRTS designation in Drake et al. (2014). MASTER network detected a new outburst on 2014 April 3 (vsnet-alert 17148). Subsequent observations detected superhumps (vsnet-alert 17154). Only single-night observation was obtained (figure 109) and only an approximate superhump period of 0.06 d was obtained.

3.81. CSS J174033.5+414756

3.81.1. Introduction

This object (=CSS130418:174033+414756, hereafter CSS J174033) was discovered by the CRTS team in 2013 April (cf. vsnet-alert 15629). The object was also detected by the ASAS-SN team (ASASSN-13ad: Prieto et al. 2013; Nesci et al. 2013). The 2013 outburst showed a sequence of early superhumps and ordinary superhumps. The object was identified as a WZ Sge-type object having a period below the period minimum. The details of the 2013 outburst is reported in T. Ohshima et al. in preparation.

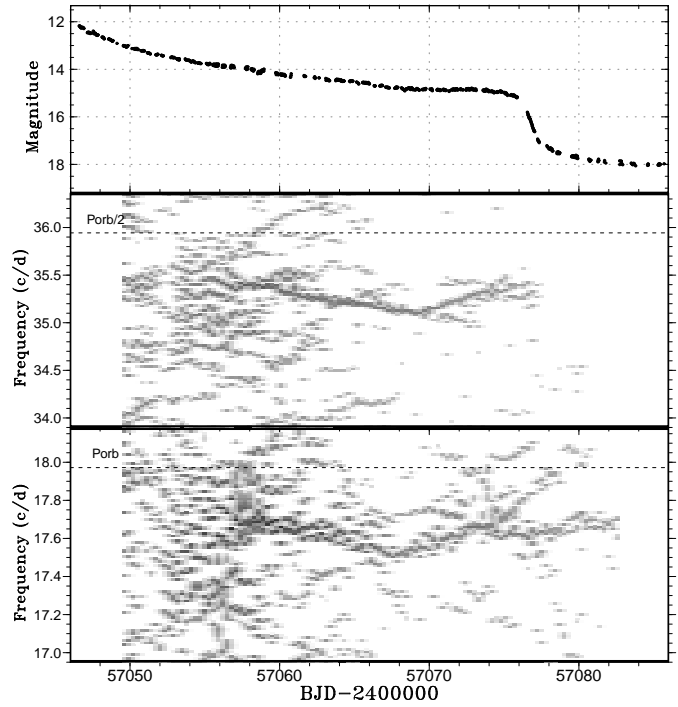


Fig. 103. Lasso period analysis of ASASSN-15bp (2015). (Upper:) Light curve. The data were binned to 0.018 d. (Middle:) First harmonics of the superhump and orbital signals. (Lower:) Fundamental of the superhump and orbital signal. The orbital signal was only weakly detected during the earliest stage (early superhumps). The signal of positive superhumps with variable frequency (around 17.6 c/d) was recorded during the superoutburst plateau post-superoutburst stage. It is obvious that the frequency decreased between BJD 2457055 and 2457059, the increased, in agreement with the $O - C$ analysis. Superhump signals before BJD 2457055 were noisy due to rapidly variable periods and contamination of early superhumps in analyzed windows. $\log \lambda = -7.8$ was used. The width of the sliding window and the time step used are 6 d and 0.3 d, respectively.

3.81.2. 2014 Outburst

The 2014 outburst was detected by C. Chiselbrook on August 6 (vsnet-alert 17610). Since there was a 6 d gap in observation before this detection and since the brightness was fainter by 0.7 mag than the peak brightness of the 2013 outburst, it was likely the peak of the 2013 outburst was missed for several days. It was a surprise that an object showing a WZ Sge-type outburst repeated a superoutburst less than 500 d after the previous outburst (vsnet-alert 17610).

As in the 2013 outburst, there was a deep dip following the plateau (BJD 2456886–2456889; figure 110). After this dip, the object showed a plateau-type rebrightening as in AL Com in 1995 (Patterson et al. 1996; Howell et al. 1996; Nogami et al. 1997) and 2001 (Ishioaka et al. 2002). Such a dip was recorded in a WZ Sge-type dwarf nova IK Leo (=OT J102146.4+234926; Uemura et al. 2008, Golovin et al. 2007, Kato et al. 2009), which was regarded as a temporary dip in a plateau rather than a dip preceding a rebrightening. After this dip, the plateau continued for

Table 77. Superhump maxima of ASASSN-15bp (2015)

E	max*	error	$O - C^\dagger$	N^\ddagger
0	57054.2881	0.0013	-0.0233	196
1	57054.3453	0.0032	-0.0228	324
5	57054.5734	0.0010	-0.0211	60
6	57054.6295	0.0012	-0.0216	66
7	57054.6930	0.0022	-0.0148	62
14	57055.1072	0.0030	0.0030	65
15	57055.1528	0.0010	-0.0081	214
16	57055.2121	0.0010	-0.0053	278
17	57055.2729	0.0008	-0.0013	192
18	57055.3294	0.0008	-0.0013	121
22	57055.5572	0.0006	-0.0000	70
23	57055.6133	0.0004	-0.0006	73
24	57055.6711	0.0004	0.0006	60
25	57055.7278	0.0006	0.0007	69
26	57055.7827	0.0006	-0.0011	102
27	57055.8424	0.0004	0.0020	172
28	57055.9020	0.0003	0.0049	105
33	57056.1867	0.0003	0.0065	118
34	57056.2433	0.0002	0.0065	131
35	57056.3013	0.0002	0.0079	123
36	57056.3544	0.0006	0.0043	92
43	57056.7520	0.0003	0.0055	45
44	57056.8083	0.0003	0.0052	45
45	57056.8658	0.0004	0.0060	45
46	57056.9222	0.0005	0.0058	40
60	57057.7204	0.0019	0.0112	18
61	57057.7629	0.0012	-0.0029	19
62	57057.8235	0.0006	0.0010	22
63	57057.8798	0.0026	0.0007	11
67	57058.1057	0.0015	0.0001	18
68	57058.1624	0.0010	0.0002	35
69	57058.2163	0.0011	-0.0026	30

*BJD-2400000.

 † Against max = 2457054.3114 + 0.056629 E . ‡ Number of points used to determine the maximum.

15 d. There was a short dip (BJD 2456902) before the termination of the entire plateau. Such a dip was recorded in KK Cnc (=OT J080714.2+113812; Kato et al. 2009).

3.81.3. Superhumps

The times of superhumps before the initial dip are listed in table 82. As in the 2013 superoutburst, there were stage B superhumps ($E \leq 166$) with a positive P_{dot} of $+2.0(0.3) \times 10^{-5}$. The value was similar to the 2013 one [$+1.6(0.1) \times 10^{-5}$]. The phases of early superhumps and stage A superhumps were not covered by the present observation since the detection was apparently several days after the peak brightness.

Before entering the dip, the superhump signal decreased and another period appeared ($E \leq 176$). The new period is 0.04505(6) d, which is identical to the orbital period within errors. We consider that the orbital signal was somehow enhanced during the decline branch to the dip minimum.

Table 77. Superhump maxima of ASASSN-15bp (2015) (continued)

E	max*	error	$O - C^\dagger$	N^\ddagger
70	57058.2766	0.0009	0.0011	29
75	57058.5569	0.0003	-0.0018	81
76	57058.6145	0.0002	-0.0008	92
77	57058.6701	0.0002	-0.0018	90
78	57058.7275	0.0002	-0.0010	83
79	57058.7846	0.0006	-0.0006	60
80	57058.8404	0.0007	-0.0014	64
81	57058.8969	0.0005	-0.0015	62
82	57058.9560	0.0025	0.0010	24
96	57059.7438	0.0006	-0.0041	42
97	57059.8028	0.0007	-0.0017	94
98	57059.8574	0.0012	-0.0037	105
99	57059.9154	0.0007	-0.0024	44
102	57060.0822	0.0020	-0.0055	28
103	57060.1404	0.0006	-0.0039	179
104	57060.1982	0.0009	-0.0027	191
105	57060.2532	0.0007	-0.0044	257
106	57060.3128	0.0007	-0.0014	152
107	57060.3687	0.0011	-0.0021	80
130	57061.6722	0.0012	-0.0011	87
142	57062.3474	0.0004	-0.0054	62
147	57062.6320	0.0005	-0.0040	15
156	57063.1501	0.0009	0.0045	119
157	57063.1999	0.0007	-0.0024	145
158	57063.2557	0.0012	-0.0033	148
159	57063.3162	0.0014	0.0006	109
167	57063.7720	0.0016	0.0034	59
168	57063.8259	0.0004	0.0007	167
169	57063.8843	0.0012	0.0025	18
170	57063.9392	0.0003	0.0007	110
173	57064.1107	0.0016	0.0023	31
174	57064.1654	0.0010	0.0004	119
175	57064.2232	0.0008	0.0015	125

*BJD-2400000.

 † Against max = 2457054.3114 + 0.056629 E . ‡ Number of points used to determine the maximum.

The times of superhump after the dip are listed in table 83. After the dip, the period was almost constant and slightly shorter than the period of stage B superhumps. The situation is clear in figure 110 that superhumps after the dip are on a smooth continuation of superhumps before the dip. Since the period was almost constant and shorter, we identified this period as that of stage C superhumps. The cycle counts listed in table 2 refer to table 83. Although these superhumps were phenomenologically identified as stage C superhumps, the variation of the period from stage B to C was smaller (0.14%) compared to $\sim 0.5\%$ in ordinary hydrogen-rich SU UMa-type dwarf novae (Kato et al. 2009). This phenomenon may be different from stage C superhumps in ordinary hydrogen-rich SU UMa-type dwarf novae. Although the entire light curve is similar to long-lasting rebrightenings in WZ Sge-type dwarf novae (such as AL Com, figure 13 in Kato et al.

Table 77. Superhump maxima of ASASSN-15bp (2015) (continued)

E	max*	error	$O - C^\dagger$	N^\ddagger
176	57064.2829	0.0011	0.0047	120
184	57064.7324	0.0009	0.0011	58
185	57064.7911	0.0010	0.0031	65
186	57064.8465	0.0010	0.0019	65
187	57064.9067	0.0012	0.0055	28
193	57065.2485	0.0048	0.0075	27
199	57065.5886	0.0007	0.0079	58
200	57065.6431	0.0008	0.0057	58
202	57065.7584	0.0009	0.0078	48
203	57065.8148	0.0010	0.0075	58
204	57065.8739	0.0013	0.0100	60
206	57065.9841	0.0010	0.0069	45
212	57066.3245	0.0034	0.0076	43
213	57066.3867	0.0029	0.0132	21
221	57066.8366	0.0021	0.0100	70
222	57066.8953	0.0028	0.0120	19
228	57067.2368	0.0025	0.0138	78
238	57067.8018	0.0016	0.0124	30
244	57068.1456	0.0045	0.0165	77
247	57068.3096	0.0026	0.0106	177
250	57068.4923	0.0029	0.0234	59
251	57068.5458	0.0017	0.0203	56
252	57068.6080	0.0023	0.0259	56
253	57068.6577	0.0023	0.0189	59
254	57068.7128	0.0028	0.0174	24
256	57068.8299	0.0028	0.0213	71
269	57069.5345	0.0009	-0.0103	46
271	57069.6489	0.0013	-0.0092	59
280	57070.1633	0.0026	-0.0045	35
287	57070.5605	0.0011	-0.0037	118

*BJD-2400000.

 † Against max = 2457054.3114 + 0.056629*E*. ‡ Number of points used to determine the maximum.

2014a), the $O - C$ behavior is different and resembles those of SU UMa-type dwarf novae with stage B-C transition. This difference needs to be further examined.

3.81.4. Comparison of superoutbursts

In figure 111, three known (super)outbursts are compared. The zero point in abscissa refers to the CRTS detection for the 2013 outburst. The object was at 14.0 mag in this detection, and the outburst was most likely detected during its rising phase. We therefore consider that zero point for the 2013 outburst refers to the start of the outburst within an error of 1 d. The 2007 outburst was detected at a much brighter magnitude (12.7). We consider that the 2007 outburst was detected near its peak brightness since the light curves well agree with the 2013 one following this assumption. The situation for the 2014 outburst is less clear. Although there was a negative observation 7 d before the initial detection by the same observer (there were four negative observations starting from 11 d before the initial detection). Since all these observations were visual observations and the detection

Table 77. Superhump maxima of ASASSN-15bp (2015) (continued)

E	max*	error	$O - C^\dagger$	N^\ddagger
288	57070.6128	0.0019	-0.0080	112
294	57070.9516	0.0012	-0.0090	60
295	57071.0033	0.0013	-0.0140	63
296	57071.0648	0.0015	-0.0091	81
305	57071.5740	0.0016	-0.0096	121
323	57072.5970	0.0012	-0.0059	116
324	57072.6486	0.0011	-0.0109	150
325	57072.7151	0.0015	-0.0010	145
327	57072.8294	0.0013	0.0000	77
328	57072.8821	0.0017	-0.0039	101
329	57072.9370	0.0013	-0.0056	103
330	57072.9839	0.0028	-0.0154	64
341	57073.6151	0.0016	-0.0071	37
342	57073.6704	0.0018	-0.0085	37
344	57073.7885	0.0031	-0.0036	32
345	57073.8327	0.0020	-0.0160	86
346	57073.8918	0.0019	-0.0136	98
347	57073.9529	0.0027	-0.0091	74
362	57074.8081	0.0025	-0.0033	61
363	57074.8591	0.0016	-0.0090	58
367	57075.0893	0.0035	-0.0053	45
368	57075.1358	0.0030	-0.0154	44
376	57075.6047	0.0005	0.0005	154
379	57075.7585	0.0025	-0.0156	35
380	57075.8186	0.0015	-0.0122	24
381	57075.8804	0.0021	-0.0070	17
395	57076.6799	0.0034	-0.0004	27
396	57076.7610	0.0035	0.0241	21

*BJD-2400000.

 † Against max = 2457054.3114 + 0.056629*E*. ‡ Number of points used to determine the maximum.

limit was close to the magnitude of the initial detection, we consider that there was a chance that the early part of the outburst was not detected by visual observations. If we consider that the actual outburst started 14 d before the initial detection, the magnitude, the epoch of the dip and the final fading agree with the 2013 ones. We adopted this assumption in figure 111. If this assumption is correct, the outburst light curves in CSS J174033 are highly reproducible.

3.82. CRTS J202731.2-224002

This object (=SSS110515:202731-224002, hereafter CRTS J202731) is a dwarf nova discovered by CRTS in 2011 May (Breidt et al. 2014). The 2014 outburst was detected by the ASAS-SN team (vsnet-alert 17857). Nine past outbursts were detected by ASAS-3 and the brightest outburst reached $V=12.2$ (vsnet-alert 17858, 17859). Subsequent observations detected superhumps (vsnet-alert 17861, 17868, 17877; figure 112). The times of superhump maxima are listed in table 84. The values for $E \leq 191$ represent post-superoutburst observations. Although stage B was not very clearly identified, a sharp

Table 78. Superhump maxima of ASASSN-15bp (2015) (post-superoutburst)

E	max*	error	$O - C^\dagger$	N^\ddagger
0	57078.2673	0.0025	0.0022	15
5	57078.5479	0.0009	0.0002	51
6	57078.6048	0.0009	0.0007	43
7	57078.6596	0.0008	-0.0011	45
8	57078.7157	0.0014	-0.0015	44
23	57079.5645	0.0013	-0.0005	42
24	57079.6252	0.0029	0.0037	41
25	57079.6767	0.0017	-0.0014	50
26	57079.7346	0.0019	-0.0001	28
28	57079.8436	0.0029	-0.0041	14
29	57079.9005	0.0037	-0.0037	12
42	57080.6398	0.0073	0.0008	10
43	57080.6990	0.0011	0.0035	48
94	57083.5838	0.0021	0.0057	37
95	57083.6352	0.0024	0.0005	40
96	57083.6926	0.0016	0.0014	40
112	57084.5893	0.0066	-0.0063	20

*BJD-2400000.

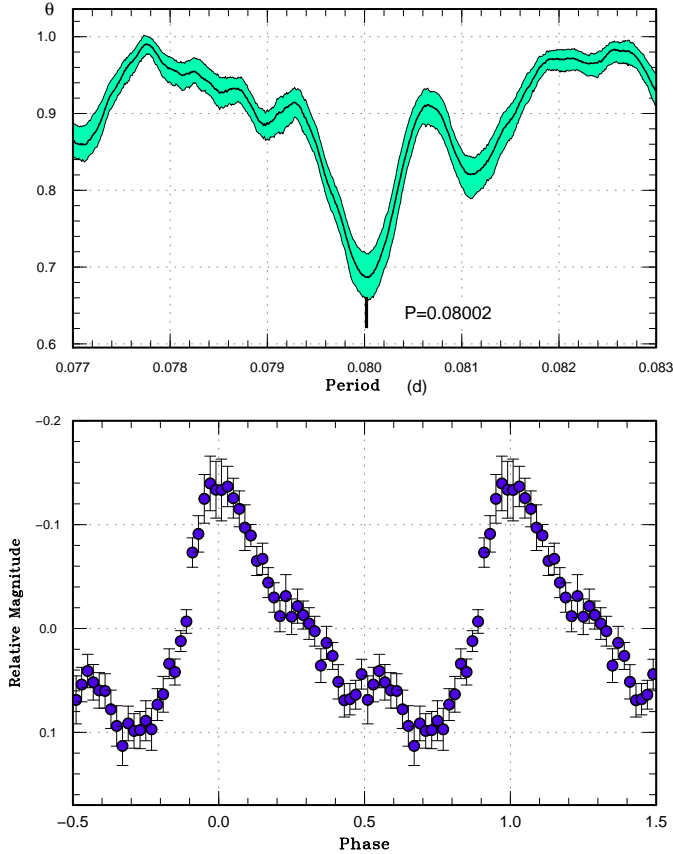
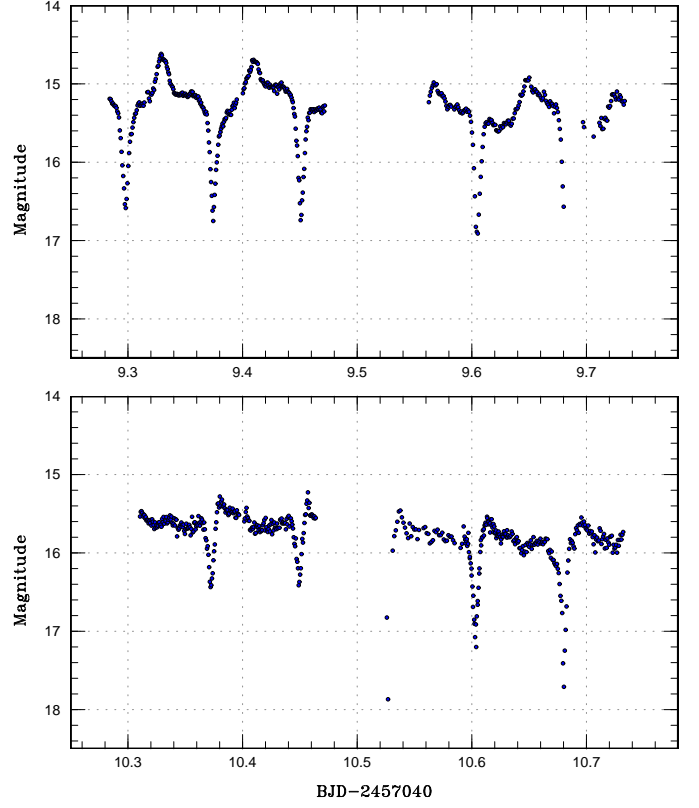
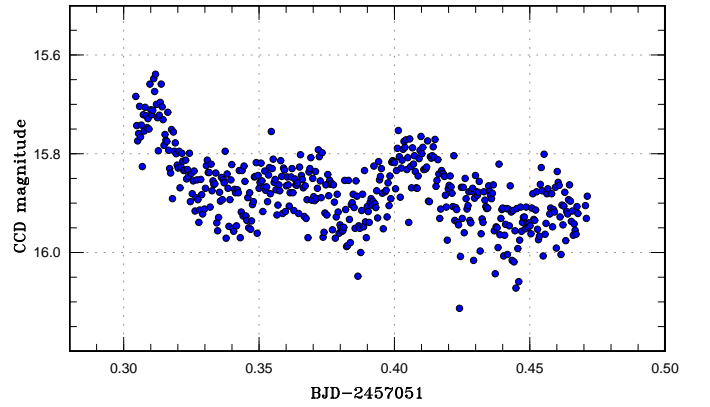
 † Against max = 2457078.2650 + 0.056523 E . ‡ Number of points used to determine the maximum.**Fig. 104.** Superhumps in ASASSN-15bu outside the eclipses (2015). (Upper): PDM analysis. (Lower): Phase-averaged profile.**Fig. 105.** Sample light curve of ASASSN-15bu in superoutburst. Superposition of superhumps and eclipse are well visible.**Fig. 106.** Likely superhumps in ASASSN-15bv (2015).

Table 79. Superhump maxima of ASASSN-15bu (2015)

E	max*	error	$O - C^\dagger$	phase ‡	N^\S
0	57049.3319	0.0006	-0.0021	0.46	88
1	57049.4138	0.0005	-0.0003	0.53	92
3	57049.5672	0.0015	-0.0070	0.52	39
4	57049.6540	0.0004	-0.0002	0.65	60
5	57049.7334	0.0016	-0.0008	0.69	30
12	57050.2921	0.0020	-0.0025	0.96	23
13	57050.3811	0.0008	0.0065	0.12	74
14	57050.4557	0.0017	0.0010	0.09	41
15	57050.5329	0.0096	-0.0019	0.09	22
16	57050.6134	0.0011	-0.0013	0.14	74
17	57050.7007	0.0014	0.0059	0.28	66
26	57051.4174	0.0005	0.0021	0.61	84
28	57051.5777	0.0006	0.0024	0.70	93
29	57051.6536	0.0008	-0.0019	0.68	76
53	57053.5811	0.0046	0.0045	0.78	71
55	57053.7416	0.0022	0.0049	0.87	60
64	57054.4507	0.0033	-0.0064	0.10	38
76	57055.4257	0.0015	0.0080	0.79	66
79	57055.6572	0.0005	-0.0007	0.80	66
80	57055.7278	0.0007	-0.0101	0.72	52

*BJD-2400000.

 † Against max = 2457049.3340 + 0.080049*E*. ‡ Orbital phase. § Number of points used to determine the maximum.**Table 80.** Superhump maxima of ASASSN-15dq (2015)

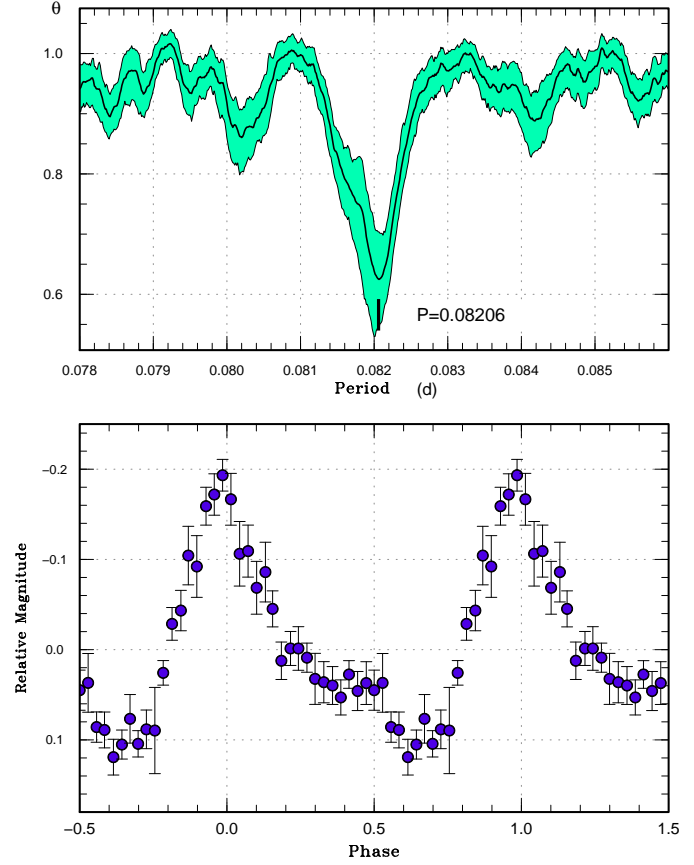
E	max*	error	$O - C^\dagger$	N^\ddagger
0	57078.5776	0.0003	-0.0031	76
13	57079.6433	0.0009	-0.0020	22
25	57080.6286	0.0007	0.0006	18
36	57081.5292	0.0005	0.0004	73
37	57081.6157	0.0012	0.0050	31
46	57082.3530	0.0008	0.0054	91
47	57082.4331	0.0038	0.0036	35
61	57083.5670	0.0040	-0.0090	9
62	57083.6569	0.0022	-0.0009	19

*BJD-2400000.

 † Against max = 2457078.5807 + 0.081889*E*. ‡ Number of points used to determine the maximum.**Table 81.** Superhump maxima of CRTS J081936 (2013)

E	max*	error	$O - C^\dagger$	N^\ddagger
0	56384.4396	0.0005	0.0008	89
1	56384.5141	0.0014	-0.0009	81
13	56385.4304	0.0007	-0.0001	90
14	56385.5069	0.0012	0.0001	87

*BJD-2400000.

 † Against max = 2456384.4387 + 0.076285*E*. ‡ Number of points used to determine the maximum.**Fig. 107.** Superhumps in ASASSN-15dq during the superoutburst plateau (2015). (Upper): PDM analysis. (Lower): Phase-averaged profile

variation in the $O - C$ values signified stage B-C transition around $E = 78$. The post-superoutburst data did not yield a significant signal of superhumps except for the initial two nights.

A list of recent outbursts is given in table 85. The intervals of known superoutburst were 473 d, 415 d and 619 d. Given the relatively frequent normal outbursts, the true supercycle appears to be 206–237 d.

3.83. CRTS J214738.4+244554

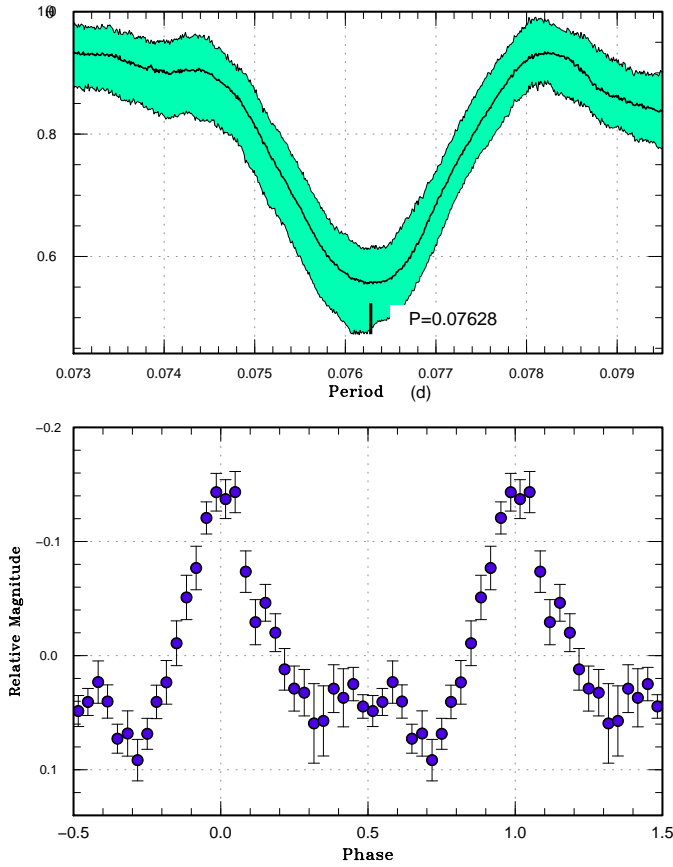
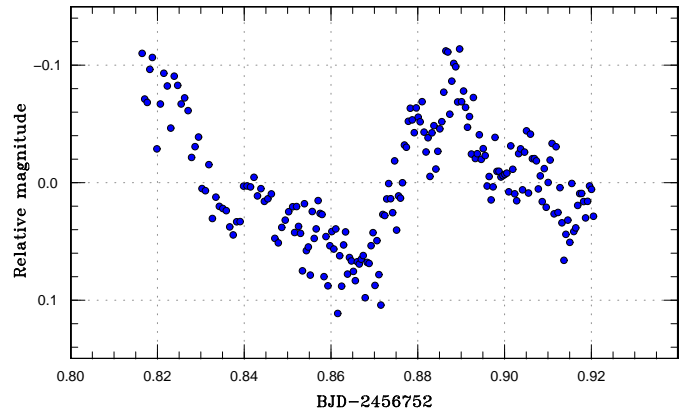
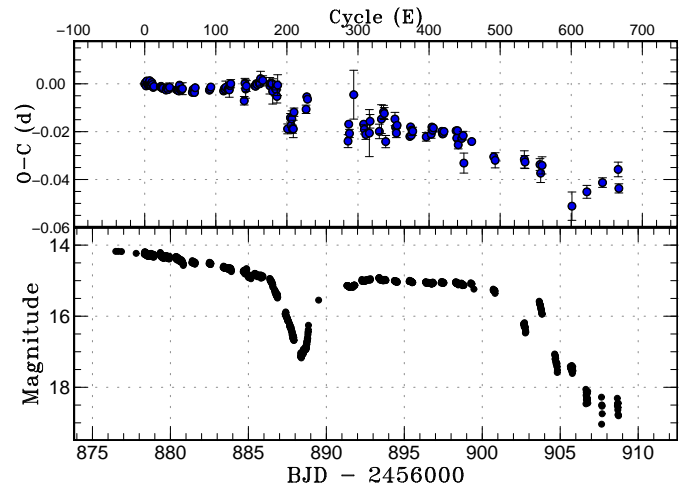
This object (=CSS111004:214738+244554, hereafter CRTS J214738) is a dwarf nova discovered by CRTS (Breidt et al. 2014). The 2011 superoutburst was relatively well observed and a positive P_{dot} for stage B superhumps was recorded in spite of the long superhump period (Kato et al. 2013a).

The 2014 superoutburst was detected by the ASAS-SN team at $V=12.81$ on September 11 (vsnet-alert 17728). On September 14, low-amplitude superhumps were detected despite that already ~ 3 d had passed since the outburst detection (vsnet-alert 17752). The superhumps further evolved ~ 4 d later (vsnet-alert 17751, 17766). The times of superhump maxima are listed in table 86. We assigned negative $O - C$ for $E \leq 2$ assuming that they are

Table 85. List of recent outbursts of CRTS J202731

Year	Month	max*	magnitude	type	source
2001	5	52053	13.0	super	ASAS-3
2001	9	52157	13.4	normal? [†]	ASAS-3
2002	9	52526	12.2	super	ASAS-3
2003	5	52770	12.8	normal? [†]	ASAS-3
2003	10	52941	12.7	super	ASAS-3
2005	7	53560	12.2	super	ASAS-3
2007	11	54409	13.0	normal? [†]	ASAS-3
2008	8	54686	13.0	normal	ASAS-3
2009	5	54976	13.0	normal	ASAS-3
2011	5	55697	13.0	normal?	CRTS
2014	10	56949	12.5	super	this paper

*JD-2400000.

[†]Single detection.**Fig. 108.** Superhumps in CRTS J081936 during the super-outburst plateau (2014). (Upper): PDM analysis. (Lower): Phase-averaged profile**Fig. 109.** Superhumps in CRTS J172038 (2014).**Fig. 110.** $O - C$ diagram of superhumps in CSS J174033 (2014). (Upper): $O - C$ diagram. We used a period of 0.045592 d for calculating the $O - C$ residuals. (Middle): Amplitudes of superhumps. (Lower): Light curve. The data were binned to 0.009 d.

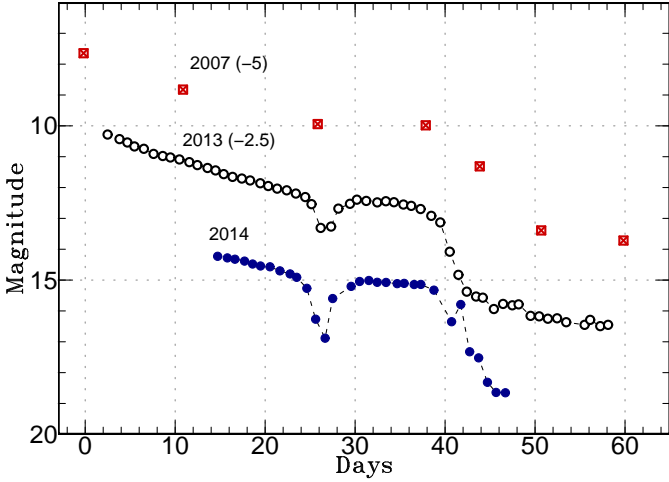


Fig. 111. Comparison of superoutbursts of CSS J174033. The data were binned to 1 d and shifted in magnitude. The dashed lines are added to aid recognizing the variation. The data for the 2013 superoutburst were from T. Ohshima et al. in preparation. The data for the 2007 superoutburst were from the CRTS public data.

Table 82. Superhump maxima of CSS J174033 (2014)

E	max*	error	$O - C^\dagger$	N^\ddagger
0	56878.3516	0.0002	-0.0003	93
1	56878.3977	0.0004	0.0003	175
2	56878.4419	0.0004	-0.0011	180
3	56878.4896	0.0006	0.0010	165
4	56878.5339	0.0009	-0.0002	52
5	56878.5790	0.0007	-0.0007	71
6	56878.6249	0.0005	-0.0003	93
7	56878.6720	0.0006	0.0013	99
8	56878.7159	0.0005	-0.0004	216
9	56878.7612	0.0004	-0.0007	185
10	56878.8081	0.0006	0.0006	150
11	56878.8528	0.0005	-0.0002	152
12	56878.8972	0.0009	-0.0014	125
13	56878.9432	0.0010	-0.0010	64
22	56879.3533	0.0004	-0.0009	24
23	56879.3991	0.0014	-0.0006	73
24	56879.4444	0.0008	-0.0009	48
25	56879.4895	0.0007	-0.0014	49
26	56879.5352	0.0015	-0.0012	48
30	56879.7167	0.0006	-0.0019	145
31	56879.7633	0.0005	-0.0009	145
32	56879.8087	0.0006	-0.0010	136
33	56879.8537	0.0011	-0.0016	119
35	56879.9458	0.0018	-0.0006	32
45	56880.4008	0.0014	-0.0013	96
46	56880.4463	0.0009	-0.0014	95
47	56880.4916	0.0009	-0.0016	58
48	56880.5370	0.0006	-0.0017	59
49	56880.5851	0.0008	0.0007	104
50	56880.6287	0.0007	-0.0012	80
51	56880.6745	0.0009	-0.0010	172
52	56880.7199	0.0007	-0.0011	185

*BJD-2400000.

† Against max = 2456878.3519 + 0.045560 E .

‡ Number of points used to determine the maximum.

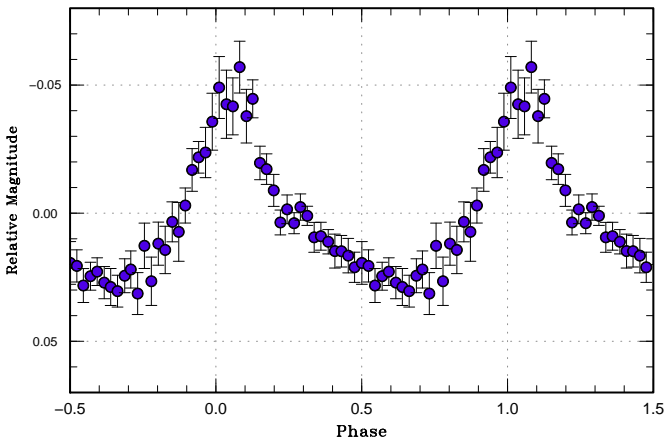
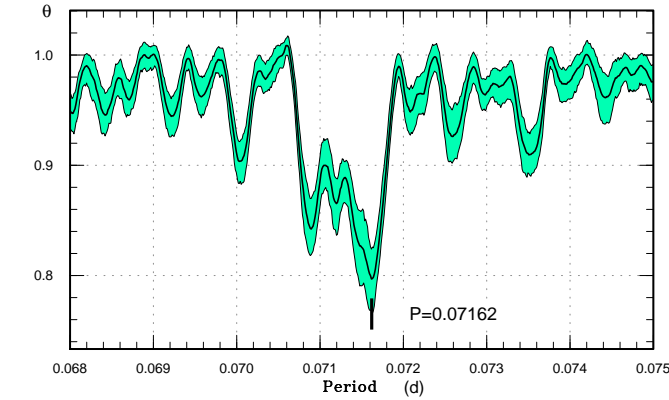


Fig. 112. Superhumps in CRTS J202731 during the superoutburst plateau (2014). (Upper): PDM analysis. (Lower): Phase-averaged profile

stage A superhumps. These counts may be in error by one cycle.

Although the observations were not sufficient, there was a suggestion of slow evolution of superhumps both in 2011 superoutburst (stage A lasting for more than 21 cycles) and the 2014 one. This indication appears to have been confirmed by a comparison of $O - C$ diagrams (figure 113). Such a slow evolution with long stage A was hypothesized for objects in the period gap as a consequence of nearly critical condition of tidal instability (Kato et al. 2014a). CRTS J214738 may be another example supporting this interpretation.

3.84. MASTER OT J031600.08+175824.4

This optical transient (hereafter MASTER J031600) was detected on 2014 December 26 at a magnitude of 15.1 (Shumkov et al. 2014). The outburst was detected in the early stage and subsequent development of superhumps

Table 82. Superhump maxima of CSS J174033 (2014) (continued)

E	max*	error	$O - C^\dagger$	N^\ddagger
53	56880.7659	0.0025	-0.0006	69
67	56881.4027	0.0005	-0.0017	48
68	56881.4495	0.0004	-0.0005	48
69	56881.4943	0.0006	-0.0012	49
70	56881.5394	0.0005	-0.0017	48
71	56881.5870	0.0013	0.0003	27
91	56882.4978	0.0007	-0.0000	88
92	56882.5440	0.0006	0.0006	87
93	56882.5903	0.0007	0.0014	67
111	56883.4093	0.0005	0.0003	47
112	56883.4559	0.0007	0.0013	47
113	56883.5012	0.0006	0.0010	46
114	56883.5476	0.0026	0.0019	17
117	56883.6836	0.0011	0.0011	31
118	56883.7292	0.0013	0.0013	40
119	56883.7745	0.0031	0.0010	41
120	56883.8219	0.0016	0.0028	40
121	56883.8683	0.0017	0.0036	40
140	56884.7274	0.0018	-0.0029	32
141	56884.7803	0.0020	0.0044	31
142	56884.8235	0.0038	0.0021	10
143	56884.8703	0.0022	0.0033	10
155	56885.4175	0.0008	0.0038	49
156	56885.4629	0.0006	0.0037	49
157	56885.5096	0.0007	0.0048	46
158	56885.5548	0.0008	0.0044	48
161	56885.6922	0.0012	0.0051	78
162	56885.7375	0.0013	0.0049	86
163	56885.7853	0.0031	0.0071	57
166	56885.9213	0.0019	0.0064	53
176	56886.3750	0.0034	0.0045	23
177	56886.4216	0.0008	0.0055	44

*BJD-2400000.

 † Against max = 2456878.3519 + 0.045560 E . ‡ Number of points used to determine the maximum.

was recorded (vsnet-alert 18112, 18138). On December 28, there were only small-amplitude variations. On 2015 January 2, fully developed superhumps were observed (figure 114). The times of superhump maxima are listed in table 87. The $O - C$ data suggest that we observed the early phase of stage B superhumps.

3.85. MASTER OT J043915.60+424232.3

This optical transient (hereafter MASTER J043915) was detected on 2014 January 21 at a magnitude of 15.7 (Balanutsa et al. 2014). The second outburst was detected also by the D. Denisenko on 2014 December 26 at a magnitude of 15.7 (vsnet-alert 18106). Subsequent observations detected superhumps (vsnet-alert 18127, 18140; figure 115). The alias selection was based on the period [0.0625(4) d] derived from the continuous observation on the first night. The times of superhump maxima are listed in table 88. The superhump stage is unknown. The mag-

Table 82. Superhump maxima of CSS J174033 (2014) (continued)

E	max*	error	$O - C^\dagger$	N^\ddagger
178	56886.4671	0.0011	0.0055	49
179	56886.5126	0.0011	0.0055	48
180	56886.5550	0.0053	0.0023	48
184	56886.7385	0.0031	0.0036	67
185	56886.7836	0.0023	0.0031	66
186	56886.8264	0.0027	0.0004	46
187	56886.8767	0.0044	0.0051	28
201	56887.4968	0.0021	-0.0127	114
205	56887.6838	0.0018	-0.0080	63
206	56887.7262	0.0011	-0.0111	79
207	56887.7745	0.0034	-0.0084	75
208	56887.8158	0.0017	-0.0126	72
209	56887.8615	0.0036	-0.0125	53
210	56887.9141	0.0017	-0.0055	35

*BJD-2400000.

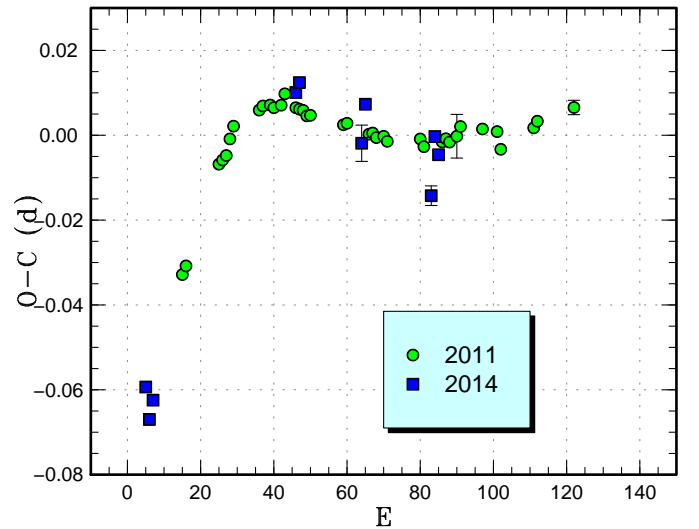
 † Against max = 2456878.3519 + 0.045560 E . ‡ Number of points used to determine the maximum.

Fig. 113. Comparison of $O - C$ diagrams of CRTS J214738 between different superoutbursts. A period of 0.09723 d was used to draw this figure. Approximate cycle counts (E) after the start of the superoutburst were used. We have shifted the 2011 $O - C$ diagram by 10 cycles to best match the 2014 one. This shift suggests that the 2011 superoutburst started 1 d earlier than the CRTS detection.

Table 83. Superhump maxima of CSS J174033 (2014) (after dip)

E	max*	error	$O - C^\dagger$	N^\ddagger
0	56888.6903	0.0017	-0.0020	73
1	56888.7412	0.0016	0.0033	94
2	56888.7857	0.0012	0.0023	81
59	56891.3669	0.0027	-0.0108	25
60	56891.4196	0.0010	-0.0036	24
61	56891.4613	0.0017	-0.0074	24
67	56891.7511	0.0102	0.0093	21
81	56892.3770	0.0013	-0.0020	68
82	56892.4205	0.0019	-0.0041	76
84	56892.5095	0.0020	-0.0061	71
89	56892.7381	0.0098	-0.0051	21
90	56892.7886	0.0028	-0.0001	21
103	56893.3771	0.0030	-0.0033	59
106	56893.5190	0.0060	0.0021	46
109	56893.6588	0.0027	0.0054	12
110	56893.7037	0.0025	0.0047	22
112	56893.7831	0.0026	-0.0068	21
125	56894.3853	0.0028	0.0036	48
126	56894.4273	0.0011	0.0002	72
127	56894.4706	0.0019	-0.0021	70
128	56894.5194	0.0013	0.0012	57
146	56895.3354	0.0007	-0.0020	23
147	56895.3850	0.0016	0.0020	62
148	56895.4271	0.0013	-0.0014	70
149	56895.4748	0.0016	0.0008	62
150	56895.5199	0.0017	0.0004	43
169	56896.3838	0.0018	-0.0004	45
176	56896.7041	0.0017	0.0013	32
177	56896.7527	0.0013	0.0043	45
178	56896.7969	0.0010	0.0030	42
179	56896.8435	0.0014	0.0041	46

*BJD-2400000.

 † Against max = 2456888.6924 + 0.045514*E*. ‡ Number of points used to determine the maximum.

nitude on 2014 January 21 would suggest a superoutburst. If this is the case, the supercycle is around 340 d.

3.86. MASTER OT J055845.55+391533.4

This optical transient (hereafter MASTER J055845) was detected on 2014 February 19 at a magnitude of 14.4 (Yecheistov et al. 2014). A retrospective examination of the MASTER data indicated that the object was already bright at 13.9 mag on February 13. There were also two outbursts (2011 November 28 and 2012 November 19) recorded in the MASTER data. Single-night observations on February 28 detected superhumps (vsnet-alert 16955; figure 116). The best superhump period using the PDM method was 0.0563(4) d. The times of superhump maxima are listed in table 89. Since the object had been in outburst already at least for 15 d, this observation most likely recorded stage C superhumps. If the three outbursts were all superoutbursts, the supercycle would be an order of 360–450 d.

Table 83. Superhump maxima of CSS J174033 (2014) (after dip, continued)

E	max*	error	$O - C^\dagger$	N^\ddagger
191	56897.3892	0.0013	0.0036	44
192	56897.4337	0.0010	0.0026	29
193	56897.4795	0.0008	0.0029	48
194	56897.5259	0.0014	0.0038	43
211	56898.3013	0.0006	0.0054	25
212	56898.3438	0.0016	0.0024	32
213	56898.3925	0.0010	0.0056	63
214	56898.4322	0.0017	-0.0002	62
219	56898.6628	0.0012	0.0028	19
221	56898.7552	0.0018	0.0041	66
222	56898.7893	0.0042	-0.0073	53
233	56899.2998	0.0016	0.0026	25
264	56900.7068	0.0010	-0.0014	18
266	56900.7965	0.0032	-0.0027	22
307	56902.6661	0.0036	0.0009	20
308	56902.7106	0.0027	-0.0001	22
329	56903.6670	0.0025	0.0005	62
330	56903.7090	0.0039	-0.0031	68
332	56903.8034	0.0036	0.0003	60
374	56905.7012	0.0059	-0.0135	45
395	56906.6647	0.0027	-0.0058	20
417	56907.6716	0.0020	-0.0002	20
439	56908.6801	0.0031	0.0070	43
440	56908.7178	0.0019	-0.0009	40

*BJD-2400000.

 † Against max = 2456888.6924 + 0.045514*E*. ‡ Number of points used to determine the maximum.

3.87. MASTER OT J085854.16-274030.7

This optical transient (hereafter MASTER J085854) was detected on 2015 January 17 at a magnitude of 13.7 (Balanutsa et al. 2015a). Four days after the detection, the object started to show short-period superhumps (vsnet-alert 18210, 18220; figure 118). After the superoutburst plateau ended, the object showed two rebrightenings (vsnet-alert 18254, 18266; figure 117).

The times of superhumps during the plateau phase are listed in table 90. Although observations started relatively early, we could not confidently detect stage A superhumps. The resultant P_{dot} for stage B superhumps was relatively large.

WZ Sge-type dwarf novae with multiple rebrightenings have been recently systematically studied by Nakata et al. (2013), C. Nakata et al. in preparation. Mroz et al. (2013) also reported two new objects (OGLE-GD-DN-001, OGLE-GD-DN-014) with multiple rebrightenings. All these objects were known to have orbital periods (or superhump periods) longer than $\gtrsim 0.06$ d. MASTER J085854 is the only known system showing multiple rebrightenings and with a very short superhump period.

C. Nakata et al. in preparation suggest that WZ Sge-type dwarf novae with multiple rebrightenings have higher mass ratios than period bouncers, which also appear to be consistent with the shortness of stage A, i.e. super-

Table 84. Superhump maxima of CRTS J202731 (2014)

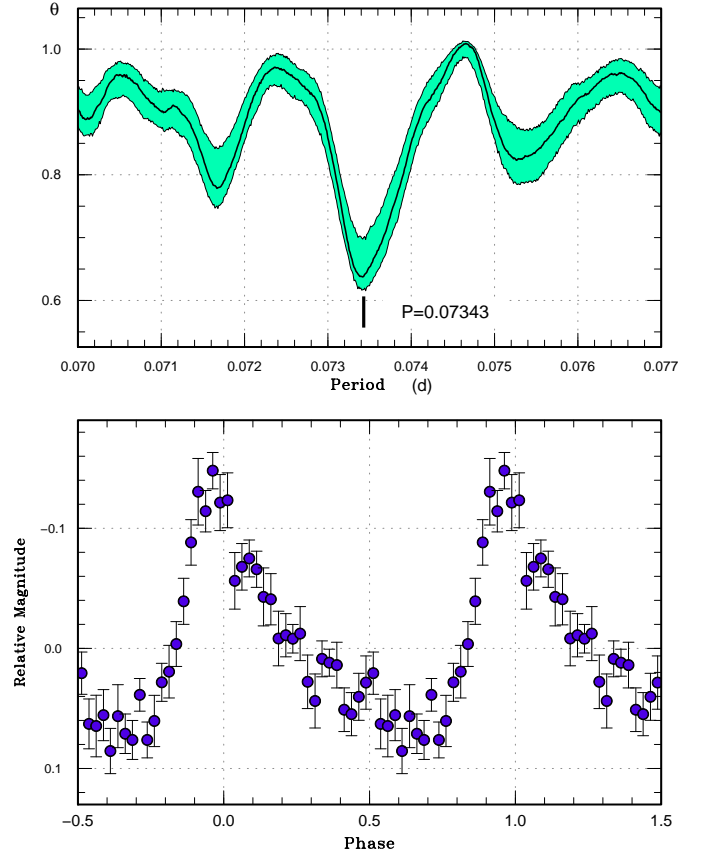
E	max*	error	$O - C^\dagger$	N^\ddagger
0	56948.9418	0.0002	-0.0129	78
1	56949.0140	0.0005	-0.0121	53
8	56949.5127	0.0044	-0.0126	10
9	56949.5858	0.0008	-0.0108	19
23	56950.5865	0.0006	-0.0085	21
36	56951.5151	0.0055	-0.0071	13
37	56951.5860	0.0034	-0.0075	19
42	56951.9434	0.0071	-0.0067	11
70	56953.9357	0.0012	-0.0112	18
78	56954.5287	0.0016	0.0113	19
83	56954.8765	0.0019	0.0025	23
84	56954.9597	0.0005	0.0144	78
92	56955.5259	0.0013	0.0101	29
93	56955.6000	0.0005	0.0128	47
94	56955.6715	0.0011	0.0130	22
106	56956.5225	0.0015	0.0082	29
107	56956.5951	0.0006	0.0095	47
108	56956.6672	0.0021	0.0102	25
121	56957.5938	0.0006	0.0098	47
122	56957.6638	0.0028	0.0085	26
126	56957.9572	0.0010	0.0165	53
127	56958.0132	0.0010	0.0013	41
135	56958.5920	0.0009	0.0095	45
136	56958.6630	0.0028	0.0092	26
139	56958.8925	0.0021	0.0247	40
140	56958.9507	0.0008	0.0116	52
149	56959.5872	0.0009	0.0063	48
150	56959.6540	0.0011	0.0018	24
163	56960.5779	0.0010	-0.0014	49
164	56960.6500	0.0013	-0.0006	29
191	56962.5409	0.0029	-0.0353	45
192	56962.6166	0.0038	-0.0309	38
205	56963.5409	0.0020	-0.0337	36

*BJD-2400000.

 † Against max = 2456948.9548 + 0.071316 E . ‡ Number of points used to determine the maximum.**Table 86.** Superhump maxima of CRTS J214738 (2014)

E	max*	error	$O - C^\dagger$	N^\ddagger
0	56915.3175	0.0009	-0.0071	187
1	56915.4071	0.0013	-0.0156	186
2	56915.5089	0.0009	-0.0118	125
41	56919.3734	0.0003	0.0306	92
42	56919.4730	0.0007	0.0321	37
59	56921.1116	0.0043	0.0047	32
60	56921.2180	0.0013	0.0131	79
78	56922.9466	0.0023	-0.0224	71
79	56923.0577	0.0005	-0.0092	200
80	56923.1507	0.0006	-0.0143	181

*BJD-2400000.

 † Against max = 2456915.3247 + 0.098004 E . ‡ Number of points used to determine the maximum.**Fig. 114.** Superhumps in MASTER J031600 (2014). (Upper): PDM analysis. (Lower): Phase-averaged profile**Table 87.** Superhump maxima of MASTER J031600 (2014)

E	max*	error	$O - C^\dagger$	N^\ddagger
0	57025.2070	0.0023	-0.0034	36
1	57025.2844	0.0008	0.0006	73
2	57025.3578	0.0009	0.0005	49
30	57027.4221	0.0032	0.0086	48
31	57027.4852	0.0025	-0.0018	75
42	57028.2964	0.0014	0.0017	76
43	57028.3730	0.0012	0.0048	67
44	57028.4308	0.0024	-0.0109	76

*BJD-2400000.

 † Against max = 2457025.2104 + 0.073438 E . ‡ Number of points used to determine the maximum.

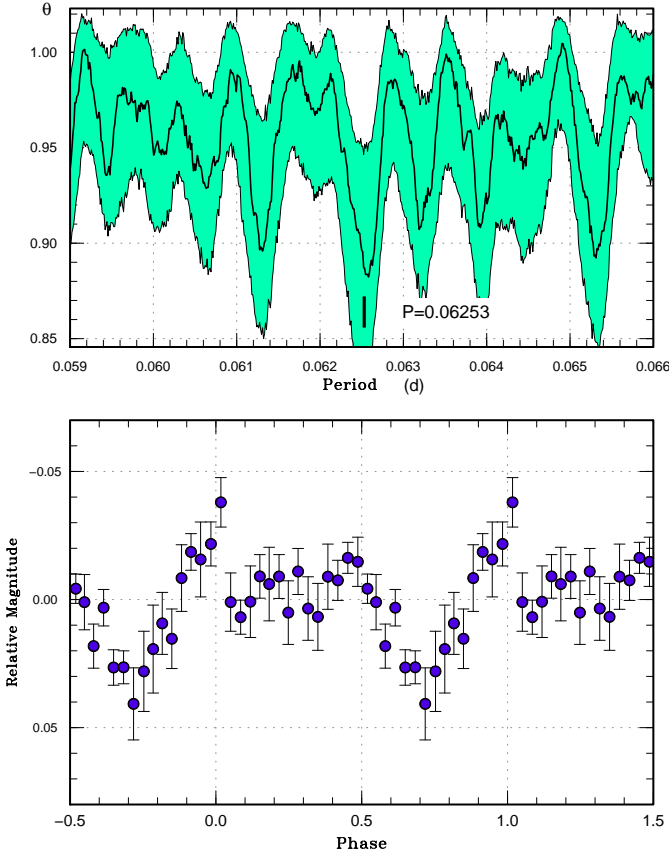


Fig. 115. Superhumps in MASTER J043915 (2014). (Upper): PDM analysis. (Lower): Phase-averaged profile

Table 88. Superhump maxima of MASTER J043915 (2014)

E	max*	error	$O - C^\dagger$	N^\ddagger
0	57019.0953	0.0018	0.0017	47
1	57019.1564	0.0010	0.0003	46
2	57019.2164	0.0017	-0.0021	27
48	57022.0914	0.0045	0.0001	45

*BJD-2400000.

† Against max = 2457019.0936 + 0.062452 E .

‡ Number of points used to determine the maximum.

Table 89. Superhump maxima of MASTER J055845 (2014)

E	max*	error	$O - C^\dagger$	N^\ddagger
0	56717.3638	0.0016	-0.0005	55
1	56717.4203	0.0019	-0.0005	54
2	56717.4796	0.0011	0.0024	54
3	56717.5322	0.0017	-0.0015	57

*BJD-2400000.

† Against max = 2456717.3643 + 0.056443 E .

‡ Number of points used to determine the maximum.

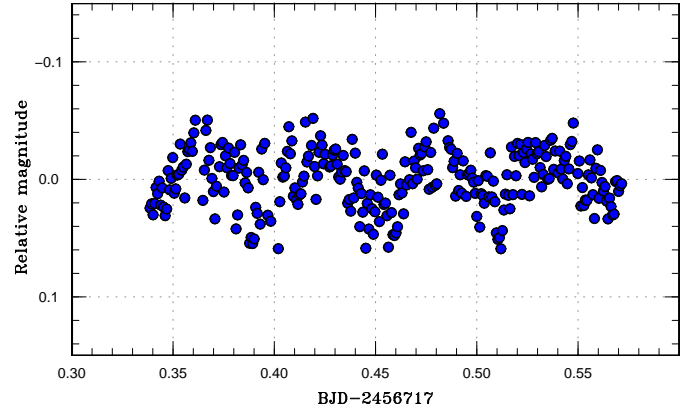


Fig. 116. Superhumps in MASTER J055845 (2014).

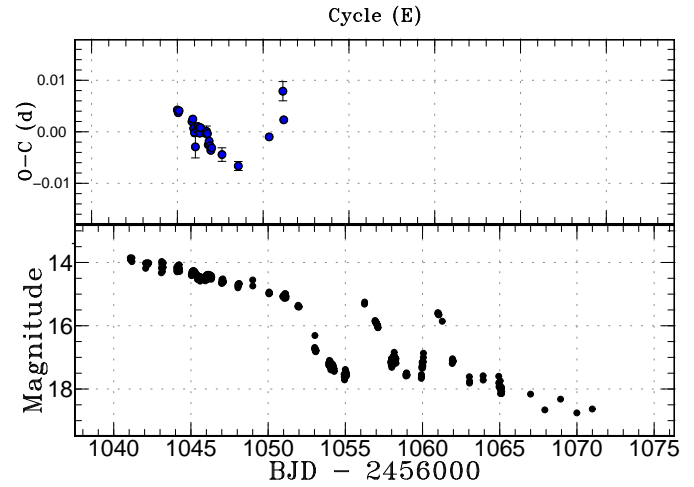


Fig. 117. $O - C$ diagram of superhumps in MASTER J085854 (2015). (Upper:) $O - C$ diagram. We used a period of 0.05556 d for calculating the $O - C$ residuals. (Lower:) Light curve. The data were binned to 0.011 d.

humps quickly grow. This also likely applies to MASTER J085854 as judged from the quick appearance of stage B superhumps. Since there was possibly a past outburst in the CRTS data (Balanutsa et al. 2015a), continued monitoring of this object will clarify the supercycle length and where there is a phase of early superhumps.

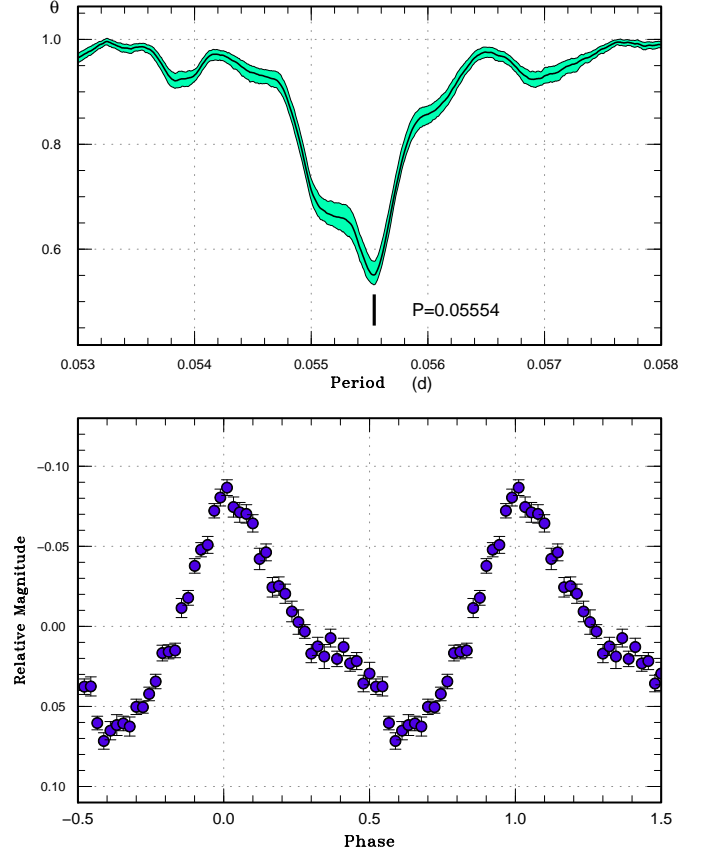
3.88. MASTER OT J105545.20+573109.7

This optical transient (hereafter MASTER J105545) was detected on 2014 March 4 at a magnitude of 15.5 (Vladimirov et al. 2014). Subsequent observations detected superhumps (vsnet-alert 17007, 17018; figure 119). The times of superhump maxima are listed in table 91. Although the stage of the superoutburst was unknown, the small amplitudes of superhumps may suggest that we observed the later stage of the superoutburst.

Table 90. Superhump maxima of MASTER J085854 (2015)

E	max*	error	$O - C^\dagger$	N^\ddagger
0	57044.1262	0.0003	0.0042	89
1	57044.1813	0.0002	0.0037	115
2	57044.2372	0.0002	0.0040	98
17	57045.0685	0.0007	0.0020	43
18	57045.1246	0.0004	0.0024	100
19	57045.1783	0.0002	0.0006	117
20	57045.2330	0.0003	-0.0002	117
21	57045.2858	0.0021	-0.0029	22
23	57045.4003	0.0004	0.0004	79
24	57045.4565	0.0002	0.0010	128
25	57045.5117	0.0002	0.0007	128
26	57045.5663	0.0002	-0.0003	127
27	57045.6229	0.0005	0.0008	70
33	57045.9552	0.0004	-0.0003	46
34	57046.0111	0.0010	0.0001	38
35	57046.0662	0.0004	-0.0004	212
36	57046.1196	0.0004	-0.0026	248
37	57046.1759	0.0006	-0.0018	236
38	57046.2306	0.0003	-0.0027	153
39	57046.2852	0.0004	-0.0036	129
40	57046.3413	0.0005	-0.0031	84
52	57047.0067	0.0013	-0.0044	53
71	57048.0601	0.0009	-0.0066	35
107	57050.0659	0.0007	-0.0010	95
123	57050.9638	0.0019	0.0079	57
124	57051.0138	0.0007	0.0023	58

*BJD-2400000.

 † Against max = 2457044.1220 + 0.055560 E . ‡ Number of points used to determine the maximum.**Fig. 118.** Superhumps in MASTER J085854 during the plateau phase (2015). (Upper): PDM analysis. (Lower): Phase-averaged profile**Table 91.** Superhump maxima of MASTER J105545 (2014)

E	max*	error	$O - C^\dagger$	N^\ddagger
0	56726.4942	0.0010	-0.0024	72
14	56727.4377	0.0016	0.0040	19
15	56727.5009	0.0006	0.0002	33
16	56727.5645	0.0007	-0.0031	60
17	56727.6369	0.0011	0.0024	94
18	56727.7015	0.0008	0.0001	65
29	56728.4369	0.0016	-0.0009	60
30	56728.5070	0.0013	0.0022	73
31	56728.5703	0.0016	-0.0014	35
45	56729.5094	0.0119	0.0006	26
46	56729.5741	0.0026	-0.0016	33

*BJD-2400000.

 † Against max = 2456726.4966 + 0.066937 E . ‡ Number of points used to determine the maximum.

3.89. OT J030929.8+263804

This object (=PNV J03093063+2638031, hereafter OT J030929) was announced as a possible nova detected by S. Ueda.¹⁴ Based on the presence of a blue counterpart and the relatively small outburst amplitude, the object was considered to be a WZ Sge-type dwarf nova rather than a nova (vsnet-alert 17907, 17908). Spectroscopic observations also indicated a dwarf nova (vsnet-alert 17912, 17919). Soon after the announcement, early superhumps were detected (vsnet-alert 17918, 17920, 17926, 17931; figure 120). The period was determined to be 0.05615(2) d. The object then showed ordinary superhumps (vsnet-alert 17934, 17959, 17972; figure 121).

The times of superhump maxima during the outburst plateau are listed in table 92. Although stage A superhumps were recorded ($E \leq 36$), there was an observational gap in the early stage B. There was a clear stage B-C transition around $E=197$. The period of stage A superhumps corresponds to $\epsilon^*=0.0291(3)$ and $q=0.078(1)$.

Superhumps after the rapid fading became less clear.

¹⁴ <<http://www.cbat.eps.harvard.edu/unconf/followups/J03093063+2638031.html>>. Also note that the reported coordinates were somewhat different from the final values.

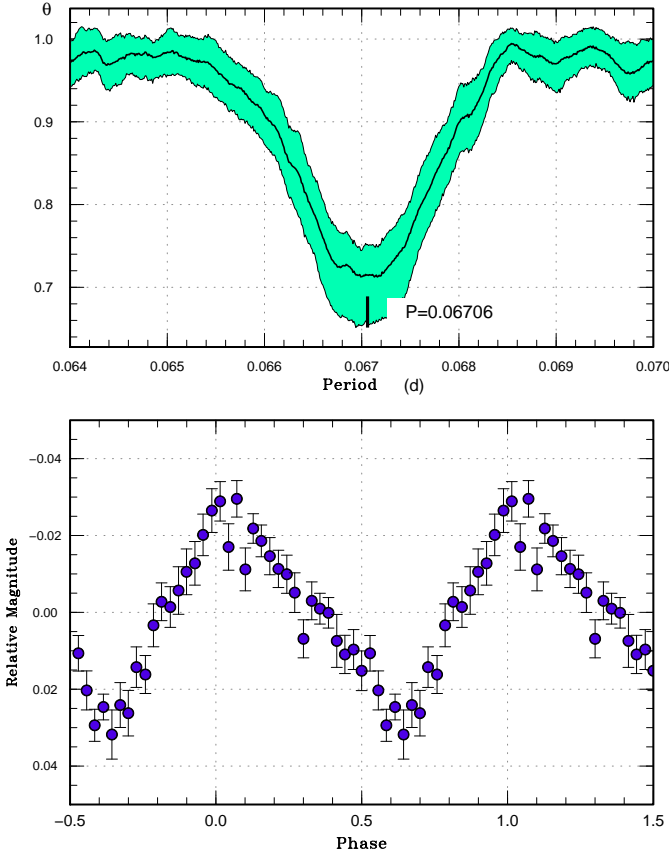


Fig. 119. Superhumps in MASTER J105545 (2014). (Upper): PDM analysis. (Lower): Phase-averaged profile

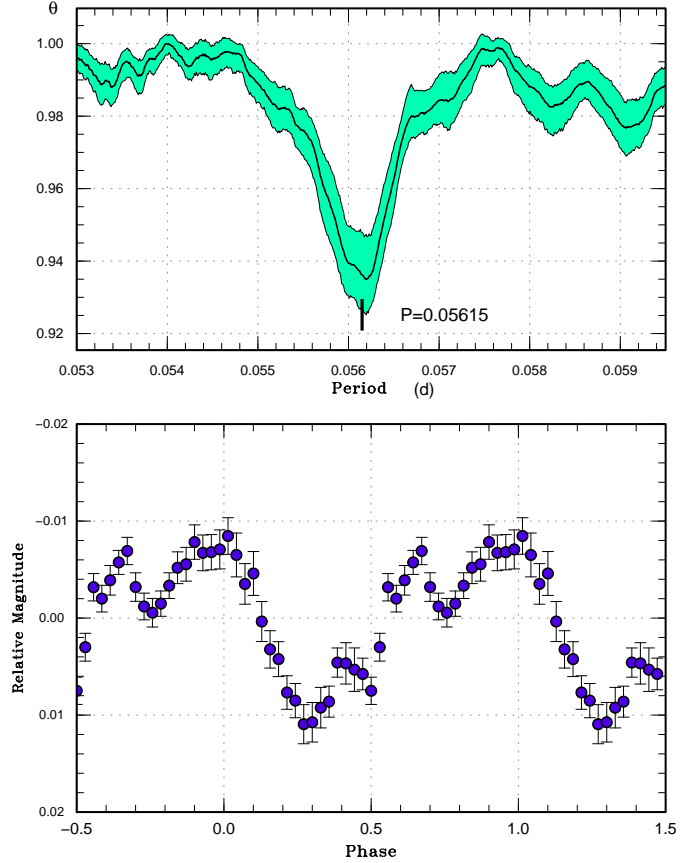


Fig. 120. Early superhumps in OT J030929 (2014). (Upper): PDM analysis. (Lower): Phase-averaged profile

The times before BJD 2456987 are listed in table 93. These post-superoutburst superhumps were on a smooth extension of stage C superhumps (figure 122). After this, the profile of superhumps became double-humped (figure 123). The secondary humps even became stronger than the original superhumps. Although this phenomenon bore some resemblance to traditional late superhumps, this change in the profile occurred more than ~ 4 d after the rapid decline, which is not the usual case in traditional late superhumps.

The relatively large P_{dot} of stage B superhumps and the transition to stage C superhumps during the plateau phase were similar to SU UMa-type dwarf novae rather than extreme WZ Sge-type dwarf novae. The object may have intermediate properties between WZ Sge-type dwarf novae and ordinary SU UMa-type dwarf novae.

3.90. OT J064833.4+065624

This object (=PNV J06483343+0656236, hereafter OT J064833) was announced as a possible nova detected at an unfiltered CCD magnitude of 11.6 on 2014 November 22 by S. Kaneko.¹⁵ The presence of a relatively bright quies-

cent counterpart made the object a good candidate for a dwarf nova (vsnet-alert 18001). Spectroscopic observation by M. Fujii indeed confirmed the dwarf nova-type nature (vsnet-alert 18004).

Subsequent observations detected growing superhumps with a long period (vsnet-alert 18012, 18014, 18018, 18027; figure 124). The times of superhump maxima are listed in table 94. Stage A superhumps are clearly detected ($E \leq 15$; figure 125). The epochs after $E = 84$ are post-superoutburst superhumps, and they are not used to determine the periods in table 2. There was no indication of a phase jump at the end of the superoutburst plateau.

The most notable feature of this object is the long-lasting stage A despite the long superhump period, which makes this object as a dwarf nova in the period gap. In Kato et al. (2014a), we have argued that in some long- P_{orb} dwarf novae, the condition of tidal instability is critically reached and it may take longer time to develop superhumps. This object appears to fit this interpretation.

The object also showed a rebrightening (vsnet-alert 18040; figure 125), which is relatively rare in long- P_{orb} systems. Well-documented rebrightenings in long- P_{orb} systems include V725 Aql (Uemura et al. 2001) and QZ Ser (T. Ohshima et al. in preparation, vsnet-alert 15567,

¹⁵ <<http://www.cbat.eps.harvard.edu/unconf/followups/J06483343+0656236.html>>.

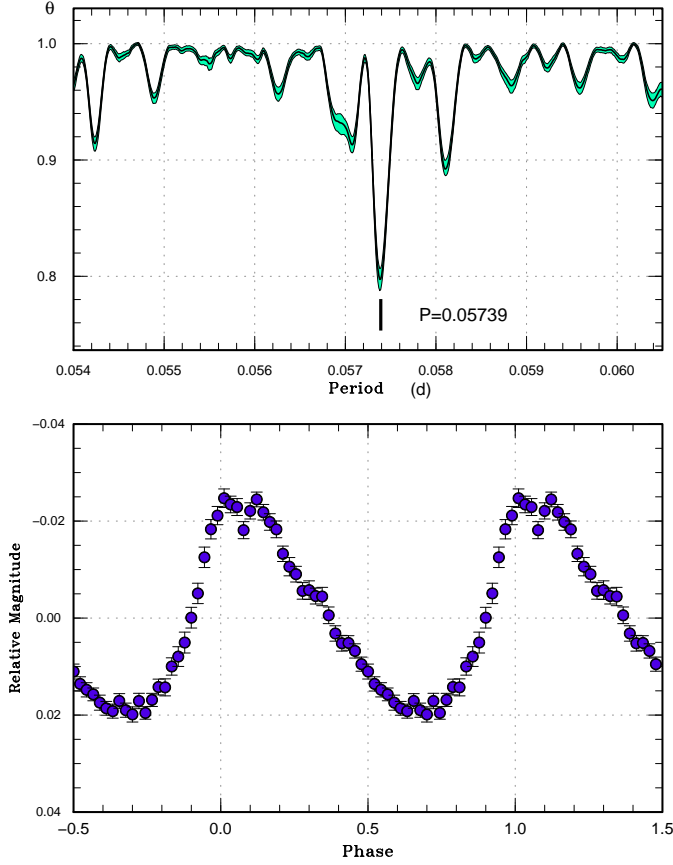


Fig. 121. Ordinary superhumps in OT J030929 (2014). (Upper): PDM analysis. (Lower): Phase-averaged profile

15620). The 1997 superoutburst of EF Peg may have also been accompanied by a rebrightening (vsnet-alert 1344). All these objects are known to have long recurrence times and are hence considered to have low mass-transfer rates. Given the lack of past detections of outbursts in OT J064833, this object also likely have a low mass-transfer rate. The features resembling short- P_{orb} (rebrightenings, positive P_{dot} and absence of phase jump at the end of superoutburst) may be a result of low mass-transfer rates and await future theoretical investigation.

Since the object has a bright quiescent counterpart (15.9 mag in J), it is a promising candidate to detect the secondary. Accurate measurement of the orbital period will lead to determination of q by using the stage A superhump method and would clarify the evolutionary state of this object.

3.91. OT J213806.6+261957

3.91.1. Introduction

This object (OT J213806) was discovered as a possible nova independently by D.-A. Yi (Yamaoka 2010) and S. Kaneko (Nakano 2010) in 2010. Spectroscopic observations demonstrated that the dwarf nova-type nature of the object (Graham et al. 2010 Tovmassian et al. 2010,

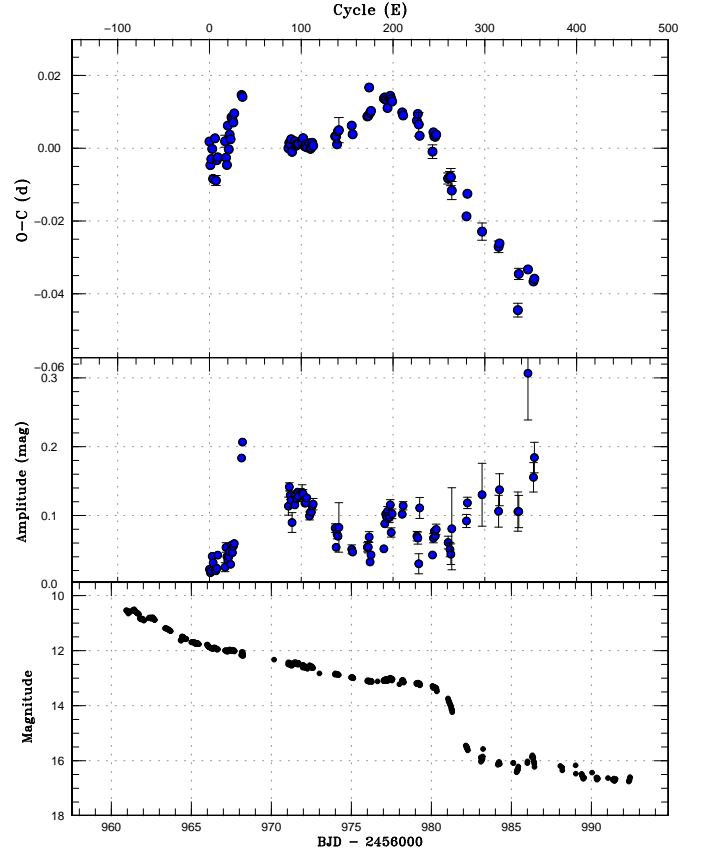


Fig. 122. $O - C$ diagram of superhumps in OT J030929 (2014). (Upper:) $O - C$ diagram. We used a period of 0.05736 d for calculating the $O - C$ residuals. (Middle:) Amplitudes of superhumps. (Lower:) Light curve. The data were binned to 0.011 d.

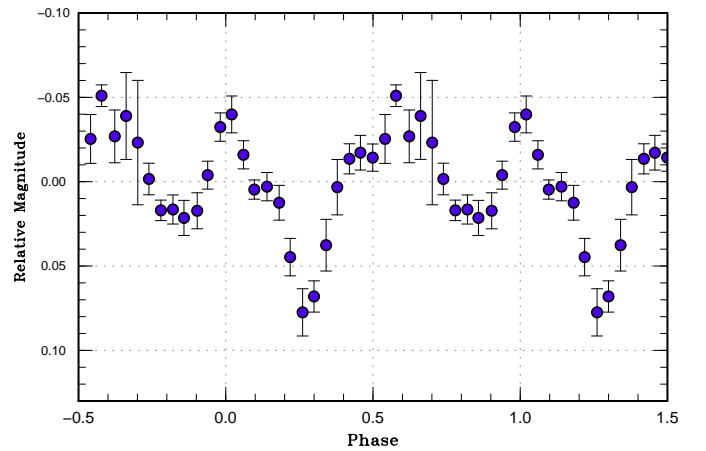


Fig. 123. Late-stage post-superoutburst superhumps in OT J030929 (2014). The data after BJD 2456987 were used. The phase corresponds to the times of maxima in table 93.

Table 92. Superhump maxima of OT J030929 (2014)

E	max*	error	$O - C^\dagger$	N^\ddagger
0	56966.1342	0.0009	0.0003	202
1	56966.1851	0.0009	-0.0062	291
2	56966.2441	0.0008	-0.0046	290
3	56966.3042	0.0005	-0.0018	209
4	56966.3534	0.0008	-0.0100	102
6	56966.4792	0.0009	0.0011	102
7	56966.5250	0.0014	-0.0105	105
8	56966.5879	0.0010	-0.0050	108
9	56966.6461	0.0008	-0.0042	82
17	56967.1094	0.0016	0.0001	89
18	56967.1622	0.0009	-0.0045	71
19	56967.2176	0.0011	-0.0065	85
20	56967.2857	0.0009	0.0043	177
21	56967.3366	0.0006	-0.0022	193
22	56967.3980	0.0007	0.0018	201
23	56967.4541	0.0007	0.0005	208
24	56967.5175	0.0004	0.0065	139
25	56967.5742	0.0006	0.0059	103
26	56967.6308	0.0006	0.0051	103
27	56967.6906	0.0006	0.0076	96
35	56968.1546	0.0001	0.0125	121
36	56968.2114	0.0001	0.0119	115
86	56971.0653	0.0009	-0.0030	40
87	56971.1242	0.0003	-0.0016	119
88	56971.1812	0.0003	-0.0019	110
89	56971.2398	0.0006	-0.0006	103
90	56971.2937	0.0011	-0.0041	94
93	56971.4687	0.0003	-0.0013	66
94	56971.5248	0.0002	-0.0025	62
95	56971.5826	0.0003	-0.0021	67
96	56971.6398	0.0003	-0.0023	66
97	56971.6974	0.0005	-0.0020	49

*BJD-2400000.

 † Against max = 2456966.1339 + 0.057377*E*. ‡ Number of points used to determine the maximum.**Table 92.** Superhump maxima of OT J030929 (2014) (continued)

E	max*	error	$O - C^\dagger$	N^\ddagger
101	56971.9272	0.0005	-0.0018	43
102	56971.9858	0.0005	-0.0006	31
104	56972.0983	0.0003	-0.0028	95
105	56972.1562	0.0002	-0.0023	109
106	56972.2127	0.0002	-0.0031	112
109	56972.3860	0.0012	-0.0021	51
110	56972.4418	0.0002	-0.0036	101
111	56972.4995	0.0002	-0.0033	112
112	56972.5582	0.0003	-0.0020	119
113	56972.6147	0.0006	-0.0028	36
137	56973.9939	0.0005	-0.0007	51
138	56974.0513	0.0008	-0.0007	149
139	56974.1065	0.0007	-0.0029	150
140	56974.1674	0.0006	0.0007	83
141	56974.2251	0.0035	0.0010	10
155	56975.0294	0.0009	0.0020	94
156	56975.0843	0.0008	-0.0004	96
172	56976.0070	0.0009	0.0042	94
173	56976.0645	0.0011	0.0043	95
174	56976.1297	0.0007	0.0121	75
175	56976.1801	0.0009	0.0051	106
176	56976.2379	0.0006	0.0056	120
190	56977.0444	0.0008	0.0088	167
191	56977.1021	0.0003	0.0091	298
192	56977.1588	0.0003	0.0084	348
193	56977.2161	0.0003	0.0084	271
194	56977.2712	0.0006	0.0061	113
196	56977.3885	0.0006	0.0087	57
197	56977.4467	0.0005	0.0094	60
198	56977.5032	0.0006	0.0086	60
199	56977.5598	0.0005	0.0079	46
210	56978.1878	0.0003	0.0047	122
211	56978.2443	0.0004	0.0038	120

*BJD-2400000.

 † Against max = 2456966.1339 + 0.057377*E*. ‡ Number of points used to determine the maximum.

vsnet-alert 11987). There was a known outburst in 1942 (Hudec 2010). The object has a bright X-ray counterpart (1RXS J213807.1+261958) and has a close visual companion (Yamaoka 2010) which dominates when the object is near quiescence. Although the 2010 superoutburst was well observed, the phase of early superhumps was not very well covered by observations (Kato et al. 2010). The 2010 superoutburst was also analyzed by Chochol et al. (2012) and Zemko, Kato (2013). Although the orbital period is not well determined yet, a possible period of (0.054523 d) was reported (Kato et al. 2010). Chochol et al. (2012) reported a period of 0.05435 d after the object started fading. Mitrofanova et al. (2014) reported a detailed spectroscopic study in quiescence and obtained Doppler tomograms. Mitrofanova et al. (2014) did not obtain the orbital period but assumed a period reported by Chochol et al. (2012).

3.91.2. 2014 Superoutburst

The 2014 superoutburst occurred only four years after the 2010 one, and the interval was surprisingly short for a WZ Sge-type dwarf nova. The outburst was detected visually by C. Chiselbrook at a magnitude of 9.7 on October 22. The same observed reported that the object was fainter than 13.8 on the night before (AAVSO observations). Approximately 1.5 d after this detection, initial CCD observations started. The object already showed ordinary superhumps (vsnet-alert 17891, 17893).

The times of superhump maxima during the superoutburst plateau are listed in table 95. As in the 2010 superoutburst, stages A-B-C were clearly present. The present observation recorded stage A superhumps much better than in the 2010 one. A PDM analysis before BJD 2456954.7 yielded a period of 0.0568(3) d, which is adopted in table 2. This period corresponds to

Table 92. Superhump maxima of OT J030929 (2014) (continued)

E	max*	error	$O - C^\dagger$	N^\ddagger
226	56979.1033	0.0007	0.0021	103
227	56979.1625	0.0010	0.0039	142
228	56979.2170	0.0032	0.0010	68
229	56979.2712	0.0010	-0.0021	123
243	56980.0699	0.0019	-0.0067	67
244	56980.1325	0.0007	-0.0014	150
245	56980.1888	0.0003	-0.0026	244
246	56980.2460	0.0004	-0.0027	212
247	56980.3040	0.0007	-0.0021	101
260	56981.0376	0.0015	-0.0144	82
262	56981.1530	0.0013	-0.0138	106
263	56981.2101	0.0024	-0.0140	69
264	56981.2637	0.0025	-0.0178	30

*BJD-2400000.

 † Against max = 2456966.1339 + 0.057377 E . ‡ Number of points used to determine the maximum.**Table 93.** Superhump maxima of OT J030929 (2014) (post-superoutburst)

E	max*	error	$O - C^\dagger$	N^\ddagger
0	56982.1744	0.0008	-0.0020	63
1	56982.2380	0.0005	0.0045	63
17	56983.1453	0.0024	-0.0011	55
35	56984.1737	0.0016	0.0002	58
36	56984.2319	0.0012	0.0014	63
56	56985.3608	0.0019	-0.0110	59
57	56985.4281	0.0015	-0.0007	45
67	56986.0030	0.0006	0.0035	10
73	56986.3438	0.0010	0.0020	59
74	56986.4019	0.0009	0.0031	54

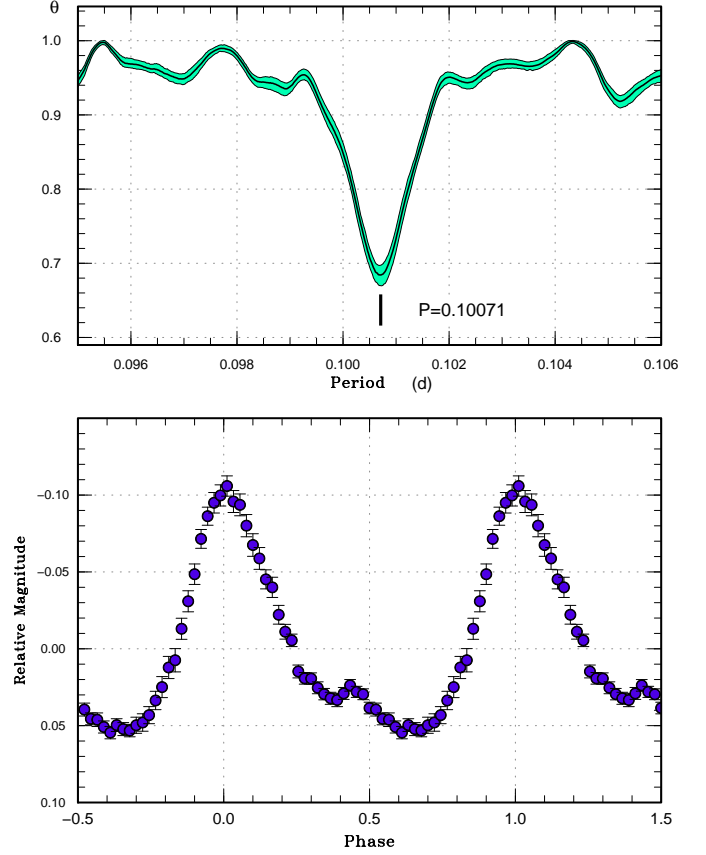
*BJD-2400000.

 † Against max = 2456982.1764 + 0.057060 E . ‡ Number of points used to determine the maximum.

$\epsilon^* = 0.041(4)$ and $q = 0.12(2)$ assuming the orbital period of 0.054523 d. The values are 0.044(4) and 0.13(2), respectively, if we adopt the period of 0.05435 d.

3.91.3. Object classification

The 2014 observation indicated that the duration of early superhumps was less than 1 d, indicating that the 2014 superoutburst was of an ordinary SU UMa-type dwarf nova rather than a WZ Sge-type dwarf nova. Since the peak brightness of the 2014 superoutburst was fainter than the 2010 one at least by 1.0 mag, it may be that the 2014 superoutburst was much less powerful as in the 2010 one, and that the 2:1 resonance was not reached during this superoutburst. The 2010 superoutburst, however, was not very well observed before the appearance of ordinary superhumps, and the existence of early superhumps was not very certain. It may be that the 2010 superoutburst did not show early superhumps at all, as was likely in the 2014 one. If it is the case, the object should be

**Fig. 124.** Superhumps in OT J064833 during the superoutburst plateau (2014). (Upper): PDM analysis. (Lower): Phase-averaged profile

better classified as an SU UMa-type dwarf nova rather than a WZ Sge-type one. The large q value (although this value has a large uncertainty), the short outburst recurrence time, the large positive P_{dot} of stage B superhumps, the short evolutionary time of stage A superhumps and the presence of stage C superhumps are better reconciled with this interpretation. We probably need to wait another bright outburst as in 2010 to test the presence of early superhumps.

3.91.4. Comparison of 2010 and 2014 superoutbursts

A comparison of $O - C$ diagrams (figure 126) indicates that the duration of stage B was different between these superoutbursts: stage B was longer in a brighter superoutburst in 2010. The behavior after transition to stage C was also different. Such features was not observed in other SU UMa-type dwarf novae and this result would provide a clue in understanding the origin of superhumps in different stages.

The duration of the superoutburst was different (figure 127). The magnitudes during the linearly fading part, which corresponds to stage B superhumps, were almost similar between these superoutbursts despite the difference of the peak brightness.

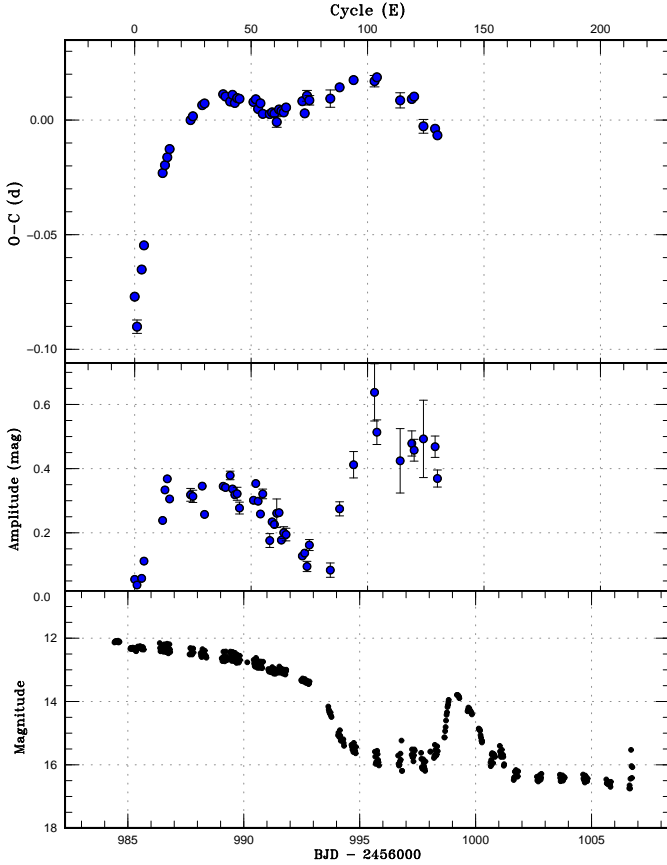


Fig. 125. $O - C$ diagram of superhumps in OT J064833 (2014). (Upper:) $O - C$ diagram. We used a period of 0.01005 d for calculating the $O - C$ residuals. (Middle:) Amplitudes of superhumps. (Lower:) Light curve. The data were binned to 0.020 d.

3.92. OT J230523.1–022546

This object (=PNV J23052314–0225455, hereafter OT J230523) was discovered as a transient at an unfiltered CCD magnitude of 12.3 on 2014 July 19 by M. Mukai.¹⁶ Since there was a 19.7-mag (*g*) SDSS blue counterpart (see also vsnet-alert 17512), the object was immediately considered as a dwarf nova. G. Masi also obtained low-resolution spectrum which did not indicate strong an H α emission line. Subsequent observations detected early superhumps (vsnet-alert 17513, 17528, 17571; figure 128), indicating that the object is a WZ Sge-type dwarf nova. On July 25, the object started to show growing ordinary superhumps (vsnet-alert 17550). The period of fully grown superhumps turned out to be very short (vsnet-alert 17566). The mean profile of stage B superhumps is shown in figure 129.

The times of superhump maxima are listed in table 96. There was clear stage A for $E \leq 17$. Although superhumps after $E = 213$ were likely stage C superhumps, the epoch when stage B-C transition occurred was not determined

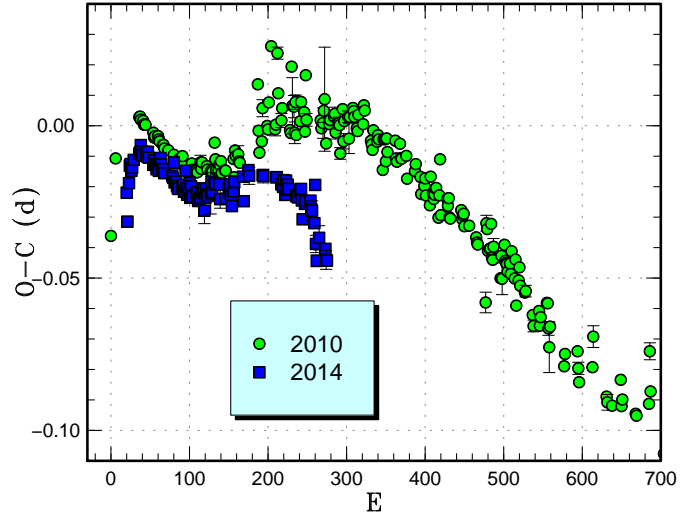


Fig. 126. Comparison of $O - C$ diagrams of OT J213806 between different superoutbursts. A period of 0.05513 d was used to draw this figure. Approximate cycle counts (E) after the appearance of superhumps were used. The 2014 superoutburst was shifted by 20 cycles to best match the 2010 one. The 2014 superoutburst was artificially shifted by 0.01 d to avoid excessive overlaps with the 2010 diagram.

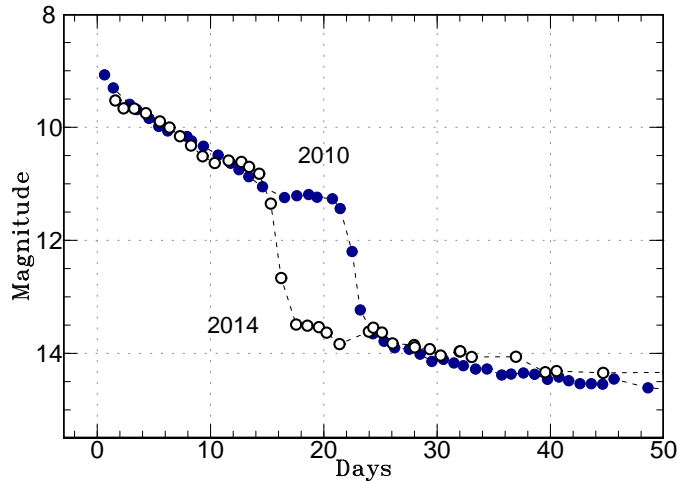


Fig. 127. Comparison of superoutbursts of OT J213806. The data were binned to 1 d and shifted in magnitude. The dashed lines are added to aid recognizing the variation. The duration of the 2014 superoutburst was shorter than the 2010 one although the magnitudes were almost similar during the linearly fading part, which corresponds to the phase of stage B superhumps.

¹⁶ <<http://www.cbat.eps.harvard.edu/unconf/followups/J23052314-0225455.html>>.

Table 94. Superhump maxima of OT J064833 (2014)

E	max*	error	$O - C^\dagger$	N^\ddagger
0	56985.2170	0.0011	-0.0538	419
1	56985.3043	0.0029	-0.0672	253
3	56985.5302	0.0007	-0.0430	353
4	56985.6411	0.0004	-0.0329	308
12	56986.4763	0.0006	-0.0042	143
13	56986.5802	0.0002	-0.0012	220
14	56986.6841	0.0002	0.0019	279
15	56986.7881	0.0006	0.0051	46
24	56987.7048	0.0008	0.0145	27
25	56987.8069	0.0007	0.0158	31
29	56988.2136	0.0002	0.0192	415
30	56988.3147	0.0004	0.0195	285
38	56989.1224	0.0002	0.0206	429
39	56989.2218	0.0002	0.0193	234
41	56989.4205	0.0006	0.0163	62
42	56989.5239	0.0002	0.0189	87
43	56989.6208	0.0004	0.0150	83
44	56989.7234	0.0008	0.0168	27
45	56989.8235	0.0009	0.0161	26
51	56990.4248	0.0006	0.0125	62
52	56990.5265	0.0003	0.0133	208
53	56990.6227	0.0003	0.0087	202
54	56990.7256	0.0005	0.0108	136
55	56990.8215	0.0007	0.0058	27
58	56991.1227	0.0009	0.0047	67
59	56991.2239	0.0004	0.0050	324
60	56991.3238	0.0003	0.0042	349
61	56991.4206	0.0023	0.0001	29
62	56991.5265	0.0005	0.0052	113
63	56991.6263	0.0007	0.0042	112
64	56991.7261	0.0011	0.0032	27
65	56991.8287	0.0016	0.0050	23

*BJD-2400000.

 † Against max = 2456985.2707 + 0.100816 E . ‡ Number of points used to determine the maximum.

due to the gap in the observation (see figure 130).

The period of stage A superhumps [0.05663(4) d] corresponds to ϵ^* of 0.037. This value gives $q=0.102(2)$, which is relatively large for a WZ Sge-type dwarf nova. The relatively large P_{dot} of stage B superhumps [$+8.2(1.3) \times 10^{-5}$], the presence of stage C and relatively short duration of stage A indicate that OT J230523 is not an extreme WZ Sge-type and but an object close to ordinary SU UMa-type dwarf novae. Thus identification is consistent with a relatively large q .

3.93. PNV J17292916+0054043

This object (hereafter PNV J172929) was discovered as a possible nova on May 22 at an unfiltered CCD magnitude of 12.1 by H. Nishimura.¹⁷ S. Kiyota reported that the blue color suggested a dwarf nova-type outburst.

¹⁷ <<http://www.cbat.eps.harvard.edu/unconf/followups/J17292916+0054043.html>>.

Table 94. Superhump maxima of OT J064833 (2014) (continued)

E	max*	error	$O - C^\dagger$	N^\ddagger
72	56992.5346	0.0006	0.0051	281
73	56992.6298	0.0008	-0.0005	131
74	56992.7379	0.0023	0.0068	28
75	56992.8364	0.0021	0.0044	18
84	56993.7412	0.0038	0.0019	27
88	56994.1479	0.0013	0.0053	143
94	56994.7537	0.0013	0.0063	40
103	56995.6573	0.0025	0.0025	18
104	56995.7595	0.0010	0.0039	41
114	56996.7539	0.0033	-0.0098	28
119	56997.2567	0.0008	-0.0111	107
120	56997.3582	0.0012	-0.0104	97
124	56997.7471	0.0030	-0.0248	37
129	56998.2483	0.0009	-0.0277	98
130	56998.3458	0.0009	-0.0310	79

*BJD-2400000.

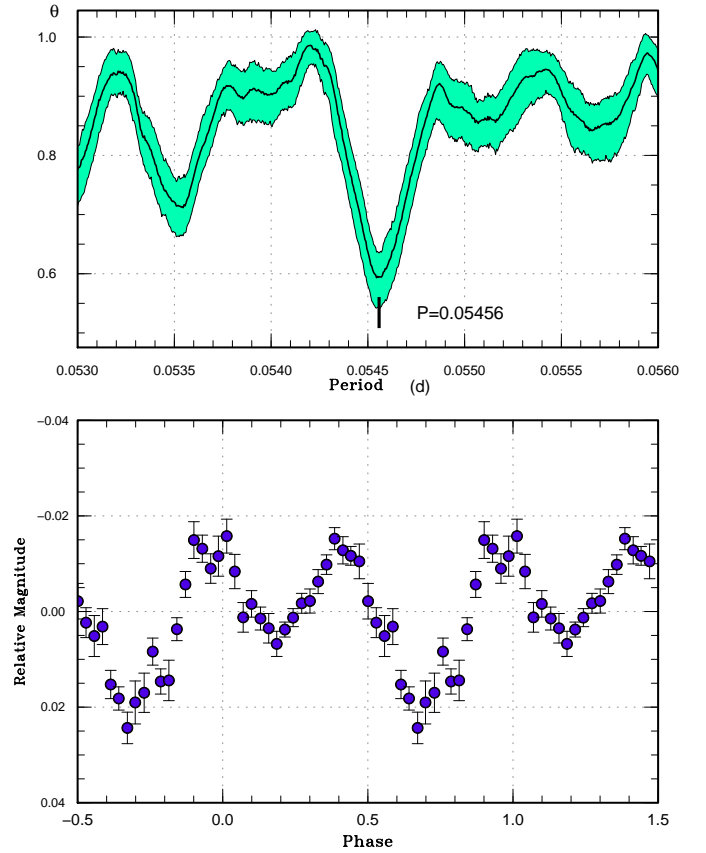
 † Against max = 2456985.2707 + 0.100816 E . ‡ Number of points used to determine the maximum.**Fig. 128.** Early superhumps in OT J230523 (2014). (Upper): PDM analysis. (Lower): Phase-averaged profile.

Table 95. Superhump maxima of OT J213806 (2014)

E	max*	error	$O - C^\dagger$	N^\ddagger
0	56954.0563	0.0005	-0.0076	160
1	56954.1018	0.0003	-0.0171	305
3	56954.2249	0.0016	-0.0042	53
4	56954.2854	0.0004	0.0012	150
5	56954.3403	0.0008	0.0011	150
6	56954.3942	0.0003	-0.0002	59
7	56954.4505	0.0005	0.0010	60
9	56954.5633	0.0006	0.0037	22
16	56954.9512	0.0002	0.0059	102
17	56955.0067	0.0002	0.0064	160
18	56955.0642	0.0001	0.0088	391
19	56955.1173	0.0001	0.0069	537
20	56955.1711	0.0001	0.0056	430
24	56955.3927	0.0009	0.0068	86
25	56955.4466	0.0002	0.0055	157
26	56955.5015	0.0003	0.0054	142
27	56955.5582	0.0003	0.0070	39
28	56955.6114	0.0005	0.0051	28
34	56955.9398	0.0005	0.0030	115
35	56955.9964	0.0004	0.0045	171
36	56956.0501	0.0002	0.0031	257
37	56956.1054	0.0001	0.0033	345
38	56956.1589	0.0004	0.0018	226
39	56956.2150	0.0007	0.0027	211
40	56956.2706	0.0005	0.0032	376
41	56956.3237	0.0006	0.0013	357
42	56956.3822	0.0008	0.0047	284
43	56956.4382	0.0007	0.0057	101
44	56956.4913	0.0008	0.0036	10
45	56956.5447	0.0003	0.0019	127
46	56956.5995	0.0003	0.0016	122
47	56956.6551	0.0003	0.0022	124

*BJD-2400000.

 † Against max = 2456954.0638 + 0.055087*E*. ‡ Number of points used to determine the maximum.**Table 95.** Superhump maxima of OT J213806 (2014) (continued)

E	max*	error	$O - C^\dagger$	N^\ddagger
48	56956.7089	0.0005	0.0009	83
58	56957.2593	0.0004	0.0004	44
59	56957.3137	0.0005	-0.0002	52
60	56957.3738	0.0021	0.0047	114
61	56957.4226	0.0004	-0.0016	57
62	56957.4778	0.0003	-0.0014	66
63	56957.5331	0.0003	-0.0012	110
64	56957.5868	0.0003	-0.0027	132
65	56957.6411	0.0003	-0.0034	74
66	56957.6960	0.0003	-0.0035	65
71	56957.9724	0.0003	-0.0026	59
72	56958.0281	0.0003	-0.0020	60
73	56958.0811	0.0003	-0.0041	56
74	56958.1363	0.0007	-0.0039	37
75	56958.1982	0.0009	0.0028	65
76	56958.2477	0.0003	-0.0028	247
77	56958.3006	0.0004	-0.0050	379
78	56958.3559	0.0006	-0.0047	202
79	56958.4126	0.0006	-0.0031	180
80	56958.4698	0.0004	-0.0010	26
81	56958.5201	0.0005	-0.0058	98
82	56958.5790	0.0004	-0.0020	41
83	56958.6311	0.0005	-0.0050	65
84	56958.6858	0.0004	-0.0054	65
89	56958.9627	0.0003	-0.0039	57
90	56959.0181	0.0003	-0.0035	142
91	56959.0703	0.0003	-0.0064	337
92	56959.1256	0.0002	-0.0062	351
93	56959.1812	0.0024	-0.0057	209
94	56959.2368	0.0004	-0.0052	212
95	56959.2950	0.0004	-0.0021	111
96	56959.3489	0.0005	-0.0033	56

*BJD-2400000.

 † Against max = 2456954.0638 + 0.055087*E*. ‡ Number of points used to determine the maximum.

There was also a faint ($g=21.5$) SDSS counterpart (vsnet-alert 17325). Spectroscopic observation by K. Ayani indicated the dwarf nova-type spectrum showing narrow emission lines of H α , H β and HeII 4686 on a blue continuum (see above URL). The amplitude and the presence of HeII emission line suggested the WZ Sge-type classification (vsnet-alert 17327).

Subsequent observations detected possible early superhumps (vsnet-alert 17337; figure 131). The object developed ordinary superhumps 12 d after the discovery (vsnet-alert 17365; figure 132). The times of maxima of ordinary superhumps are listed in table 97. After a relatively long stage A ($E \leq 28$), stage B appeared (figure 133). There was no strong hint of transition to stage C superhumps during the superoutburst plateau.

The signal of early superhump was weak and the data were not sufficient to uniquely determine the period. Although a signal around 0.0586 d was slightly stronger,

we have selected a period of 0.05973(3) d because this value gave a more reasonable value of ϵ^* . The period of stage A superhumps corresponds to $\epsilon^*=0.0273(5)$ and $q=0.073(2)$.

The orbital period is apparently longer than the period minimum and the system parameters resemble those of period bouncers although q is not so extreme. This object appears to be similar to recently identified objects with superhump periods of 0.058–0.061 d having properties intermediate between ordinary hydrogen-rich dwarf novae and period bouncers (C. Nakata et al. in preparation). There was no indication of rebrightenings in PNV J172929, which makes a difference from the objects mentioned in C. Nakata et al. in preparation.

3.94. PTF1 J071912.13+485834.0

This object (hereafter PTF1 J071912) is an AM CVn-type object detected in outburst by Palomar Transient

Table 95. Superhump maxima of OT J213806 (2014) (continued)

E	max*	error	$O - C^\dagger$	N^\ddagger
97	56959.4047	0.0008	-0.0026	63
98	56959.4588	0.0014	-0.0036	36
99	56959.5082	0.0042	-0.0093	43
100	56959.5675	0.0006	-0.0050	100
101	56959.6258	0.0004	-0.0018	118
102	56959.6788	0.0003	-0.0039	148
103	56959.7335	0.0004	-0.0043	82
107	56959.9549	0.0068	-0.0032	13
108	56960.0138	0.0006	0.0006	106
109	56960.0656	0.0006	-0.0027	121
112	56960.2335	0.0007	-0.0000	66
113	56960.2890	0.0010	0.0003	161
118	56960.5642	0.0013	0.0001	127
119	56960.6147	0.0030	-0.0045	40
126	56961.0007	0.0012	-0.0041	59
130	56961.2246	0.0020	-0.0006	203
131	56961.2783	0.0011	-0.0020	442
132	56961.3362	0.0008	0.0009	249
133	56961.3872	0.0017	-0.0032	222
134	56961.4392	0.0012	-0.0063	57
136	56961.5544	0.0027	-0.0013	38
137	56961.6126	0.0020	0.0019	11
148	56962.2208	0.0006	0.0040	246
149	56962.2678	0.0010	-0.0040	175
155	56962.6089	0.0013	0.0065	104
156	56962.6621	0.0028	0.0046	25
173	56963.5994	0.0008	0.0055	128
174	56963.6542	0.0022	0.0052	87
190	56964.5360	0.0018	0.0056	22
191	56964.5912	0.0012	0.0057	24
197	56964.9195	0.0004	0.0035	128
199	56965.0290	0.0007	0.0029	173
200	56965.0864	0.0006	0.0051	143

*BJD-2400000.

 † Against max = 2456954.0638 + 0.055087*E*. ‡ Number of points used to determine the maximum.

Factory (PTF) (Levitan et al. 2011). Levitan et al. (2011) identified the orbital period of 26.77(2) min [0.01859(1) d] and reported superoutbursts recurring with intervals longer than 65 d together with normal outbursts. Levitan et al. (2011) recorded superhumps with amplitudes of ~ 0.1 mag. Due to the shortness of the observation, the only approximated period of 26–27 min was obtained.

The 2014 outburst was detected by the ASAS-SN team on August 31 at $V=15.57$ (vsnet-alert 17685). Subsequent observations detected superhumps (vsnet-alert 17688). This single-night observation determined the period of 0.0186(3) d, better than in Levitan et al. (2011). We obtained time-resolved observations three nights later. Although there was a long gap, we have selected a period of 0.01881(1) d among alias periods based on the knowledge that superhump periods of AM CVn-type objects are 0.67–2.18% longer than the orbital periods

Table 95. Superhump maxima of OT J213806 (2014) (continued)

E	max*	error	$O - C^\dagger$	N^\ddagger
202	56965.1918	0.0016	0.0003	155
203	56965.2516	0.0005	0.0051	247
204	56965.3037	0.0006	0.0021	245
205	56965.3605	0.0007	0.0038	247
206	56965.4143	0.0011	0.0025	242
216	56965.9631	0.0003	0.0005	317
217	56966.0187	0.0003	0.0009	367
218	56966.0730	0.0004	0.0002	316
221	56966.2406	0.0017	0.0025	173
222	56966.2965	0.0014	0.0033	277
223	56966.3476	0.0008	-0.0006	279
224	56966.3966	0.0008	-0.0067	140
227	56966.5671	0.0008	-0.0015	125
228	56966.6231	0.0008	-0.0006	99
234	56966.9540	0.0009	-0.0002	61
235	56967.0064	0.0006	-0.0029	61
236	56967.0610	0.0032	-0.0034	21
239	56967.2223	0.0004	-0.0073	102
240	56967.4001	0.0019	0.1154	121
241	56967.3257	0.0029	-0.0141	176
242	56967.3753	0.0019	-0.0196	105
245	56967.5483	0.0040	-0.0119	24
253	56967.9857	0.0019	-0.0152	36
254	56968.0372	0.0031	-0.0188	41
255	56968.0921	0.0018	-0.0189	33

*BJD-2400000.

 † Against max = 2456954.0638 + 0.055087*E*. ‡ Number of points used to determine the maximum.

(Pearson 2007)¹⁸, corresponding to 0.01871–0.01900 d in the present case. figure 134). Table 98 is based on this identification.

3.95. *SDSS J033449.86–071047.8*

This object (hereafter SDSS J033449) was selected as a CV during the course of the SDSS (Szkody et al. 2007). The 2009 superoutburst was reported in Kato et al. (2009). The 2014 superoutburst was detected by the ASAS-SN team (vsnet-alert 17711). Single-night observation was available and the following superhump maxima were obtained: BJD 2456909.1948(33) ($N=69$), 2456909.2738(4) ($N=143$) and 2456909.3576(11) ($N=57$). Two other outbursts (likely normal outbursts) were recorded on 2013 February 16 (15.5 mag, unfiltered CCD, vsnet-outburst 15132) and 2014 March 26 (16.6 mag, unfiltered CCD, AAVSO data).

3.96. *SDSS J081408.42+090759.1*

This object (hereafter SDSS J081408) was selected as a CV by its variability by Wils et al. (2010). Kato et al. (2012b) estimated the orbital period to be 0.11–0.14 d

¹⁸ The superhump period in Pearson (2007) was an old value. A more updated period 0.018728 d (Kato et al. 2004b) corresponds to 1.3%.

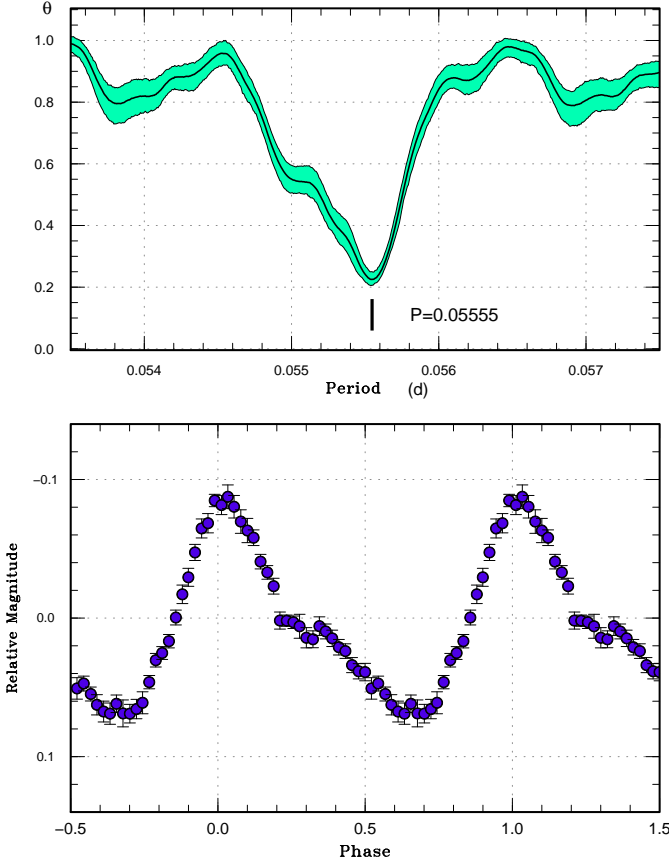


Fig. 129. Ordinary superhumps in OT J230523 (2014) for the interval BJD 2456865–2456871. (Upper): PDM analysis. (Lower): Phase-averaged profile.

from the SDSS colors of the quiescent counterpart. CRTS detected an outburst on 2014 March 8. Subsequent observations detected superhumps (vsnet-alert 16994, 17000; figure 135). The resultant superhump period qualified this object as an SU UMa-type dwarf nova in the period gap. The times of superhump maxima are listed in table 99. There was a large decrease in the superhump period, which is often seen in long- P_{orb} systems [cf. section 4.10 in Kato et al. (2009)].

3.97. SDSS J090221.35+381941.9

This object (hereafter SDSS J090221) is an AM CVn-type object identified by Rau et al. (2010). The object underwent a superoutburst preceded by a precursor in 2014 March. This superoutburst made SDSS J090221 the longest P_{orb} object which ever showed outbursts among AM CVn-type objects. The analysis of the superhumps, evolution of the outburst, estimation of q from stage A superhumps and their implications were discussed in Kato et al. (2014c). Here, we present materials used in Kato et al. (2014c). Since the evolution of the outburst was so complex, we show here the times of superhump maxima separately in different stages of the outburst (tables 100, 101, 102, 103). The E values given in table 2 refer to those

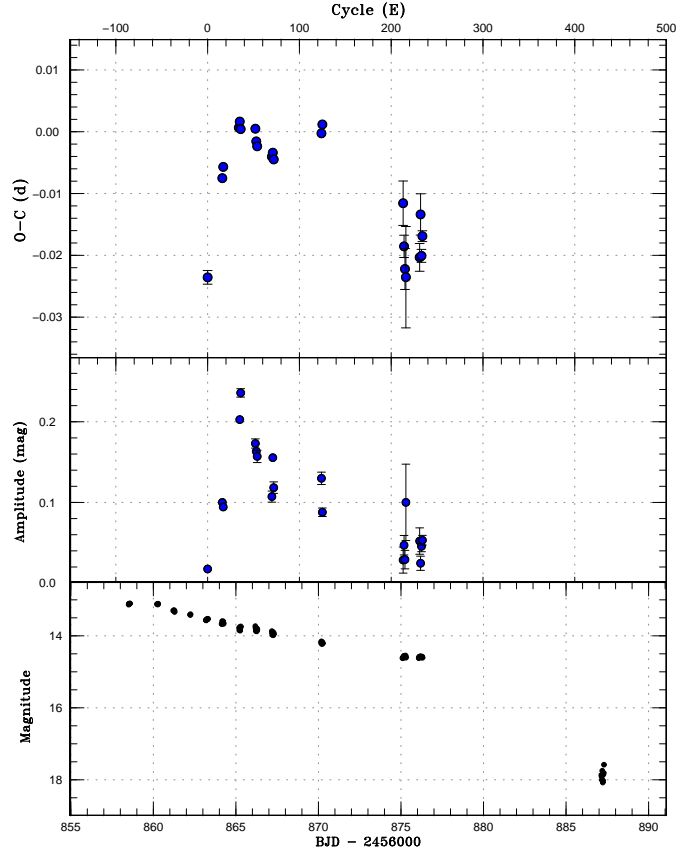


Fig. 130. $O - C$ diagram of superhumps in OT J230523 (2014). (Upper): $O - C$ diagram. We used a period of 0.05560 d for calculating the $O - C$ residuals. (Middle:) Amplitudes of superhumps. (Lower:) Light curve. The data were binned to 0.011 d.

in table 102.

The enlarged $O - C$ diagram of figure 1 in Kato et al. (2014c) illustrates the stage B–C transition as well as a phase hump associated with the “dip” phenomenon.

Mean superhump profiles of stages B and C are shown in figures 137 and 138, respectively. The mean profile of stage A superhumps was already shown in Kato et al. (2014c). The small amplitudes of superhumps are consistent with the small q estimated from stage A superhumps Kato et al. (2014c). Superhumps persisted after the rapid fading, and the mean profile is shown in figure 139. After the rebrightening, the superhump signal became weaker (full amplitude 0.05 mag) and the period could not be uniquely determined due to the small number of observations. The variations, however, could be well expressed by a period close to 0.0336 d.

3.98. SDSS J120231.01+450349.1

This object (hereafter SDSS J120231) was selected as a CV during the course of SDSS (Szkody et al. 2006). The SDSS spectrum was indicative of a low mass-transfer rate with absorption lines of a white dwarf. The spectrum itself resembled that of a WZ Sge-type dwarf nova.

Table 96. Superhump maxima of OT J230523 (2014)

E	max*	error	$O - C^\dagger$	N^\ddagger
0	56863.2644	0.0011	-0.0226	117
16	56864.1701	0.0002	-0.0054	118
17	56864.2275	0.0002	-0.0036	119
34	56865.1791	0.0007	0.0039	28
35	56865.2356	0.0002	0.0050	119
36	56865.2900	0.0001	0.0039	97
52	56866.1797	0.0003	0.0050	39
53	56866.2332	0.0002	0.0030	61
54	56866.2880	0.0003	0.0023	57
70	56867.1760	0.0006	0.0017	40
71	56867.2322	0.0002	0.0024	61
72	56867.2867	0.0004	0.0014	58
124	56870.1821	0.0005	0.0092	29
125	56870.2392	0.0004	0.0107	41
213	56875.1192	0.0036	0.0039	94
214	56875.1679	0.0018	-0.0030	95
215	56875.2198	0.0033	-0.0066	79
216	56875.2741	0.0082	-0.0078	44
231	56876.1113	0.0022	-0.0036	88
232	56876.1738	0.0033	0.0034	130
233	56876.2227	0.0010	-0.0032	185
234	56876.2815	0.0009	0.0000	199

*BJD-2400000.

 † Against max = 2456863.2870 + 0.055532 E . ‡ Number of points used to determine the maximum.

Quimby, Mondol (2006) detected an outburst on 2006 March 21.15 UT at 13.4 mag with ROTSE-IIIb telescope. This outburst faded to 14.8 mag over the ten days. The quiescent SDSS colors also suggested a short (0.056 d) orbital period (Kato et al. 2012b).

The 2014 outburst was detected by ASAS-SN on May 27 at $V=13.88$. The object was not detected in outburst on May 25 (vsnet-alert 17341).

Subsequent observations recorded well-developed superhumps (vsnet-alert 17348). Considering that the outburst detection was made sufficiently early, the lack of a stage with early superhumps indicates that this object is an ordinary SU UMa-type dwarf nova rather than a WZ Sge-type object as suggested from spectroscopy.

The times of superhump maxima are listed in table 104. Although there was a gap in the observation, the entire observation can be well interpreted by stage B with a large positive P_{dot} and a transition to stage C. The P_{dot} of $+9.0(1.3) \times 10^{-5}$ in stage B is typical for this P_{SH} . The profiles of superhumps are given separately for stages A and B (figures 140, 141) since the large change in the period, which is supposed to be present in the later part of stage B but was not covered by observation, caused a split in the superhump signal if the combined data are used. It would be worth mentioning that the superhump periods of early stage B and stage C are almost the same (as described in Kato et al. 2009).

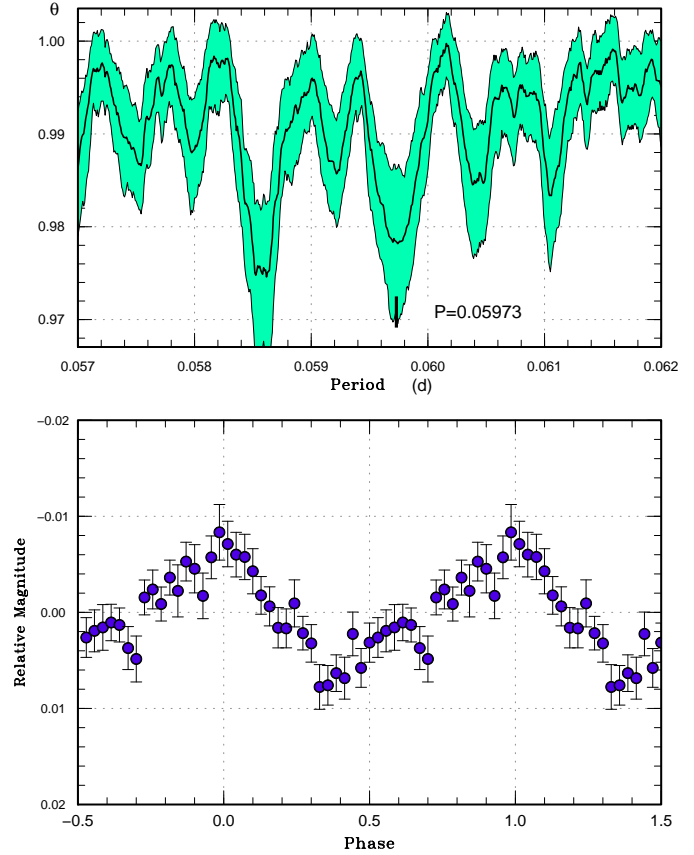


Fig. 131. Early superhumps in PNV J172929 (2014). (Upper): PDM analysis. The selection of the period was based on comparison with the period of ordinary superhumps. (Lower): Phase-averaged profile.

3.99. *SDSS J140037.99+572341.3*

This object (hereafter SDSS J140037) was selected from SDSS and spectroscopically confirmed as a CV by Carter et al. (2013a). No previous outburst was known. The 2015 outburst was detected by the ASAS-SN team on February 2 (vsnet-alert 18257). Superhumps were immediately detected (vsnet-alert 18263, 18265; figure 142). The times of superhump maxima are listed in table 105. There remains ambiguity in cycle count between $E = 8$ and $E = 123$. Among the possible aliases (see figure 142), we have selected the most likely period based on the period determined by the PDM method from the observations on the first night was 0.0639(2) d. This selection, however, may not be true if there were significant variations in the period during the 8 d gap. The object already faded from the superoutburst on February 17, 15 d after the initial detection.

3.100. *SDSS J172325.99+330414.1*

This object (hereafter SDSS J172325) was reported in outburst by the ASAS-SN team (=ASASSN-14gz, Davis et al. 2014) at $V=14.2$ on 2014 September 9. Since the spectrum in quiescence was already obtained in the SDSS

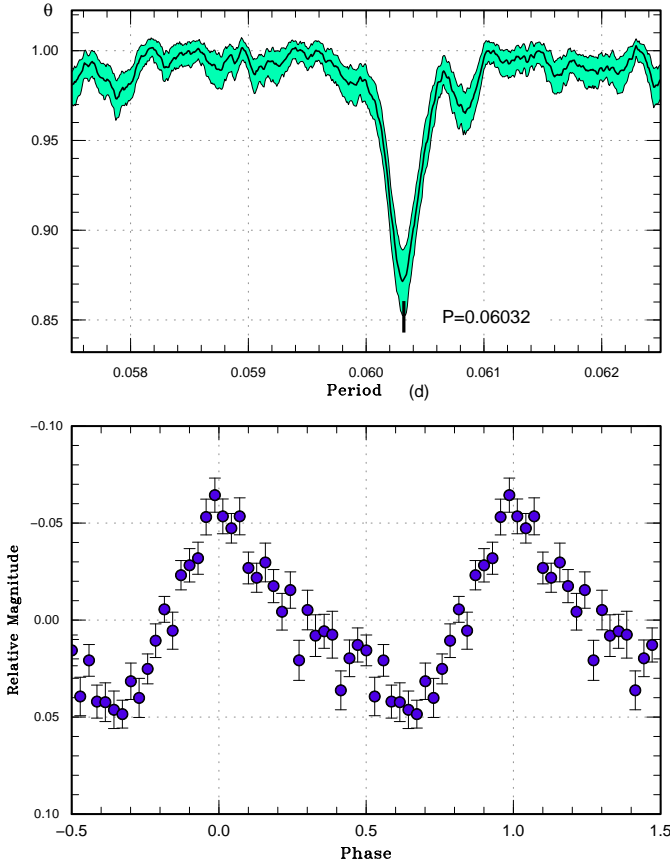


Fig. 132. Ordinary superhumps in PNV J172929 (2014). (Upper): PDM analysis. (Lower): Phase-averaged profile.

archive and was clearly recognized as a CV, we call this object by the SDSS name. The large outburst amplitude (7.7 mag) was suggestive of a WZ Sge-type dwarf nova (Davis et al. 2014). On September 16, this object started to show ordinary superhumps (vsnet-alert 17737, 17755, 17800; figure 143). The times of superhump maxima are listed in table 106. Although $E \leq 1$ most likely corresponded to stage A superhumps as judged from the growing amplitude, the period of stage A superhumps was not determined due to the lack of the data.

After fading to $V=16.6$ on September 26, the object underwent a rebrightening to $V=15.8$ on October 4 (vsnet-alert 17824) and remained at this level at least until October 24 (figure 144).

There was no convincing signal of early superhumps before the appearance of ordinary superhumps.

3.101. SDSS J173047.59+554518.5

This object (hereafter SDSS J173047) was selected as an AM CVn-type object from the SDSS photometric catalog by Carter et al. (2014). Carter et al. (2014) obtained time-resolved spectroscopy and found an orbital period of 35.2(2) min, possibly allowing one-day aliases. Although the emission lines showed double peaks, Carter et al. (2014) suggested a low orbital inclination since the

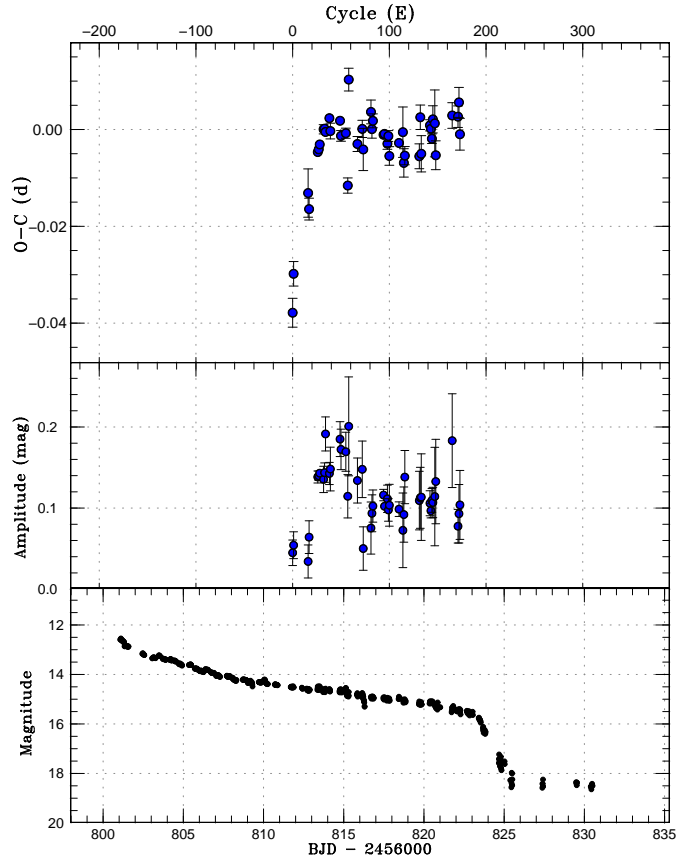


Fig. 133. $O - C$ diagram of superhumps in PNV J172929 (2014). (Upper): $O - C$ diagram. A period of 0.06028 d was used to draw this figure. (Lower): Light curve. The observations were binned to 0.012 d.

lines were narrow. A single outburst was detected in the past CRTS data.

The 2014 outburst was detected by CRTS on April 2 at 14.5 mag (cvnet-outburst 5889). On the first night of the observation, there were no significant modulations (vsnet-alert 17143). On April 6, the object was found to show prominent superhumps (vsnet-alert 17160; figure 145). These superhumps developed somewhere between April 4 and 6, and we probably missed stage A superhumps. The object started fading rapidly on April 10 (lower panel of figure 146). The object was again observed bright on April 15, accompanied by rapid fading.

The times of superhump are listed in table 107. During the rebrightening, superhumps were still strongly seen. The epochs $E \geq 367$ in table 107 represent these superhumps during the rebrightening, although the continuity of the phase or the cycle count between $E = 166$ and $E = 367$ is unclear. The mean superhump period of 0.024597(6) d confirmed the alias selection in Carter et al. (2014). The fractional superhump excess is 0.006(6), where the source of the error is mostly due to the uncertainty of the orbital period. Future refinement of the orbital period is desired to estimate q from the fractional superhump excess.

Table 97. Superhump maxima of PNV J172929 (2014)

E	max*	error	$O - C^\dagger$	N^\ddagger
0	56811.7769	0.0030	-0.0283	14
1	56811.8452	0.0025	-0.0203	14
16	56812.7661	0.0050	-0.0048	15
17	56812.8231	0.0023	-0.0082	16
26	56813.3774	0.0004	0.0029	75
27	56813.4382	0.0003	0.0034	83
28	56813.4995	0.0003	0.0044	68
32	56813.7437	0.0010	0.0072	16
33	56813.8042	0.0006	0.0073	25
34	56813.8638	0.0009	0.0065	22
38	56814.1077	0.0006	0.0090	43
39	56814.1653	0.0016	0.0063	16
49	56814.7703	0.0009	0.0077	17
50	56814.8274	0.0011	0.0045	30
55	56815.1294	0.0010	0.0047	77
57	56815.2391	0.0016	-0.0063	85
58	56815.3213	0.0024	0.0155	37
67	56815.8505	0.0015	0.0016	28
72	56816.1550	0.0018	0.0043	101
73	56816.2111	0.0044	-0.0000	115
81	56816.7010	0.0025	0.0071	13
82	56816.7578	0.0019	0.0035	16
83	56816.8198	0.0014	0.0051	29
94	56817.4800	0.0004	0.0015	47
95	56817.5404	0.0003	0.0016	47
98	56817.7192	0.0011	-0.0007	18
99	56817.7811	0.0011	0.0008	18
100	56817.8373	0.0019	-0.0034	17
110	56818.4428	0.0007	-0.0014	33
114	56818.6861	0.0052	0.0005	11
115	56818.7400	0.0029	-0.0059	19
116	56818.8018	0.0019	-0.0045	17

*BJD-2400000.

 † Against max = 2456811.8052 + 0.060354*E*. ‡ Number of points used to determine the maximum.

The outburst behavior of SDSS J173047 is characterized by the short duration of the plateau phase, consisting only 5 ± 1 d after the appearance of superhumps. This behavior is similar to another AM CVn-type object, SDSS J012940.05+384210.4 (Kato et al. 2010; Shears et al. 2012).

3.102. TCP J16054809+2405338

This object (hereafter TCP J160548) is a transient discovered by H. Nishimura at an unfiltered CCD magnitude of 12.6 on 2014 December 20. The object was not detected on December 2 and 3.¹⁹ The object was readily identified with a blue SDSS object and a GALEX source (vsnet-alert 18085). The object was also detected in outburst by ASAS-SN survey (vsnet-alert 18107, 18109). The object was also selected as a candidate for an AM CVn-type

¹⁹ <<http://www.cbat.eps.harvard.edu/unconf/followups/J16054809+2405338.html>>.

Table 97. Superhump maxima of PNV J172929 (2014) (continued)

E	max*	error	$O - C^\dagger$	N^\ddagger
131	56819.7059	0.0026	-0.0057	18
132	56819.7742	0.0025	0.0022	18
133	56819.8270	0.0037	-0.0054	18
142	56820.3754	0.0012	-0.0002	30
143	56820.4349	0.0007	-0.0010	31
144	56820.4932	0.0010	-0.0031	32
145	56820.5574	0.0028	0.0008	11
147	56820.6772	0.0069	-0.0001	10
148	56820.7309	0.0030	-0.0068	18
165	56821.7638	0.0026	0.0001	18
171	56822.1253	0.0022	-0.0005	216
172	56822.1885	0.0031	0.0023	97
173	56822.2422	0.0033	-0.0043	98

*BJD-2400000.

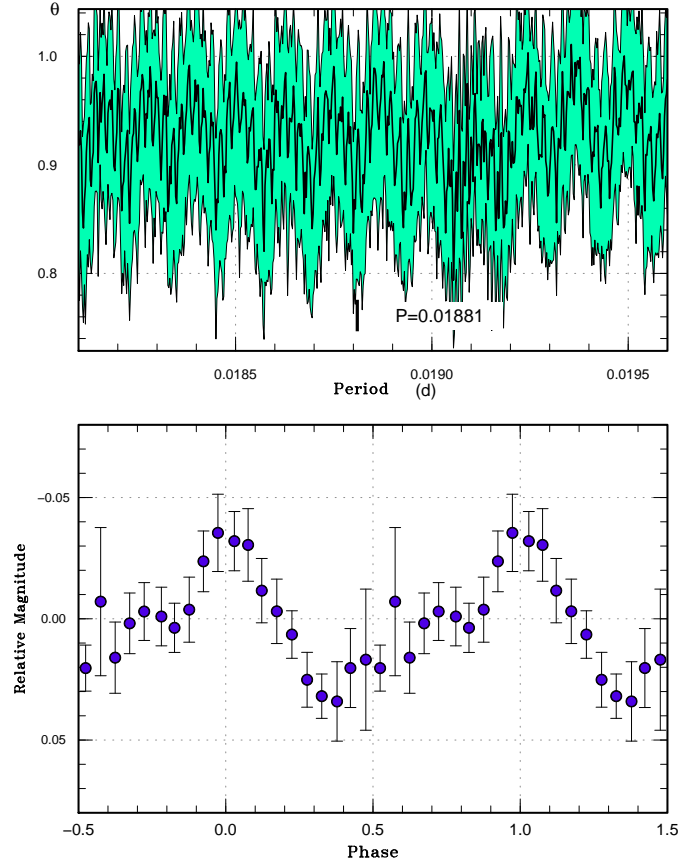
 † Against max = 2456811.8052 + 0.060354*E*. ‡ Number of points used to determine the maximum.**Fig. 134.** Superhumps in PTF1 J071912 (2014). (Upper): PDM analysis. (Lower): Phase-averaged profile.

Table 98. Superhump maxima of PTF1 J071912 (2014)

E	max*	error	$O - C^\dagger$	N^\ddagger
0	56902.6058	0.0006	0.0010	32
1	56902.6244	0.0008	0.0009	36
2	56902.6423	0.0006	-0.0000	36
3	56902.6593	0.0012	-0.0019	33
153	56905.4829	0.0019	-0.0009	9
155	56905.5218	0.0014	0.0004	9
158	56905.5772	0.0018	-0.0007	10
159	56905.5979	0.0006	0.0012	7

*BJD-2400000.

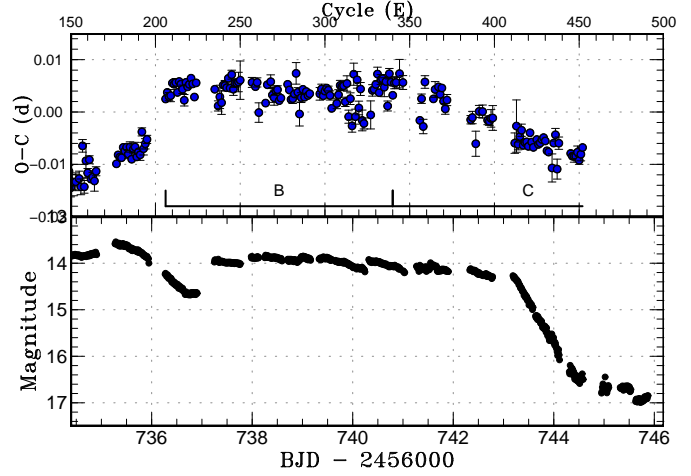
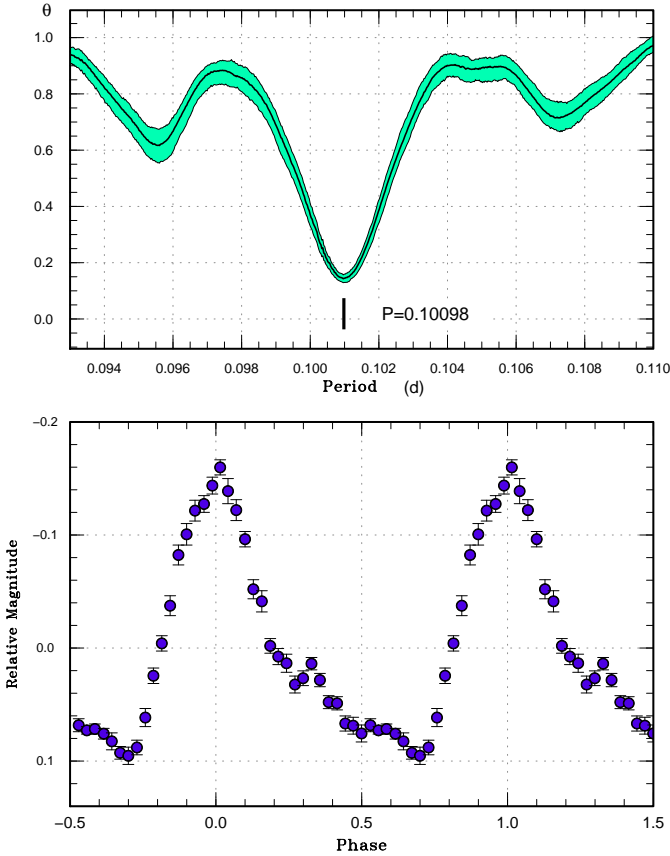
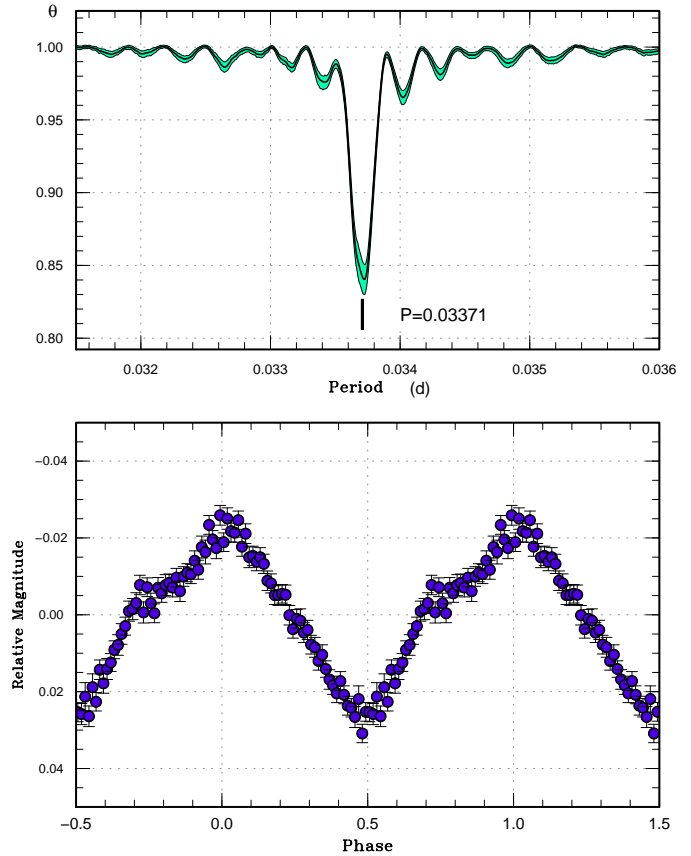
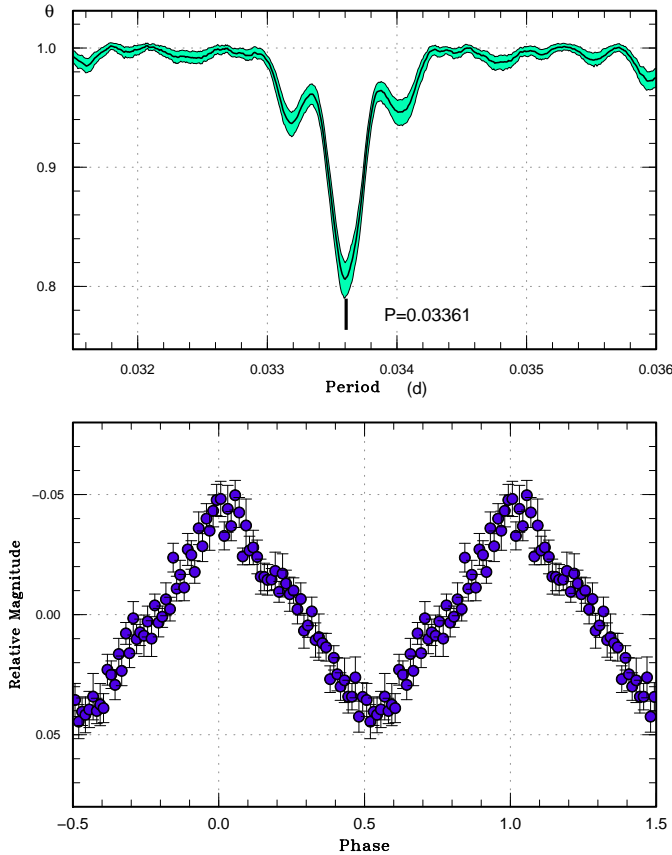
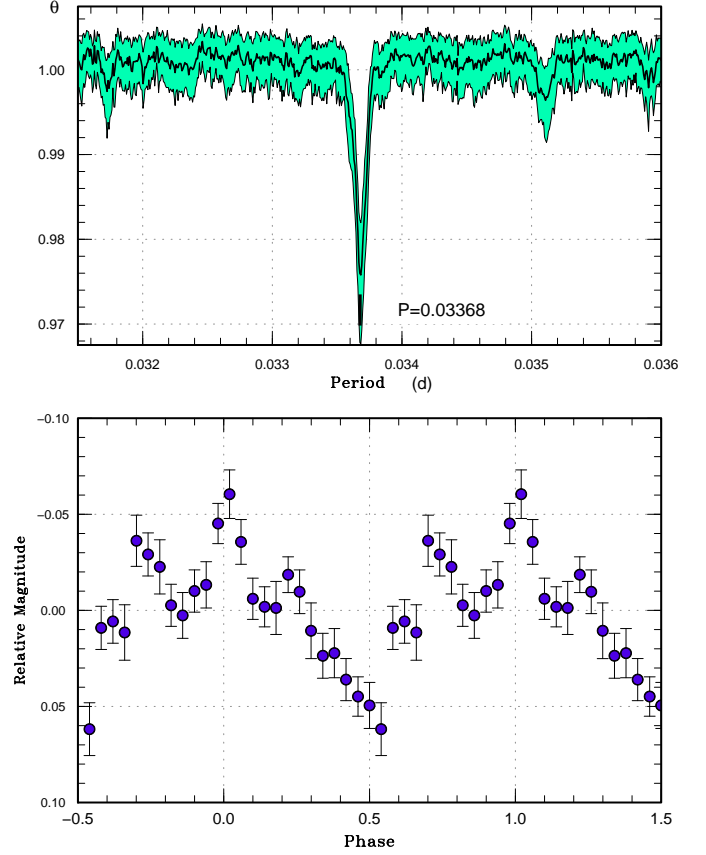
 † Against max = 2456902.6047 + 0.018818 E . ‡ Number of points used to determine the maximum.**Fig. 136.** $O - C$ diagram of superhumps in SDSS J090221 (2014) showing the stage B-C transition. (Upper): $O - C$ diagram. A period of 0.03372 d was used to draw this figure. (Lower): Light curve. The observations were binned to 0.01 d.**Fig. 135.** Superhumps in SDSS J081408 (2014). (Upper): PDM analysis. (Lower): Phase-averaged profile.**Fig. 137.** Stage B superhumps in SDSS J090221 (2014). (Upper): PDM analysis. (Lower): Phase-averaged profile.

Table 99. Superhump maxima of SDSS J081408 (2014)

E	max*	error	$O - C^\dagger$	N^\ddagger
0	56724.7195	0.0003	-0.0022	101
11	56725.8337	0.0003	0.0018	97
16	56726.3384	0.0007	0.0019	88
17	56726.4390	0.0004	0.0015	113
18	56726.5377	0.0008	-0.0007	96
27	56727.4444	0.0007	-0.0023	58

*BJD-2400000.

 † Against max = 2456724.7217 + 0.100929 E . ‡ Number of points used to determine the maximum.**Fig. 138.** Stage C superhumps in SDSS J090221 (2014). (Upper): PDM analysis. (Lower): Phase-averaged profile.**Fig. 139.** Superhumps in the post-superoutburst stage before the rebrightening in SDSS J090221 (2014). (Upper): PDM analysis. (Lower): Phase-averaged profile.

object from SDSS colors (Carter et al. 2013a). Although the object received attention, the difficult visibility in the morning sky and unstable weather hindered early observations. On December 21, apparent large-amplitude variations were recorded (vsnet-alert 18102). Although short-term variations were recorded on December 26 and 27 (vsnet-alert 18126), the nature of the variation was unclear. It was only on 2015 January 1, when clear superhumps were detected (vsnet-alert 18131, 18134; figure 147). Although the data were rather fragmentary and with long gaps, a period of 0.05501 d was found to express observations after BJD 2457019 (December 27). The times of superhump maxima based on this period are listed in table 108. Although there was a possibility of stage A superhumps or early superhumps before BJD 2457019, this could not be confirmed due to the lack of observations.

4. Discussion

4.1. Statistics of Objects

Up to Kato et al. (2009), a large fraction of objects studied in our survey were known variable stars in the General Catalog of Variable Stars (GCVS: Kholopov et al. 1985). Since 2007, the CRTS started to produce new transients,

Table 100. Superhump maxima of SDSS J090221 (2014) (slow rising part)

E	max*	error	$O - C^\dagger$	N^\ddagger
0	56729.2778	0.0059	0.0016	18
1	56729.3088	0.0015	-0.0016	18
2	56729.3462	0.0014	0.0018	12
3	56729.3805	0.0009	0.0019	18
5	56729.4408	0.0027	-0.0061	14
29	56730.2652	0.0012	-0.0005	17
30	56730.2994	0.0011	-0.0004	18
31	56730.3356	0.0021	0.0016	16
32	56730.3661	0.0010	-0.0020	25
33	56730.4020	0.0012	-0.0002	27
34	56730.4373	0.0018	0.0010	16
35	56730.4716	0.0011	0.0011	21
36	56730.5050	0.0016	0.0004	31
37	56730.5415	0.0028	0.0028	25
38	56730.5742	0.0016	0.0014	18
58	56731.2540	0.0011	-0.0012	19
59	56731.2894	0.0010	0.0000	17
60	56731.3215	0.0013	-0.0019	11
61	56731.3570	0.0010	-0.0005	16
64	56731.4581	0.0013	-0.0018	13
90	56732.3503	0.0011	0.0033	39
91	56732.3852	0.0012	0.0041	40
92	56732.4176	0.0008	0.0024	40
93	56732.4518	0.0015	0.0024	27
94	56732.4836	0.0009	0.0001	27
95	56732.5165	0.0016	-0.0012	23
96	56732.5524	0.0013	0.0007	60
97	56732.5858	0.0006	-0.0001	115
98	56732.6193	0.0009	-0.0007	73
99	56732.6537	0.0009	-0.0004	80
100	56732.6862	0.0014	-0.0020	23
101	56732.7183	0.0021	-0.0040	15
102	56732.7545	0.0011	-0.0020	14

*BJD-2400000.

 † Against max = 2456729.2763 + 0.034120*E*. ‡ Number of points used to determine the maximum.**Table 101.** Superhump maxima of SDSS J090221 (2014) (rise to superoutburst)

E	max*	error	$O - C^\dagger$	N^\ddagger
0	56733.3333	0.0018	0.0026	32
1	56733.3633	0.0006	-0.0012	65
3	56733.4342	0.0015	0.0022	65
4	56733.4672	0.0010	0.0013	65
5	56733.4996	0.0014	-0.0001	61
6	56733.5372	0.0036	0.0037	40
7	56733.5660	0.0005	-0.0013	30
10	56733.6707	0.0041	0.0021	31
11	56733.7031	0.0021	0.0007	37
12	56733.7366	0.0011	0.0004	93
14	56733.8041	0.0014	0.0003	109
15	56733.8406	0.0037	0.0030	106
30	56734.3442	0.0011	-0.0004	37
31	56734.3748	0.0017	-0.0036	64
32	56734.4096	0.0015	-0.0026	65
34	56734.4771	0.0017	-0.0027	52
36	56734.5451	0.0014	-0.0023	74
37	56734.5773	0.0015	-0.0039	69
38	56734.6188	0.0012	0.0038	64
39	56734.6447	0.0012	-0.0041	69
40	56734.6834	0.0033	0.0008	91
41	56734.7148	0.0008	-0.0016	79
42	56734.7510	0.0008	0.0009	59
43	56734.7811	0.0007	-0.0029	75
44	56734.8151	0.0009	-0.0026	61
45	56734.8481	0.0020	-0.0034	39
46	56734.8837	0.0009	-0.0016	38
58	56735.2898	0.0002	-0.0011	139
59	56735.3252	0.0003	0.0005	198
60	56735.3585	0.0003	-0.0000	206
61	56735.3921	0.0005	-0.0002	236
62	56735.4278	0.0004	0.0017	98
63	56735.4608	0.0004	0.0009	190

*BJD-2400000.

 † Against max = 2456733.3307 + 0.033797*E*. ‡ Number of points used to determine the maximum.

most of which were initially supernovae. The first CRTS CV studied in our survey was CRTS J021110.2+171624 in 2008 (Djorgovski et al. 2008). The CRTS then became the dominant source of new CVs for the subsequent five years (figure 148). Since the main targets of the CRTS are moving Solar system objects, the observation strategy (approximately once in 10 d) was not necessarily suitable for detecting CV outbursts in the early phase. Starting from 2012, the MASTER network started to produce new transients. The first MASTER CV studied in our survey was MASTER OT J072948.66+593824.4 (Balanutsa et al. 2012). Since the observation strategy was more suitable for early detection of CV outbursts, the contribution of outburst detections by the MASTER network increased up to 2013. A large number of newly discovered WZ Sge-type dwarf novae was a remarkable product of this survey (e.g. Kato et al. 2013a; Kato et al. 2014b; Nakata et al.

2013). Starting from 2013, the ASAS-SN system (Shappee et al. 2014a) started to produce new transients. The first ASAS-SN CV we studied was ASASSN-13cf and the number of ASAS-SN CVs rapidly increased thanks to the high frequency of observations (observations up to every night) and large sky coverage up to 15000 square degrees. As a result, the fraction of ASAS-SN CVs and detections of CV outbursts by the ASAS-SN team dramatically increased. If we restrict the objects to those studied in our series of papers, the number of objects designated by the ASAS-SN survey has already surpassed the number registered in the GCVS. It is likely that the majority of CVs within the reach of small telescopes have ASAS-SN names (currently 452 at the time of writing in 2015 June) in the near future unless the GCVS names (currently 581, including NSV) are given more quickly. The ASAS-SN transients are mostly not very faint as in the CRTS ones and

Table 101. Superhump maxima of SDSS J090221 (2014) (rise to superoutburst, continued)

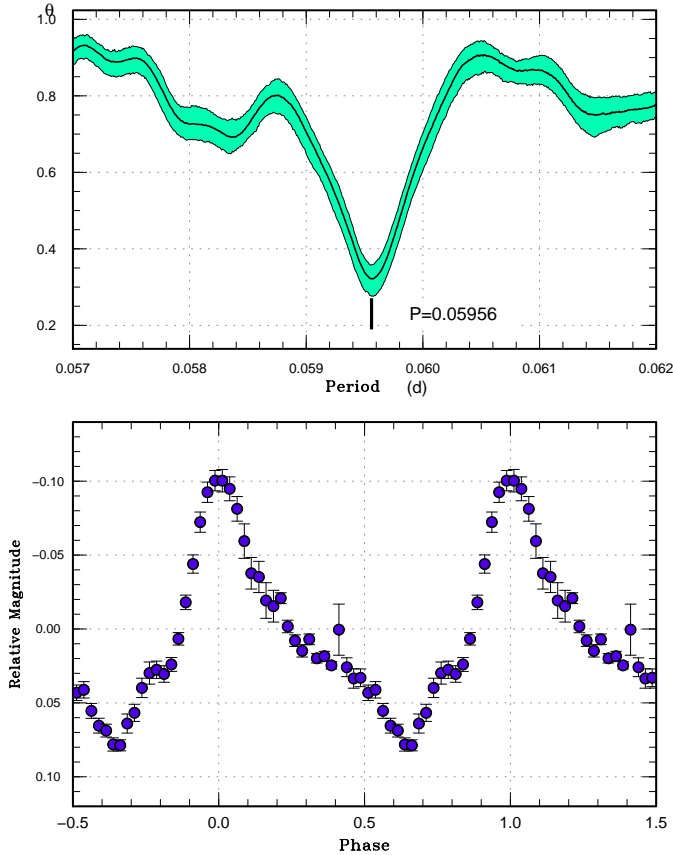
E	max*	error	$O - C^\dagger$	N^\ddagger
64	56735.4953	0.0006	0.0016	152
65	56735.5277	0.0009	0.0002	136
66	56735.5628	0.0010	0.0015	52
67	56735.5941	0.0005	-0.0010	50
68	56735.6298	0.0008	0.0009	45
69	56735.6639	0.0009	0.0012	56
70	56735.6957	0.0006	-0.0007	80
71	56735.7304	0.0007	0.0002	41
72	56735.7636	0.0011	-0.0005	39
73	56735.8017	0.0008	0.0038	39
74	56735.8322	0.0012	0.0005	43
75	56735.8668	0.0010	0.0014	43
76	56735.9014	0.0008	0.0021	21

*BJD-2400000.

 † Against max = 2456733.3307 + 0.033797 E . ‡ Number of points used to determine the maximum.**Table 102.** Superhump maxima of SDSS J090221 (2014) (superoutburst plateau)

E	max*	error	$O - C^\dagger$	N^\ddagger
0	56736.2800	0.0006	-0.0048	109
1	56736.3150	0.0007	-0.0035	111
2	56736.3479	0.0008	-0.0042	145
3	56736.3818	0.0012	-0.0040	111
4	56736.4180	0.0006	-0.0016	34
5	56736.4515	0.0007	-0.0017	47
6	56736.4855	0.0008	-0.0013	36
7	56736.5173	0.0006	-0.0032	42
8	56736.5531	0.0006	-0.0010	101
9	56736.5864	0.0007	-0.0015	96
10	56736.6191	0.0008	-0.0024	79
11	56736.6507	0.0011	-0.0045	135
12	56736.6879	0.0005	-0.0010	166
13	56736.7207	0.0007	-0.0018	164
14	56736.7549	0.0005	-0.0013	167
15	56736.7898	0.0005	-0.0001	166
16	56736.8224	0.0004	-0.0011	135
17	56736.8537	0.0006	-0.0036	126
18	56736.8901	0.0005	-0.0008	102
29	56737.2598	0.0004	-0.0015	37
31	56737.3240	0.0010	-0.0045	37
32	56737.3595	0.0022	-0.0028	75
33	56737.3921	0.0022	-0.0038	75
34	56737.4292	0.0007	-0.0004	120
35	56737.4628	0.0010	-0.0005	142
36	56737.4961	0.0007	-0.0008	139
37	56737.5316	0.0007	0.0010	135
38	56737.5635	0.0007	-0.0008	137
39	56737.5998	0.0008	0.0018	164
40	56737.6307	0.0012	-0.0009	57
41	56737.6656	0.0008	0.0003	196
42	56737.6993	0.0006	0.0004	182
43	56737.7332	0.0019	0.0006	203

*BJD-2400000.

 † Against max = 2456736.2848 + 0.033669 E . ‡ Number of points used to determine the maximum.**Fig. 140.** Superhumps in SDSS J120231 (2014, stage B). (Upper): PDM analysis. (Lower): Phase-averaged profile.

are reachable by relatively small telescopes. This present statistics would provide a clue for strategy of surveys in maximizing the scientific gain for small telescopes.

4.2. Period Distribution

In figure 149, we give distribution of superhump and estimated orbital periods, greatly updated since Kato et al. (2009). Since most of non-magnetic CVs below the period gap are SU UMa-type dwarf novae, this figure is expected to well represent the distribution of superhump periods of non-magnetic CVs. It is quite noticeable that there is a sharp cut-off at a period of 0.053 d (the objects below this period are either AM CVn-type systems and EI Psc-type objects). This finding has strengthened the modern observational identification of the period minimum (e.g. Knigge 2006; Gänsicke et al. 2009; Knigge et al. 2011) and there is no indication of systems below this period,

Table 102. Superhump maxima of SDSS J090221 (2014) (superoutburst plateau, continued)

E	max*	error	$O - C^\dagger$	N^\ddagger
44	56737.7673	0.0037	0.0010	48
51	56738.0029	0.0010	0.0010	19
53	56738.0696	0.0006	0.0003	25
54	56738.1041	0.0009	0.0011	21
55	56738.1321	0.0019	-0.0046	15
59	56738.2687	0.0005	-0.0026	36
60	56738.3060	0.0004	0.0010	37
62	56738.3740	0.0013	0.0017	111
63	56738.4052	0.0014	-0.0008	106
64	56738.4384	0.0014	-0.0013	72
65	56738.4734	0.0009	0.0001	73
66	56738.5073	0.0007	0.0003	67
67	56738.5390	0.0005	-0.0017	73
68	56738.5732	0.0006	-0.0012	36
72	56738.7107	0.0007	0.0017	66
73	56738.7433	0.0004	0.0006	75
74	56738.7752	0.0005	-0.0011	75
75	56738.8091	0.0009	-0.0009	75
76	56738.8437	0.0007	0.0000	75
77	56738.8814	0.0021	0.0040	70
78	56738.9115	0.0009	0.0004	75
79	56738.9411	0.0023	-0.0037	74
80	56738.9779	0.0009	-0.0005	24
81	56739.0132	0.0005	0.0012	74
82	56739.0454	0.0006	-0.0003	85
83	56739.0802	0.0004	0.0008	74
84	56739.1132	0.0005	0.0001	69
85	56739.1473	0.0006	0.0005	68
91	56739.3496	0.0012	0.0008	73
92	56739.3842	0.0009	0.0018	75
93	56739.4166	0.0005	0.0005	94
94	56739.4512	0.0006	0.0015	101
95	56739.4855	0.0007	0.0021	101

*BJD-2400000.

 † Against max = 2456736.2848 + 0.033669 E . ‡ Number of points used to determine the maximum.**Table 102.** Superhump maxima of SDSS J090221 (2014) (superoutburst plateau, continued)

E	max*	error	$O - C^\dagger$	N^\ddagger
96	56739.5188	0.0008	0.0018	102
97	56739.5516	0.0009	0.0008	35
98	56739.5828	0.0007	-0.0016	22
101	56739.6849	0.0010	-0.0005	81
102	56739.7203	0.0010	0.0012	78
103	56739.7558	0.0010	0.0030	84
104	56739.7893	0.0007	0.0029	85
105	56739.8232	0.0008	0.0031	78
106	56739.8538	0.0009	0.0000	84
107	56739.8910	0.0015	0.0036	75
108	56739.9184	0.0012	-0.0027	136
109	56739.9556	0.0011	0.0008	160
110	56739.9841	0.0012	-0.0044	172
111	56740.0277	0.0021	0.0056	219
112	56740.0533	0.0014	-0.0025	183
113	56740.0941	0.0016	0.0046	196
114	56740.1224	0.0013	-0.0007	215
115	56740.1598	0.0012	0.0029	164
116	56740.1875	0.0020	-0.0030	122
117	56740.2206	0.0011	-0.0035	122
121	56740.3571	0.0027	-0.0017	98
122	56740.3955	0.0011	0.0030	114
123	56740.4294	0.0007	0.0033	180
124	56740.4641	0.0007	0.0043	175
125	56740.4998	0.0013	0.0063	195
126	56740.5300	0.0007	0.0028	206
127	56740.5662	0.0009	0.0054	207
128	56740.6001	0.0008	0.0056	238
129	56740.6322	0.0018	0.0040	108
130	56740.6670	0.0006	0.0051	211
131	56740.6960	0.0010	0.0005	309
132	56740.7359	0.0010	0.0067	300
133	56740.7680	0.0005	0.0052	249

*BJD-2400000.

 † Against max = 2456736.2848 + 0.033669 E . ‡ Number of points used to determine the maximum.

contrary to what was suggested by Uemura et al. (2010). Since there have been a sizeable number of genuine candidates for period bouncers (Kato et al. 2013b; Kato, Osaki 2013b; Nakata et al. 2014), it is unlikely that the mass-transfer rate quickly decreases as systems approach the period minimum and this identification of the period minimum appears to be secure.

There is a peak of distribution just above the period minimum and it is compatible with the period spike (Gänsicke et al. 2009). The distribution monotonically decreases towards the longer period, and, rather surprisingly, there is no clear indication of a sudden decrease of the number at the supposed lower edge of the period gap. This tendency is the same as reported in Pavlenko et al. (2014). This result may even cast a doubt against the presence of the period gap, at least for SU UMa-type dwarf novae and the lower edge of the gap (we should

note, our surveys of superhumps systems are not sensitive to the upper edge of the period gap, above which almost all dwarf novae are not SU UMa-type stars).

4.3. Period Derivatives during Stage B

Figure 150 represents updated relation between P_{dot} for stage B versus P_{orb} . The objects studied in this paper are heavily concentrated in the region of $P_{\text{orb}} < 0.065$ d, and most of the object showed positive P_{dot} as in earlier studies. The longer-period systems studied in this work generally followed the trend shown in previous works. OT J064833 showed an exceptionally large P_{dot} . As discussed in subsection 3.90, this object has features common to short- P_{orb} systems and warrants further study.

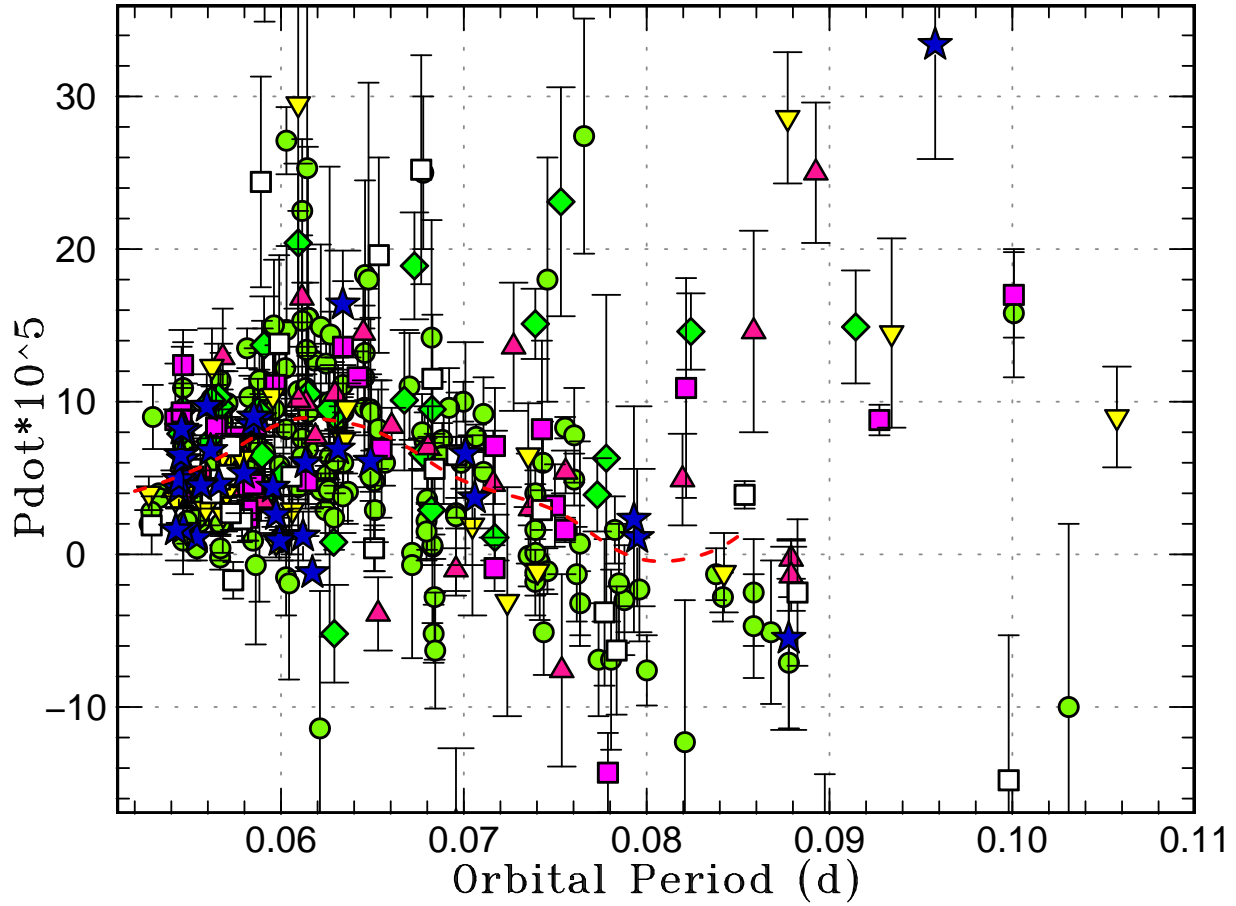


Fig. 150. P_{dot} for stage B versus P_{orb} . Filled circles, filled diamonds, filled triangles, filled squares, filled lower-pointed triangles, open square and filled stars represent samples in Kato et al. (2009), Kato et al. (2010), Kato et al. (2012a), Kato et al. (2013a), Kato et al. (2014b), Kato et al. (2014a) and this paper, respectively. The curve represents the spline-smoothed global trend.

4.4. Mass Ratios from Stage A Superhumps

We have proposed that the precession rate of stage A superhumps represents the dynamical precession rate of at the 3:1 resonance, thereby enabling estimation of mass ratios without experimental calibration (Kato, Osaki 2013b). We list new estimates for the binary mass ratio from stage A superhumps in table 109. This table includes two objects in C. Nakata et al. in preparation. In table 110, we list stage A superhumps recorded in the present study.

A updated distribution of mass ratios is shown in figure 151. The Kepler DNe shown in this figures are V516 Lyr (Kato, Osaki 2013a), KIC 7524178 (Kato, Osaki 2013c) and the unusual short- P_{orb} object GALEX J194419.33+491257.0 in the field of KIC 11412044 (Kato, Osaki 2014) (located at $P_{\text{orb}}=0.05282$ d, $q=0.14$). The present study has strengthened the concentration of WZ Sge-type dwarf novae around $q = 0.07$ just above the period minimum.

4.5. Development of Superhumps Following Precursor Outburst

In Kato et al. (2012a), we showed from the Kepler data of V1504 Cyg and V344 Lyr that superhumps start to develop following precursor outbursts. This finding was examined in more detail using the Kepler data of the same objects in Osaki, Kato (2013a), Osaki, Kato (2013b). The same phenomenon was also confirmed in the Kepler data of the background dwarf nova of KIC 4378554 and V516 Lyr (Kato, Osaki 2013a). These findings have strengthened the universal application of the TTI model to various SU UMa-type dwarf novae.

In this paper, we have observed similar evolution of superhumps following the precursor outburst in Z Cha. Although only one superhump was recorded, superhumps likely started to grow just before the final rise to the main superoutburst also in CY UMa. An $O - C$ analysis of SU UMa also suggested that superhumps likely started to appear around the maximum of the precursor outburst. All of these findings are in good agreement with what the TTI model predicts (cf. Osaki, Kato 2013a).

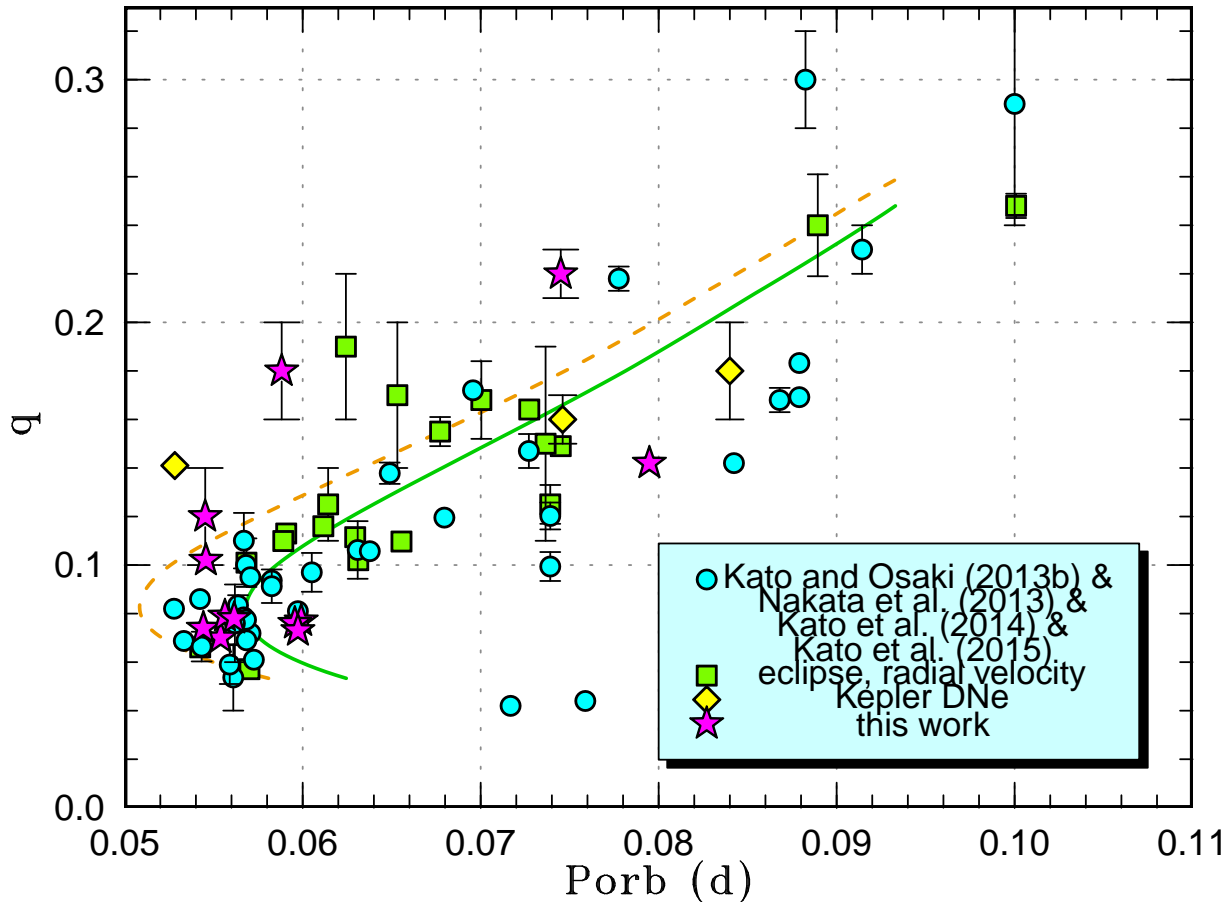


Fig. 151. Mass ratio versus orbital period. The dashed and solid curves represent the standard and optimal evolutionary tracks in Knigge et al. (2011), respectively. The filled circles, filled squares, filled stars, filled diamonds represent q values from a combination of the estimates from stage A superhumps published in four preceding sources (Kato, Osaki 2013b; Nakata et al. 2013; Kato et al. 2014b; Kato et al. 2014a), known q values from quiescent eclipses or radial-velocity study (see Kato, Osaki 2013b for the data source), q estimated in this work and dwarf novae in the Kepler data (see text for the complete reference), respectively. The objects in “this work” includes two objects in C. Nakata et al. in preparation

4.6. AM CVn-Type Objects and Related Objects

In recent years, an increasing number of AM CVn-type objects [for recent reviews of AM CVn-type objects, see e.g. Nelemans (2005); Solheim (2010)] have been recorded in outbursts and superhumps were detected during outbursts: CR Boo (observation in atypical state in Patterson et al. 1997, more regular superoutburst in Kato et al. 2001); V803 Cen (observation in atypical state in Patterson et al. 2000); KL Dra (Wood et al. 2002); V406 Hya (Nogami et al. 2004); SDSS J012940.05+384210.4 (Kato et al. 2010; Shears et al. 2012); YZ LMi (partial coverage in Copperwheat et al. 2011); PTF1 J071912.13+485834.0 (Levitan et al. 2011); CP Eri (Armstrong et al. 2012; Kato et al. 2014a); SDSS J172102.48+273301.2 (Kato et al. 2013a); CSS J045019.7–093113 (Woudt et al. 2013).

In Kato et al. (2013a), we also studied superhumps and outburst patterns in an AM CVn star CR Boo and found that the basic $O-C$ variation of superhumps in AM CVn-type superoutburst is the same as in hydrogen-rich systems. K. Isogai et al. in preparation also detected stage

A superhumps in CR Boo, first time in AM CVn-type objects with typical supercycles.

In this paper, we added new examples of AM CVn-type systems PTF1 J071912, SDSS J090221 (see also Kato et al. 2014c) and SDSS J173047. During the present survey, two further objects ASASSN-14ei and ASASSN-14mv have been identified as AM CVn-type objects showing superoutbursts and multiple rebrightenings (K. Isogai et al. in preparation; for spectroscopic identifications, see Prieto et al. 2014a, see also vsnet-alert 18160). ASASSN-14cn was also found to be an eclipsing AM CVn-type object in outburst (vsnet-alert 17879; superhumps are yet to be detected). ASASSN-14fv was also found to be an outbursting AM CVn-type object (Wagner et al. 2014 for spectroscopic identification; superhumps are yet to be detected). These data suggest that about 8% of objects showing dwarf nova-type outbursts are AM CVn-type objects. This fraction is much larger than the hitherto known statistics (about 1% in RKcat Edition 7.21 Ritter, Kolb 2003). AM CVn-type objects may be more populous than have been considered.

There have also been an increasing number of EI Psc-

Table 102. Superhump maxima of SDSS J090221 (2014) (superoutburst plateau, continued)

E	max*	error	$O - C^\dagger$	N^\ddagger
134	56740.7992	0.0006	0.0027	233
135	56740.8353	0.0011	0.0051	216
136	56740.8691	0.0011	0.0053	189
138	56740.9382	0.0027	0.0070	72
140	56741.0040	0.0013	0.0055	49
150	56741.3340	0.0004	-0.0013	76
151	56741.3718	0.0009	0.0029	97
152	56741.4002	0.0014	-0.0023	117
153	56741.4425	0.0012	0.0062	85
158	56741.6078	0.0007	0.0032	117
159	56741.6434	0.0015	0.0051	84
161	56741.7113	0.0005	0.0057	104
162	56741.7436	0.0007	0.0043	104
163	56741.7785	0.0005	0.0056	102
164	56741.8097	0.0007	0.0031	102
165	56741.8420	0.0010	0.0017	102
166	56741.8774	0.0011	0.0034	102
180	56742.3457	0.0008	0.0004	41
181	56742.3798	0.0012	0.0008	54
183	56742.4423	0.0024	-0.0041	39
185	56742.5159	0.0011	0.0022	25
187	56742.5833	0.0012	0.0023	34
190	56742.6828	0.0009	0.0008	64
191	56742.7163	0.0008	0.0006	62
192	56742.7506	0.0017	0.0012	64
193	56742.7844	0.0024	0.0014	32
206	56743.2179	0.0019	-0.0028	17
207	56743.2549	0.0050	0.0005	13
208	56743.2851	0.0010	-0.0029	32
209	56743.3204	0.0010	-0.0014	30
210	56743.3553	0.0012	-0.0001	30
211	56743.3861	0.0006	-0.0030	71
212	56743.4204	0.0004	-0.0024	93

*BJD-2400000.

 † Against max = 2456736.2848 + 0.033669 E . ‡ Number of points used to determine the maximum.

type objects (CVs containing but depleted hydrogen with orbital period below the period minimum): V485 Cen (Augusteijn 1995; Olech 1997); EI Psc (Thorstensen et al. 2002; Uemura et al. 2002; Skillman et al. 2002); CRTS J102842.9-081927 (Kato et al. 2009; Kato et al. 2013a; Kato et al. 2014b); CRTS J112253.3-111037 (Kato et al. 2010); SBS 1108+574 (Kato et al. 2013a; Littlefield et al. 2013; Carter et al. 2013b); CSS J174033.5+414756 (T. Ohshima et al. in preparation). Candidate systems include CRTS J233313.0-155744 (Woudt, Warner 2011).

We have added another object of this class, V418 Ser, in this paper. In all well-observed cases, the development of superhumps in these systems follow the same pattern as in hydrogen-rich systems. Although the number of these objects is smaller than AM CVn-type objects, these object may be more abundant than have been considered.

Table 102. Superhump maxima of SDSS J090221 (2014) (superoutburst plateau, continued)

E	max*	error	$O - C^\dagger$	N^\ddagger
213	56743.4542	0.0004	-0.0022	97
214	56743.4871	0.0005	-0.0030	92
215	56743.5234	0.0005	-0.0003	89
216	56743.5553	0.0004	-0.0021	37
217	56743.5880	0.0006	-0.0030	22
219	56743.6570	0.0004	-0.0014	70
220	56743.6898	0.0002	-0.0023	64
221	56743.7238	0.0005	-0.0020	66
222	56743.7582	0.0003	-0.0013	72
223	56743.7922	0.0003	-0.0009	70
224	56743.8253	0.0004	-0.0015	72
225	56743.8571	0.0003	-0.0033	54
226	56743.8906	0.0005	-0.0035	72
228	56743.9550	0.0027	-0.0064	15
229	56743.9935	0.0005	-0.0016	39
230	56744.0288	0.0012	0.0000	83
231	56744.0560	0.0019	-0.0065	95
232	56744.0946	0.0012	-0.0015	92
239	56744.3287	0.0006	-0.0031	45
240	56744.3619	0.0007	-0.0036	72
241	56744.3956	0.0011	-0.0035	97
242	56744.4293	0.0006	-0.0035	99
243	56744.4638	0.0012	-0.0026	63
244	56744.4960	0.0008	-0.0041	45
245	56744.5309	0.0013	-0.0029	35
246	56744.5659	0.0006	-0.0016	24

*BJD-2400000.

 † Against max = 2456736.2848 + 0.033669 E . ‡ Number of points used to determine the maximum.

4.7. Long-Term Variation of Supercycles

In this paper, we studied long-term variation of supercycles in MM Hya (subsection 3.15) and CY UMa (subsection 3.27). In MM Hya, variations of the supercycle in the range of 330 d and 386 d were recorded. In CY UMa, a sudden decrease of the supercycle from 362(3) d to 290(1) d was observed in 2003. In both systems, the supercycle tended to be constant for several to ten years, and there was a tendency of a sudden switch to a different period.

Similar systematic variations of cycle lengths were studied in SS Cyg-type dwarf novae [cf. AR And, UU Aql, RU Peg: Andronov, Shakun (1990)]. Andronov, Shakun (1990) suggested the Solar-type activity as a possible cause, but the phenomenon still remained a puzzle. In recent years, Zemko et al. (2013) recorded variations of supercycles from 43.6 to 59.2 d in ER UMa. The variations of the supercycle in ER UMa was an order similar to those in the two systems studied in this paper. Although there was a possibility that a disk tilt, which is supposed to produce negative superhumps (Wood, Burke 2007; Montgomery 2012), could affect the outburst properties, Zemko et al. (2013) could not find a correlation between the appearance of negative superhumps and the

Table 103. Superhump maxima of SDSS J090221 (2014) (rapid fading)

E	max*	error	$O - C^\dagger$	N^\ddagger
0	56754.9713	0.0008	-0.0009	64
1	56755.0049	0.0007	-0.0011	64
2	56755.0385	0.0009	-0.0014	65
3	56755.0758	0.0013	0.0021	65
4	56755.1058	0.0028	-0.0017	23
9	56755.2813	0.0007	0.0046	32
10	56755.3099	0.0010	-0.0007	45
11	56755.3451	0.0007	0.0007	70
12	56755.3784	0.0006	0.0002	72
13	56755.4114	0.0012	-0.0007	87
14	56755.4461	0.0007	0.0002	74
15	56755.4803	0.0008	0.0005	61
16	56755.5134	0.0010	-0.0002	39
22	56755.7168	0.0007	0.0002	72
23	56755.7495	0.0004	-0.0009	72
24	56755.7831	0.0008	-0.0011	70
22	56755.7169	0.0007	0.0003	70

*BJD-2400000.

 † Against max = 2456754.9722 + 0.033836 E . ‡ Number of points used to determine the maximum.**Table 104.** Superhump maxima of SDSS J120231 (2014)

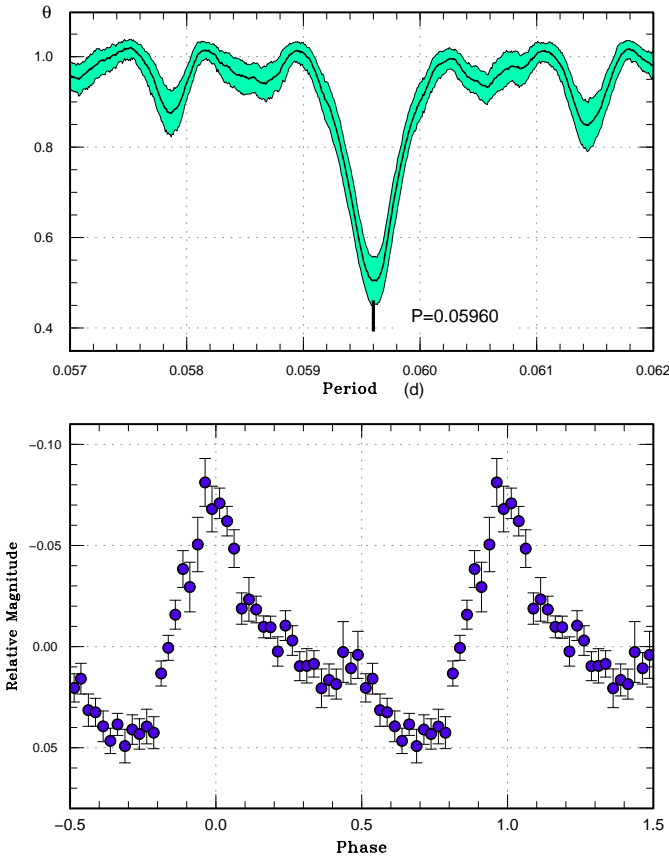
E	max*	error	$O - C^\dagger$	N^\ddagger
0	56806.4104	0.0002	0.0022	94
1	56806.4700	0.0002	0.0020	92
2	56806.5297	0.0003	0.0019	68
16	56807.3663	0.0004	0.0013	62
17	56807.4272	0.0002	0.0024	143
18	56807.4826	0.0003	-0.0021	124
19	56807.5441	0.0005	-0.0004	87
51	56809.4493	0.0003	-0.0088	47
52	56809.5098	0.0002	-0.0081	61
53	56809.5711	0.0008	-0.0065	33
134	56814.4280	0.0004	0.0066	49
135	56814.4894	0.0005	0.0081	53
150	56815.3838	0.0006	0.0055	36
151	56815.4452	0.0006	0.0071	52
152	56815.5047	0.0004	0.0068	41
167	56816.3978	0.0009	0.0029	20
168	56816.4560	0.0009	0.0013	53
169	56816.5139	0.0018	-0.0006	31
184	56817.4124	0.0006	0.0009	52
185	56817.4698	0.0007	-0.0015	54
200	56818.3587	0.0010	-0.0096	19
201	56818.4223	0.0018	-0.0058	28
202	56818.4822	0.0013	-0.0057	21

*BJD-2400000.

 † Against max = 2456806.4082 + 0.059800 E . ‡ Number of points used to determine the maximum.**Table 105.** Superhump maxima of SDSS J140037 (2015)

E	max*	error	$O - C^\dagger$	N^\ddagger
0	57057.4814	0.0013	0.0005	73
1	57057.5429	0.0015	-0.0018	99
2	57057.6082	0.0010	-0.0006	81
5	57057.8007	0.0006	0.0001	48
6	57057.8627	0.0005	-0.0019	67
7	57057.9250	0.0008	-0.0035	61
8	57057.9998	0.0009	0.0073	19
123	57065.3426	0.0023	-0.0046	37
124	57065.4116	0.0018	0.0005	35
125	57065.4789	0.0014	0.0039	35

*BJD-2400000.

 † Against max = 2457057.4808 + 0.063954 E . ‡ Number of points used to determine the maximum.**Fig. 141.** Superhumps in SDSS J120231 (2014, stage C). (Upper): PDM analysis. (Lower): Phase-averaged profile.

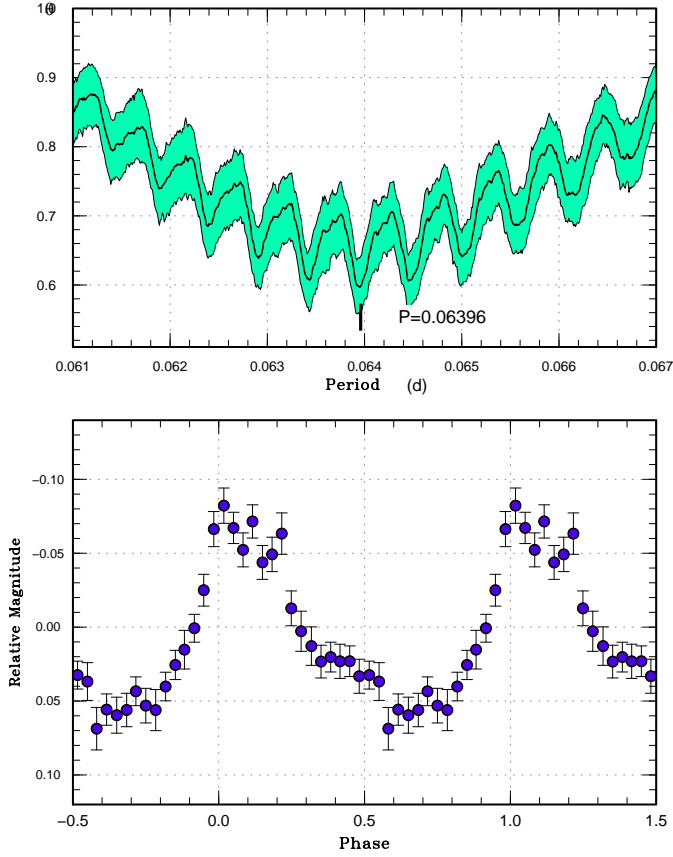


Fig. 142. Superhumps in SDSS J140037 during the plateau phase (2015). (Upper): PDM analysis. The shown period is one of possible aliases, which has been selected based on the long, continuous data on the first night. (Lower): Phase-averaged profile.

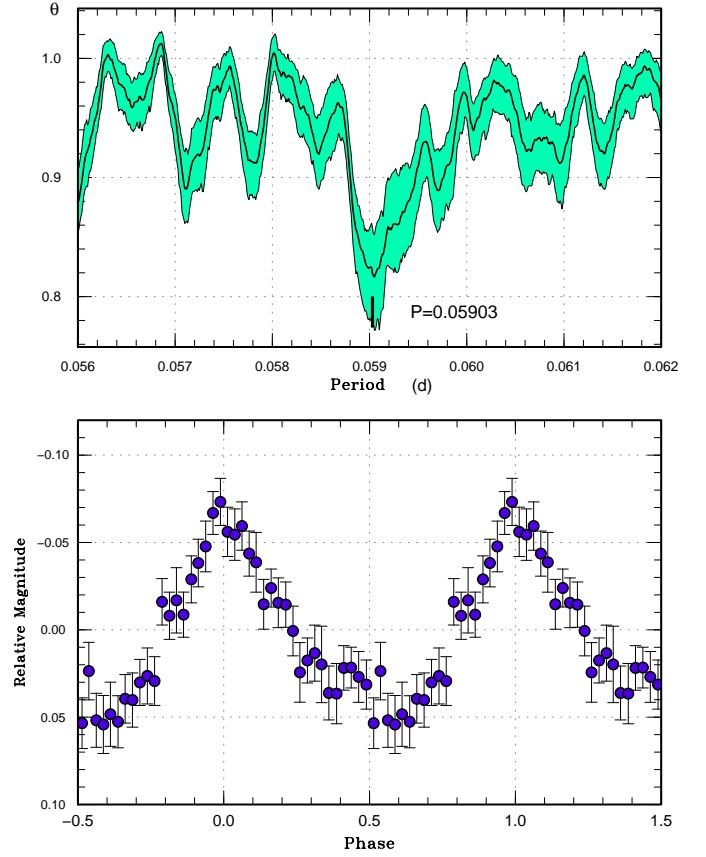


Fig. 143. Superhumps in SDSS J172325 (2014). The data between BJD 2456916.5 and BJD 2456928 were used. (Upper): PDM analysis. (Lower): Phase-averaged profile.

Table 106. Superhump maxima of SDSS J172325 (2014)

E	max*	error	$O - C^\dagger$	N^\ddagger
0	56916.9409	0.0005	-0.0018	66
1	56917.0029	0.0018	0.0009	19
6	56917.2979	0.0008	-0.0001	37
7	56917.3568	0.0004	-0.0004	61
8	56917.4193	0.0005	0.0029	89
9	56917.4757	0.0005	0.0001	51
22	56918.2486	0.0036	0.0034	31
23	56918.3057	0.0014	0.0013	34
39	56919.2531	0.0017	0.0014	49
40	56919.3062	0.0007	-0.0047	58
41	56919.3666	0.0005	-0.0035	24
92	56922.3873	0.0013	-0.0020	62
93	56922.4451	0.0022	-0.0035	60
109	56923.3976	0.0017	0.0018	40
110	56923.4591	0.0037	0.0041	29

*BJD-2400000.

† Against max = 2456916.9428 + 0.059202 E .

‡ Number of points used to determine the maximum.

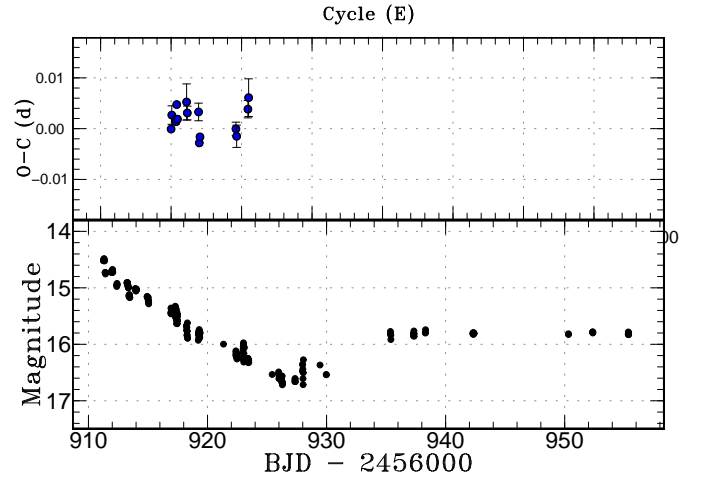


Fig. 144. $O - C$ diagram of superhumps in SDSS J172325 (2014). (Upper): $O - C$ diagram. A period of 0.05920 d was used to draw this figure. (Lower): Light curve. The observations were binned to 0.011 d.

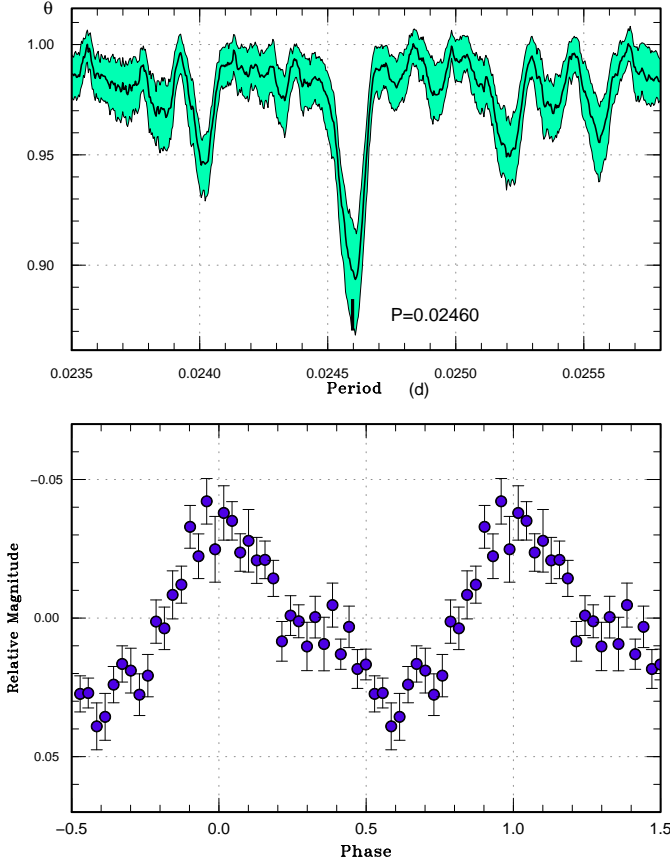


Fig. 145. Superhumps in SDSS J173047 (2014). The data between BJD 2456753 and BJD 2456758 were used. (Upper): PDM analysis. (Lower): Phase-averaged profile.

Table 107. Superhump maxima of SDSS J173047 (2014)

E	max*	error	$O - C^\dagger$	N^\ddagger
0	56753.5318	0.0003	-0.0025	39
1	56753.5570	0.0004	-0.0020	38
2	56753.5814	0.0004	-0.0021	39
3	56753.6061	0.0006	-0.0020	39
4	56753.6303	0.0004	-0.0024	33
5	56753.6575	0.0007	0.0002	39
6	56753.6776	0.0014	-0.0043	39
78	56755.4506	0.0007	-0.0015	13
79	56755.4830	0.0002	0.0064	12
80	56755.5004	0.0005	-0.0008	13
81	56755.5258	0.0005	-0.0000	51
82	56755.5500	0.0004	-0.0004	53
83	56755.5749	0.0004	-0.0001	46
84	56755.5995	0.0005	-0.0001	29
85	56755.6244	0.0005	0.0002	30
86	56755.6485	0.0006	-0.0003	31
87	56755.6720	0.0005	-0.0014	31
88	56755.6975	0.0006	-0.0005	31
96	56755.8933	0.0007	-0.0013	26
97	56755.9209	0.0008	0.0016	25
98	56755.9445	0.0008	0.0007	25
99	56755.9695	0.0025	0.0011	25
100	56755.9920	0.0010	-0.0010	24
104	56756.0877	0.0009	-0.0036	26
108	56756.1860	0.0041	-0.0036	23
122	56756.5356	0.0014	0.0018	49
123	56756.5625	0.0008	0.0041	46
124	56756.5836	0.0006	0.0006	33
125	56756.6092	0.0008	0.0016	27
126	56756.6361	0.0018	0.0039	25
127	56756.6599	0.0012	0.0031	23

*BJD-2400000.

† Against max = 2456753.5344 + 0.024586 E .

‡ Number of points used to determine the maximum.

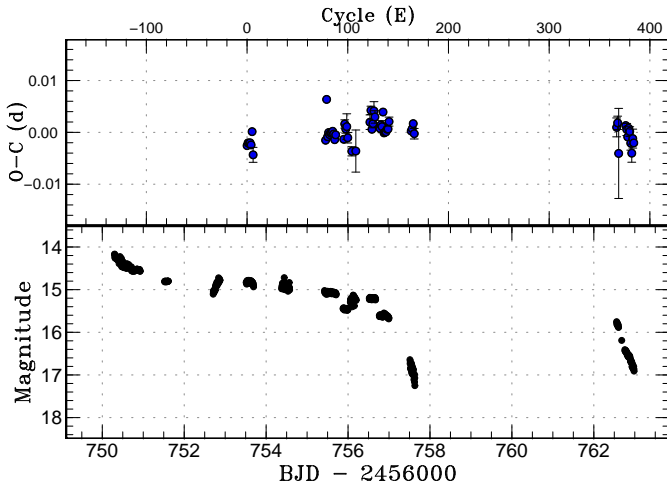


Fig. 146. $O - C$ diagram of superhumps in SDSS J173047 (2014). (Upper): $O - C$ diagram. A period of 0.024586 d was used to draw this figure. (Lower): Light curve. The observations were binned to 0.005 d.

supercycle length. Since a disk tilt is less likely to occur in systems with lower mass-transfer rate like MM Hya and CY UMa supposing a theoretical interpretation by Montgomery, Martin (2010), we consider it less likely that a disk tilt can explain the variations of the supercycle commonly seen in a variety of dwarf novae. The mechanism needs to be sought further.

5. Summary

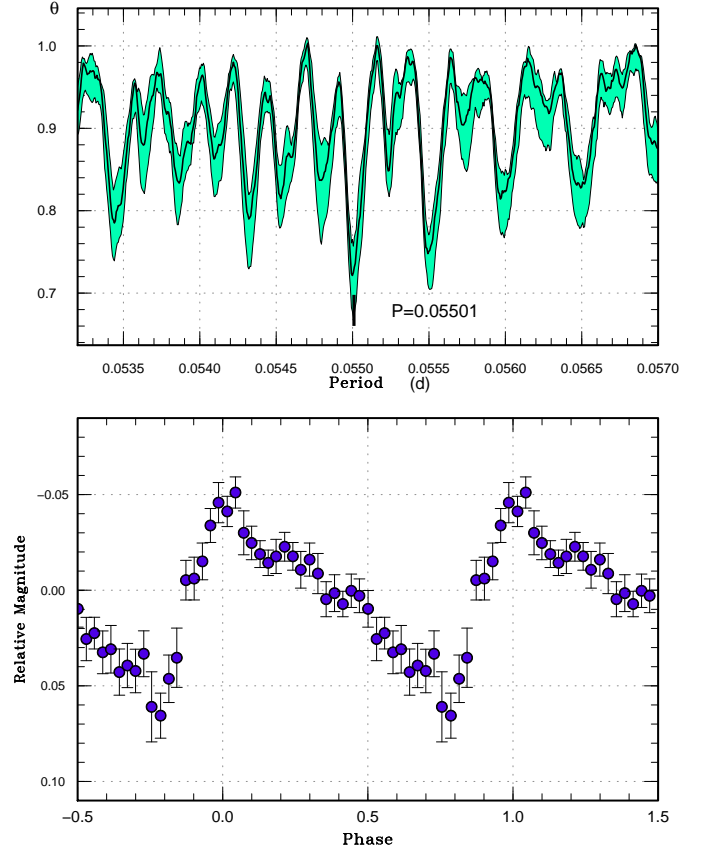
In addition to results of observations superhumps of the objects studied in this paper, the major findings we obtained can be summarized as follows.

- The contribution of various surveys in detecting SU UMa-type dwarf novae have dramatically changed in the last ten years. The advantage of a wide-field survey on nightly basis (such as ASAS-SN survey) has become obvious.
- Thanks to the increase of samples of SU UMa-type

Table 107. Superhump maxima of SDSS J173047 (2014)
(continued)

E	max*	error	$O - C^\dagger$	N^\ddagger
132	56756.7805	0.0005	0.0008	26
133	56756.8058	0.0006	0.0015	25
134	56756.8300	0.0012	0.0011	23
135	56756.8574	0.0007	0.0040	26
136	56756.8780	0.0006	-0.0001	26
137	56756.9027	0.0006	0.0000	25
138	56756.9274	0.0007	0.0001	26
139	56756.9525	0.0006	0.0006	25
140	56756.9771	0.0006	0.0007	25
141	56757.0031	0.0009	0.0021	6
163	56757.5421	0.0010	0.0002	24
164	56757.5671	0.0010	0.0007	27
165	56757.5927	0.0011	0.0017	23
166	56757.6152	0.0015	-0.0004	27
367	56762.5584	0.0018	0.0010	18
368	56762.5839	0.0013	0.0019	31
369	56762.6026	0.0087	-0.0040	22
376	56762.7800	0.0006	0.0014	25
377	56762.8039	0.0012	0.0006	22
378	56762.8270	0.0007	-0.0008	26
379	56762.8533	0.0004	0.0008	26
380	56762.8772	0.0009	0.0002	26
381	56762.8996	0.0013	-0.0020	26
382	56762.9222	0.0017	-0.0040	24
383	56762.9496	0.0018	-0.0012	26
384	56762.9734	0.0006	-0.0020	25

*BJD-2400000.

 † Against max = 2456753.5344 + 0.024586 E . ‡ Number of points used to determine the maximum.**Fig. 147.** Superhumps in SDSS J173047 (2014). The data after BJD 2457019 were used. (Upper): PDM analysis. (Lower): Phase-averaged profile.**Table 108.** Superhump maxima of TCP J160548 (2014)

E	max*	error	$O - C^\dagger$	N^\ddagger
0	57019.3296	0.0009	0.0087	29
79	57023.6644	0.0007	-0.0006	70
80	57023.7192	0.0003	-0.0009	101
81	57023.7720	0.0016	-0.0030	32
187	57029.6010	0.0010	-0.0029	54
188	57029.6547	0.0008	-0.0042	56
189	57029.7077	0.0029	-0.0062	45
315	57036.6494	0.0015	0.0068	42
316	57036.6998	0.0012	0.0023	41

*BJD-2400000.

 † Against max = 2457019.3209 + 0.054989 E . ‡ Number of points used to determine the maximum.**Table 109.** New estimates for the binary mass ratio from stage A superhumps

Object	ε^* (stage A)	q from stage A
Z Cha	0.0707(4)	0.22(1)
BR Lup	0.0488(12)	0.142(4)
QZ Vir	0.059(5)	0.18(2)
ASASSN-14cv	0.0286(3)	0.077(1)
ASASSN-14jf	0.026(2)	0.070(5)
ASASSN-14jv	0.0278(9)	0.074(3)
ASASSN-15bp	0.0293(6)	0.079(2)
OT J030929	0.0291(3)	0.078(1)
OT J213806	0.041(4)	0.12(2)
OT J230523	0.0366(7)	0.102(2)
PNV J171442	0.0284(3)	0.076(1)
PNV J172929	0.0273(5)	0.073(2)

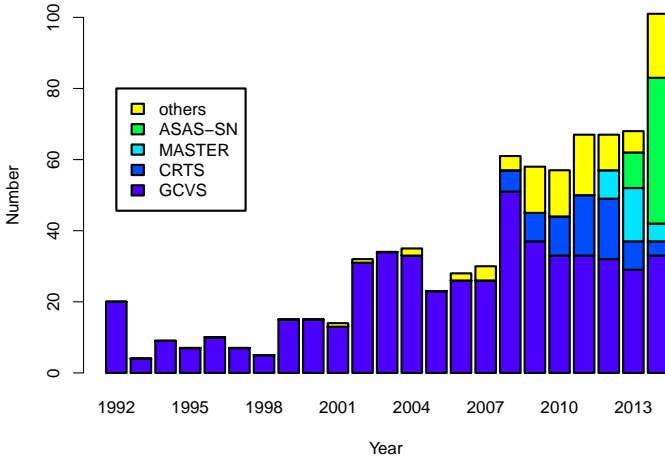


Fig. 148. Object categories in our survey. Superoutbursts with measured superhump periods are included. The year represents the year of outburst. The year 1992 represents outbursts up to 1992 and the year 2014 includes the outbursts in 2015, respectively. The category GCVS includes the objects named in the General Catalog of Variable Stars Kholopov et al. (1985) in the latest version and objects named in New Catalog of Suspected Variable Stars (NSV). The categories CRTS, MASTER, ASAS-SN represent objects which were discovered in respective surveys. A small fraction of objects discovered by the CRTS are already named in GCVS and are included in the category GCVS.

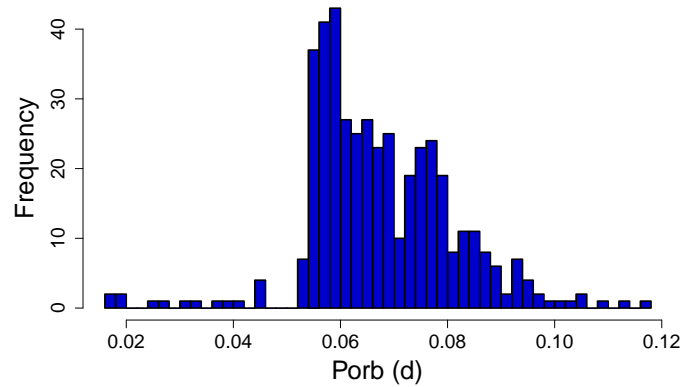
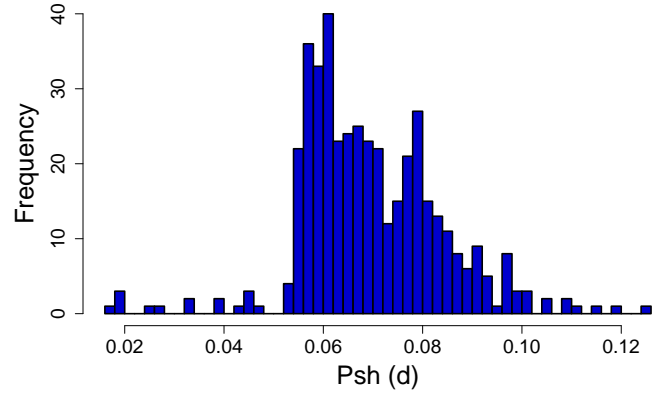


Fig. 149. Distribution of superhump periods in this survey. The data are from Kato et al. (2009), Kato et al. (2010), Kato et al. (2012a), Kato et al. (2013a), Kato et al. (2014b), Kato et al. (2014a) and this paper. The mean values are used when multiple superoutbursts were observed. (Upper) distribution of superhump periods. (Lower) distribution of orbital periods. For objects with superhump periods shorter than 0.053 d, the orbital periods were assumed to be 1% shorter than superhump periods. For objects with superhump periods longer than 0.053 d, we used the new calibration in Kato et al. (2012a) to estimate orbital periods.

Table 110. Superhump Periods during Stage A

Object	Year	period (d)	err
Z Cha	2014	0.08017	0.00031
BR Lup	2014	0.08357	0.00011
QZ Vir	2014	0.06248	0.00034
ASASSN-14cl	2014	0.06082	0.00014
ASASSN-14cv	2014	0.06168	0.00002
ASASSN-14jf	2014	0.05687	0.00009
ASASSN-14jv	2014	0.05597	0.00006
ASASSN-14md	2014	0.06943	0.00035
ASASSN-15bp	2015	0.05731	0.00003
OT J030929	2014	0.05783	0.00008
OT J060009	2014	0.06458	0.00005
OT J064833	2014	0.10519	0.00040
OT J213806	2014	0.05684	0.00026
OT J230523	2014	0.05663	0.00004
PNV J171442	2014	0.06130	0.00002
PNV J172929	2014	0.06141	0.00009
SDSS J090221	2014	0.03409	0.00001

dwarf novae, we could clarify the distribution of orbital periods in SU UMa-type dwarf novae, which approximate the CV population with short orbital periods. There is a sharp cut-off at a period of 0.053 d, which is considered to be the period minimum. There is a high concentration of objects just above the period minimum, which can be interpreted as the “period spike”. The distribution monotonically decreases towards the longer period, and there is little indication of the period gap.

- We observed a precursor outburst in Z Cha and found that superhumps developed just following the precursor outburst. $O-C$ analyses in CY UMa and YZ Cnc also support this finding. The agreement of the time of growing superhumps with the rising branch following the precursor outburst has been confirmed in all SU UMa-type systems so far studied. This finding provides a strong support to the thermal-tidal disk instability model which predicts that a superoutburst develops as a result of the de-

velopment of superhumps.

- We detected possible negative superhumps in Z Cha. During the phase of negative superhumps, the outburst cycle apparently lengthened. This finding seems to support a suggestion that a disk tilt suppresses normal outbursts.
- We studied secular variations of the quiescent brightness and the amplitude of orbital humps throughout one supercycle in Z Cha. The quiescent brightness decreased as the system approached the next superoutburst. There was no enhanced orbital humps just before the superoutburst.
- We studied long-term trends in supercycles in MM Hya and CY UMa and found systematic variations of supercycles of $\sim 20\%$. This degree and characteristics of variations are similar to those recorded in other SS Cyg-type dwarf novae and the SU UMa-type system ER UMa. A disk tilt is unlikely a common source of this variation.
- The WZ Sge-type object ASASSN-15bp showed a phase jump of superhumps during the plateau phase.
- A sizable number of AM CVn-type objects (PTF1 J071912, SDSS J090221, SDSS J173047) were studied in this paper and four more AM CVn-type objects (ASASSN-14cn, ASASSN-14ei, ASASSN-14fv and ASASSN-14mv) were found in this period. This number suggests that about 8% of objects showing dwarf nova-type outbursts are AM CVn-type objects.
- We have added another EI Psc-type object V418 Ser in this paper. These object may be more abundant than have been considered.
- CSS J174033, an EI Psc-type object, showed a similar type of superoutbursts in 2012 and 2014, comprising of a dip and the second plateau phase. This finding suggests that the same type of superoutbursts tend to be reproduced in EI Psc-type objects as in hydrogen-rich systems.
- OT J213806, a WZ Sge-type object, exhibited a remarkably different peak brightness and $O - C$ diagrams between the 2010 and 2014 superoutbursts. The fainter superoutburst in 2014 was shorter and the difference was most striking in the later part of the plateau phase.
- MASTER J085854 showed two post-superoutburst rebrightenings. This object had a rather exceptionally short superhump period among the objects showing multiple rebrightenings.
- Four deeply eclipsing SU UMa-type dwarf novae were identified (ASASSN-13cx, ASASSN-14ag, ASASSN-15bu, NSV 4618). ASASSN-14id also showed shallow eclipses.

Acknowledgements

This work was supported by the Grant-in-Aid “Initiative for High-Dimensional Data-Driven Science through Deepening of Sparse Modeling” (25120007) from the Ministry of Education, Culture, Sports, Science and

Technology (MEXT) of Japan. The authors are grateful to observers of VSNET Collaboration and VSOLJ observers who supplied vital data. We acknowledge with thanks the variable star observations from the AAVSO International Database contributed by observers worldwide and used in this research. We are also grateful to the VSOLJ database. This work is deeply indebted to outburst detections and announcement by a number of variable star observers worldwide, including participants of CVNET and BAA VSS alert. The CCD operation of the Bronberg Observatory is partly sponsored by the Center for Backyard Astrophysics. We are grateful to the Catalina Real-time Transient Survey team for making their real-time detection of transient objects available to the public. R. Modic acknowledge the Bradford Robotic Telescope for the detection of the 2014 outburst of QZ Vir. The work by A. Sklyanov is partially performed according to the Russian Government Program of Competitive Growth of Kazan Federal University.

References

- Andronov, I. L., & Shakun, L. I. 1990, *Ap&SS*, 169, 237
- Armstrong, E., Patterson, J., & Kemp, J. 2012, *MNRAS*, 421, 2310
- Augusteijn, T. 1995, in *Cataclysmic Variables*, ed. A. Bianchini, M. della Valle, & M. Orio (Dordrecht: Kluwer Academic Publishers), p. 129
- Baade, W. 1928, *Astron. Nachr.*, 232, 65
- Baba, H., et al. 2002, *PASJ*, 54, L7
- Bailey, J. 1979, *MNRAS*, 187, 645
- Bailey, J., & Ward, M. 1981, *MNRAS*, 194, 17
- Balanutsa, P., et al. 2014, *Astron. Telegram*, 5787
- Balanutsa, P., et al. 2015a, *Astron. Telegram*, 6946
- Balanutsa, P., et al. 2015b, *Astron. Telegram*, 6967
- Balanutsa, P., et al. 2012, *Astron. Telegram*, 3935
- Barwig, H., & Schoembs, R. 1981, *IBVS*, 1989
- Beljawsky, S. 1927, *Astron. Nachr.*, 230, 349
- Berardi, P. 2014, *Astron. Telegram*, 6684
- Boyd, D., Kracj, T., Shears, J., & Poyner, G. 2007, *J. Br. Astron. Assoc.*, 117, 198
- Breedt, E., et al. 2014, *MNRAS*, 443, 3174
- Brown, A., et al. 2015, *AJ*, 149, 67
- Brown, S. J., Mills, O. F., Osborn, W., & Hoette, V. 2010, *J. American Assoc. Variable Star Obs.*, 38, 176
- Bruch, A., Fischer, F.-J., & Wilmsen, U. 1987, *A&AS*, 70, 481
- Buat-Ménard, V., & Hameury, J.-M. 2002, *A&A*, 386, 891
- Carter, P. J., et al. 2013a, *MNRAS*, 429, 2143
- Carter, P. J., et al. 2013b, *MNRAS*, 431, 372
- Carter, P. J., Steeghs, D., Marsh, T. R., Kupfer, T., Copperwheat, C. M., Groot, P. J., & Nelemans, G. 2014, *MNRAS*, 437, 2894
- Ceraski, W. 1908, *Astron. Nachr.*, 177, 173
- Chochol, D., Katysheva, N. A., Shugarov, S. Y., Zemko, P. O., & Andreev, M. V. 2012, *Contr. of the Astron. Obs. Skalnaté Pleso*, 42, 39
- Cleveland, W. S. 1979, *J. Amer. Statist. Assoc.*, 74, 829
- Cook, M. C., & Warner, B. 1981, *MNRAS*, 196, 55P
- Copperwheat, C. M., et al. 2011, *MNRAS*, 410, 1113
- Cowley, A. P., Crampton, D., Hutchings, J. B., Helfand, D. J., Hamilton, T. T., Thorstensen, J. R., & Charles, P. A. 1984, *ApJ*, 286, 196

- Croom, S. M., Smith, R. J., Boyle, B. J., Shanks, T., Miller, L., Outram, P. J., & Loaring, N. S. 2004, *MNRAS*, 349, 1397
- Dai, Z., Qian, S., & Fernández Lajús, E. 2009, *ApJ*, 703, 109
- Davis, A. B., Shappee, B. J., Archer Shappee, B., & ASAS-SN 2015, American Astron. Soc. Meeting Abstracts, 225, #344.02
- Davis, A. B., et al. 2014, *Astron. Telegram*, 6455
- Denisenko, D. 2011, *Perem. Zvezdy*, 31, 3
- Denisenko, D. V. 2009, *Astron. Telegram*, 2282
- Denisenko, D. V., & Sokolovsky, K. V. 2011, *Astron. Lett.*, 37, 91
- D'Esterre, C. R. 1912, *Astron. Nachr.*, 190, 163
- D'Esterre, C. R. 1913, *Astron. Nachr.*, 193, 281
- Djorgovski, S. G. ., et al. 2008, *Astron. Telegram*, 1416
- Downes, R. A., & Shara, M. M. 1993, *PASP*, 105, 127
- Drake, A. J., et al. 2009, *ApJ*, 696, 870
- Drake, A. J., et al. 2014, *MNRAS*, 441, 1186
- Echevarria, J., Pocock, A. S., Penston, M. V., & Blades, J. C. 1983, *MNRAS*, 205, 559
- Elvey, C. T., & Babcock, H. W. 1943, *ApJ*, 97, 412
- Erastova, L. K. 1973, *Astron. Tsirk.*, 774, 5
- Fernie, J. D. 1989, *PASP*, 101, 225
- Gänsicke, B. T., et al. 2009, *MNRAS*, 397, 2170
- Garnavich, P., Littlefield, C., Terndrup, D., & Adams, S. 2014, *Astron. Telegram*, 6287
- Glasby, J. S. 1970, *The Dwarf Novae* (London: Constable)
- Golovin, A., et al. 2007, *IBVS*, 5763
- Graham, M. L., Broekhoven-Fiene, H., Parker, A. H., Sadavoy, S., Maxwell, A. J., Hsiao, E. Y., & Balam 2010, *Cent. Bur. Electron. Telegrams*, 2275, 6
- Green, R. F., Ferguson, D. H., Liebert, J., & Schmidt, M. 1982, *PASP*, 94, 560
- Greenhill, J. G., Hill, K. M., Dieters, S., Fienberg, K., Howlett, M., Meijers, A., Munro, A., & Senkbeil, C. 2006, *MNRAS*, 372, 1129
- Guthnick, P., & Prager, R. 1933, *Astron. Nachr.*, 249, 253
- Han, Z.-T., Qian, S.-B., Fernández Lajús, E., Liao, W.-P., & Zhang, J. 2015, *New Astron.*, 34, 1
- Hartwig, E. 1915, *Astron. Nachr.*, 201, 287
- Hartwig, E. 1917, *Astron. Nachr.*, 204, 11
- Hartwig, E. 1920, *Astron. Nachr.*, 212, 79
- Harvey, D., Skillman, D. R., Patterson, J., & Ringwald, F. A. 1995, *PASP*, 107, 551
- Harvey, D. A., & Patterson, J. 1995, *PASP*, 107, 1055
- Hirose, M., & Osaki, Y. 1990, *PASJ*, 42, 135
- Hodgkin, S. T., et al. 2014, *Astron. Telegram*, 6407
- Hoffmeister, C. 1963, *Veröff. Sternw. Sonneberg*, 6, 1
- Hornby, P. W. 1975, *J. Br. Astron. Assoc.*, 85, 528
- Horne, K. 1984, *Nature*, 312, 348
- Howarth, I. D. 1978, *J. Br. Astron. Assoc.*, 89, 47
- Howell, S. B., De Young, J., Mattei, J. A., Foster, G., Szkody, P., Cannizzo, J. K., Walker, G., & Fierce, E. 1996, *AJ*, 111, 2367
- Hudec, R. 2010, *Astron. Telegram*, 2619
- Imada, A., Kubota, K., Kato, T., Nogami, D., Maehara, H., Nakajima, K., Uemura, M., & Ishioka, R. 2006, *PASJ*, 58, L23
- Imada, A., & Monard, L. A. G. B. 2006, *PASJ*, 58, L19
- Ishioka, R., et al. 2002, *A&A*, 381, L41
- Isles, J. E. 1974, *J. Br. Astron. Assoc.*, 84, 365
- Kato, T. 1990, *IBVS*, 3522
- Kato, T. 1995, *IBVS*, 4236
- Kato, T. 1997a, *PASJ*, 49, 583
- Kato, T. 1997b, *VSOLJ Variable Star Bull.*, 25, 2
- Kato, T. 2002, *PASJ*, 54, L11
- Kato, T. 2015, *PASJ*, submitted
- Kato, T., et al. 2014a, *PASJ*, 66, 90
- Kato, T., Fujino, S., Iida, M., Makiguchi, N., & Koshiro, S. 1988, *VSOLJ Variable Star Bull.*, 5, 18
- Kato, T., et al. 2013a, *PASJ*, 65, 23
- Kato, T., et al. 2014b, *PASJ*, 66, 30
- Kato, T., Hamsch, F.-J., Oksanen, A., Starr, P., & Henden, A. 2015, *PASJ*, 67, 3
- Kato, T., et al. 2009, *PASJ*, 61, S395
- Kato, T., & Maehara, H. 2013, *PASJ*, 65, 76
- Kato, T., et al. 2012a, *PASJ*, 64, 21
- Kato, T., Maehara, H., & Uemura, M. 2012b, *PASJ*, 64, 62
- Kato, T., et al. 2010, *PASJ*, 62, 1525
- Kato, T., & Matsumoto, K. 1999, *IBVS*, 4763
- Kato, T., Monard, B., Hamsch, F.-J., Kiyota, S., & Maehara, H. 2013b, *PASJ*, 65, L11
- Kato, T., et al. 2004a, *MNRAS*, 347, 861
- Kato, T., Nogami, D., Baba, H., Matsumoto, K., Arimoto, J., Tanabe, K., & Ishikawa, K. 1996, *PASJ*, 48, L21
- Kato, T., et al. 2014c, *PASJ*, 66, L7
- Kato, T., & Osaki, Y. 2013a, *PASJ*, 65, 97
- Kato, T., & Osaki, Y. 2013b, *PASJ*, 65, 115
- Kato, T., & Osaki, Y. 2013c, *PASJ*, 65, L13
- Kato, T., & Osaki, Y. 2014, *PASJ*, 66, L5
- Kato, T., et al. 2001, *IBVS*, 5120, 1
- Kato, T., Stubbings, R., Monard, B., Butterworth, N. D., Bolt, G., & Richards, T. 2004b, *PASJ*, 56, S89
- Kato, T., & Uemura, M. 2012, *PASJ*, 64, 122
- Kato, T., Uemura, M., Ishioka, R., Nogami, D., Kunjaya, C., Baba, H., & Yamaoka, H. 2004c, *PASJ*, 56, S1
- Kazarovets, E. V., Samus, N. N., Durlevich, O. V., Kireeva, N. N., & Pastukhova, E. N. 2006, *IBVS*, 5721
- Kazarovets, E. V., Samus, N. N., Durlevich, O. V., Kireeva, N. N., & Pastukhova, E. N. 2008, *IBVS*, 5863, 1
- Kazarovets, E. V., Samus, N. N., Durlevich, O. V., Kireeva, N. N., & Pastukhova, E. N. 2011, *IBVS*, 6008, 1
- Kholopov, P. N., et al. 1985, *General Catalogue of Variable Stars*, fourth edition (Moscow: Nauka Publishing House)
- Khruslov, A. V. 2005, *Perem. Zvezdy, Prilozh.*, 5, 4
- Knigge, C. 2006, *MNRAS*, 373, 484
- Knigge, C., Baraffe, I., & Patterson, J. 2011, *ApJS*, 194, 28
- Krzeminski, W., & Vogt, N. 1985, *A&A*, 144, 124
- Kubiak, M., & Krzeminski, W. 1989, *PASP*, 101, 667
- Kubiak, M., & Krzeminski, W. 1992, *Acta Astron.*, 42, 177
- Levitán, D., et al. 2011, *ApJ*, 739, 68
- Littlefield, C., et al. 2013, *AJ*, 145, 145
- Lubow, S. H. 1991, *ApJ*, 381, 259
- Luyten, W. J. 1938, *Publ. of the Astron. Obs. Univ. of Minnesota*, 6, 1
- Mayall, M. W. 1966, *JRASC*, 60, 301
- Mennickent, R. E., & Sterken, C. 1998, *PASP*, 110, 1032
- Misselt, K. A., & Shafter, A. W. 1995, *AJ*, 109, 1757
- Mitrofanova, A. A., Borisov, N. V., & Shimansky, V. V. 2014, *Astrophys. Bull.*, 69, 82
- Monard, L. A. G., & Africa, S. 2005, *IAU Circ.*, 8540, 3
- Montgomery, M. M. 2012, *ApJ*, 745, L25
- Montgomery, M. M., & Martin, E. L. 2010, *ApJ*, 722, 989
- Mroz, P., et al. 2013, *Acta Astron.*, 63, 135
- Munari, U., & Zwitter, T. 1998, *A&AS*, 128, 277
- Nakano, S. 2010, *Cent. Bur. Electron. Telegrams*, 2275, 2
- Nakata, C., et al. 2014, *PASJ*, 66, 116
- Nakata, C., et al. 2013, *PASJ*, 65, 117

- Nelemans, G. 2005, in ASP Conf. Ser. 330, *The Astrophysics of Cataclysmic Variables and Related Objects*, ed. J.-M. Hameury, & J.-P. Lasota (San Francisco: ASP), p. 27
- Nesci, R., Caravano, A., Falasca, V., & Villani, L. 2013, IBVS, 6059
- Nijland, A. A. 1914, *Astron. Nachr.*, 199, 131
- Nijland, A. A. 1915, *Astron. Nachr.*, 201, 347
- Nijland, A. A. 1918, *Astron. Nachr.*, 206, 223
- Nijland, A. A. 1924, *Astron. Nachr.*, 221, 243
- Nogami, D., Kato, T., Baba, H., Matsumoto, K., Arimoto, J., Tanabe, K., & Ishikawa, K. 1997, *ApJ*, 490, 840
- Nogami, D., Kato, T., Masuda, S., Hirata, R., Matsumoto, K., Tanabe, K., & Yokoo, T. 1995, *PASJ*, 47, 897
- Nogami, D., Monard, B., Retter, A., Liu, A., Uemura, M., Ishioka, R., Imada, A., & Kato, T. 2004, *PASJ*, 56, L39
- Nogami, D., et al. 2004, *PASJ*, 56, S99
- O'Donoghue, D. 1987, *Ap&SS*, 136, 247
- Ohshima, T., et al. 2014, *PASJ*, 66, 67
- Ohshima, T., et al. 2011, *PASJ*, submitted
- Olech, A. 1997, *Acta Astron.*, 47, 281
- Olech, A., Cook, L. M., Złoczewski, K., Mularczyk, K., Kędzierski, P., Udalski, A., & Wisniewski, M. 2004, *Acta Astron.*, 54, 233
- Olech, A., Kędzierski, P., Złoczewski, K., Mularczyk, K., & Wiśniewski, M. 2003, *A&A*, 411, 483
- Osaki, Y. 1989, *PASJ*, 41, 1005
- Osaki, Y. 1996, *PASP*, 108, 39
- Osaki, Y., & Kato, T. 2013a, *PASJ*, 65, 50
- Osaki, Y., & Kato, T. 2013b, *PASJ*, 65, 95
- Osaki, Y., & Kato, T. 2014, *PASJ*, 66, 15
- Osaki, Y., & Meyer, F. 2002, *A&A*, 383, 574
- Osborne, J. P., et al. 2011, *A&A*, 533, A41
- Pagnotta, A., & Schaefer, B. E. 2014, *ApJ*, 788, 164
- Patterson, J., Augusteijn, T., Harvey, D. A., Skillman, D. R., Abbott, T. M. C., & Thorstensen, J. 1996, *PASP*, 108, 748
- Patterson, J., Bond, H. E., Grauer, A. D., Shafter, A. W., & Mattei, J. A. 1993, *PASP*, 105, 69
- Patterson, J., et al. 1997, *PASP*, 109, 1100
- Patterson, J., et al. 2002, *PASP*, 114, 721
- Patterson, J., et al. 2003, *PASP*, 115, 1308
- Patterson, J., Walker, S., Kemp, J., O'Donoghue, D., Bos, M., & Stubbings, R. 2000, *PASP*, 112, 625
- Pavlenko, E. P., et al. 2014, *PASJ*, 66, 111
- Pearson, K. J. 2007, *MNRAS*, 379, 183
- Perez, A., & McNaught, R. H. 1986, *IAU Circ.*, 4222, 2
- Petit, M. 1960, *Journal des Observateurs*, 43, 33
- Petit, M., & Brun, A. 1956, *Journal des Observateurs*, 39, 37
- Pojmański, G. 2002, *Acta Astron.*, 52, 397
- Pojmanski, G. 2005, *IAU Circ.*, 8539, 3
- Prager, R., & Shapley, H. 1941, *Annals of the Astron. Obs. of Harvard Coll.* 111, 1
- Price, A., et al. 2003, *IBVS*, 5488
- Prieto, J. L., et al. 2013, *Astron. Telegram*, 4999
- Prieto, J. L., et al. 2014a, *Astron. Telegram*, 6475, 1
- Prieto, J. L., et al. 2014b, *Astron. Telegram*, 6293
- Quimby, R., & Mondol, P. 2006, *Astron. Telegram*, 787
- Rau, A., Roelofs, G. H. A., Groot, P. J., Marsh, T. R., Nelemans, G., Steeghs, D., Salvato, M., & Kasliwal, M. M. 2010, *ApJ*, 708, 456
- Ritter, H. 1980, *A&A*, 85, 362
- Ritter, H., & Kolb, U. 2003, *A&A*, 404, 301
- Robertson, J. W., Honeycutt, R. K., & Turner, G. W. 1995, *PASP*, 107, 443
- Ross, F. E. 1925, *AJ*, 36, 99
- Ross, F. E. 1928, *AJ*, 38, 144
- Rykoff, E. S., et al. 2004, *IBVS*, 5559
- Schmidtke, P. C., Cowley, A. P., Hutchings, J. B., & Crampton, D. 2002, *AJ*, 123, 3210
- Schoembs, R., & Hartmann, K. 1983, *A&A*, 128, 37
- Shafter, A. W., & Hessman, F. V. 1988, *AJ*, 95, 178
- Shafter, A. W., & Szkody, P. 1984, *ApJ*, 276, 305
- Shappee, B. J., et al. 2014a, *ApJ*, 788, 48
- Shappee, B. J., et al. 2014b, *Astron. Telegram*, 6676
- Shears, J., & Boyd, D. 2007, *J. Br. Astron. Assoc.*, 117, 25
- Shears, J., Brady, S., Koff, R., Goff, W., & Boyd, D. 2012, *J. Br. Astron. Assoc.*, 122, 49
- Shears, J., et al. 2011a, *J. Br. Astron. Assoc.*, 121, 355
- Shears, J. H., Gaensicke, B. T., Brady, S., Dubovsky, P., Miller, I., & Staels, B. 2011b, *New Astron.*, 16, 311
- Sherrington, M. R., Jameson, R. F., Bailey, J., & Giles, A. B. 1982, *MNRAS*, 200, 861
- Shumkov, V., et al. 2014, *Astron. Telegram*, 6851
- Simonian, G., et al. 2015, *Astron. Telegram*, 6981
- Simonian, G., et al. 2014, *Astron. Telegram*, 6608
- Skillman, D. R., et al. 2002, *PASP*, 114, 630
- Smak, J. 1985, *Acta Astron.*, 35, 357
- Smak, J. 2004, *Acta Astron.*, 54, 221
- Smak, J. 2008, *Acta Astron.*, 58, 55
- Smak, J. I. 1991, *Acta Astron.*, 41, 269
- Smart, R. L. 2013, *VizieR Online Data Catalog*, 1324
- Smith, D. A., et al. 2002, *IBVS*, 5226
- Soejima, Y., Imada, A., Nogami, D., Kato, T., & Monard, L. A. G. 2009, *PASJ*, 61, 395
- Solheim, J.-E. 2010, *PASP*, 122, 1133
- Stanek, K. Z., et al. 2014a, *Astron. Telegram*, 6233
- Stanek, K. Z., et al. 2014b, *Astron. Telegram*, 6479
- Stellingwerf, R. F. 1978, *ApJ*, 224, 953
- Still, M. D., Marsh, T. R., Dhillon, V. S., & Horne, K. 1994, *MNRAS*, 267, 957
- Swope, H. H., & Caldwell, I. W. 1930, *Harvard Coll. Obs. Bull.*, 879
- Szkody, P., et al. 2002, *AJ*, 123, 430
- Szkody, P., et al. 2006, *AJ*, 131, 973
- Szkody, P., et al. 2007, *AJ*, 134, 185
- Szkody, P., & Mattei, J. A. 1984, *PASP*, 96, 988
- Templeton, M. R. 2011, *AAVSO Alert Notice*, 434
- Teyssier, F. 2014, *Astron. Telegram*, 6235
- Thorstensen, J. R., Fenton, W. H., Patterson, J. O., Kemp, J., Krajci, T., & Baraffe, I. 2002, *ApJ*, 567, L49
- Thorstensen, J. R., Patterson, J. O., Shambrook, A., & Thomas, G. 1996, *PASP*, 108, 73
- Thorstensen, J. R., & Skinner, J. N. 2012, *AJ*, 144, 81
- Thorstensen, J. R., & Taylor, C. J. 1997, *PASP*, 109, 1359
- Thorstensen, J. R., Wade, R. A., & Oke, J. B. 1986, *ApJ*, 309, 721
- Tibshirani, R. 1996, *J. R. Statistical Soc. Ser. B*, 58, 267
- Tovmassian, G., Clark, D., & Zharikov, S. 2010, *Cent. Bur. Electron. Telegrams*, 2283, 1
- Udalski, A. 1988, *IBVS*, 3239
- Udalski, A. 1989, *IAU Circ.*, 4885
- Udalski, A. 1990, *AJ*, 100, 226
- Udalski, A., & Pych, W. 1992, *Acta Astron.*, 42, 285
- Uemura, M., et al. 2008, *PASJ*, 60, 227
- Uemura, M., et al. 2002, *PASJ*, 54, L15
- Uemura, M., Kato, T., Nogami, D., & Ohsugi, T. 2010, *PASJ*, 62, 613
- Uemura, M., Kato, T., Pavlenko, E., Baklanov, A., & Pietz, J. 2001, *PASJ*, 53, 539

- Uemura, M., et al. 2005, *A&A*, 432, 261
- van Amerongen, S., Bovenschen, H., & van Paradijs, J. 1987, *MNRAS*, 229, 245
- van Amerongen, S., Kuulkers, E., & van Paradijs, J. 1990, *MNRAS*, 242, 522
- Vladimirov, V., et al. 2014, *Astron. Telegram*, 5950
- Vogt, N. 1979, *IAU Circ.*, 3375
- Vogt, N. 1980, *A&A*, 88, 66
- Vogt, N. 1982, *ApJ*, 252, 653
- Vogt, N. 1983, *A&A*, 128, 29
- Vogt, N. 1983, *A&A*, 118, 95
- Vogt, N., & Bateson, F. M. 1982, *A&AS*, 48, 383
- Vogt, N., Schoembs, R., Krzeminski, W., & Pedersen, H. 1981, *A&A*, 94, L29
- Wagner, R. M., et al. 2014, *Astron. Telegram*, 6669
- Walker, A. D., & Olmsted, M. 1958, *PASP*, 70, 495
- Warner, B. 1974, *MNRAS*, 168, 235
- Warner, B. 1976, in *IAU Colloq. 29, Multiple Periodic Variable Stars*, ed. W. S. Fitch (Dordrecht: D. Reidel Publishing Company), p. 247
- Warner, B. 1995, *Cataclysmic Variable Stars* (Cambridge: Cambridge University Press)
- Watanabe, M., Hirosawa, K., Kato, T., & Narumi, H. 1989, *VSOLJ Variable Star Bull.*, 10, 40
- Whitehurst, R. 1988, *MNRAS*, 232, 35
- Williams, S. C., Darnley, M. J., Bode, M. F., & Copperwheat, C. M. 2015, *Astron. Telegram*, 6992
- Wils, P., Gänsicke, B. T., Drake, A. J., & Southworth, J. 2010, *MNRAS*, 402, 436
- Wolf, M. 1912, *Astron. Nachr.*, 192, 7
- Wood, M. A., & Burke, C. J. 2007, *ApJ*, 661, 1042
- Wood, M. A., Casey, M. J., Garnavich, P. M., & Haag, B. 2002, *MNRAS*, 334, 87
- Woudt, P. A., & Warner, B. 2011, *Astron. Telegram*, 3705
- Woudt, P. A., Warner, B., & Motsoaledi, M. 2013, *Astron. Telegram*, 4726
- Yamaoka, H. 2010, *Cent. Bur. Electron. Telegrams*, 2273
- Yecheistov, V., et al. 2014, *Astron. Telegram*, 5905
- Zemko, P., Kato, T., & Shugarov, S. 2013, *PASJ*, 65, 54
- Zemko, P. O., & Kato, T. 2013, *Astrophysics*, 56, 203